Refining marine polysaccharides and their immunomodulatory effects

Monica Daugbjerg Christensen

Thesis for the degree of Philosophiae Doctor

October 2025

School of Health Sciences

FACULTY OF FOOD SCIENCE AND NUTRITION

UNIVERSITY OF ICELAND

Refining marine polysaccharides and their immunomodulatory effects

Monica Daugbjerg Christensen

Thesis for the degree of Philosophiae Doctor

Supervisors

Prof. Guðjón Þorkelsson
Dr. Hildur Inga Sveinsdóttir
Prof. Guðmundur Óli Hreggviðsson
Prof. Jóna Freysdóttir

Doctoral committee

Dr. Ólafur H. Friðjónsson
Prof. Eva Nordberg Karlsson

October 2025

School of Health Sciences
FACULTY OF FOOD SCIENCE AND NUTRITION
UNIVERSITY OF ICELAND

Einangrun og niðurbrot sjávarfjölsykra og mat á ónæmismótandi áhrifum þeirra

Monica Daugbjerg Christensen

Ritgerð til doktorsgráðu

Leiðbeinendur

Próf. Guðjón Þorkelsson
Dr. Hildur Inga Sveinsdóttir
Próf. Guðmundur Óli Hreggviðsson
Próf. Jóna Freysdóttir

Doktorsnefnd

Dr. Ólafur H. Friðjónsson
Prof. Eva Nordberg Karlsson

Október 2025

Heilbrigðisvísindasvið
MATVÆLA- OG NÆRINGARFRÆÐIDEILD
HÁSKÓLI ÍSLANDS

ISBN 978-9935-9665-8-2

ORCID:0000-0002-5151-9932

Reykjavik, Iceland 2025

Ágrip

Brúnþörungar (þang og þari) mynda megnið af fjörugróðri við strendur Íslands. Í þeim finnast fjölsykrur sem hægt er að nýta í heilsuvörur vegna fjölbreyttrar lífvirkni þeirra, t.d. ónæmismótandi eiginleika. Einnig er hægt að umbreyta þessum verðmætu fjölsykrum með aðferðum líftækninnar, með það að markmiði að framleiða nýjar vörur sem hægt er að nýta í lyfja-, fæðubótar- og öðrum iðnaði. Þannig er unnt að nýta lífmassa stórþörunganna á sjálfbæran hátt og skapa ný verðmæti.

Þessi ritgerð fjallar um rannsóknir á sjávarfjölsykrum og ónæmismótandi áhrifum þeirra. Í ritgerðinni er lögð áhersla á fjögur viðfangsefni: i) ítarlega greiningu á nýjum súlfatasa sem hægt er að nota við ummyndun á sjávarfjölsykrum, ii) rannsóknir á flókinni byggingu laminarin sameinda og afleiðum þeirra og ónæmismótandi áhrifum, iii) rannsóknir á ónæmismótandi áhrifum fúkóídan sameinda, og iv) rannsóknir á algínati og algínat smásykrum sem útbúnar voru með hjálp ensíma. Eitt aðal markmið þessa verkefnis var að kanna hvernig unnt er að nota ensím til að breyta byggingu fjölsykra úr brúnþörungum og rannsaka hvernig slíkar breytingar hafa áhrif á sérhæft ónæmissvar. Lífefnafræðilegar aðferðir, frumuræktir og nákvæmar mæliaðferðir voru notaðar til að greina myndbyggingu fjölsykra og afleiddra fásykra úr þremur þarategundum og meta ónæmismótandi áhrif þeirra.

Nýr súlfatasi, SulA1, úr sjávarbakteríunni *Arthrobacter* ISCAR3885, var framleiddur með erfðatæknilegum aðferðum og rannsakaður ítarlega. Markmiðið var að rannsaka SulA1 með tilliti til hagnýtingar í iðnaði. SulA1 súlfatasinn gat fjarlægt súlfathóp af *N*-Acetyl-D-galactosamine-4-sulfate (GalNAc4S) sem er önnur byggingareining kondroítin súlfats sem fyrirfinnst í brjóski sjávarlífvera og spendýra. Eiginleikar súlfatasans endurspegla hlutverk hans og sjávarbakteríunnar *Arthrobacter* í niðurbrotsferlum kondroítin súlfats. Þetta er mikilvægt því með því að fjarlægja súlfathópa fjölsykra er unnt að hafa áhrif á leysni þeirra, seigju og lífvirkni, t.d. möguleg áhrif á ónæmiskerfið.

Laminarin sameindir eru forðasykrur sem finnast aðallega í brúnþörunum. Þær samanstanda af stuttum β−1,3-glúkan keðjum með β−1,6-greinum. Í þessu verkefni voru laminarin sameindir úr þremur gerðum brúnþörunga eingangraðar og hreinsaðar og bygging þeirra greind. Þær voru einnig klipptar niður í smásykrur með laminaripentaosa-myndandi endo−1,3−β-glúkanasa (LPHase). Markmiðið var að greina samband byggingar og ónæmisvirkni sem metin var í angafrumulíkani. Niðurstöðurnar sýndu að afleiður af laminarini, sérstaklega stuttar smásykrur, höfðu áhrif á ræsingu angafrumna með því að draga úr seytingu þeirra á TNF-α og bólguhvetjandi boðefnunum IL-12p40 og IFN-. Þetta benti til þær hefðu bólguhamlandi áhrif, að hluta til með því að draga úr Th1 ónæmissvari. Aftur á móti leiddi samrækt angafrumna sem

voru meðhöndlaðar með laminarini frá *L. hyperborea,* sem inniheldur fáar og stuttar hliðargreinar (eina glúkósaeiningu), og $CD4^+$ T frumna til aukinnar seytingar á IL-17 og IL-10 og þannig til virkjunar á Th17 ónæmissvari. Þessar niðurstöður benda til þess að hugsanlega sé unnt að nota laminarin sameindir og afleiður þeirra í meðferðarskyni á sjúkdómum tengdum bólgu og að meðferðarmöguleikinn færi eftir mólstærð þeirra og hvernig greinamunstur þeirra er.

Fúkóídan, sem er fjölsykra með súlfathópa, fyrirfinnst í frumuvegg stórþörunga og utanfrumu efni (extracellular matrix). Þar gegnir sykran mikilvægu hlutverki í byggingu frumuveggsins, hún hefur áhrif á osmótískan þrýsting, aðstoðar við samskipti milli frumna og þjónar sem varnarkerfi fyrir lífveruna. Fúkóídan einkennist af flókinni byggingu þar sem aðalkeðjan samanstendur af af α–1,3- og α–1,4-tengdum fúkósa einingum. Í þessari rannsókn var fúkóídan fjölsykra úr *S. latissima* einangruð og brotin niður með ensíminu endo-α-(1,3)-fukóídanasa (Psf1) í mismunandi stórar smásykrur. Því næst var ónæmisvirkni smásykranna metin. Stuttar smásykrur höfðu bólguhamlandi áhrif með því að minnka IL-12p40 seytingu angafrumna og koma þannig í veg fyrir Th1 ónæmissvar. Stuttar fúkóídan smásykrur gætu því hugsanlega nýst við meðferð á bólgusjúkdómum og þá einkum þeim sem eru tengdir Th1 ónæmissvari.

Algínat er byggingarfjölsykra sem finnst í frumuveggjum brúnþörunga. Algínat er línuleg keðja sem samanstendur úr blokkum α–L–guluronic (GulA) sýru eininga og β–D–mannuronic (ManA) sýru eininga. Þessi fjölsykra gegnir hlutverki í styrk og liðleika frumuveggs þörunga. Í þessari rannsókn kom í ljós að tvær algínat fásykur, sem útbúnar voru með algínat lyasa ensíminu AlyRm3, annars vegar með hlutmeltingu og hins vegar fullu niðurbroti, juku setyingu IL-6 og IL-10 angafrumna. Fullmelta fásykran jók líka seytingu á IL-12p40. Auk þess leiddi AlyRm3 fullmelta fásykran til Th1 ónæmissvars í samrækt angafrumna og ósamgena $CD4^+$ T frumna með því að auka seytingu á IFN-γ og IL-10.

Niðurstöður rannsóknarinnar sem greint er frá í ritgerð þessari sýna fram á að niðurbrot þarafjölsykra í smásykrur með þar til gerðum ensímum getur breytt ónæmismótandi áhrifum sykranna og gert notkun þeirra í meðferðum við sjúkdómum tengdum ónæmiskerfinu mögulega. Vinnsla á fjölsykrum úr brúnþörungum með ensímum er umhverfisvæn og getur aukið verðmæti þeirra og notkunargildi í lyfja- og fæðubótariðnaði.

Lykilorð: Sjávarfjölsykur, ensímmeðhöndlun, smásykrur, ónæmismótandi áhrif, brúnþörungar, súlfatasi.

Abstract

Marine-derived polysaccharides, particularly those sourced from abundant and renewable seaweeds like brown algae, offer remarkable potential as valuable compounds for various health applications due to their diverse and bioactive properties, including immunomodulating activities. Through innovative biorefining processes and enzymatic modification, it is possible to efficiently modify and utilize these valuable polysaccharides, with potential of creating novel products with targeted functionalities for use in pharmaceuticals, nutraceuticals, and other industrial applications. This sustainable approach not only optimizes seaweed biomass utilization but also represents a critical step forward in developing environmentally friendly, high-value products from marine resources.

In this study, refinement of marine polysaccharides and their immunomodulatory effects were investigated, focusing on four major aspects i) detailed characterization of a novel sulfatase for potential enzymatic refining processes, ii) the structural complexity of laminarin and its derivatives and their immunomodulating effects, iii) the immunomodulating effects of fucoidan, iv) and the enzymatic refinement of alginate. The primary aim of this research was to examine how enzymatic refining processes, which cause structural modifications of marine polysaccharides derived mainly from brown seaweed, affected adaptive immune responses. Biochemical assays, cell culture experiments, and advanced analytical techniques were used to characterize the biomass and evaluate the immunomodulatory effects of various polysaccharides and oligo-derivatives.

A novel sulfatase, SulA1, was cloned and extensively characterized from a marine *Arthrobacter* strain. SulA1 was found to modify the sulfate group of the chondroitin sulfate monosaccharide *N*-Acetyl-D-galactosamine-4-sulfate (GalNAc4S), underscoring its role in the chondroitin sulfate degradation pathway of the identified *Arthrobacter* strain. The purpose was to gather detailed understanding of SulA1, which potentially could reveal industrial applications, such as selective desulfation of polysaccharides, which might alter their solubility, viscosity, or bioactivity. Understanding the specific actions and optimal conditions for SulA1 might enable targeted modification and refinement of marine polysaccharides like chondroitin sulfate, and possibly alter their immunomodulatory potential.

Laminarin, a storage polysaccharide predominantly found in brown seaweed, is a β–1,3-glucan with β–1,6-branches. In this study laminarin from three species of brown seaweed were extracted, purified, structurally analyzed, and enzymatically modified using the laminaripentaose-producing endo–1,3–β-glucanase, LPHase. The aim was to

unravel structure-function relationships with immune-modulating activity using a human monocyte-derived dendritic cell (DC) model. Results showed that derivatives of laminarin, particularly those with short degree of polymerization (DP) range, altered the activation of DCs by down-regulating their TNF-α secretion and secretion of the pro-inflammatory 12p40 and IFN-γ cytokines, thus promoting an anti-inflammatory immune environment partly by modulating Th1 responses. In contrast, co-cultures of DCs treated with simple branched laminarin from *L. hyperborea* and $CD4^+$ T-cells led to increased IL-17 and IL-10 secretion, thus inducing Th17 responses. These data suggest that laminarin and their derivatives may have different therapeutic applications depending on the molecular size and branching pattern of laminarin and laminari-oligosaccharides.

Fucoidan, a sulfated polysaccharide primarily found in the cell walls, plays a crucial structural role in maintaining the integrity and flexibility of the seaweed. It is characterized by its complex structure, which includes a backbone of α–1,3- and α–1,4-linked fucose residues. In this study, fucoidan from *S. latissima* was enzymatically refined by the endo- α-(1,3)-fucoidanase Psf1 into different molecular-sized fractions to assess their potential therapeutic applications. The low molecular weight fractions exhibited significant anti-inflammatory effects by decreasing IL-12p40 secretion by DCs and inhibiting Th1 responses and possible key signaling pathways, highlighting their promise in treating inflammatory diseases.

Alginate, a structural polysaccharide found in the cell walls of brown seaweed, is composed of linear chains of α–L–guluronic acid (GulA) and β–D–mannuronic acid (ManA) residues. This polysaccharide plays a key role in providing strength and flexibility to the seaweed's cell walls. In this study, the two alginate oligosaccharide fractions, AlyRm3 partially digestion and AlgRm3 full digestion, respectively, were both found to significantly enhance the secretion of IL-6 and IL-10 by DCs. The fully digested fraction also notably increased IL-12p40 secretion. Furthermore, the fully digested AlyRm3 fraction was effective in promoting a Th1 response during co-culture of DCs with allogeneic $CD4^+$ T-cells, as shown by increased levels of IFN-γ and IL-10 in the co-culture supernatant.

These findings collectively reveal that specific enzymatic modifications, and various enzyme treatments, can alter the immunomodulatory effects of marine-derived polysaccharides, making them a potential target for therapeutic applications. This approach not only optimizes the use of seaweed biomass but also advances the development of environmentally sustainable, high-value products with potential applications as pharmaceuticals and nutraceuticals.

Keywords: Marine polysaccharides, Enzymatic refinement, Immunomodulation, Brown seaweed, Sulfatase.

Acknowledgements

The work of this thesis was carried out at the Division of Biotechnology, Matís ohf, at the Department of Immunology, Landspítali - the National University Hospital of Iceland, and the Faculty of Food Science and Nutrition, University of Iceland. The research was funded by the MARIKAT JPI Cofound Blue BioEconomy project (grant number 9082-00021B), the European Union's Horizon Europe program SeaMark (Seaweed-based market applications) project (grant number 101060379), and the Landspítali Science Fund (grants number A-2020-034, A-2021-027 and A-2022-025).

First and foremost, I would like to express my sincere gratitude to my supervisors Professor Jóna Freysdóttir and Professor Guðmundur Óli Hreggviðsson, for their invaluable supervision, guidance, support, and collaboration throughout my studies. Their insightful feedback, encouragement, and unwavering dedication have been contributory in shaping the direction and success of my research. I am deeply grateful for the opportunities they provided me to explore new ideas, develop my skills, and grow both academically and personally. Their expertise and mentorship have profoundly influenced my academic journey, and I am truly fortunate to have had the privilege of working under their supervision.

I am sincerely grateful to my co-supervisor and committee member, Dr. Ólafur H. Friðjónsson, and my committee member, Professor Eva Nordberg Karlsson, for their exceptional supervision, scientific sparring, and invaluable collaboration. Their profound expertise and insightful advice have enriched my research, guiding me through complex challenges and encouraging me to think critically and innovatively. Their significant contributions to my scientific writing, particularly in preparing and reviewing manuscripts for publication, have been vital in enhancing the quality and impact of my work. The intellectual exchange and support I received from them have been pivotal in advancing my research and have significantly contributed to my academic development. I deeply appreciate their commitment to my success and the generous sharing of their knowledge and experience.

A special note of gratitude is extended to my coworkers and co-authors, Hörður Guðmundsson, Dr. Leila Allahgholi, Associated professor Javier Linares-Pastén, Justyna M. Dobruchowska, and Antoine Moenaert. Their contributions to my research, valuable feedback, and great assistance during this project have been invaluable. It has been a distinct pleasure to work with them.

I would like to express my deepest gratitude to Professor Anne S. Meyer of the Technical University of Denmark (DTU) for her unwavering trust in my abilities to carry

out the immunomodulating tests. I am also profoundly grateful for the opportunity to contribute to and be part of the resulting publication (paper III).

I also want to express my gratitude to my administrative supervisors Professor Guðjón Þorkelsson and Dr. Hildur Inga Sveinsdóttir for their understanding, expert guidance, and help in bringing this PhD thesis to completion.

A special thanks to my current and former colleagues at Matís and at the Department of Immunology, especially Lara Chrystina Malta Neri, Brynja Einarsdóttir, Associate Professor Stefanía P. Bjarnarson, Associate Professor Siggeir Fannar Brynjólfsson, and Dr. Kirstine Nolling Jensen, for their help, support, and encouragement throughout the years.

Finally, I want to express my deepest gratitude to my family. I sincerely thank my parents for their endless love, encouragement, and belief in my capabilities, my sister for always standing by my side and lastly but not least my husband, Henrik, for his patience, and consistent support throughout this journey.

Contents

List of Abbreviations

^{1}H-NMR	^{1}H Nuclear Magnetic Resonance
1D	One-Dimensional
2D	Two-Dimensional
AA	Auxiliary activities
aa	Amino acid
APCs	Antigen-presenting cells
CAZy database	Carbohydrate-Active enZymes database
CAZymes	Carbohydrate-active enzymes
cDCs	Conventional dendritic cells
CEs	Carbohydrate esterases
CLRs	C-type lectin receptors
C-PAGE	Carbohydrate polyacrylamide gel electrophoresis
CR3	Complement receptor 3
CS	Chondroitin sulfate
DAMPs	Damage associated molecule patterns
DB	Degree of branching
DC	Dendritic cell
DCs	Dendritic cells
DP	Degree of polymerization
DSF	Differential scanning fluorimetry
dw	Dry weight
EDTA	Ethylenediaminetetraacetic acid
ELISA	Enzyme-linked immunosorbent assay
EPS	Exopolysaccharides
FACS	Fluorescence-Activated Cell Sorting
FGly	Formylglycine
FT-IR	Fourier transform infrared spectrometry

GAG	Glycosaminoglycan
GalNAc	*N*-acetyl-galactosamine
GalNAc4S	*N*-Acetyl-D-galactosamine-4-sulfate
GHs	Glycoside hydrolases
GlcA	Glucuronic acid
Glcp	Glucose pyranose form
GTs	Glycoside transferases
GulA	α–L-guluronic acid units
HSQC	Heteronuclear Single Quantum Coherence
HMW	High molecular weight
HPAEC-PAD	High-performance anion-exchange chromatography with pulsed amperometric detection
IFN	Interferon
IL	Interleukin
imDCs	Immature dendritic cells
LMW	Low molecular weight
LPHase	Laminaripentaose-producing endo-1,3–β-glucanase
LPS	Lipopolysaccharide
MACS	Magnet associated cell sorting
M:G	Mannitol:Glucose ratio
MALDI-TOF MS	Matrix-Assisted Laser Desorption/Ionization Time-of-Flight Mass Spectrometry
MalE	Maltose-binding protein domain
ManA	β-D-mannuronic acid
mDC	Mature dendritic cells
MHC	Major histocompatibility complex
MMW	Medium molecular weight
moDCs	Monocyte-derived DCs
NLRs	NOD-like receptors
PAMPs	Pathogen associated molecule patterns
PBMCs	Peripheral blood mononuclear cells
PGE	Phloroglucinol equivalents

PI	Proportional index
pLDDT	Predicted local distance difference test
PLs	Polysaccharide lyases
PMF	Peptide mass fingerprinting
*p*NCS	*p*-nitrocatechol sulfate
ppm	Parts per million
PRRs	Pathogen recognition receptors
SD	Standard deviation
SDS-PAGE	Sodium dodecyl-sulfate polyacrylamide gel electrophoresis
SEC	Size exclusion chromatography
SEM	Standard error of mean
SI	Secretion index
TFF	Tangential flow filtration
Tfh	T follicular cells
TGF	Transforming growth factor
Th	T-helper cells
TLC	Thin-layer chromatography
TLRs	Toll-like receptors
T_m	Melting temperature
TNF-α	Tumor necrosis factor alpha
TPC	Total phenolic content
Tregs	T regulatory cells

List of Figures

List of Tables

List of Original Papers

This thesis is based on the following original publications, which are referred to in the text by their Roman numerals (I, II, III):

I. Christensen MD, Allahgholi L, Linares-Pastén JA, Friðjónsson Ó, Guðmundsson H, Kale V, Sardari RRR, Hreggviðsson GÓ, Karlsson EN. Cloning and Characterization of a Novel *N*-Acetyl-D-galactosamine-4-*O*-sulfate Sulfatase, SulA1, from a Marine *Arthrobacter* Strain. Mar Drugs. 2024 Feb 23;22(3):104.

II. Christensen MD, Allahgholi L, Dobruchowska JM, Moenaert A, Guðmundsson H, Friðjónsson Ó, Karlsson EN, Hreggviðsson GÓ, Freysdottir J. Laminarins and their derivatives affect dendritic cell activation and their crosstalk with T cells. Int J Biol Macromol. 2025 Feb 19;306(Pt 1):141287. doi: 10.1016/j.ijbiomac.2025.141287.

III. Trang VTD, Mikkelsen MD, Christensen MD, Meier S, Hunt CJ, Holck J, Hreggviðsson GÓ, Freysdottir J, Cao HTT, Khanh HHN and Meyer AS. A cold-adapted endo-fucoidanase Psf1 from *Pseudoalteromonas sp.* that catalyzes production of T-cell activating fucoidan oligosaccharides from *Saccharina latissima* fucoidan. Int J Biol Macromol. 2025 Jul 11; 320:145930. doi: 10.1016/j.ijbiomac.2025.145930

Declaration of Contribution

Paper I: In this paper, we characterized a novel sulfatase, SulA1, from a marine *Arthrobacter* strain. I planned the study and conducted the protein expression and enzyme purification, performed optimization, thermostability, and storage experiments, and investigated the enzyme's activity on various natural substrates. Additionally, I analyzed and interpreted the data. The determination of specific activity on GalNAc4S and kinetic parameters using the HPAEC-PAD system was carried out with assistance from Hörður Guðmundsson and Ólafur H. Friðjónsson. I designed the figures included in the paper. The multiple sequence alignment, enzymatic modeling, and related figures were completed by Leila Allahgholi and Javier Linares-Pastén from Dr. Eva Nordberg Karlsson's research group at the Division of Biotechnology, Department of Chemistry, Lund University. Finally, I wrote the manuscript in collaboration with my mentors Dr. Guðmundur Óli Hreggviðsson, Dr. Ólafur H. Friðjónsson, and Dr. Eva Nordberg Karlsson from Lund University and coordinated the editing and revision of the manuscript with co-authors and submitted the manuscript as the corresponding author.

Paper II: In this paper, we investigated the structural relationships of purified laminarin, and laminarin-oligosaccharides derived from *L. digitata*, *L. hyperborea* and *S. latissima* and their immunomodulatory effects on dendritic cells (DCs) and their T-cell crosstalk. I had a major role in planning and designing the research. Particularly, it was I who extracted and purified laminarin from the three species of brown seaweed, with assistance from Antoine Moenaert (Matís) and former Matís staff member Brynja Einarsdóttir, specialist in tangential-flow filtration systems. Carbohydrate composition analyses, laminarin profiling, and Fourier transform infrared spectrometry (FT-IR) analyses were conducted by former Ph.D. student Leila Allahgholi in Dr. Eva Nordberg Karlsson's research group at Lund University. I analyzed the data output and interpreted it, as well as designing the figures and tables used in the publication.

The experimental setup for enzymatic laminarin-oligosaccharide generation was planned in collaboration with my supervisor Dr. Guðmundur Óli Hreggviðsson and Hörður Guðmundsson and carried out by me. I purified and collected the laminarin-oligosaccharide fractions using the Äkta purification system under Hörður Guðmundsson's supervision and analyzed and visualized the data. Structural analysis of the laminarin with MALDI-TOF and ^{1}H-NMR were outsourced to Dr. Justyna M. Dobruchowska from Utrecht University, who also contributed to the manuscript writing of this section. I interpreted the data in relation to other structural information obtained, as well as immunomodulating data.

I planned and carried out the studies analyzing the immunomodulating effects of laminarin and laminarin-oligosaccharide samples by collecting supernatants from DCs and DCs co-cultured with allogeneic $CD4^+$ T-cells. Flow cytometry panels for surface molecule expression on DCs were set up with the help of former PhD student Kirstine Nolling Jensen and my mentor Dr. Jóna Freysdóttir. I performed all assays (cell culture, cell isolation, flow cytometry and ELISA), analyzed the data, and designed the figures included in the paper. Finally, I wrote the original manuscript in collaboration with Dr. Jóna Freysdóttir, Dr. Guðmundur Óli Hreggviðsson, and Dr. Ólafur H. Friðjónsson at Matís, as well as Dr. Eva Nordberg Karlsson and Leila Allahgholi from Lund University and coordinated the editing and revision of the manuscript with co-authors and submitted the manuscript as the corresponding author.

Paper III: In this paper, the α-(1,3)-fucoidanase, Psf1, was characterized and used to generate different sized fucoidan fractions, which were structurally analyzed. This part of the work was carried out by scientists in the research group of Dr. Anne S. Meyer, Department of Biotechnology and Biomedicine, Section for Protein Chemistry and Enzyme Technology (DTU). My contribution to this paper includes all immunomodulating experiments, such as cell-related work (cell culture and cell isolation) and protein assays (flow cytometry and ELISA), analysis of the data, interpreting the data in relation to structural information, and construction of figures for the publication. My part of the project required planning and execution of the experiments in close communication with DTU. Finally, I was involved in writing the original draft, contributing with my knowledge in immunology by writing the part for the introduction, materials & methods, results, and discussion.

Contribution not included in the thesis

Allahgholi L, Jönsson M, **Christensen MD**, Jasilionis A, Lavasani S, Karlsson EN. Fermentation of the Brown Seaweed *Alaria esculenta* by a Lactic Acid Bacteria Consortium Able to Utilize Mannitol and Laminari-Oligosaccharides. Fermentation 2023; 9: 499.

Hreggviðsson GÓ, Nordberg-Karlsson EM, Tøndervik A, Aachmann FL, Dobruchowska JM, Linares-Pastén J, **Daugbjerg Christensen M**, Moenaert A, Kristjansdottir T, Sletta H, Fridjonsson OH, Aasen IM. (2020). Biocatalytic refining of polysaccharides from brown seaweeds. In MD Torres Pérez, S Kraan, & H Domínguez González (Eds.), *Sustainable Seaweed Technologies: Cultivation, Biorefinery, and Applications: Vol. Chapter 16* (1st ed.). Elsevier. https://doi.org/10.1016/B978-0-12-817943-7.00016-0

1 Introduction

Sustainable bioactive compounds, particularly those derived from marine sources, have gained significant interest due to their potential usage in various industries, including pharmaceuticals and nutraceuticals. This chapter introduces the fundamental concepts of marine-derived polysaccharides and the innovative approaches to refine and enhance their bioactivity. The unique bioactivity of these compounds, combined with the increasing need for sustainable resources, underscores the importance of developing effective methods for their extraction and refinement.

Utilizing refining processes holds significant potential due to the diverse and complex structures of many marine-derived compounds. Seaweeds, especially brown seaweed, are abundant and rapidly renewable resources that do not compete with terrestrial food crops for farmland. The unique polysaccharides found in seaweed, such as laminarin, fucoidan, and alginate, exhibit a variety of bioactive properties, including antioxidant, anti-inflammatory, and anticancer effects, making them valuable for numerous industrial applications. Biorefining these polysaccharides through enzymatic processes allows for the extraction and modification of these valuable compounds in an environmentally friendly manner. This approach not only maximizes the utilization of seaweed biomass but also opens up possibilities for developing novel bioactive products with specific functionalities tailored for use in pharmaceuticals, nutraceuticals, and other industrial applications.

1.1 Marine-derived polysaccharides

The marine environment is one of the most diverse ecosystems on the planet and harbors a wealth of biological diversity, much of which remains unused and unexplored. Within this vast marine ecosystem lies a multitude of organisms that produce a diverse range of natural compounds, including polysaccharides. These polysaccharides can be found in marine organisms such as seaweed [1], microalgae [2], and marine bacteria [3]. In contrast to their terrestrial relatives, marine-derived polysaccharides stand out for their structural complexity, functional diversity, and biological activities, making them potential candidates to be used for various industries, including food and non-food products.

1.2 Biorefining marine polysaccharides

Biorefining is the process that utilizes biomass e.g., sourced from plants, animals, or microorganisms, to extract and refine valuable components, resulting in high-value products. The primary goal is to optimize the utilization of renewable resources while

minimizing environmental impact. The story on biorefining often involves three generations of biomass feedstock. First-generation biomass feedstocks involve traditional crops, leading to concerns about competition with food production, land scarcity, and potential negative impacts on food security. In contrast, second-generation and third-generation biomass feedstock offer more sustainable alternatives, as they do not directly compete with food production. Third-generation biomass feedstocks are derived from algae and microorganisms. Seaweed, in particular, holds immense potential for biorefineries due to its widespread availability, rapid growth rate, and independence from fertile land, fertilizer, pesticides, and irrigation, as in contrast to traditional crops [4]. Brown seaweed has emerged as a focal point for biorefineries due to the potential for large-scale production across many species and its high carbohydrate content, which can reach up to 70% of dry weight (*dw*) [5,6]. However, the full potential of these carbohydrates remains to be fully explored. The extractions and purification of seaweed-derived polysaccharides offer numerous opportunities, whether for their physical or bioactive properties, or as a carbon source for microbial conversions to biofuels and common industrial chemicals. Likewise, other marine organisms contribute valuable complex polysaccharides, such as the sulfated glycosaminoglycan (GAG) from crustaceans, chondroitin sulfate, found primarily in cartilage tissue [7], and exopolysaccharides (EPS) produced by microorganisms, which has also captured significant interest [8,9] especially as resources for the pharmaceutical industry [10,11]. Nevertheless, the structural complexity and heterogeneous composition of these polysaccharides pose challenges in biorefinery processes, requiring solutions to and several processing problems in order to make them a real option.

In biorefinery we often talk about primary and secondary products extracted from the processed biomass. Primary products refer to the unaltered/native components obtained through biocatalytic tools like enzymes and microbes. Not only do they offer heightened resource efficiency, but they also present environmentally benign alternatives to harsh physicochemical processes, thus paving the way for new product development. Secondary products are derivatives of the primary products obtained by enzymatic and microbial conversions. This encompasses derivatives such as modified polysaccharides as investigated in this study.

1.3 Brown seaweed

Brown seaweeds belong to the class Phaeophyceae and are a diverse group of marine macroalgae predominantly found in cold and temperate ocean waters, including regions such as Iceland. Their characteristic brown color is attributed to the presence of fucoxanthin pigment in addition to chlorophyll a and c. Notably, members of the Phaeophyceae include several well-known species, such as kelp (*Laminaria* and *Saccharina*), rockweed (*Fucus*), and bladderwrack *(Ascophyllum*).

Within marine ecosystems, brown seaweeds play pivotal roles, serving as both habitat and food for a variety of marine organisms. Beyond their ecological significance, they hold considerable economic value due to their rich nutritional composition. Brown seaweeds boast a diverse profile of vitamins, proteins, minerals, carbohydrates, polyphenols, and fatty acids, making them prized substrates in various industries.

1.4 Polysaccharides from brown seaweed

Polysaccharides are carbohydrates composed of long chains of monosaccharide units linked by glycosidic bonds. These macromolecules exhibit notable diversity in size, structure, and functions. These properties are influenced by various factors, including source orientation, arrangement of sugar units, types of bonds present, and decoration with functional groups such as sulfate. Brown seaweeds are particularly rich sources of polysaccharides, which can comprise up to 50% of their *dw* depending on factors such as species, harvesting season, and harvesting site [12,13]. Within brown seaweeds, polysaccharides can be categorized into two types: structural and storage carbohydrates. Structural carbohydrates, including fucoidan, alginate, and cellulose, are integral components of the seaweed's cell wall, providing stability and resilience to the unpredictable marine environment. Meanwhile, storage carbohydrates, comprising laminarin and mannitol, serves as energy reserves. Laminarin is stored in granules within the cytoplasm of the cells, while mannitol accumulates in the vacuoles. This study focuses primarily on laminarin and, to some extent, fucoidan and alginate.

1.4.1 Laminarin

Laminarin is a low-molecular-weight polysaccharide ranging from 2-7 kDa, corresponding to a DP of 25-40 [1,14,15]and constitutes approximately 1-25% of the seaweed's *dw*. Its concentration peaks during the summer months, serving as an energy reserve for tissue growth, but declines over the winter [5]. This water-soluble β-glucan is composed of a β–1,3–D-glucose backbone, interspersed with β–1,6-linked glucose moieties (Figure 1). The content and position of β–1,6-linkages within laminarin vary by species, season, environmental factors, and extraction techniques, contributing to its structural diversity. These linkages may occur internally in the linear β–1,3-backbone (intrachain) or form β–1,6-linked branch-points within the linear backbone [1,16]. Additionally, laminarin glucan chains are capped at their reducing end with either mannitol or glucose moiety, known as the M-chains and G-chains, respectively. These variants also vary among species [16,17].

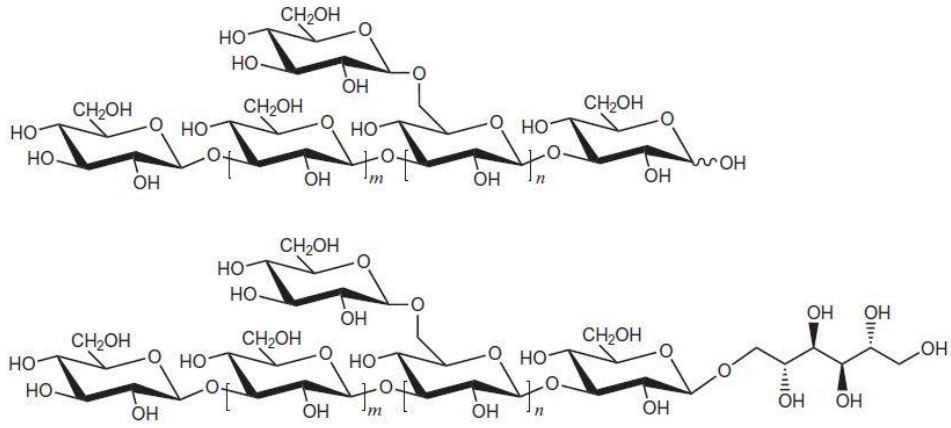

Figure 1: General Structure of Laminarin.
Laminarin consists of a β–(1,3)-linked glucose backbone with intermittent β–(1,6)-linked glucose unit branches. The top figure represents the G-chain laminarin, which has a glucose unit at the reducing end, while the bottom figure represents the M-chain laminarin, featuring a terminal mannitol unit. In the diagram, *m* denotes the number of β–(1,3)-linked glucose units, and *n* represents the number of β–(1,3;1,6)-linked glucose branching points. Figure adapted from [61].

Laminarin polysaccharides exhibit a diverse range of bioactive properties, including antioxidant, anti-inflammatory, anti-apoptotic, immunomodulatory, and anti-cancer effects [15,18–22]. Their non-toxic nature makes them attractive candidates as bioactive molecules. These effects have been demonstrated to be closely linked to the laminarin's structural characteristics, such as the DP, degree of branching (DB), ratio of β–1,3 to β–1,6-glycosidic linkages, molecular weight, and purity [15,21,23,24].

1.4.2 Fucoidan

Fucoidan is defined by its high molecular weight (HMW) and negatively charged sulfated structure, predominantly comprising fucose residues. These fucose units can make up 90% of the total carbohydrate composition [25]. The length, branching, and sulfation pattern of the polysaccharide can vary, influenced by factors such as geographical origin, harvesting season, and extraction process. In addition to fucose residues, fucoidan molecules may feature branching points where other monosaccharides are attached, such as galactose, xylose, mannose, glucuronic acid, and acetyl groups, which form a structurally diverse composition [5,13]. Two structural types of fucoidan have been identified: Type I fucoidan, characterized by repeating units of α–1,3-linked L-fucose, and Type II fucoidan, containing alternately repeating units of α–1,3 and α–1,4-linked L-fucose (Figure 2) [26,27]. Fucoidan has gathered increasing attention for its biomedical potential, including antioxidant, anti-inflammatory, anticoagulant, and anticancer properties, as reviewed several times [27,28].

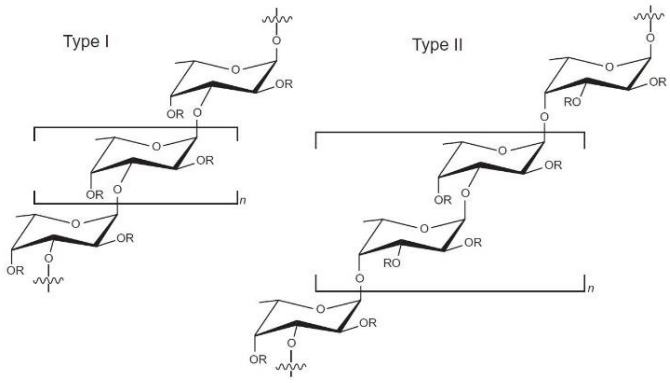

Figure 2: Structural variations of type I and type II fucoidan.
Type I fucoidan consists of repeating units of α–1,3-linked L-fucose, and Type II fucoidan contains alternately repeating units of α–1,3 and α–1,4-linked L-fucose. R groups can be fucose, sulfate groups, or glucuronic acid, while the location of galactose, mannose, and xylose remains unknown. *n* denotes the number of α–1,3 and α–1,4-linked L-fucose. Figur is from [26].

1.4.3 Alginate

Like fucoidan, alginates serve as structural carbohydrates, constituting 25-40% of the seaweed *dw* [29]. Alginate is a linear polysaccharide composed of β–D-mannuronic acid (ManA) units linked by β–1,4-linkages and α–L-guluronic acid (GulA) units linked by α–1,4-linkages. These residues can organize into homogeneous regions composed solely of one type of unit or into regions containing both units, known as M- and G-blocks and MG-blocks (Figure 3) [30,31]. Variance in the percentages of these block segments contribute to the distinct properties observed in alginate across different species of brown seaweed. The average molecular weight of commercial alginate from brown seaweeds has been reported to range between 32 and 400 kDa [32].

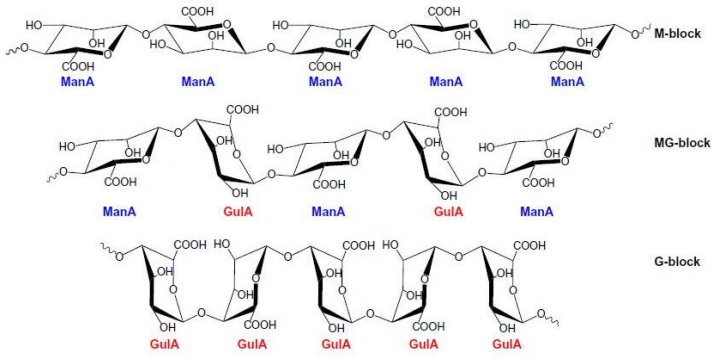

Figure 3: Structural illustartion of M-, MG-, and G-block alginate.
β-D-mannuronic acid (ManA) is bound by β–1,4-linkages and α–L-guluronic acid units (GulA), is bound by α–1,4-linkages, making up the M- and G-blocks, as well as the heterogenic MG-block. Figure from [61].

Alginate finds extensive applications across diverse industries. In the food industry, it serves as prominent product, functioning as a thickener, stabilizer, and emulsifier in various food and beverage formulations. Similarly, in the pharmaceutical sector, alginate is employed in drug delivery systems, wound healing applications, and dental impressions. Its usefulness extends to the textile industry, where it acts as a thickener in printing and dyeing processes. Moreover, alginate features prominently in the cosmetic industry, offering skin moisturizing and restoring properties [33,34].

1.5 Polysaccharides from other marine resources

1.5.1 Chondroitin sulfate

Chondroitin sulfate (CS) is a type of GAG found in cartilage tissue of land and marine animals [7], ranging from 50-100 kDa [35]. It is composed of repeating disaccharide units of glucuronic acid (GlcA) and *N*-acetyl-galactosamine (GalNAc), linked by β−1,4-glycisidic bonds (Figure 4). Depending on the heterogeneous length and degree of sulfation, which are influenced by the species of origin, the CS are classified into different classes [36].

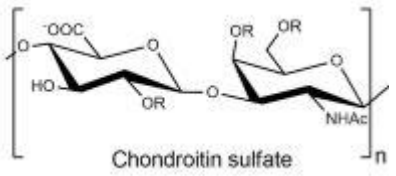

Figure 4: Structural illustration of chondroitin sulfate.
The chain consists of glucuronic acid (GlcA) linked by β−1,4-likage to *N*-acetyl-galactosamine (GalNAc). R =H or SO_3^-, and n denotes the number of β-1,4-likages. The figure is modified from [213].

The two major classes of CS are CS-A and CS-C, distinguished by the position of the sulfate group on the GalNAc unit. In CS-A, the sulfate group is located at C4 position on the GalNAc molecule, while in CS-C, it is positioned at C6 position. Additionally, more distinct and complex CS structures exist, such as CS-AC, which features alternating C4 and C6 sulfation on the GalNAc unit, and fucosylated CS from sea cucumber [37].

Compared to the seaweed-derived polysaccharides, CS is well recognized for its functional properties and diverse bioactivities, including anti-inflammatory [38,39], anti-cancer [40], and anti-coagulating [41] effects. It is also used as a treatment for osteoarthritis [10]. These bioactivities are primarily attributed to the sulfate content of the CS molecules, the positions of the sulfate groups, and the size of the polymer.

These characteristics make CS molecules interesting for pharmaceutical and nutraceutical applications.

1.6 Enzymatic refining of marine polysaccharides

Enzymes and enzymatic processes serve as valuable tools in biorefining of marine-derived polysaccharides. They facilitate the efficient release and extraction of individual compounds (the primary product) and enable highly specific tasks, such as modifying the structures of poly- and oligosaccharides by introducing or removing side groups and branches (the secondary product). This capability opens possibilities for producing products with specialized bioactivities. Compared to traditional chemical processing of polysaccharides, enzymatic degradation provides great advantageous properties, such as substrate specificity, the capability to achieve either complete or selective degradation of the polysaccharides depending on the type of enzyme used, and a process usually simpler and more eco-friendly.

These enzymes, which are involved in the synthesis, degradation, and modification of carbohydrates, are classified in the Carbohydrate-Active enZymes (CAZy; http://www.cazy.org/) database [42]. These enzymes, commonly referred to as carbohydrate-active enzymes or CAZymes, are categorized based on their catalytic activities, carbohydrate-based products, and their amino acid similarities. The main classes of CAZymes include glycoside hydrolases (GHs), glycoside transferases (GTs), polysaccharide lyases (PLs), carbohydrate esterases (CEs), and auxiliary activities (AA). By offering insights into enzyme functions and their evolutionary relationships, the CAZy database serves as an essential tool for researchers in fields such as biochemistry, biotechnology, bioenergy, and biorefining

1.7 Enzymatic refining of the brown seaweed polymers laminarin, fucoidan, and alginate

1.7.1 β–1,3–1,6-glucanases

Laminarin is an attractive feedstock for enzymatic processes owing to its solubility and its availability as a by-product in a cascading biorefinery. Enzymes which are capable of hydrolyzing β–1,3-1,6-glucans, such as laminarin, belong to several GH families within the CAZy database. The GH16 and GH17 families harbor most of the β–1,3-*endo*-enzymes (EC 3.2.1.6 and EC 3.2.1.39 [43]), which are involved in complete hydrolysis of laminarin into glucose (Figure 5). Exhibiting endo-acting activity means they cleave randomly within β–1,3-linked backbone, leading to the breakdown of the polymer into smaller oligosaccharides, mainly laminaribiose and in a few cases glucose [44,45]. In addition to GH16 and GH17, newer GH families, including GH55, GH64,, GH128, GH157, and GH158, also contain members with β–1,3 endo-activity (http://www.cazy.org/). In contrast, the β–1,3-*exo*-enzymes (EC 3.2.1.58 [43]),

releasing glucose, and in some cases, laminaribiose from the non-reducing ends of laminarin oligosaccharides [46]. The main families comprising these enzymes are GH3 and GH5 (http://www.cazy.org/). Since laminarins contain β–1,6-linked branches, complete depolymerization of laminarin requires the cleavage of this linkage. Enzymes responsible for this task have been characterized and are found in the GH30 family (http://www.cazy.org/).

In this study, a laminaripentaose-producing endo-1,3–β-glucanase (LPHase) belonging to the GH64 family was reported to release a laminaripentaose [47], was used to generate different laminari-oligosaccharides with different DP-range and branching patterns, aiming to investigate the structure-function relationship in the context of immunomodulation.

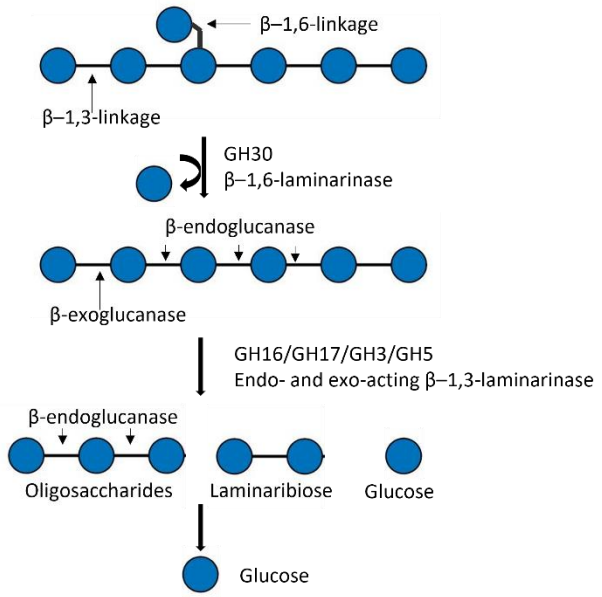

Figure 5: Laminarin degradation pathways by CAZymes

The figure illustrates the enzymatic breakdown of laminarin into glucose by carbohydrate-active enzymes (CAZymes). The oligosaccharide shown at the top represents a section of a larger laminarin chain, composed of β–1,3 and β–1,6 linkages, indicated by arrows. Depolymerization of laminarin occurs through the action of endo-β-glucanases (e.g., from the GH16 and GH17 families), which cleave randomly within the β–1,3-linked backbone, and exo-β-glucanases (e.g., from the GH3 and GH5 families), which release laminaribiose or glucose units from the non-reducing ends of laminarin oligosaccharides. In the final step, specific β-glucosidases further process laminaribiose into glucose after its transport into the cell. This complete breakdown allows the resulting glucose monomers to enter metabolic pathways for energy production or storage. Blue symbols represent glucose in its pyranose form (Glcp), following the Symbol Nomenclature for Glycans (SNFG; https://www.ncbi.nlm.nih.gov/glycans/snfg.html). The figure was generated using the DrawGlycan SNFG online software (http://www.virtualglycome.org/DrawGlycan/) and modified in PowerPoint.

1.7.2 Fucoidanases and fucosidases

Fucoidanases and fucosidases have attracted considerable attention for their capacity to degrade fucoidan into bioactive fragments, making them a valuable tool in the pharmaceutical, nutraceutical, and biotechnological industries. These enzymes belong to the GH families in CAZy, as seen for the β−1,3-1,6-glucanases. Both fucoidanases and fucosidases catalyze similar reactions. However, there are key differences between these two enzyme classes.

Characterized fucoidanases specifically target the glycosidic bond within the fucoidan backbone, particularly in the marine environments where brown seaweeds are abundant. These enzymes exhibit both endo-acting and exo-acting activities and are all classified under the GH107 family. *Endo*-fucoidanases can be further subdivided based on their catalytic activity [27] into Type 1 (catalyzing 1,4−α-L-Fucoidan endohydrolysis [47]) and Type 2 (catalyzing 1,3−α-L-Fucoidan endohydrolysis [49]). The exo-fucoidanases (Type 3) cleave the terminal glycosidic bond, removing one fucose from the end of the fucoidan chain [50].

The fucosidases are classified under several GH families (GH29, GH95, GH139, GH141, and GH151; CAZy May 2024). Their primary function is to catalyze the hydrolysis of fucose residues from various substrates, including fucoidan fucosylated glycoproteins, glycolipids, and oligosaccharides. Fucosidases typically exhibit exo-acting activity, leading to the release of fucose as a monosaccharide and leaving a de-fucosylated product [27].

In this study, a novel α-(1,3)-fucoidanase named Psf1, classified within the GH107 family, was isolated from *Pseudoalteromonas* sp. S.1378 from the Arctic Ocean was employed to generate fucoidan fractions of varying molecular sizes from *S. latissima*. Subsequently, these fractions were examined for their immunomodulatory effects.

1.7.3 Sulfatases

Sulfatases play a significant role in modifying fucoidan and other sulfated marine-derived products, such as fucoidan, carrageenans, and GAGs. Many of the reported bioactivities of these compounds are attributed to their sulfate content and the positions of the sulfate groups [38,51,52]. Given the potential importance of sulfation for the bioactivity of such compounds, it is of great interest to enzymatically modify their sulfate content to control and investigate the bioactive properties. For this purpose, enzymes with sulfatase activity are particularly valuable in refining marine polysaccharides.

Sulfatases are categorized into four families designated S1-S4 according to SulfAtlas nomenclature (https://sulfatlas.sb-roscoff.fr/sulfatlas/, May 2024; [53]). Most sulfatases belong to the S1 family, also known as Type I or formylglycine (FGly)-dependent sulfatases [54,55]. The name is derived from the essential generation of a C_α-formylglycine residue in the pentameric core motif C/S-X-P-X-R within the active site,

located in the larger N-terminal domain. This FGly residue is generated via enzymatic posttranslational modification of the conserved C/S residue and is crucial for the catalytic activity of these enzymes [54,56,57]. Although more sulfatase families exist, only Type I sulfatases have been reported to be active on carbohydrates [54].

As seen for the GH enzymes described above, sulfatases are suggested to display either endo- or exo-activity. Endo-acting sulfatases cleave sulfate groups located along the poly- or oligosaccharide chain, while *exo*-sulfatases cleave sulfate groups from either the nonreducing or reducing end of substrate molecules. Moreover, a substantial collection of genomic data exists in the SulfAtlas database. However, despite the discovery of new enzymes and the extensive genomic data available, sulfatases remain largely underexplored in terms of substrate specificity and kinetic properties [57,58], and to our knowledge, they have not yet been implanted in enzymatic refining processes.

In this study, a novel sulfatase, SulA1, derived from the marine *Arthrobacter* strain MAT3885, was originally investigated to modify sulfation patterns of sulfated marine-derived polysaccharides. The aim was to explore how different sulfation patterns affect immunomodulation.

1.7.4 Alginate lyases

In contrast to the GH families that hydrolyze the glycosidic bonds, lyases cleave glycosidic bonds through a non-hydrolytic mechanism. This involves the elimination of a group (e.g., a carboxyl or hydroxyl group), typically resulting in the formation of a double bond or a new ring structure. Lyases are classified into different families based on the type of bond they cleave. Carbohydrate-active lyases are grouped into the polysaccharide lyases (PL) families (PL5, 6, 7, 14, 15, 17, and 18) in the CAZy database [59,60]. Alginate lyases depolymerize alginate via β-elimination mechanism. They cleave the glycosidic linkages between sugar monomers and leaving a 4-deoxy-L-erythro-hex-4-enopyranosyluronic acid at the non-reducing end [61]. These lyases are generally categorized into G- or M-lyases based on their preferences for cleaving either G- or M-rich alginate (Figure 3). However, most lyases exhibit some level of activity toward more than one type of the four glycosidic linkages present in alginates, MM, MG/GM, and GG, as reviewed in e.g., [62,63], making them interesting as they can break both α-and β-linkages. Like the previously described enzymes in this thesis, alginate lyases exhibit endo-or exo-acting activity. Endo-acting lyases cleave the alginate polymer internally, producing oligosaccharides, whereas exo-acting lyases cleave from the ends, resulting in unsaturated monomers, which are then converted into 4-deoxy-L-erythro-5-hexoseulose uronic acid (Figure 6; [62,63]), and enter the alternative glycolytic pathway, the Entner-Doudoroff pathway, for the catabolism of glucose to pyruvate.

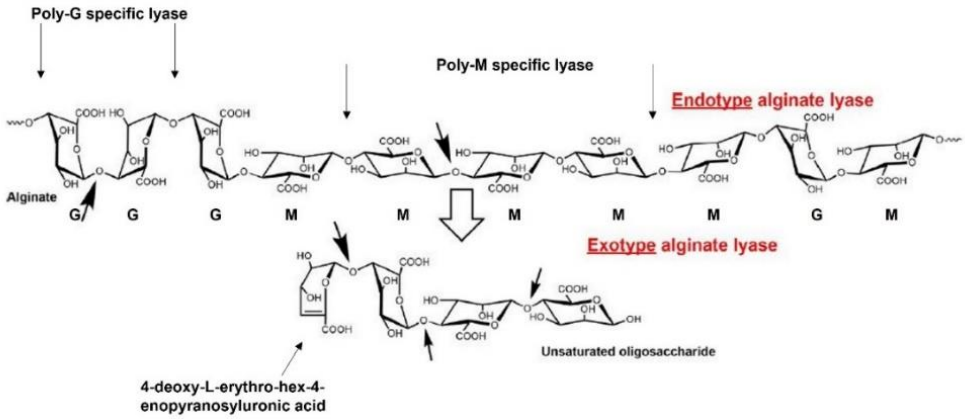

Figure 6: The degradation of alginate by endolytic (top) and exolytic (bottom) alginate lyases. The endolytic alginate lyase cleaves the internal linkages within the alginate polymer, forming a 4-deoxy-L-erythro-hex-4-enopyranosyluronic acid on the none-reducing end of the resulting unsaturated oligosaccharide (bottom). The exolytic alginate lyase cleaves terminal linkages, releasing unsaturated monosaccharides, which are then funneled into the Entner Doudoroff glycolytic pathway. In the top, the thin arrows indicate the cleavage sites for the correspond alginate lyases. M and G indicates the mannuronic and guluronic residues in the alginate polymer. The figure is modified from [61].

1.8 Immunomodulation

Immunomodulation refers to the adjustment or regulation of the immune response through various mechanisms or agents. This can involve enhancing the immune response to combat infections and cancers or suppressing it to prevent excessive inflammation and autoimmune diseases. Immunomodulatory therapies are pivotal in managing a wide range of medical conditions, from infectious diseases to chronic inflammatory disorders and cancers. Many marine-derived molecules have been shown to have immunomodulating effects, including the stimulation of both pro-inflammatory and anti-inflammatory responses, as well as having regulatory effects on the immune system.

1.8.1 Inflammation

One of the critical aspects of immunomodulation is its role in managing inflammation. Inflammation is a complex biological response triggered when the body encounters harmful insults such as pathogens and tissue damage. Its primary aim is to remove the injurious stimuli and initiate the healing process. The classic signs of acute inflammation are redness, swelling, heat, pain, and loss of function [64]. Acute inflammation typically involves four central elements: inflammatory inducers, sensors, mediators, and target tissue [64], leading to the activation of the innate immune system. The inducers include infectious agents, sterile tissue injury, hypoxia, and metabolic stressors. When an inducer affects the body, tissue-resident antigen-presenting cells (APCs), such as

macrophages and DCs, as well as endothelial cells, act as sensors. These sensors interact with the pathogen and damage associated molecule patterns (PAMPs and DAMPs) from the inducer via pathogen recognition receptors (PRRs) expressed on the innate immune cells. This interaction leads to the release of inflammatory mediators, such as cytokines, chemokines, eicosanoids, bioactive amines, and molecules from the proteolytic cascade. These mediators then act on target tissues, subsequently attracting more immune cells into the infection site [64].

Under normal circumstances, this process is resolved by a tightly organized cellular and molecular response to regain homeostasis [65]. However, failure to resolve the acute inflammation can result in its progression to chronic inflammation, which is involved in the pathogenesis of many prevalent diseases, such as cardiovascular diseases, atherosclerosis, rheumatoid arthritis, inflammatory bowel disease, and cancer [66]. Typically, if the innate immune system is unable to eliminate an intruder, the adaptive immune system is activated. Compared to the innate system, the adaptive system is highly specialized and takes longer to activate, but results in immunological memory. APCs, especially DCs, play a key role in initiating the adaptive immune response and are regarded as a link between the innate and adaptive immune systems.

1.8.2 Dendritic cells and their activation and differentiation of naïve T-cells

DCs are white blood cells belonging to the innate immunity. They are important for the immune system by being the primary APCs responsible for bridging the innate and adaptive immune system. They are easily recognized by their long dendrites, well-suited to their function as sentinels, scanning for danger signals through different tissues in the body [67,68]. The main role of DCs involves capturing, processing, and presenting their antigens to naïve T-cells.

DCs originate from hematopoietic stem cells in the bone marrow, where they undergo differentiation into various subsets, each with specialized functions and locations within the body. The main subsets include conventional DCs (cDCs), which are further divided into cDC1 and cDC2. These cells can be distinguished by their expression of specific surface molecules: CD141 expression by cDC1s and CD1c expression by cDC2s. Additionally, these two subsets activate different T-cells: cDC1s are involved in cross-presenting antigens to $CD8^+$ T-cells, while cDC2s are more involved in activating $CD4^+$ T-cells [69,70]. Besides cDCs, the body also contains monocyte-derived DCs (moDCs), plasmacytoid DCs, and Langerhans cells [69].

Immature DCs (imDCs) reside in tissues where they are on constant look-out for foreign or harmful molecules, upon encountering such molecules, in the form PAMPs or DAMPs, through PRRs such as the toll-like receptors (TLRs), C-type lectin receptors (CLRs), NOD-like receptors (NLRs), and others, the imDCs are activated and undergo phenotypic and functional changes, transitioning into their activated stage and become

mature DCs (mDCs; Figure 7). This maturation involves the upregulation of surface molecules vital for antigen presentation, such as major histocompatibility complex (MHC) molecules, as well as the co-stimulatory molecules CD80 and CD86 [68]. Subsequently, mDCs migrate to draining lymph nodes where they prime $CD4^+$ or $CD8^+$ naïve T-cells, steering them toward becoming effector cells, including T-helper cells (Th1, Th2 and Th17 subsets), T regulatory cells (Tregs), or cytotoxic T-cells [71,72]. The repertoire of cytokines secreted by the mDCs during this process is responsible for the different type of immune response and depends on the specific PAMPs or DAMPs encountered [67,68].

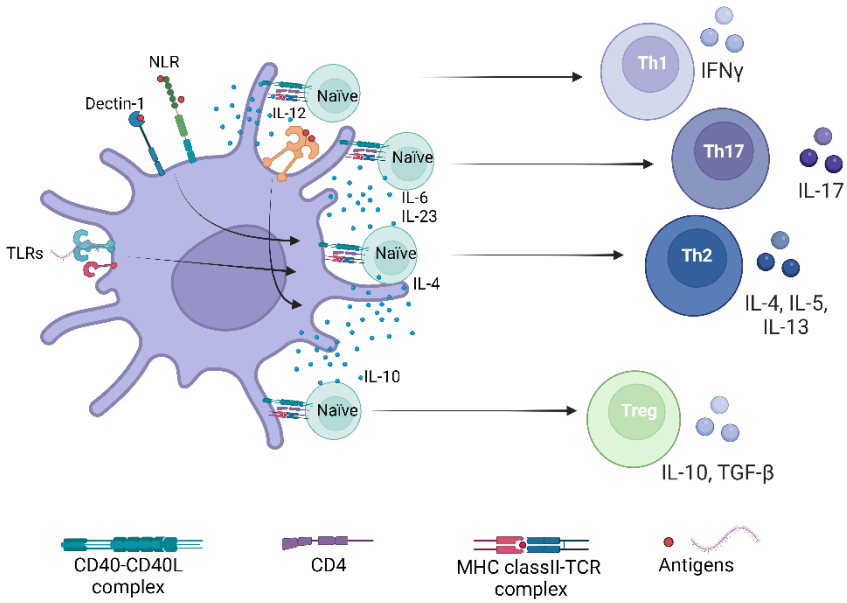

Figure 7: Dendritic cell differentiation and activation of naïve $CD4^+$ T-cells into Th subtypes by various cytokines.
The figure illustrates the differentiation and activation of naïve $CD4^+$ T-cells into Th subtypes mediated by cytokines (IL-12, IL-6, IL-23, and IL-10). It also specifies examples of pathogen recognition receptors (TLRs, dectin-1, and NLR) on the dendritic cell, blue dots indicating cytokine secretions. Note that IL-4 is not derived from dendritic cells. Inspiration gathered from [72,214]. Created with BioRender.com

1.8.3 T-cell subtypes

As described above, upon activation by DCs, naïve T-cells proliferate and differentiate into various effector T-cell subsets, each tailored to address specific types of pathogens or infected cells, depending on the molecules they express and cytokines they secrete.

Human Th1 cells are central to the type 1 immune response and are derived from interleukin (IL)-12 producing DCs [72], often in combination with interferon (IFN)γ secreted by non-DCs. These cells are induced in response to viral, protozoan, and

intracellular bacterial infections. Th1 cells are easily identified by their secretion of the cytokine IFN-γ (Figure 7) [71,72]. The release of this pro-inflammatory cytokine activates macrophages, making them more potent in phagocytosing and killing pathogens. Furthermore, Th1 cells ensure the activation of cytotoxic $CD8^+$ T-cells by producing IFN-γ and IL-2, which enhance antigen presentation and directly activate and stimulate $CD8^+$ T-cells, ensuring their proliferation, survival, and differentiation [74,75], leading to effective pathogen-killing capabilities. Moreover, IFN-γ can inhibit the differentiation and function of Th2 cells. Cross-regulation helps prevent the immune system from launching a mixed or inappropriate response, which could be inefficient or harmful [74].

Human Th2 cells are the main players of Type 2 immune responses and play a central protective role against extracellular parasites by secreting IL-4, IL-5, and IL-13 (Figure 7). Effective Th2 differentiation require the presence of IL-4, which is secreted by non-DCs and can directly or indirectly influence other cells, such as basophils and mast cells, to produce more IL-4. Furthermore, IL-4 and IL-5 secreted by Th2, and T follicular (Tfh)2 cells are crucial for antibody isotype class-switching to IgE in B cells [76]. IL-13 is important for the epithelia cell repair and mucus secretion, which accelerate the removal of parasite and increases mucosal smooth muscle activity [77]. Additionally, Th2-type responses are involved in many allergic disorders, atopic disorders and involved in transplantation tolerance [78].

The human Th17 subset, which is at the center of type 3 immune response, can be induced by the pro-inflammatory cytokines IL-6, IL-23, and IL-1β by DCs (Figure 7). Th17 cells, like Th1 cells, are easily distinguished from the other subtypes by their specific secretion of the key inflammatory cytokine IL-17 and are highly potent against extracellular fungi and bacteria. Through the secretion of IL-17 and IL-22, Th17 cells indirectly recruit neutrophils and other phagocytes to infection sites, while also inducing antimicrobial peptide production, which directly kills bacteria [79,80]. Additionally, Th17 cells have been implicated in numerous autoimmune diseases [81,82].

Tregs are induced by the presence of the anti-inflammatory cytokines IL-10 and/or transforming growth factor (TGF)-β. Unlike the previously mentioned Th cells, Tregs are responsible for maintaining immune balance, preventing autoimmunity, and modulating the immune response during various physiological and pathological conditions. They achieve this by secreting the same cytokines as induced their formation, i.e., IL-10 and/or TGF-β (as depicted in Figure 7). Elevated levels of IL-10 can lead to reduced expression of MHC- and co-stimulatory molecules on APCs, while also inhibiting the production of pro-inflammatory cytokines, such as IL-1, IL-6, tumor necrosis factor alpha (TNF-α), and IL-12 [83]. In contrast, TGF-β inhibits the proliferation of T-cells and B-cells, thereby controlling their activation and expansion [84]. Thus, the unique ability of Tregs

to suppress immune activity makes them a critical focus of research in immunology and a promising target for therapeutic interventions.

1.8.4 Evaluation of immunomodulating activities of marine-derived polysaccharides

Natural compounds, such as laminarin, fucoidan, alginate, and chondroitin sulfate, have all been explored for their ability to interact with the immune system (Table 1 below highlights some examples).

Pro-inflammatory responses induced by a natural compound refer to the process of activating an immune response through the interaction of PAMPs or DAMPs with different PRRs on immune cells. This interaction can lead to the production of pro-inflammatory mediators to combat the intruders. These pro-inflammatory mediators can be effectively measured through different techniques, and subsequently, the inflammatory response monitored. Inducing a pro-inflammatory response using natural compounds can have several beneficial applications in both research and therapeutic contexts. For instance, promoting a pro-inflammatory response can be beneficial in developing an anti-viral or anti-bacterial drug. These compounds can enhance the body's ability to fight infections by recruiting immune cells, such as macrophages, to the site of infection and activating their pathogen-fighting capabilities [85–90]. Moreover, using natural compounds as vaccine adjuvants to boost and enhance the immune response towards a specific antigen, or in the development of anti-cancer drugs to recruit immune cells to the tumor site and enhance the anti-tumor immune response, are also important research areas [91–93]. Additionally, inducing a pro-inflammatory response can promote the initial stages of wound healing by helping to clear debris and pathogens from the wound, which is a critical part of the healing process [94,95].

In contrast to pro-inflammatory effects, anti-inflammatory responses counteract inflammation with the primary goal of reducing its intensity and duration. This is crucial in preventing excessive or chronic inflammation that can result in severe tissue damage. The anti-inflammatory response typically involves the inhibition of pro-inflammatory mediators, such as cytokines (e.g., TNF-α, IL-6, and IL-12) and chemokines, while upregulating anti-inflammatory mediators, such as IL-10. This shift leads to suppressed immune cell activities, thereby controlling and limiting the inflammatory response during the active phase and restoring homeostasis [83,96,97].

Despite the significant knowledge gained through both *in vivo* and *in vitro* models (Table 1), there are contradictory data regarding whether the different marine polysaccharides harbor pro- or anti-inflammatory properties, especially in relation to seaweed-derived polysaccharides, such as laminarin. Moreover, many research papers are only investigating innate immune responses and often rely on cultured RAW 264.7 mouse macrophages [85–90] or rodent *in vivo* models [98–102], which may not

reflect what would occur in human immune cell models or during adaptive immune responses. Lastly, there is limited knowledge regarding which specific structures of the marine-derived polysaccharides are responsible for the immunomodulating activities reported.

Using DCs to investigate the possible immunomodulatory effect of marine-derived polysaccharides is a promising research area with significant potential to advance immunotherapy in cancer research, vaccine development, and the treatment of various inflammatory-mediated diseases [103–105]. Moreover, it allows researchers to explore the interaction between health-benefitting molecules and gain new insights into their underlying mechanism of action on the human immune system, as well as understanding the DCs biology, critical for designing strategies to modulate immune responses.

Table 1. Marine-derived polysaccharides and some of their documented activities.

Resource	Bioactivity	Type/research methods	Species	References
Laminarin	Anti-tumor	Apoptotic cell death of cancer cells	*Laminaria japonica*	[106,107]
	Anti-cancer immunity	*In vivo* C57BL/6 mice model *i.v* injected with laminarin	Not specified	[98]
	Anti-inflammation	*In vivo* Male Wistar rat LPS-induced model and Wistar rats ear edema model	*Laminaria digitata, Sargassum crassifolium*	[99,108]
	Immunomodulation	*In vitro* stimulation of RAW 264.7 mouse macrophages with laminarin - enhanced cytokine secretion and enhance the phagocytic activity	Not specified	[85]
	Wound healing	*In vivo* Wistar female rat wounds induction mode, topical application of laminarin-based creams	*Cystoseira barbata*	[109]
Fucoidan	Anti-tumor /Anti-cancer immunity	*in vitro* models with human microvascular endothelial cells – tube formation and migration assays, human prostate cancer cells – viability, proliferation, migration, and tube formation assays.	*Undaria pinnatifida, Laminaria angustata, Fucus vesiculosus, Fucus evanescens, Sargassum fusiforme*	[110–114]

		Mouse breast cancer cells – apoptosis and VEGF expression analysis. *In vivo* Athymic nude mice xenograft model with DU-145 prostate cancer cells. BALB/c mice xenograft models with 4T1 breast cancer cells and A549 lung cancer cells.		
	Anti-inflammation	Acute peritonitis rat model and Wistar rats ear edema model	*Saccharina latissima, Laminaria digitata, Cladosiphon okamuranus, Fucus evanescens, Fucus vesiculosus, Fucus serratus, Fucus distichus, Fucus spiralis, Ascophyllum nodosum, Sargassum vulgare*	[100,101]
	Immunomodulation	RAW264.7 murine macrophages, enhanced cytokine secretion and enhance the phagocytic activity	*Ascophyllum nodosum, Laminaria japonica*	[86,87]
	Anti-allergy	BALB/c mice models and mast cell line (RBL-2H3 cells)	*Sargassum graminifolium Squatina japonica*	[115,116]
	Wound healing	Promoting angiogenesis, granulation formation and collagen deposition	Not specified	[117,118]
Alginate	Anti-tumor	C57BL/6 mice melanoma model - Enhances Memory Properties of Antitumor CD8+	Not specified	[119,120]

		T cells B16-OVA Cancer Model - Serve as a carrier and adjuvant for immunotherapy		
	Immunomodulation	RAW264.7 murine macrophages, enhanced cytokine secretion and enhance the phagocytic activity Induced pro-inflammatory cytokine release from monocyte derived DCs	Not specified	[88–90]
	Wound healing	Diabetic wound model in Sprague-Dawley rats	*Laminaria hyperborea*	[102]
Chondroitin sulfate	Anti-inflammation	*In vitro* mouse-bone-marrow-derived macrophages model: NO inhibitory activity and decrease pro-inflammatory cytokines and increase IL-10 level *In vitro* chondrocytes model: Inhibition of NF-κB pathway Murine splenocyte model: Increase Th1 responses	Chondroitin sulfate from shark cartilage and from bovine trachea Not specified	[121,122]
	Immunomodulation	Experimental autoimmune encephalomyelitis mouse model: Induced IFN-γ production and Th1 CD4 T cell differentiation and up-regulated STAT3 and IL-23 expression and thus increased IL-17 producing T cells	Chondroitin sulfate from bovine tracheal cartilage Chondroitin sulfate A (source not specified)	[123,124]
	Wound healing	*In vivo* full thickness infected skin defect mouse model	Hydrogel with chondroitin sulfate	[125]

2 Aims

The main objective of this project was to identify and characterize the structural complexity and functional diversity of marine-derived polysaccharides and their role in immunomodulation by employing an enzymatic refinement approach to modify and potentially alter immunomodulating activities. The immunomodulating activities were assessed using a human monocyte-derived dendritic cell model.

Specific aims:

1. To characterize in detail a newly identified marine-derived sulfatase's enzymatic activity and substrate specificity.
2. To refine laminarin from three species of brown seaweed.
3. To assess the immunomodulating potential of laminarin and enzymatically modified laminarin structures purified from the three species of brown seaweed.
4. To study the immunomodulating potential of various molecular-sized fucoidan fractions.
5. To investigate the immunomodulating potential of enzymatically produced alginate derivatives.

3 Materials and Methods

3.1 Production of recombinant enzymes

This thesis describes the cloning and expression of two enzymes in *Escherichia coli* (*E. coli*), a novel sulfatase designated the name SulA1 derived from a marine *Arthrobacter* strain (Paper I), and a previously described laminaripentaose-producing endo-1,3−*β*-glucanase (LPHase) from *Streptomyces matensis* DIC-108 [47] (Paper II).

3.1.1 Cloning of the sulfatase gene *sulA1* (Paper I)

The *sulA1* gene from the marine *Arthrobacter* strain (MAT3885) was amplified via PCR using forward primer, SulA1-Nde-f (5′-CGAATTCCATATGGTCAGCTCGTCCCCTGCG-3′), targeting the 5′ end of the orf including the deduced ATG start codon and the reverse primer, SulA1- BamHI-r-his (5′-CGCGGATCCGATTCCATCCCAGTTCGGCG-3′), targeting the 3′ end of the orf excluding the stop codon. The PCR product was digested with *Nde*I and *Bam*HI and ligated into *Nde*I- and *Bam*HI-digested pJOE3075 vector. The resulting plasmid with *sulA1* was designated pVK13. As the reverse primer did not include a stop codon, the sulA1 gene was cloned upstream of and in frame with 6 × 3′ histidine codons. *E. coli* BL21(C43) was transformed with the expression vector containing the inserted gene by electroporation [126]. The transformed cells were screened for the *sulA1* gene by performing PCR using the above-described primers. Correct sequence and fusion in the plasmid were verified with sequence analysis.

3.1.2 Production, purification, and storage of the SulA1 (Paper I)

The *E. coli* BL21(C43) strain transformed with pVK13 was inoculated in LB broth containing ampicillin (100 µg/mL) overnight at 37°C. The overnight culture was diluted in fresh LB-amp broth (1:100) and cultivated at 37°C and 200 rpm until an OD_{600} between 0.7 and 0.9 was reached. Gene expression was induced with 10% (w/v) L-rhamnose (final concentration of 0.1%). The culture was then grown overnight at room temperature. Cells were harvested via centrifugation (3400 × g for 10 min at 4°C) and resuspended in a lysis buffer (1.2 mL; 50 mM sodium citrate, pH 6, 150 mM NaCl, 15% glycerol) and further disrupted via sonication. The cells were kept on ice and centrifugated at 16,000× g for 30 min at 4°C to separate the supernatant from the insoluble debris. Thereafter, SulA1 was purified using PureCube His Affinity MagBeads (Cube Biotech; https://cube-biotech.com/solubilization-database (accessed on 2 February 2024), Monheim, Germany) using the protocol provided by the manufacturer. In brief, protein purifications were made with PureCube 100 INDOGO Ni-MagBeads, using the recommended lysis, wash, and elution buffers. Lysis, binding, and elution

buffers consisted of 50 mM NaH_2PO_4 and 300 mM NaCl (pH 8.0) with varying concentrations of imidazole (10, 20, and 500 mM, respectively). After purification, the elution buffer was exchanged with 100 mM acetate buffer pH 5.5 using Amicon Ultra-0.5 centrifugal filter unit with a 30 K cut-off (Merck Millipore). The expression level and purification of SulA1 were verified with SDS-PAGE, as described in section 3.5.1

3.1.3 Cloning and expression of recombinant LPHase (Paper II)

The LPHase (376 amino acids) was obtained from *Streptomyces matensis* DIC-108 and extended with maltose-binding protein domain (MalE) to confer solubility as follows. The encoding gene was amplified using the forward primer f(CCATCGTGAACAGATTGGTGGCGCCGCCGTTCCAGCGACCATTC) and the reverse primer r(TTAATGATGATGATGATGATGG*GATCC*ATCGAACGGGTCCAGAGTCAG). The expression vector pHWG1106 [127] was linearized with *Kas*I and *Bam*HI and subsequently, the gene was inserted into the vector using the NEBuilder® HiFi DNA Assembly Cloning Kit (New England Biolabs Inc.). The resulting plasmid, pHG247, was introduced into *E. coli* NEB10 beta competent cells by transformation. Expression was achieved by cultivating pHG247/NEB10 in 30 mL LB broth supplemented with ampicillin (100 µg/ml) at 37°C until reaching OD_{600} 0.7. The culture was then moved to room temperature and allowed to grow until reaching OD_{600} of approximately 0.9. Gene expression, cell harvesting, cell disruption, and supernatant collection were achieved in a similar manner as described above. The expression level of LPHase was verified with SDS-PAGE, as described in section 3.5.1.

3.1.4 Total protein content and protein distribution

To determine the protein concentration of purified SulA1, the Bradford method [128] was used. Dilutions of 1/3, 1/6, and 1/10 were made of the purified SulA1 solution using 100 mM acetate buffer, pH 5.5. As standard, BSA was used, ranging from 0-2.00 mg/mL. Five µl of samples/standards were pipetted into Flat-bottom 96-well plates (Thermo Scientific) together with 250 µl Bradford Reagent (Sigma). The plate was incubated for 15 min in the dark at room temperature. Absorbance was measured at 595 nm using a BioTek Epoch microplate reader coupled to the Gen5 software (BioTek). Protein concentrations were determined by subtracting blank measurements from the absorbances. Then the data from the BSA standard measurements were plotted, and an equation for the standard curve was determined with linear regression. The equation derived from the standard curve was then used to calculate the protein concentration of the different dilutions of purified SulA1, based on the absorbance values.

3.2 Bioinformatic analysis for SulA1 (Paper I)

Several bioinformatic methods were used to predict and gain valuable information regarding SulA1 (Table 2), including determining whether it acts intracellularly or extracellularly, identifying structurally conserved regions and functional motifs within the protein sequence, gaps, and variations with other identified FGly-dependent sulfatases, as specified in Paper I.

Table 2. List of bioinformatic programs.

Program	Application
SignalP v5.0 (https://services.healthtech.dtu.dk/services/SignalP-5.0/ (accessed 2024-01-25))	Identification of signal peptides in the aa* sequence
BLASTp against PDP database (NCBI) (https://blast.ncbi.nlm.nih.gov/Blast.cgi?PAGE=Proteins (accessed 2024-02-18))	Structure similarities with structure determine sulfatases
Interpro (https://www.ebi.ac.uk/interpro/ (accessed on 2024-01-25))	Domain annotations and functional prediction
Clustal Omega Multiple Sequence Alignment tool (https://www.ebi.ac.uk/ (accessed on 2024-01-25))	Multiple sequence alignment, with 3D-structural identified FGly-SULFs aa Multiple sequence alignment, with identified CS/Dermantan sulfate sulfatases and SulA2 found with tin the chondroitin lyase cluster
SulfAtlas database (https://sulfatlas.sb-roscoff.fr/ (accessed on 2024-02-18))	Consulted to confirm the novelty of SulA1

*aa = amino acid

3.3 Structure modeling using YASARA and AlphaFold2 (Paper I)

Two approaches were followed: a homology-based structural modeling using YASARA and structural prediction using AlphaFold2, to obtain structural-function information of SulA1. Table 3 and Table 4 summarize the programs used to obtain the 3D-structures and information concerning substrate specificity and enzyme-ligand interaction. The specifics can be found in Paper I.

Table 3. List of programs used for structure modeling of SulA1.

Program	Application
Protein Data Bank (PDB)	Matching SulA1 aa* sequence with five best matching 3D-structural identified sulfatases
YASARA Software [129]	Structural 3D-modeling of SulA1 Docking of the enzyme with the different sulfated sugars, Gal4S, GalNAc4S, and GalNAc6S
AlphaFold2 [130] colab.research.google.com/github/sokrypton/ColabFold/blob/main/AlphaFold2.ipynb (accessed on 2024-02-02)	Structural prediction of SulA1
PyMOL v2.5.4 program [130,131]	Illustration of the 3D model and docking
LigPlot+ [132]	The enzyme–ligand interaction

*aa = amino acid

Table 4: Crystallographic structures used as templates for 3D-modeling of SulA1 in YASARA.

Template (PDB Code)	Source	Sequence Coverage (%)	Amino Acid Sequence Identity (%)	Transferred Region to the Model (Residue Numbering)
5G2V	*Bacteroides thetaiotaomicron* VPI-5482	76	32.09	1–459
6B0K	*Pseudoalteromonas* sp.	89	27.27	168–180, 435–483
2QZU	*Bacteroides fragilis* YCH46	90	24.79	1–9, 283–282, 433–441
6BIA	*Pseudoalteromonas fuliginea*	90	27.20	452–484
6UST	*Hungatella hathewayi*	94	30.60	86–89

3.4 Activity test for SulA1 characterization

To investigate the sulfatase activity, a standard assay based on the synthetic substrate *p*-nitrocatechol sulfate (*p*NCS) dipotassium salt was used. This type of assay was used to investigate the temperature and pH optimum, thermal deactivation, storage capacity, and cations and Ethylenediaminetetraacetic acid (EDTA)s effect on the sulfatase activity as elaborated in paper I.

3.4.1 *p*-nitrocatechol sulfate (*p*NCS) assay

In short, 5 µL SulA1 enzyme extract (~1.10 mg/ml) was mixed with 20 µL 6.5 mM *p*NCS, 10 µL 100 mM acetate buffer, pH 5.5, and 15 µL water, and the reaction was carried out at 40°C for 30 min. The reaction was stopped by adding 100 µL 1 M NaOH. The activity was determined spectrophotometrically at 515 nm.

3.4.2 Differential scanning fluorimetry (DSF)

The DSF assay was used to investigate the thermal stability of SulA1 under various pH, $CaCl_2$, and EDTA conditions, conducted with the Prometheus NT 48 nanoDSF instrument (NanoTemper Technologies, GmbH) by determining the melting temperature (T_m), as described in Paper I.

In short, the assay utilizes the ability to measure changes in the protein's intrinsic fluorescence intensity as a function of temperature under various conditions. When the protein of interest unfolds with increasing temperature, the exposure of tryptophan residues, which are often buried in the hydrophobic core of the protein, to different surroundings leads to changes in fluorescence, allowing the detection of the protein's thermal stability. For each experiment, 10 µL of protein sample (SulA1) was prepared under various conditions (different pH, different $CaCl_2$, or different EDTA concentrations) and loaded in the instrument capillaries. Under each experiment, the sample was subjected to a temperature ramp from 20°C to 90°C, with a gradual increase of 1°C per min. To monitor the unfolding of the protein intrinsic fluorescence at emission, wavelengths of 330 and 350 nm were used. This allows the identification of the T_m, which represents the temperature at which 50% of the protein population is unfolded.

3.4.3 SulA1 activity assay against natural substrates

Different sulfated mono-, di-, and oligosaccharides were tested as substrates for SulA1 (Table 5). In short, the natural compound of interest was mixed with 15 µL 1/3 diluted pure SulA1 (1.1 mg/mL; 0.0165 mg in reaction), 10 µL 100 mM acetate buffer, pH 5.5, and 5 µL Milli-Q water. Enzyme activity was assayed after 30 min, at 40°C. As controls, for each reaction, 20 µL of the substrate was mixed with 10 µL of 100 mM acetate buffer pH 5.5 and 20 µL of ultrapure water (Milli-Q grade, hereafter referred to as Milli-

Q water) without the addition of SulA1. To verify the activity of SulA1 on the different substrates, thin-layer chromatography (TLC) was generated (Section 3.5.2).

Moreover, the kinetic parameters of SulA1 were estimated by quantifying the amount of *N*-Acetyl-D-galactosamine (GalNAc) formed after 30 min of incubation at 40°C with different molarities (0–20 mM) of GalNAc4S, using purified SulA1 (16.5 µg). Similarly, specific activity was determined by quantifying the amount of GalNAc formed after 30 min incubation at 40°C using 20 mM GalNAc4S, with purified SulA1 (16.5 µg). The reactions were analyzed using high-performance anion exchange chromatography with pulsed amperometric detection (HPAEC-PAD), using a PA-20 column for the quantification of the substrate and product. Both the column and compartments were maintained at a constant temperature of 30°C. The eluents, 200 mM sodium hydroxide (5%) and MilliQ water (95.0%); were used to equilibrate the system. The samples were eluted after injection under the same conditions for 14 min.

Table 5. Natural substrate used to investigate SulA1 activity.

Substrate	Manufacturer
Chondroitin sulfate AC dp4 (contain both 4S and 6S)	Iduron
Chondroitin without sulfation (Δdi0S)	Dextra laboratories Ltd
Chondroitin sulfate (Δdi4S)	Dextra laboratories Ltd
Chondroitin sulfate (Δdi6S)	Dextra laboratories Ltd
N-Acetyl-D-galactosamine-4-sulfate (GalNAc4S)	Dextra laboratories Ltd
N-Acetyl-D-galactosamine-6-sulfate (GalNAc6S)	Dextra laboratories Ltd
Heparin disaccharide I-H	Sigma-Aldrich
N-Acetyl-D-glucosamine-6-sulfate (GlcNac-6S)	Sigma-Aldrich
D-galactose-4-sulfate (Gal-4S)	Sigma-Aldrich
Neocarrabiose-4-*O*-sulfate	Dextra laboratories Ltd
Neocarratetraose-41,43-di-*O*-sulfate	Dextra laboratories Ltd
L-fucose from Chorda filum cut-off <10 kDa Fuc310)	ProSea
Fucoidan	ProSea

3.4.4 Peptide mass fingerprinting (PMF) of SulA1

The primary purpose of this approach was to validate the amino acid sequence of the purified SulA1 and the conformation of its identity. Moreover, combining the PMF with tamed mass spectrometry (MS/MS) analysis, it is possible to reveal post-translational modifications present in the protein of interest, such as phosphorylation, glycosylation, or acetylation. In this case, we attempted to confirm the post-translationally modification of the formyl glycine residue, necessary for the activity of SulA1. Shortly, PMS was performed using ESI-Orbitrap MS/MS and MASCOT [133] to validate the amino acid sequence of the purified SulA1. Then gel fragment with the correct molecular weight (51.9 kDa) was cut from a sodium dodecyl-sulfate polyacrylamide gel electrophoresis (SDS-PAGE) and digested with trypsin in-gel [134]. After in-gel digestion, peptide fragments were determined using MS/MS analysis and compared with the deduced amino acid sequence.

3.4.5 Statistical analysis of sulfatase activity (Paper I)

Sulfatase activity tests and DFS data are presented as mean values ± standard deviation (SD) from triplicate experiments. The specific activity experiment was completed in duplicate and is displayed as mean ± SD.

3.5 Common analysis used in Paper I and Paper II

3.5.1 Sodium dodecyl-sulfate polyacrylamide gel electrophoresis (SDS-PAGE)

SDS-PAGE was used to check the protein expression of both SulA1 and LPHase, using Mini-PROTEAN® TGX Stain-Free™ Precast Gels (4-20%, 15-well; Bio-Rad), in Tris-glycine-SDS (TGS) running buffer. Briefly, samples of interest were mixed with 4 x SDS-loading buffer (Merck) and heated for 5 min at 95°C to denature the proteins. An equal amount of sample was loaded onto the gel together with Precision Plus Protein Unstained Standard (10-250 kD; Bio-Rad). The settings were 200 V for 45 min, and the stain-free gel images were generated using Stain-Free Image Lab software (Bio-Rad) for protein gels application.

3.5.2 Thin-Layer Chromatography (TLC)

TLC was applied in the studies, including the SulA1 (paper I) and laminarin (paper II) research. For the SulA1 study, TLC was used to verify the activity of SulA1 on natural substances, where 2 µL of each reaction were taken and spotted near the bottom of the TLC Silica gel 60 F_{254} (10 × 20; Merck). Similarly, TLC was applied in the laminarin study for a comprehensive assessment of laminari-oligosaccharides distribution and approximate sizes. After LPHase digestion, 0.8 µL or 2 µL samples, containing the laminari-oligosaccharide fractions from one of three seaweed species, were spotted

near the bottom of the TLC Silica gel 60 F_{254} plate. The mobile phase was the same in both studies and consisted of a mixture of 1-butanol, acetic acid, and Milli-Q water (2:1:1). The running time was 1.5 h. Afterwards, the TLC plate was dried. The developing solutions, however, were different in the two studies. For SulA1 study, the developing solution consisted of diphenylamine–aniline–phosphoric acid in acetone in accordance with the published procedure [135]. While for the laminarin study, the detection solution was the orcinol reagent (100 mg orcinol in 95 mL methanol and 5 mL sulfuric acid). As the last step, the plates were dried and heated at 120°C, using the TLC Plate Heater III (CAMAG®) until bands became visible.

3.6 Seaweed refining

3.6.1 Biomass for laminarin experiments

Dried biomass from *S. latissima* was kindly provided by Annette Bruhn from the Department of Bioscience at Aarhus University, AlgeCenter Danmark. Similarly, dried biomass of *L. digitata* and *L. hyperborea* was provided by Íslensk Bláskel og Sjávargróður, Stykkishólmur, Iceland. All biomasses were harvested during summer, when laminarin yield is anticipated to be highest. Purified laminarin from *L. digitata* (harvested in Iceland) was obtained from Merck (Lot #SLCG6449).

3.6.2 Biomass for fucoidan experiments

S. latissima seaweed was kindly provided by Ocean Rainforest (Faroe Islands).

3.6.3 Biomass for alginate experiments

Alginic acid sodium salt derived from the brown seaweed *Macrocystis pyrifera* was obtained from Sigma (Lot 76H0592).

3.7 Laminarin refinement process

3.7.1 Laminarin extractions, filtration, and purification

A sustainable and gentle two-step water extraction protocol was used to extract laminarin from *L. digitata*, *L. hyperborea*, and *S. latissima*. First, the dried biomasses were milled into fine powder using the redesigned IKA® A10 basic batch mill (Staufen, Germany). To extract the crude laminarin, 100 g of the seaweed powder was mixed with 1.5 L of distilled water. Initially, extraction occurred at 30°C for 2 hours at 75 rpm, after which the temperature was increased to 70°C and the extraction continued for 3 hours under continuous shaking. The resulting extracts were cooled down at 4°C overnight. The seaweed pellets and the extracts were separated by centrifugation at ~12,000 g for 20 min, and the supernatants (soluble extracts) were collected. To maximize extraction yield, the pellets were recentrifuged (~12,000 g for 20 min).

To remove traces of alginate, the extracts underwent alginate precipitation, using 1% $CaCl_2$ at 4°C overnight, whereafter the alginate was removed from the extracts by centrifugation at ~12,000 g for 20 min. For further refinement, laminarin extracts underwent filtration and dialysis, using the Cogent®10 M1 tangential flow filtration (TFF) system (Merck Millipore, Darmstadt, Germany) equipped with 10 kDa filters to improve the quality of the laminarins, and further purified via dialysis on the TFF-system using 1 kDa filters. The laminarin extracts were lyophilized and stored at -20°C until further use (Figure 8).

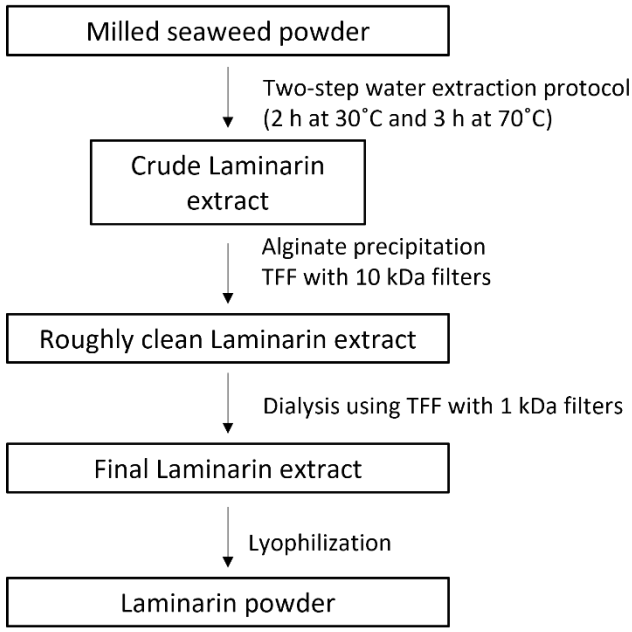

Figure 8: Flow chart of the two-step water extraction protocol of laminarin.

3.7.2 Separation of *L. hyperborea* derived laminarin and fucoidan polysaccharides by Anion-Exchange Chromatography

To remove fucoidan from the laminarin extracted derived from *L. hyperborea*, additional purification was necessary. A laminarin sample of 10 mg/mL was dissolved in 1 mL of distilled water and loaded onto a DEAE-cellulose (Sigma-Aldrich) column (1 x 20 cm), which was pre-equilibrated with distilled water. The fractions containing laminarin were eluted with water and afterwards lyophilized. The sulfated fucoidan was remaining in the column and was removed from the column using 1 M ammonium bicarbonate buffer.

3.7.3 Preparation of laminarin oligosaccharide by enzymatic hydrolysis

To obtain laminari-oligosaccharide fractions with different branching and DP range, laminarin from the three species was hydrolyzed using the laminaripentaose-producing

endo-1,3–β-glucanase, LPHase (Section 3.1.3). The hydrolysis was carried out at 50°C and pH 5.7, the conditions optimized for LPHase activity. Concurrently, dialysis was conducted to separate the laminari-oligosaccharides from the substrate. The procedure was as follows: A 4% (*w/v*) solution of lyophilized laminarin from *L. digitata*, *L. hyperborea*, or *S. latissima* was prepared by mixing the powder with 50 mL 20 mM sodium citrate buffer (pH 5.7). The laminarin solutions were mixed with 200 µl of the LPHase crude extract, corresponding to approximately 1.2 mg per reaction. The prepared mixtures were transferred into Slide-A-Lyzer® 3.5K Dialysis cassettes (Thermo Scientific) and placed within 1 L beakers. The beakers were filled to the 550 mL mark with a 20 mM sodium citrate buffer (pH 5.7) and securely covered with food film and aluminum foil to prevent potential evaporation. The sealed beakers were incubated in a 50°C heating cabinet for two days, with manual shaking 4-5 times daily throughout the incubation period. Upon completion of the incubation, the surrounding buffer, containing the targeted oligosaccharides, was collected for each reaction, frozen, and subsequently lyophilized to yield the desired product (Figure 9).

3.7.4 Laminari-oligosaccharide purification using size exclusion chromatography (SEC)

To purify the laminari-oligosaccharides mixtures, 12% (*w/v*) solutions of lyophilized laminari-oligosaccharide mixtures were prepared by mixing the extracted laminarins with Milli-Q water. The solutions were filtered through non-sterile Phenex RC membrane filters (0.45 µm, 26 mm, Phenomenex). The purification process of the laminari-oligosaccharide mixtures was executed using an ÄKTA system with a size exclusion Superdex™ 30 HiLoad 26/600 column (Cytiva). To establish optimal conditions, the column was equilibrated with low ionic strength buffer (50 mM NaCl) and the running buffer was in this case degassed Milli-Q water. A total of 12 mL of the 12% oligosaccharide solution plus an additional 5 mL of Milli-Q water was loaded onto the column. The separation was initiated by allowing 0.37 column volume to flow into 50 mL tubes, utilizing the running buffer at a 2 mL/min flow rate. Subsequently, 1.7 mL fractions of laminari-oligosaccharide mixtures were collected in a 2.2 mL V-shaped 96 squared deep well microplate (4titude, Azenta Life Science) using a flow rate of 2 mL/min. The laminari-oligosaccharide size-distribution was analyzed using TLC (Section 3.5.2), where from distinct oligosaccharide fractions were carefully collected, subjected to lyophilization, and thereafter stored at –20°C for future utilization.

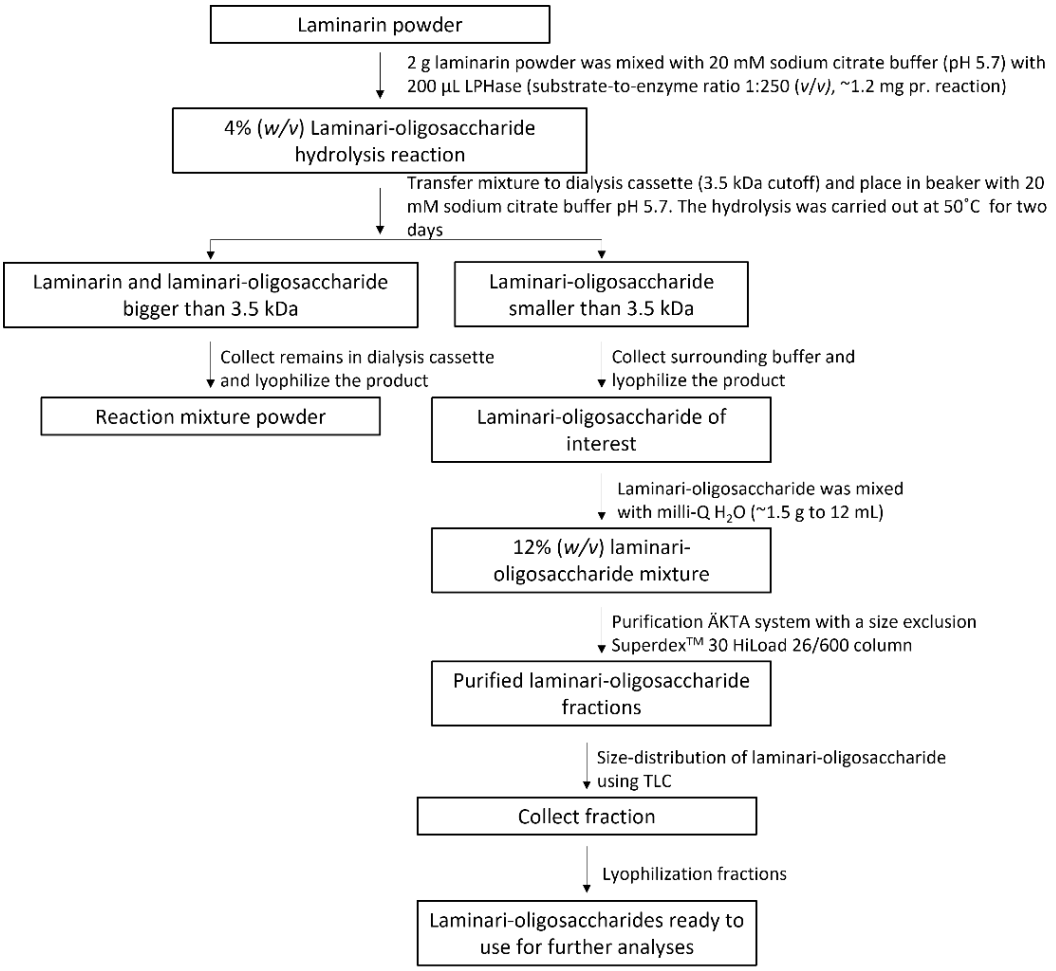

Figure 9: Flow chart of laminari-oligosaccharide fraction generation.

3.7.5 Ash content

To determine the ash content in the laminarin extracts, the lyophilized laminarin samples were subjected to combustion at a high temperature of 550°C for 10 hours [137]. During this process, organic materials in the sample combust and are oxidized, leaving behind the inorganic residue or ash. After cooling, the samples were collected, weighed, and recorded. The analyses were done in duplicates, and data were expressed as % *dw*.

3.7.6 High-performance anion-exchange chromatography with pulsed amperometric detection (HPAEC-PAD)

HPAEC-PAD was applied for carbohydrate composition analysis and laminarin profiling derived from *L. digitata*, *L. hyperborea*, and *S. latissima*. Laminarin samples were

prepared using a two-step sulfuric acid hydrolysis, adjusted for algal biomass [138], as described in Paper II. The HPAEC-PAD system was equipped with a Dionex CarboPac PA-20 analytical column and a corresponding guard column (Thermo Fisher Scientific) for monosaccharide separation. The separation of monosaccharides and uronic acid was performed under isocratic conditions at a flow rate of 0.5 mL/min. Eluents for separation of monosaccharides and mannitol were (A) MilliQ-water, (B) 2 mM NaOH, and (C) 200 mM NaOH. Separation was done using an eluent mixture of 62.5% (A) and 37.5% (B) for 30 min. To investigate the presence of uronic acids, eluent (B) was 1 M sodium acetate in 200 mM NaOH, while eluent (A) and (C) were the same as for monosaccharide separation. The uronic acids were eluted by an eluent mixture of 55% (A), 15% (B), and 30% (C) for 18 min. The column and compartment temperature were kept at 30°C. All the experiments were performed in duplicate, and the mean value and SD were calculated. Total carbohydrates were estimated as the sum of all individual monomeric sugars.

Similarly, laminarin profiles of same species were generated using HPAEC-PAD equipped with a Dionex CarboPac PA-200 analytical column (Thermo Fisher Scientific) and a corresponding guard column. The dried extracts were dissolved in Milli-Q water and filtered through the PTFE 0.2 µm syringe filter (Pall). Eluents were (A) Milli-Q water, (B) 1 M sodium acetate in 200 mM sodium hydroxide, and (C) 200 mM sodium hydroxide. Oligosaccharides were separated at a flow rate of 0.5 mL/min by a linear gradient from zero to 50% (B) in (C) while eluent (A) was kept at 50% for 20 min.

3.7.7 Fourier transform infrared spectrometry (FT-IR) analysis

FT-IR was applied to obtain valuable information regarding the molecular structure and purity of the extracted laminarins from the three different species of brown seaweed (*L. digitata*, *L. hyperborea*, and *S. latissima*), including the identification of functional groups characteristic for laminarin, structural variation, and validation of the extraction protocol. The procedure was as follows: Freeze-dried laminarin was analyzed to identify its functional groups using an FT-IR spectrometer (Nicolet iS5, Thermo Scientific) with a spectral range of 400−4000 cm^{-1}.

3.7.8 ^{1}H Nuclear Magnetic Resonance (^{1}H-NMR)

To achieve comprehensive structural characterization and assess the purity of laminarin and laminari-oligosaccharides, both 1D (One-Dimensional NMR) and 2D (Two-Dimensional NMR) NMR spectra were recorded using a 600 MHz Bruker Avance Neo NMR spectrometer equipped with a 5mm TCI Prodigy CryoProbe (Bruker). 1D NMR provided information about individual proton resonances, enabling the assignment of chemical shifts to different functional groups and anomeric carbons. Additionally, coupling constants obtained from 1D spectra helped determine the connectivity between adjacent atoms, allowing us to identify the glycosidic linkage types (e.g., α or β) in laminarin and laminari-oligosaccharide fractions. In contrast, 2D NMR techniques

were employed to analyze the spatial proximity of nuclei, providing insight into molecular conformation and intra-molecular interactions. By examining cross-peaks in 2D NMR spectra, interactions between protons were elucidated, further supporting structural assignments. To resolve signal overlap observed in the 1D spectrum, Heteronuclear Single Quantum Coherence (HSQC) spectroscopy was utilized. HSQC enabled direct carbon-proton correlation, improving the accuracy of chemical shift assignments, especially in crowded spectral regions where overlapping signals complicated analysis. The following protocol was used: Samples were dissolved in D_2O (0.5 ml, 99.9%; Cambridge Isotope Laboratories) and transferred to 5 mm NMR tubes. All spectra were recorded using standard Bruker pulse programs with water suppression. Chemical shifts were reported in parts per million (ppm) relative to the solvent HOD signal (4.84 ppm for ^{1}H-NMR, 292K). Data were processed using TopSpin™ software (Bruker).

3.7.9 Matrix-Assisted Laser Desorption/Ionization Time-of-Flight Mass Spectrometry (MALDI-TOF MS)

MALDI-TOF MS was utilized to elucidate the molecular weight distribution of the laminarins and laminari-oligosaccharide fractions, focusing on their DP. Analysis of the mass spectra of each laminarin sample facilitated the estimation of the DP range and identification of the dominant peak, representing the most prevalent polymer within the laminarin samples. Similarly, the DP range of each laminari-oligosaccharide fraction was investigated. The experiments were conducted using a Bruker ultrafleXtreme (Bruker Daltonics) mass spectrometer in reflector positive-ion mode, with a mass acquisition range of 200–6000 Da. Sample preparation involved mixing 0.5 µL of sample solutions with 0.5 µL of aqueous 10% 2,5-dihydroxybenzoic acid as the matrix solution.

3.7.10 Statistical analysis of composition data (paper II)

Composition analysis data in Paper II, including Total Polyphenol Content (TPC; n = 3), ash content (n = 2) and monosaccharides composition analysis (n = 2), are data expressed as mean values ± SD.

3.8 Fucoidan refinement process

3.8.1 Enzyme-assisted extractions of fucoidan and purification (published by Nguyen et al. 2020)

Fucoidan was extracted from *S. latissima* using an enzyme-assisted extraction protocol, as described by Nguyen and colleagues 2020. Since the detailed methodology is beyond the scope of this thesis, only a brief summary is provided here. The extraction involved a one-step enzyme-assisted process using a combination of a commercial

cellulase preparation (Cellic®CTec2, Novozymes Bagsværd, Denmark, known to catalyze depolymerization of cellulose and laminarin) and an alginate lyase from *Sphingomonas* sp. (SALy), which was purified from an *E. coli* expression system by DTU. This combination ensured the degradation of the seaweed glucans, e.g., cellulose and laminarin, and alginate [139]. The enzymatic extraction was performed by mixing dried, milled seaweed with 55 mM phosphate—38 mM citrate buffer pH 6 (5% *w/v* substrate concentration) along with 5% (*v/w*) cellulase and 0.35% (*w/w*) alginate lyase (DTU production). The mixture was incubated at 40°C for 24 hours on a horizontal mixer at 100 rpm. To terminate the reaction, the mixture was heated to 90°C for 10 min and then cooled on ice. The supernatant, containing the fucoidan, was collected after removal of insoluble residues by centrifugation at 10,000 g for 10 min and subjected to 2% $CaCl_2$ precipitation to remove the alginate. The crude fucoidan was then isolated from the supernatant by ethanol precipitation (72%), recovered by centrifugation at 10,000 g for 30 min, and lyophilized.

To further purify the crude fucoidan, it was dissolved in aqueous solution (5 g in 100 mL) and applied to an anion exchange-column (2.6 cm × 40 cm), manually packed with DEAE-Macroprep resin (Bio-Rad, CA, USA) and equilibrated with acidic NaCl (0.04 N HCl in 0.1 M NaCl). Unbound materials were washed from the column with 0.1 M NaCl, and fucoidans were eluted at a flow rate of 5 mL/min using a sequential concentration gradient of NaCl from 0.1 to 2M, yielding three fractions designated SlF1-SlF3 [139]. Fractions SlF2 and SlF3 were considered pure fucoidan samples based on monosaccharide analysis [139]. The fractions were passed through a 10 kDa membrane to concentrate the fucoidan and remove salt, followed by lyophilized. In this thesis this sample is considered as the native structure of fucoidan of *S. latissima* (Sl native).

3.8.2 Preparation and isolation of fucoidan oligosaccharide fractions (unpublished and Vuillemin et al. 2020)

To generate the fucoidan oligosaccharide fractions, a 0.9% (*w/v*) fucoidan solution was prepared by dissolving 180 mg Sl native fucoidan in 200 mL of 10 mM Tris-HCl buffer (pH 7), containing 100 mM NaCl, 10 mM $CaCl_2$. The solution was incubated at 25°C for 24 hours with 0.3 mg/mL Psf1 fucoidanase. The separation of medium molecular weight (MMW) and low molecular weight (LMW) fractions was performed using a method like that described by Vuillemin and colleagues (2020). Briefly, MMW products were precipitated by adding ice-cold ethanol to a final concentration of 75%. The mixture was then centrifuged at 10,000 × g for 15 min at 4°C, and the resulting pellet was collected. Likewise, the supernatant containing the LMW products was collected and concentrated under vacuum. The concentrated supernatant was applied to a Q-Sepharose HP anion exchange column (1 × 10 cm) pre-equilibrated with water. The LMW oligosaccharides were eluted from the column using sequential linear gradients of ammonium bicarbonate (NH_4HCO_3) buffer at concentrations of 0-0.75 M,

0.5-1.5 M, and 1–2 M, with a flow rate of 1 mL/min. Fractions containing the LMW products were pooled, concentrated, and desalted by vacuum evaporation or passed through a Sephadex G-10 column to remove salts, yielding the purified LMW fraction [140]. The reaction and separated fractions were analyzed by Carbohydrate Polyacrylamide Gel Electrophoresis (C-PAGE). This process led to the generation of the two fractions named Sl MMW and Sl LMW, respectively, in this thesis and in the unpublished manuscript for paper III.

3.9 Preparation and isolation of alginate oligosaccharide fractions

In this study, alginate lyases (AlyRm2, AlyRm3, AlyRm4, and AlyPx8) were obtained from *Rhodothermus marinus* MAT378 and MAT4696, which affiliates with the species *Petroclostridium xylanilyticum* (99% sequence identity) according to 16S rRNA analysis (Matís, unpublished results). These enzymes were cloned and expressed at Matís, using an *E. coli* cloning system ([141] and unpublished results). Utilizing these different alginate lyases, which exhibit distinct enzymatic activities (Table 6), enabled production of alginate oligosaccharide fractions with varying sizes and compositions.

Solutions of 1.5% alginic acid derived from *M. pyrifera* were prepared by mixing the alginate with different buffer solutions depending on the enzyme used, see specificity in Table 6. Reactions were conducted in glass Erlenmeyer flasks with a final volume of 70 mL for AlyRm2, AlyRm4, and AlyPx8, while a larger 400 mL volume was used for reactions involving AlyRm3. The protein concentrations used in these reactions were estimated based on SDS-PAGE band intensity analysis: AlyRm2 (~0.100 mg/mL), AlyRm3 (fully digested, ~0.050 mg/mL; partially digested, ~0.013 mg/mL), AlyRm4 (~0.036 mg/mL), and AlyPx8 (~0.009 mg/mL). All reactions were performed at 40°C with shaking at 150 rpm to ensure adequate mixing overnight. The choice of 40°C was based on preliminary observations showing that higher temperatures resulted in a significantly darker solution, which was undesirable. Following the incubation period, the resulting fractions were purified using a two-step ethanol precipitation process. Initially, a 50% ethanol solution was employed to remove larger impurities. Subsequently, a 76% ethanol solution was used to isolate the alginate oligosaccharide fractions of interest.

Two distinct fractions using AlyRm3 were prepared using slightly different methodologies. The AlyRm3 partially digested fraction was obtained by subjecting the sample to partial digestion, using 2.5 mL crude AlyRm3 (one-fourth the volume of the fully digestion reaction, see Table 6, resulting in a mixture of intermediate-sized oligosaccharides. In contrast, the AlyRm3 fully digested fraction was produced after using 10 mL crude AlyRm3. Both fractions were then precipitated using the two-step ethanol precipitation method previously described.

Table 6. Overview of Alginate lyases used to generate the alginate oligosaccharide fractions.

Alginate lyase	Reported Activity	Specificities	Stock Concentration (mg/mL)*	Final Concentration in Reaction (mg/mL)	Alginate oligosaccharide fraction ID
AlyRm2	Exotype and endotype alginate lyase Major activity: M-G bonds Major activity: G-G bonds Minor activity: M-M bonds [142]	20 mM sodium citrate buffe, pH 6.6, incubated overnight 40°C 70 mL reaction The crude enzyme-to-total-volume ratio was 1:70 (1 mL crude enzyme)	~7 mg/mL	0.100 mg/mL	AlyRm2
AlyRm3	Endo-type alginate lyase active on both M and G blocks of alginate [141]	20 mM sodium citrate buffer, pH 5.7, incubated overnight at 40°C 400 mL reaction volume Full digestion: Crude enzyme-to-total-volume ratio: 1:40 (10 mL crude enzyme) Partial digestion: Crude enzyme-to-total-volume ratio: 1:160 (2.5 mL crude enzyme)	~2 mg/mL	0.050 mg/mL Partial digestion: 0.013 mg/mL	AlyRm3 fully digested AlyRm3 partially digested
AlyRm4	Exo-type enzyme Active on both	20 mM sodium citrate buffer, pH 6.6,	~2.5 mg/mL	0.036 mg/mL	AlyRm4 dialyzed

	M, G and MG-blocks [141]	incubated overnight 40°C 70 mL reaction The crude enzyme-to-total-volume ratio 1:70 (1 mL crude enzyme			
AlyPx8	Endo-type Major activity: M-G bonds Major activity: G-G bonds [unpublished]	Potassium phosphate buffer, pH 7.0, incubated overnight 40°C 70 mL reaction The crude enzyme-to-total-volume ratio 1:70 (1 mL crude enzyme)	~0.6 mg/mL	0.009 mg/mL	AlyPx8

*Stock enzyme concentrations were estimated from SDS-PAGE band intensity analysis

To enrich the G-block content, a process involving AlyRm4, an alginate lyase that predominantly cleaves M-M bonds, was utilized [141]. Post-reaction, the mixture was dialyzed using Slide-A-Lyzer® 3.5K Dialysis Cassettes (Thermo Scientific) placed in a beaker filled with 2 L water. This step allowed smaller alginate oligosaccharides to diffuse out of the membrane, theoretically enriching the G-block content within the dialysis membrane. The dialyzed fractions were subsequently precipitated using approximately 50% ethanol.

To verify the activity of the different alginate lyases, TLC was applied using the same protocol as described for laminarin (Section 3.5.2) but was separated on a larger Silica gel 60 F_{254} (20 × 20; Merck 20x20 cm plate) for 4-5 hours to obtain better band separation.

Through these methods, various alginate oligosaccharide fractions were successfully prepared and purified, allowing for further investigation into their properties as immunomodulating agents

3.10 Immunomodulatory activity assay

Human peripheral blood mononuclear cells (PBMCs) were isolated from either buffy coat obtained from the Icelandic Blood Bank or fresh venous EDTA blood from healthy volunteers at the Department of Immunology, Landspítali – the National University Hospital of Iceland. Informed consent was obtained from all blood donors in accordance with the guidelines for ethical research described by the Directorate-General for Research and Innovation of the European Commission. Permission was granted by the National Bioethics Committee of Iceland (# 06-068-V1).

3.10.1 Samples of investigation for immunomodulation

In this PhD study, a comprehensive high-throughput screening was conducted on various marine-derived polysaccharides to identify potential immunomodulatory agents, with a primary focus on laminarin, fucoidan, and alginate. In addition to the previously described poly- and oligosaccharides from brown seaweed, more than 20 other fucoidan samples were screened (Appendix A, Table 10, and Table 11). Moreover, several polysaccharides and their derivatives from the cell walls of red and green seaweed were also screened, as well as EPSs derived from *Rhodothermus marinus* and *β*-glucans from *Agrobacterium* species and yeast (Appendix A, Table 11). The primary evaluation criteria used to identify potential immunomodulatory agents was centered on the modulation of key cytokines, such as IL-6, TNF-α, IL-12p40, and IL-10, by DCs.

3.10.2 Monocyte isolation and differentiation

Buffy coats were diluted in PBS and layered on top of Histopaque-1077 (Sigma-Aldrich). After centrifugation with minimum acceleration and no break at 400 G, the PBMC-rich layer was carefully harvested. Then PBMCs were washed 3 times with magnet associated cell sorting (MACS) buffer (0.5% BSA (Sigma-Aldrich), 2 mM EDTA (Sigma-Aldrich) in PBS), and counted using Neubauer cell counting using trypan blue, and resuspended at a concentration of 12.5×10^7 cells/mL.

$CD14^+$ monocytes were isolated using positive selection using CD14 Microbeads (Miltenyi Biotec). Briefly, PMBCs were incubated with $CD14^+$ microbeads and then washed with MACS buffer. The $CD14^+$ labeled cell solution was applied to an LS^+ MACS column (Miltenyi Biotec) attached to a magnetic field. The unlabeled cells ran through the column while the $CD14^+$ monocytes were retained. To retrieve the $CD14^+$ monocytes, the columns were taken from the magnetic field and put onto a 15 mL tube. MACS buffer was added to the column and the $CD14^+$ monocytes were pushed through with the column plunger. Following positive selection, the purified $CD14^+$ monocytes were counted by Neubauer cell counting with trypan blue, pelleted, and resuspended in complete RPMI medium (Gibco, Invitrogen), supplemented with 10% fetal calf serum (FCS; Gibco) and 1% penicillin/streptomycin (Gibco) to a concentration of 0.5×10^6 cells/mL. Then 1 mL of the cell solution was pipetted into 48-well plates (Nunc) and stimulated with IL-4 at 12.5 ng/mL and GM-CSF at 25. ng/mL (both from R&D Systems, Bio-Techne~~)~~ to ensure monocyte differentiation to imDCs. The cells were incubated at 37°C, with 5% CO_2 and 95% humidity for 7 days and resupplied with RPMI medium, IL-4 and GM-CSF after 3-4 days.

3.10.3 Dendritic cell activation and maturation

On day 7, the imDCs were harvested and matured and activated by culturing them for 24 hours in RPMI medium supplemented with FCS and antibiotics in 48-well plates at a concentration of 2.5 x 10^5 cells/mL in the presence of IL-1β at 10 ng/mL, TNF-α at 50 ng/mL (both from R&D Systems) and lipopolysaccharide (LPS) from *E. coli*, serotype 055:B5 (Sigma-Aldrich) at 0.5 µg/mL. Seaweed derived polysaccharides and oligosaccharides (or other compounds of interest – Appendix A, Table 10 and 11) were dissolved in complete RPMI medium to stock solutions of 5 mg/mL and added to the imDCs at a concentration of 100 µg/mL together with cytokines and LPS. Only the fucoidan fraction, Sl Psf1 LMW, was investigated for its dose-dependent effect at 1, 10, and 100 µg/mL. Cell cultured with cytokines and LPS without any added sample (Neg-DCs) were used as a negative control in each experiment. After 24 hours, the matured DCs were harvested. The effect of the samples of interest on their activation and maturation was evaluated by measuring cytokine secretion using Enzyme-linked immunosorbent assay (ELISA). In some instances (Paper II and Paper III), the effect of the samples on activation and maturation of the DCs was evaluated by measuring expression of surface molecules by flow cytometry. Additionally, the effect of some samples on DC activation and maturation was further evaluated by co-culturing them with allogeneic $CD4^+$ T cells (paper II and unpublished data Results section 4.4).

3.10.4 Co-culture of DCs and allogeneic $CD4^+$ T cells

Allogeneic $CD4^+$ T cells were obtained from PBMCs using CD4 microbeads (Miltenyi Biotec) using the same procedure for isolating $CD14^+$ monocytes described in section 3.11.2. DCs, which were matured and activated for 24 hours with LPS, TNF-α, and IL-1β in the presence or absence of 100 µg/ml laminarin, laminari-oligosaccharides, the alginate oligosaccharide fraction, AlyRm3 fully digested, or the fucoidan fraction, Sl Psf1 LMW, were co-cultured at 2 x 10^5 cell/mL with allogeneic $CD4^+$ T cells at 2 x 10^6 cells/mL (mDCs:T cells ratio 1:10) in 96-well round-bottom culture plates (Nunc) for six days. Then supernatants were collected and stored at –80°C for cytokine measurement by ELISA.

3.10.5 Determination of cytokine secretion by ELISA

The concentration of TNF-α, IL-6, IL-12p40, and IL-10 from DCs culture supernatants and IFN-γ, IL-17, IL-12p40, and IL-10 in supernatants from co-cultured DCs and allogeneic $CD4^+$ T cells were measured by sandwich ELISA using DuoSets from R&D Systems according to the protocol from the manufacturer. The results were expressed as secretion index (SI), which was obtained by dividing the cytokine concentration (pg/mL) in the supernatant from DCs matured in the presence of the seaweed-derived compound of interest or in co-cultures of these DCs with allogeneic $CD4^+$ T cells, by the cytokine concentration (pg/mL) in supernatants from DCs cultured in the absence of samples or in co-cultures of these DCs with allogeneic $CD4^+$ T cells. Proportional index

(PI) was used to evaluate the overall effect of the samples in DCs cultures on the IL-12p40 and IL-10 cytokine secretion, calculated by dividing the SI for IL-12p40 by SI for IL-10. PI<1, obtained with IL-10-SI of >1 and/or IL-12p40-SI of <1, is indicative of anti-inflammatory effect, whereas PI>1, obtained with IL-10-SI of <1 and/or IL-12p40-SI of >1, is indicative of pro-inflammatory effect.

3.10.6 Flow cytometry

Cells were collected for flow cytometry, washed with Fluorescence-Activated Cell Sorting (FACS) buffer (3.8 M sodium azide, 0.5% BSA, and 2 mM EDTA in PBS) and divided into FACS tubes. To minimize background staining by blocking the Fc-receptors of the cells, they were incubated with 2% normal human and normal mouse serum (AbD Serotec, BioRad) for 10 min. Then the cells were stained with monoclonal antibodies against surface molecules or isotype antibodies, specified in Table 7, by incubating for 20 min at 4°C. Hereafter, the cells were washed with FACS buffer and subsequently pelleted by centrifugation (300 g, 10 min, 4°C). Hereafter, cells were fixed using 2% paraformaldehyde (Sigma-Aldrich) and kept for maximum of 48 hours at 4°C. The cells were then evaluated by flow cytometry on a Sony SH800 Cell Sorter (Sony Biotechnology).

Table 7. Antibodies used for human in vitro studies for flow cytometry.

Antigen	Fluorophore	Clone	Manufacturer
HLA-DR	BV421	L243	*BioLegend*
Dectin-1 (CLEC7A)	AF488	259931	*R&D Systems, Bio-Techne*
CD40	PE	5C3	*BioLegend*
CD86	AF700	Bu63	*Bio-Rad*
CD14	BV421	M5E2	*BioLegend*
CD1c	AF488	L161	*BioLegend*
CD141	AF700	501733	*R&D Systems, Bio-Techne*
PD-L1 (CD274)	PE	5C3	*BioLegend*
TLR2 (CD282)	AF488	383936	*R&D Systems, Bio-Techne*
TLR4 (CD284)	BV421	HTA125	*BioLegend*
TLR6 (CD286)	PE	TLR6.127	*BioLegend*
Isotype antibodies			
Mouse IgG2a, κ	BV421	MOPC-21	*BioLegend*
Mouse IgG2b, κ	AF488	MPC-11	*BioLegend*
Mouse IgG1, κ	PE	MOPC-21	*BioLegend*
Mouse IgG1, κ	AF700	MOPC-21	*BioLegend*

To evaluate the data, a singlet gate was made using FSC-A and FSC-H (forward scatter; area and height of cells) and then a live gate using FSC-A and SSC-A (forward scatter and side scatter) of a minimum of 10,000 events, which allowed successive exclusion

of doublet events, non-intact cells, and debris, respectively, using Kaluza analysis Software (Beckman Coulter). Histograms of the live-gated isotype antibody stained DCs was used to set positive gating limits, where signals under the limit represented unspecific binding of the isotype antibodies (Figure 10). Results were expressed as percentage positive cells.

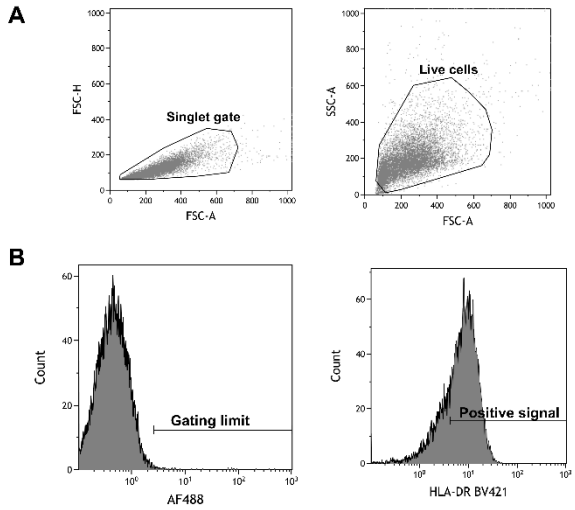

Figure 10: Gating strategy to assess surface molecule expression following 24-hour incubation with or without experimental treatment.
(A) Human dendritic cells (DCs) were first single-gated based on forward scatter area (FSC-A) and forward scatter height (FSC-H; left), followed by gating for live cells using their FSC-A and side scatter area (SSC-A; right) properties. (B) Histograms to distinguish a positive antibody signal using live-gated isotype antibody stained mature DCs (mDCs) to set the gating limit (left), and the positively stained mDCs (right).

3.10.7 Statistical analysis of immunomodulating data (paper II)

Results from the immunomodulating experiments are shown as mean values ± standard error of mean (SEM). Experimental treatments were compared to the negative control (Neg-DCs) using one-way ANOVA utilizing Dunnett comparison test, in GraphPad Prism version 10.2.1 (395). Significance markers in the results are denoted as follows: * for $p \leq 0.033$, ** for $p \leq 0.002$, and *** for $p < 0.001$, for donor size $n \geq 3$. For the co-culture experiments, data were compared using an unpaired t-test statistical model in GraphPad Prism (version 10.2.1 (395)). The asterisks indicate $p \leq 0.033$ (*), $p \leq 0.002$ (**), and $p < 0.001$ (***), with $n = 5$-6.

4 Results

This results chapter aims to present the findings from various experiments and analyses conducted during this research. Each section within this chapter corresponds to a specific objective outlined in the thesis.

4.1 Section I: Cloning and characterization of SulA1 from a marine *Arthrobacter* strain (Paper I and unpublished data)

The objective was to clone and characterize the sulfatase enzyme SulA1 from a marine *Arthrobacter* strain, including exploring its sequence homology, structural features, and enzymatic properties. This section will highlight the successful cloning process, the structural predictions made through comparative modeling, and the characterization of the enzyme's optimal activity conditions and substrate specificity.

4.1.1 Exploring sequence homology and structural features of SulA1 (Paper I)

In previous work conducted by Matís, a marine chondroitin degrading *Arthrobacter* strain, MAT3885, was isolated and sequenced [143]. The *sulA1* gene was located within a chondroitin lyase gene cluster, along with another potential sulfatase gene, *sulA2* (Paper I, Fig. 1). In this study, the deduced amino acid sequence of SulA1 was compared against the PDB database, revealing that the closest related structures were enzymes from *Bacteroides thetaiotaomicron* VPI-5482 (PDB 5G2V) *Pseudoalteromonas* sp. (PDB 6B0K), *Bacteroides fragilis* YCH46 (PDB 2QZU), *Pseudoalteromonas fuliginea* (PDB 6BIA), and *Hungatella hathewayi* (PDB 6UST). These candidates shared low sequence homology with SulA1 but exhibited high query coverage (Paper I; Table 1), which indicated an overall conserved topology. Moreover, analysis of the SulA1 amino acid sequence in Interpro revealed conserved motifs and residues throughout the aligned sequences (Paper I, Fig. 2). The obtained sequences mentioned above, contained the formylglycine-dependent sulfatases (FGly-SULF) signature motif C/S-X-P-X-R, which is essential for the post-translationally generation of the FGly catalytic residue, found in the active site of type I sulfatases. The two catalytic residues, Cys57 (converted to FGly) and His190, were identified. Four calcium-binding residues (Asp17, Asp18, Asp277, and Asn278) were identified, shown to be conserved across the enzymes, and located close to the active site (Paper I, Fig. 2). Comparing the deduced amino acid sequence of SulA1 with the potential SulA2 (Paper I, Fig. 1), two recently characterized GalNAc4S-acting CS sulfatases (GenBank UFQ91287.1 and QAB47431.1), and one GalNAc6S CS sulfatase (GenBankUFQ91288.1), higher query coverage was observed

than observed for the PDB sequences, but the sequence identity remained low (26.6 to 28.01%). It was also confirmed that SulA1 shared a higher conserved topology with the GalNAc4S-acting CS sulfatases (90% query coverage) and lowest with the GalNAc6S-acting CS sulfatases (67% query coverage), while SulA2 shared 96% query coverage with the GalNAc6S-acting CS sulfatases.

4.1.2 Comparative three-dimensional modeling and structural prediction of SulA1 (Paper I)

Two alternative approaches were used for three-dimensional modeling of SulA1 a homology-based structural modeling with YASARA and a structural prediction using AlphaFold2. Both methods resulted in a monomeric 3D molecular model, with $Ca2^{+}$ included as a ligand.

For the homology model, the five templates from PDB (Paper I, Table 1) were used to obtain a hybrid model. Despite the low sequence similarity with the crystallographic structures, the model was assessed as "satisfactory" according to the overall Z-score (Z = −1.786) (Paper I, Table 2). Similarly, the AlphaFold2 model displayed good quality and showed high predicted local distance difference test (pLDDT) score above 90% (Paper I, Fig. 3A). Low PLDDT scores were only observed for the loop Ala360-Val376 (ADDGTGDAAGRAENAVV) and the C-terminal part of the model (Paper I, Fig. 3A)).

Despite using different approaches, both 3D models exhibited a typical sulfatase fold composed of a large N-terminal domain and a smaller C-terminal domain, each centered on a β-sheet. Detailed comparison of the models revealed discrepancies, particularly in the size and orientation of loops (Paper I; Fig. 3B and Fig. S1) and in the orientation of the active site residue Arg61 (Paper I; Fig. 3C). Given the relatively low sequence identity to the structure-determined candidates (Paper I; Table 1), the prediction from AlphaFold2 was used for a further evaluation of the 3D structure of SulA1.

The N-terminal domain (Domain I) encompassed the β-strands β1, β2, and β4-β8, β11, β14, and β15 surrounded by the α-helixes α1, α2, α5, α6, α7, α8, α10, and α13 (Paper I; Fig. 4). The C-terminal domain (Domain II) consisted of a β–sheet formed by β17-20 strands, surrounded by α-helices α17-α21 (Paper I; Fig. 4). The catalytic site was in the interdomain region, which also contained the calcium-binding site with the conserved residues Asp17, Asp18, Asp277, and Asn278 (Paper I; Fig. 4B).

Based on the location of *sulA1* in the genome (Paper I, Fig. 1), it was suspected that SulA1 had potential activity on CS-AC degradation products produced by the nearby chondroitin lyase (ChoA1). Therefore, GalNAc4S and GalNAc6S were docked into the active site (Paper I, Fig. S2). However, the sulfate groups of the two substrates were oriented in opposite directions in the active site of the model. Moreover, the 4S-group did not interact with the calcium-binding site (Paper I, Fig. S2) but showed higher

binding energy compared to the GalNAc6S substrate. Lastly, the distance between the sulfate group and the catalytic residues was longer for GalNAc4S than for GalNAc6S.

4.1.3 Recombinant protein production in *E. coli*, and purification of SulA1 (Paper I)

The *sulA1* gene was successfully cloned into vector pJOE3075. The resulting plasmid, designated pVK13, was brought into E. coli Bl21(C43) by transformation. Subsequently, the gene was expressed, and the recombinant enzyme purified in a soluble form (Paper I, Fig. 5A,B). The molecular weight of the recombinant protein, estimated with SDS-PAGE, aligned closely with the calculated weight of 51.9 kDa (Paper I; Fig. 5). Purification of the recombinant protein was efficiently achieved using his-tag affinity beads (Paper I, Fig. 5A,B).

The activity of SulA1 was confirmed in crude extract and in purified form using *para*-nitrocatechol-sulfate (*p*NCS). It was observed that the specific activity of purified SulA1 increased approximately four-fold compared to the corresponding activity in the crude extract under standard conditions (Paper I, Table 3).

Additionally, peptide mass fingerprinting (PMF) was applied to validate the SulA1 amino acid sequence used in structural modeling. This approach confirmed the accuracy of the sequence, achieving 100% identity with peptide fragments generated in silico using the software MASCOT (https://www.matrixscience.com/). The fragments also showed 40% query coverage of the SulA1 amino acid sequence, matching the peptide fragments identified in the mass spectrometry analysis (Paper I, Fig. 6).

4.1.4 Insights into optimal activity conditions, thermal stability, cation dependence and storage stability of SulA1 using *p*NCS as substrate (Paper I)

SulA1 exhibited pH-sensitive activity on *p*NCS, reaching maximum relative activity at pH 5.5, with reductions to 21% and 54% of the optimal activity observed at pH 5.0 and pH 6.0, respectively (Paper I, Fig. S3A). The optimal temperature range was between 40°C and 50°C at pH 5.5 using *p*NCS, while significant activity loss (83%) occurred at 60°C, lower than its unfolding temperature determined by DSF (T_m=67°C at pH 6.0, increasing up to 72.4°C at pH 7.0; Paper I, Fig. 7).

The presence of the potential calcium-binding site progressed into an investigation into the effects of mono- and divalent cations on SulA1 activity using *p*NCS as substrate (Paper I; Fig. S4). The divalent cation, Ca^{2+}, at concentrations ranging from 15 to 30 mM $CaCl_2$, increased the relative SulA1 activity three-fold, while EDTA efficiently chelated Ca^{2+} ions and reduced SulA1 activity by ~90% (Paper I; Fig. S4). Moreover, DSF analysis indicated that higher $CaCl_2$ concentrations marginally decreased SulA1's unfolding temperature, while EDTA had no such effect (Paper I, Table 4).

Lastly, purified SulA1 exhibited varying stability during storage under different conditions. Storage at 4°C and –20°C resulted in precipitation and loss of activity. Optimizing storage conditions using *p*NCS as the substrate revealed that storing SulA1 in 100 mM sodium acetate buffer with 20% glycerol at pH 5.5 maintained stable enzyme activity for at least 5 weeks at –80°C. in contrast, storage at –20°C in the same buffer showed a slight decrease in relative activity after one week, with 86% remaining activity after 5 weeks. Storage at 4°C in sodium acetate buffer pH 5.5 led to a substantial reduction in relative activity, with activity dropping to 26% after one week of storage and to 13% of the initial activity after 5 weeks of storage.

4.1.5 Specific activity towards GalNAc4S and Michaelis-Menten kinetics (Paper I and unpublished data)

Investigating the SulA1's natural substrate specificity, various CS sulfated mono-, di-, and oligo/polysaccharides with different sulfation patterns were screened (Paper I, Table 5). It was found that SulA1 exclusively exhibited activity towards GalNAc4S. This activity was confirmed through a TLC mobility shift (Paper I, Fig. 8A) and HPAEC-PAD (Paper I, Fig. 8B,C). Moreover, it was observed that the optimal pH range for SulA1 activity was pH 6.0-6.5 (Paper I, Fig. 9A), higher than the initially expected pH (pH 5.5 for *p*NCS, Paper I, Fig. S1A).

The specific activity of purified SulA1 was determined to be 6.8 mU/mg SulA1 at pH 5.5 with 20 mM GalNAc4S and 14.0 mM/mg SulA1 at pH 6.5 with 15 mM GalNAc4S (Paper I, Table 6). Initially, attempts to investigate kinetic parameters with *p*NCS were unsuccessful. However, activity assays using different concentrations of GalNAc4S confirmed that SulA1 followed Michaelis-Menten kinetics at pH 5.5 (Paper I, Fig. 9B), with a K_m value of 6.94 ± 0.053. The V_{max} at saturation corresponded to the specific activity of 6.8 mU/mg SulA1 at pH 5.5 and 40°C. Michalis-Menten behavior was also indicated at pH 6.5 when the reaction rate was plotted against different GalNAc4S (mM) concentrations, yet less distinctly (Figure 11).

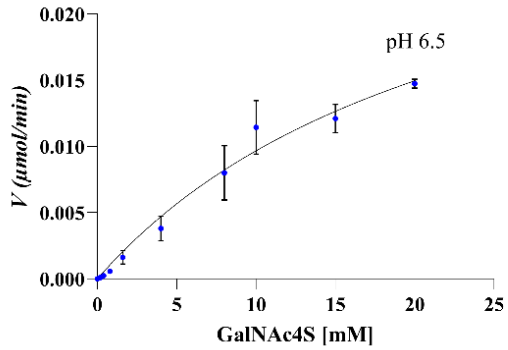

Figure 11: Michalis-Menten behavior of SulA1 at pH 6.5.
The reaction rate *V* (µmol/min) was plotted against the concentration of GalNAc4S (mM). The graph shows the GalNAc formation after the SulA1 reaction with Michaelis–Menten nonlinear curve fitting (black line); data are represented as mean ± SD of two individual experiments (unpublished data).

4.2 Section II: Laminarin refinement and immunomodulating potential of laminarin and enzymatically modified laminarin (Paper II and unpublished data)

The purpose was to investigate the structural complexity and enzymatic modification of laminarin extracted from various species of brown seaweed (*L. digitata*, *L. hyperborea*, and *S. latissima*). Thus, this result section includes detailed structural analyses, information on the production of laminari-oligosaccharide fractions, and assessment of their immunomodulatory effects on DCs and T-cell responses by investigating the cytokine secretion.

4.2.1 Laminarin extraction and purification (Paper II and unpublished data)

Laminarins from *L.* digitata, *L. hyperborea*, and *S. latissima* were extracted using a two-step water extraction protocol, followed by treatment with $CaCl_2$ to precipitate traces of alginate. Larger molecules, such as fucoidan, were removed using a 10 kDa filtration step, and smaller products and minerals were removed via dialysis using 1 kDa filters (Paper I, Table 1). The use of $CaCl_2$ resulted in increased ash content in the laminarin extracts. To ensure the effectiveness of the filtration process, conductivity was measured during filtration, and a drop in conductivity was observed after the 1 kDa filtration step (Figure 12), confirming successful removal of smaller ions and minerals. The conductivity data were expressed as the concentration of ions in g/L.

The %yield of extracted laminarin was 10% and 12% of the *L. hyperborea* and *S. latissima* biomass (100 g seaweed powder in 1.5 L distilled water), respectively. In contrast, laminarin extracted from a locally sourced *L. digitata* resulted in a low yield, due to low laminarin content in the raw material verified by subsequent monosaccharide analysis (Paper II, Table S1). Additionally, the ash and mannitol content remained relatively high (Paper II, Table S1), despite low conductivity measurement (Figure 12, Paper II, Table S1).

To obtain *good purity of L. digitata laminarin*, commercially available laminarin (Sigma Aldrich) was used for structural analyses and immunomodulation trials.

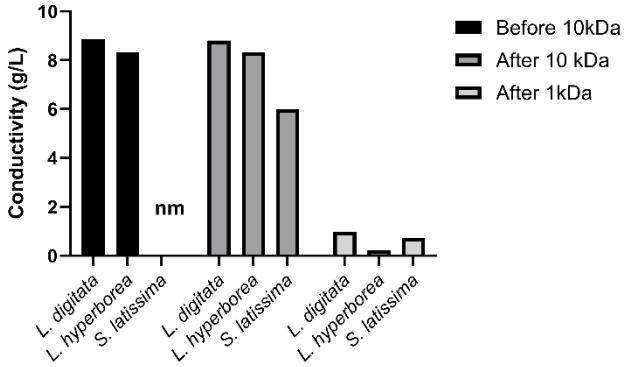

Figure 12: Conductivity profiles of laminarin extracts from brown seaweed species before and after tangential flow (TTF)-filtrations.
Conductivity was measured for laminarin extracts from *L. digitata*, *L. hyperborea*, or *S. latissima* (as labeled on the x-axis) at three stages: before 10 kDa TTF-filtration (black), after 10 kDa TTF-filtration (grey), and after 1 kDa TFF-filtration (white). nm indicates Not measured. The conductivity is expressed as the concentration of ions in grams pr. liter (g/L).

Monosugar analysis of the extracted laminarins (*L. hyperborea* and *S. latissima*) and the commercial laminarin (*L. digitata*) revealed distinct compositions. Laminarin from *L. digitata* contained 78% glucose (*w/dw*), with minimal levels of mannitol and ash (Paper II, Table 1). The *L. hyperborea* extract predominately consisted of glucose (53% *w/dw*) and minor amount of mannitol (2% *w/dw*), alongside traces of fucose, galactose, and xylose, indicating contamination with fucoidan. This was further confirmed by ^{1}H-NMR analysis (Paper II, Fig. S3). The successful removal of fucoidan was achieved by DEAE-cellulose anion-exchange chromatography. Similarly, the *S. latissima* extract was dominated by glucose (75% *w/dw*) and mannitol (5% *w/dw*), comprising a total carbohydrate content of 80%, indicative for high purity of the laminarin extract (Paper II, Table 1).

Furthermore, ^{1}H-NMR characterization of the three different laminarins confirmed the coexistence of M- and G-type laminarin. This was observed as a chemical shift at 4.18 ppm for mannitol connected to glucose or as glucose in its α or β configuration at the reducing end (Gα/β) [(1 → 3)−β−D−Glc*p*] at δ 5.22/4.67 ppm (Paper II, Fig. 1). Variations in the M-type:G-type ratio between the three extracts were observed: 2.5:1 for *L. digitata* and *S. latissima* and 1:1 for *L. hyperborea*.

The TPC in the laminarin extracts was below detection levels for *L. digitata* and *L. hyperborea*, while *S. latissima* laminarin contained 1.03 ± 0.05 mg PGE/100 g lyophilized laminarin sample (Paper II, Table 1). However, phenolic content was not detected by ^{1}H-NMR (Paper II, Fig. 1).

4.2.2 Structural insights and polymerization characteristics of laminarins from the three brown seaweed species (Paper II)

The FT-IR spectra of the laminarin from *L. digitata*, *L. hyperborea*, and *S. latissima* demonstrated the characteristic pyranose absorption peak around 890 cm^{-1}, confirming the presence of β-glycosidic bond typical of β−1,3−D-glucans, such as laminarin. Additionally, the characteristic absorption peaks for -OH groups were detected at 3347 cm^{-1} for *L. digitata*, 3361 cm^{-1} for *L. hyperborea*, and 3314 cm^{-1} for *S. latissima*. Peaks corresponding to C-H stretching vibrations in -CH3 or -CH2 groups were observed at 2917 cm^{-1} for *L. digitata* and *L. hyperborea*, and at 2887 cm^{-1} for *S. latissima*. Lastly, the strong absorption in the range of 1000-1200 cm^{-1} indicated polysaccharides as the predominant components in the lyophilized extracts (Paper II, Fig. 2).

Moreover, 1D/2D ^{1}H-NMR spectroscopy analysis revealed that laminarins from *L. digitata*, *L. hyperborea*, and *S. latissima* were composed of a mix of β−1,3 and β−1,6-linkages with varying DB. *S. latissima* showed a notable DB with 21% β−1,6-linkages, where 15% were branches and 6% were intrachain links. *L. digitata* had a lower content of β−1,6-branching with 6.5% branches and 3.5% intrachain links. *L. hyperborea* predominantly featured a linear β−1,3-linked backbone with minimal branching, approximately 4%. These branches are predicted to consist solely of single glucose units (Paper II. Fig. S4). No intrachain links were detected (Paper II, Fig. 1, and Table 3 or Table 8 in this thesis).

Finally, MALDI-TOF MS analysis confirmed that the extracted laminarins were fitting with the average size of approximately 5 kDa of other reported laminarins, with the dominant signal observed at DP25 for *L. digitata* and at DP24 for *L. hyperborea* and *S. latissima* (Paper II, Fig. 3, and Table 2).

4.2.3 Structural analysis of LPHase generated laminari-oligosaccharides (Paper II and unpublished data)

Laminari-oligosaccharide fractions from the three species were carefully selected after TLC analysis. Close-up views were generated by spotting 2 µL at the TLC plate from the end wells in row C to the E12 for each species (Figure 13), and the different fractions were collected and hereafter analyzed structurally (Table 8).

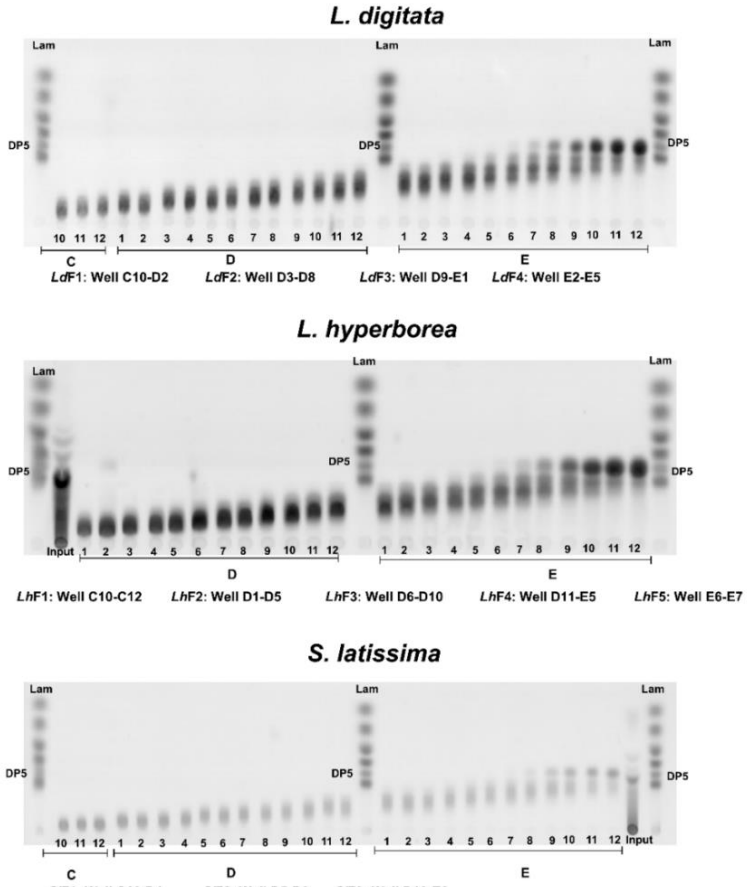

Figure 13: TLC close-up views of laminari-oligosaccharide.
Distribution in *L. digitata* (Top), *L. hyperborea* (Middle), and *S. latissima* (Bottom). The distributions were generated by hydrolyzing laminarin from the three species using pentamer-producing laminarinase (LPHase) and purifying the products on a Superdex™ 30pg column. Numbers at the bottom of each image indicate well numbers, while letters (C, D, and E) represent rows of the 96-well plate into which the samples were eluted. "Lam" denotes a laminarin ladder ranging from a single glucose unit to DP6, with DP5 specifically highlighted as the main product of LPHase. For *L. hyperborea* and *S. latissima*, "Input" indicates partially hydrolyzed laminarin prior to separation on the Superdex™ 30 HiLoad 26/600 column; this input is absent for *L. digitata*. Fraction names and the wells, from which they were merged to generate the samples, are indicated beneath each TLC image for each species.

MALDI-TOF-MS and ^{1}H-NMR analyses revealed that laminari-oligosaccharide fractions derived from *L. hyperborea* exhibited increased β–1,6-branching compared to the laminarin polymer. Specifically, the oligosaccharide fraction *Lh*F1 contained 11% β–1,6-branching, compared to 4% in undigested laminarin. Fraction *Lh*F2 showed 7% β–1,6-branching. Both fractions were excluded from immunomodulation analysis due to fucoidan contamination. Intermediate-sized fractions (*Lh*F3 and *Lh*F4) exhibited 3% β–1,6-branching, while the smaller oligosaccharide fraction (*Lh*F5) contained 7% β–1,6-branching. No intrachain links were observed (absence of the GB residue indicative for β–1,6-intrachain, Table 8) in any of these fractions, as observed for the laminarin polymer (Table 8). In contrast, the laminarin fractions derived from *L. digitata* and *S. latissima* showed a gradual reduction in β–1,6-links as the oligosaccharide mixtures decreased in DP range. For instance, the *L. digitata* fractions *Ld*F1 and *Ld*F2 contained 10% and 7% β–1,6-linkage, respectively, while *Ld*F3 and *Ld*F4 contained 3% β–1,6-linkages without intrachain links (Table 8). The *S. latissima* oligosaccharide fractions (*Sl*F1, *Sl*F2, and *Sl*F3) displayed a higher percentage of β–1,6-linkages (20%, 16%, and 11%, respectively, Table 8), all of which contained intrachain links. Furthermore, the obtained fractions from each species were estimated to be with in the same DP-range (Table 8).

Table 8. Overview of laminarin and laminari-oligosaccharide samples, detailing the degree of polymerization range as determined by MALDI-TOF-MS, branching content, and the mannitol-to-glucose (M:G)ratio as measured by ^{1}H-NMR.

Sample	Degree of polymerization	Branching	M:G chains
L. digitata laminarin	DP10-DP36 Highest signal DP25	~ 10% β–1,6-linkages (6.5% branching, 3.5% intrachain) Residues ratio GD:GB* ~ 2:1	~2.5:1
*Ld*F1 (well: C10-D2)[a]	DP-12-DP15	10% β–1,6-linkage Residues ratio GD:GB 2:1	
*Ld*F2 (well: D3-D8)	DP9-DP12	7% β–1,6-linkage Residues ratio GD:GB 2:1	
*Ld*F3 (well: D9-E1)	DP8-DP10	3% β–1,6-branching GB residue nd[a]	
*Ld*F4 (well: E2-E5)	DP6-DP8	3% β–1,6-branching GB residue nd	
L. hyperborea laminarin	DP8-DP33 highest signal at DP24	~ 4% β–1,6-branching, GB traces	~ 1:1
*Lh*F1 (well: C10-C12)	DP12-DP15	11% β–1,6-branching	

		NB: contamination with fucoidan	
*Lh*F2 (well: D1-D5)	DP10-DP13	7% β–1,6-branching **NB:** contamination with fucoidan	
*Lh*F3 (well: D6-D10)	DP8-DP11	3% β–1,6-branching	
*Lh*F4 (well: D11-E5)	DP6-DP10	3% β–1,6-branching	
*Lh*F5 (well: E6-E7)	DP5-DP8	7% β–1,6-branching	
S. latissima laminarin	DP7-DP36 highest signal detected at DP24	~ 21% β–1,6-linkages (~ 15% branching, ~ 6% intrachain) Residues ratio GD:GB ~ 2:1	~ 2.5:1
*Sl*F1 (well: C10-D2)	DP10-DP14	20% β–1,6-linkages (~ 15% branching, ~ 5% interchain) Residues ratio GD:GB ~2:1	
*Sl*F2 (well: D9-E1)	DP9-DP11	16% β–1,6-linkages (~ 11% branching, ~ 5% interchain) Residues ratio GD:GB ~2:1	
*Sl*F3 (well: E2-E5)	DP6-DP9	11% β–1,6-linkages (~7% branching, ~4% interchain) Residues ratio GD:GB ~2:1	

[a] Wells merged in Figure 13

*The GD:GB ratio reflects the β–1,6-branch to β–1,6-intrachain ratio

[a] nd = not detected

^{1}H-NMR analysis revealed the presence of citric acid to varying extents in all the laminari-oligosaccharide fractions (Figure 14 is an example from *L. digitata*-derived oligosaccharide fractions).

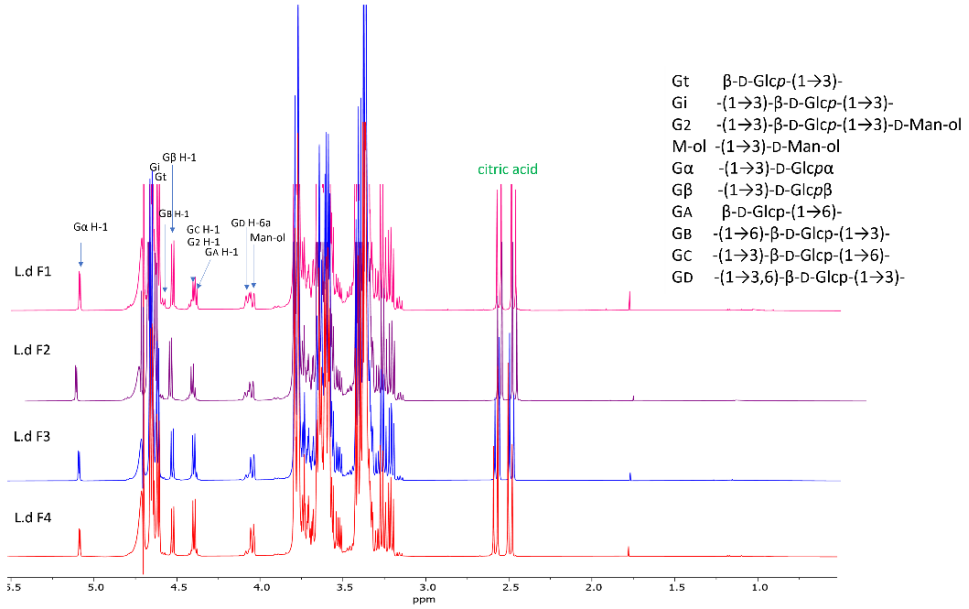

Figure 14: 1H-NMR spectra of laminari-oligosaccharide fractions from *L. digitata*.
The spectra were recorded in D_2O at 292 K. The x-axis represents chemical shift in parts per million (ppm). Potential linkages are annotated in the spectra, with detailed explanations provided in the top right corner. Peaks corresponding to citric acid are highlighted in green text.

No impact on the appearance or viability of DCs treated with 100 µg/mL laminarin or laminari-oligosaccharides for 24 hours was observed compared to Neg-DCs, with viability count exceeding 80% for most treatments (Paper II, Table S2 and Fig. 4a). Additionally, the maturation of imDCs into mDCs was confirmed by the low expression of CD14 and high percentages of DCs expression HLA-DR, CD40, and CD86, which were not affected by laminarin treatments (Paper II, Fig. 4b). Furthermore, laminarin treatments did not affect the expression of CD1c and CD141 by DCs, with a higher percentage of DCs expressing CD1c than CD141 (Paper II, Fig. 4b and Figure15). Notably, cells expressing CD141 were also CD1c positive (22.5%; Figure 15) irrespective of whether they were matured in the absence or presence of any of the laminarin samples (data not shown). Additionally, all matured DCs, regardless of the presence or absence of experimental treatments, exhibited high expression of PD-L1 (Paper II, Fig. 4b).

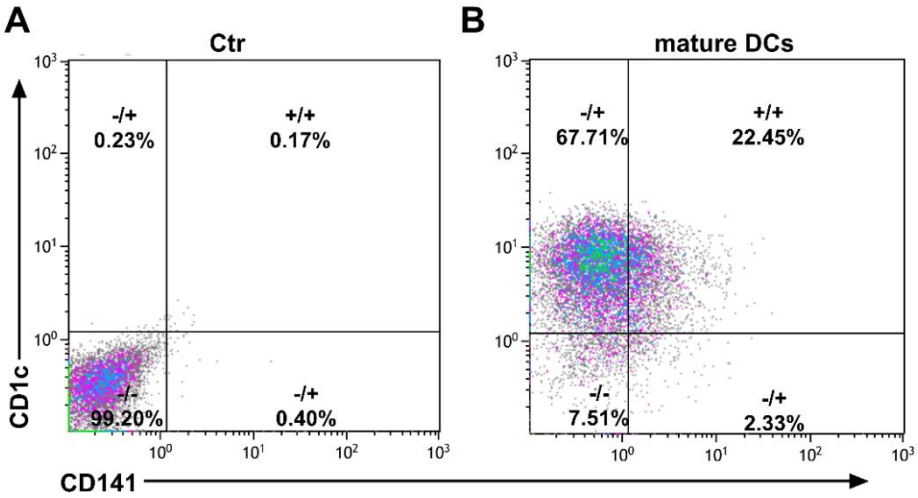

Figure 15: Expression of CD1c and CD141 on dendritic cells after 24-hour culture.
DCs were cultured for 24 hours, stained with antibodies against CD1c and CD141, and analyzed by flow cytometry. Gating was performed using DCs stained with isotype control antibodies. The figure shows representative dot plots of mature DCs expressing CD1c and CD141 in cells stained with (A) isotype control antibodies and (B) specific antibodies against CD1c and CD141.

Furthermore, the expression of Dectin-1 was investigated in DCs treated with laminarin with a yeast derived β-glucan (Nutramunity) serving as a positive control. Significantly higher proportion of DCs treated with Nutramunity expressed Dectin-1 compared to Neg-DCs (Figure 16).

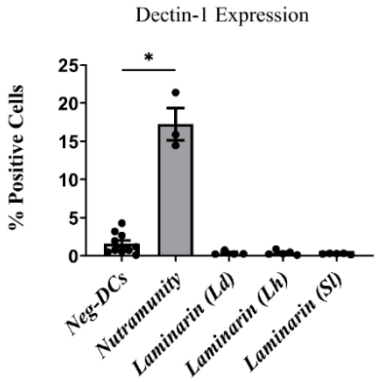

Figure 16: Dectin-1 expression of dendritic cells treated with β-glucans.
DCs were treated for 24 hours in the absence (Neg-DCs) or presence of yeast-derived β-glucan Nutramunity or laminarin derived from *L. digitata* (*Ld*), *L. hyperborea* (*Lh*), and *S. latissima* (*Sl*). Expression of Dectin-1 was measured by flow cytometry. Dectin-1 expression was compared between DCs treated with Nutramunity or laminarin and Neg-DCs using one-way ANOVA with Dunnett's post hoc test in GraphPad Prism version 10.2.1 (395). Significance is denoted as * for $p \leq 0.033$, with sample sizes ranging from n=3-10.

4.2.4 Laminari-oligosaccharides from *L. hyperborea* and *S. latissima* decrease TNF-α cytokine secretion by DCs (Paper II)

No impact on the four cytokines evaluated (TNF-α, IL-6, IL-12p40, and IL-10) was observed when DCs were treated with 100 µg/mL laminarin, or laminari-oligosaccharides derived from *L. digitata* (Paper II; Fig. 5a-5e, light grey graphs) compared to Neg-DCs. Treating DCs with laminarin from *L. hyperborea* did not affect their TNF-α secretion but treating the DCs with the smaller laminari-oligosaccharide fractions *Lh*F4 and *Lh*F5 significantly decreased their TNF-α levels by 35% and 32%, respectively, as compared to Neg-DCs (Paper II, Fig. 5a, middle grey graph). Moreover, DCs treated with laminarin polymer and *Lh*F5 secreted higher levels of IL-6 than Neg-DCs (24% and 34%, respectively) (Paper II, Fig. 5b, middle grey graph). Additionally, treating DCs with *L. hyperborea*-derived laminarin increased their IL-10 secretion compared to Neg-DCs, resulting in a 26% decrease in the PI (PI<1; Paper II, Fig. 5e, middle grey graph). No effect on IL-12p40 secretion by the DCs was observed after any of the *L. hyperborea*-derived treatments. Treatment of DCs with laminarin derived from *S. latissima*, as well as the two laminari-oligosaccharide fractions *Sl*F1 and *Sl*F2, had no impact on their secretion of any of the evaluated cytokines (Paper II, Fig. 5a-5d, dark grey graphs). However, treatment of DCs with *Sl*F3 from *S. latissima* resulted in an 18% decrease in their TNF-α secretion compared with Neg-DCs (Paper II, Fig. 5a, dark grey graph), without affecting their secretion of the other cytokines. Similarly, no impact of sodium citrate buffer on cytokine secretion by DCs was observed for any of the tested cytokines (TNF-α, IL-6, IL-12p40, or IL-10 (Paper II, Fig. S5)).

4.2.5 Modulation of cytokine secretion in DC-CD4$^+$ T-cell co-cultures in response to laminarin from *L. hyperborea*, *Lh*F5 and *Sl*F3 (Paper II)

When DCs matured in the presence of laminarin extracted from *L. hyperborea* were co-cultured with allogeneic CD4$^+$ T-cells, significantly increased IL-17, and IL-10 secretion was observed (Paper II, Fig. 6a). When DCs treated with *Lh*F5 were co-cultured with allogeneic CD4$^+$ T-cells a non-significant decrease in IFN-γ and IL-12p40 was observed (Paper II, Fig. 6b). When DCs were treated with *Sl*F3 and subsequently co-cultured with allogeneic CD4$^+$ T-cells it resulted in a significant decrease in IFN-γ, IL-12p40, and IL-10 levels by 26%, 16%, and 38%, respectively (Paper II, Fig. 6c).

4.3 Section III: The immunomodulating potential of various molecular-sized fucoidan fractions (Paper III - submitted manuscript)

This section presents the key findings from the isolation and fractionation of fucoidan derived from *S. latissima*, utilizing the endo-acting fucoidanase Psf1 to generate oligosaccharide fractions of varying sizes. The focus was on examining how these different molecular sizes of fucoidan impacted DC and T-cell responses. This is highlighted by investigating the cytokine secretions by DCs under treatment of different sized fucoidan fractions, as well as investigating the dose-dependent response of one specific sample, and how this specific sample affected T-cell responses.

4.3.1 Fucoidan fractions generated with Psf1 (Paper III - submitted manuscript)

Fucoidan from *S. latissima* (Type 1 fucoidan) was successfully isolated by researchers at DTU using a procedure similar to that described by Nguyen and colleagues (2020). These researchers also investigated the enzymatic activity of Psf1 on fucoidan samples derived from eight different species of seaweed, finding that Psf1 exhibited the highest activity on *S. latissima* fucoidan, confirmed with C-PAGE analysis (Submitted paper III, Figure 3). The C-PAGE gel revealed clear and distinct oligosaccharide bands, allowing the visualization of size distribution of resulting fucoidan oligosaccharides, with the furthest migrating oligosaccharides after 24 hours of reaction estimated to have molecular sizes of approximately DP10 to DP12, based on comparisons with the Fhf1 standard (products from a previously characterized GH107 fucoidanase [140]; Submitted paper III, Figure 6A). This result is consistent with the size-exclusion chromatography (SEC) data (Submitted paper III, Figure 6B), which showed that degradation products accumulated in the 10-30 kDa range, with no significant amounts of smaller products below 2000-3000 Da, even after an extended reaction time of 8-24 hours. The presence of multiple bands indicated that Psf1 functions as an endo-enzyme, specifically an α-endo−(1,3)-fucoidanase, given that *S. latissima* fucoidan predominantly contains α−(1,3)-linked fucose residues, which was also confirmed by ^{1}H-NMR spectrometry.

After the enzymatic reaction, a Sl MMW fraction was successfully isolated using the method outlined by Vuillemin et al. (2020). To estimate the molecular size of the samples used for immunomodulating studies, the samples underwent SEC. The results indicated that the native Sl fucoidan exhibited a peak at around 400-500 kDa, and a population of 2000-3000 kDa representing very high molecular weight fucoidan. The Sl MMW fucoidan fraction ranged between 110 and 400 kDa.

Furthermore, ^{1}H-NMR spectrometry and monosaccharide composition analysis confirmed the presence of sulfation and with fucose being abundant in all samples as

well as galactose in both fractions (Submitted paper III, Figure 7 and Table S4). The ^{1}H-NMR data also showed that both the Sl Psf1 MMW and Sl Psf1 LMW fractions, and the released oligo-/polymeric fucoidans were predominantly 4-sulfated (Submitted paper III, Figure 7).

4.3.2 Fucoidan and fucoidan oligosaccharides showed size-dependent and dose-dependent effect on IL-12p40 secretion by DCs and subsequent IFN-γ secretion by co-cultured allogeneic T cells (Paper III - Submitted manuscript)

Treating DCs with 100 µg/mL of either native fucoidan (Sl native) and its derivatives (Sl Psf1 MMW and Sl Psf1 LMW) for 24 hours had no impact on cell viability as compared to untreated DCs (Neg-DCs; Submitted Paper III, supplementary Table S2). In addition, secretion of IL-12p40 and IL-10 by DCs was not affected by the three treatments (Submitted Paper III, Fig. 8A). However, as Sl native and Sl Psf1 MMW induced non-significantly higher levels of IL-12p40 secretion and non-significantly lower levels of IL-10 secretion (22% and 25%, respectively) than that of Neg-DCs, which led to significantly increased PI (ratio of Sl-IL-12p40/Sl-IL-10), as compared to Neg-DCs (Submitted Paper III, Fig. 8A).

In contrast, DCs treated with Sl Psf1 LMW secreted non-significantly lower levels of IL-12p40 (29%) without IL-10 secretion being affected as compared to Neg-DCs (Paper III, Fig. 8A). In a subsequent experiment, treating the DCs with different concentrations of Sl Psf1 LMW (1, 10, and 100 µg/mL) a significant dose-dependent reduction in IL-12p40 secretion was observed (by 15%, 22%, and 32%, respectively), again without affecting IL-10 secretion (Submitted Paper III, Fig. 8C). This led to reduced PI ratio for Sl Psf1 LMW at 100 µg/ml as compared to Neg-DCs (Submitted Paper III, Fig. 8C). Notably, the decrease in IL-12p40 secretion with LMW fucoidan was similar to the inhibition of IL-12 secretion observed with the active form of vitamin D3 (Submitted Paper III, Figure S7).

Neither the buffer (50 mM NaCl and 10 mM $CaCl_2$) nor the enzyme present in the samples influenced the cytokine secretion or the cell viability in the DC model (Submitted Paper III, supplementary Figure S5 and Table S3).

The maturation of DCs was confirmed by the low percentage of DCs expressing the surface molecule CD14 and a high percentage of DCs expressing HLA-DR. Treatment of DCs with Sl Psf1 LMW at 100 µg/mL did not affect the ratio of DCs expressing CD14 and HLA-DR, as well as CD40, CD86, PD-L1, CD1c, and CD141 (Submitted Paper III, Fig. 8B).

DCs treated with Sl Psf1 LMW at 100 µg/mL for 24 hours and subsequently co-cultured with allogeneic $CD4^{+}$ T-cells led to significantly reduced IFN-γ levels (37%) and IL-10 levels (24%) in the co-culture supernatant compared to when untreated DCs were co-

cultured with allogeneic CD4+ T-cells (Submitted Paper III, Fig 8D). No effect on IL-17 secretion was observed (Submitted Paper III, Fig. 8D).

4.4 Section IV: The immunomodulating potential of enzymatically produced alginate derivatives (unpublished data)

The purpose of this part of the study was to investigate the immunomodulatory potential of alginate derivatives produced using different alginate lyases. Thus, this section includes the analysis of various alginate oligosaccharide fractions, including possible structural features, screening of their effects on cytokine secretion by DCs, and their possible involvement in T-cell responses.

4.4.1 Purification of alginate fractions (previous reported data by Dobruchowska et al. 2022, patent WO2015104723A1 by Hreggvidsson et al., and report for SeaMark, and unpublished data)

Alginate oligosaccharide fractions were obtained via a two-step ethanol precipitation method, and their size distribution was analyzed using TLC (Figure 17). The fractions and their proposed theoretical structural compositions—based on assumptions drawn from published and unpublished data on the enzymes' reported activities (Table 6 in Materials and Methods), as well as the TLC results presented in this chapter (Figure 17)—are summarized in Table 9. The AlyRm2 reaction produced a mixture of smaller and larger oligosaccharides, comprising predominantly G-rich and MG-rich oligosaccharides. The partially digested fractions with AlyRm3 (Figure 17, AlyRm3 (P2), top image) contained predominantly intermediate-small sized oligosaccharides, whereas the full digestion fraction with AlyRm3 (Figure 17, AlyRm3full, top image) showed a reduction in intermediate-sized oligosaccharides. Both samples comprised a mixture of M-rich, G-rich, and MG-rich oligosaccharides. Digestion with AlyPx8 resulted in a mixture of larger and smaller oligosaccharides, possibly consisting of both M, G, and MG-rich oligosaccharides, according to the TLC (Figure 17, AlyPx8(P2)) and unpublished data. AlyRm4 digestion displayed an intense band corresponding to saturated cyclic monomers (4-deoxy-L-erythro-hex-4-enopyranosyluronic acid; Figure 17, top and lower image AlyRm4). Additionally, a faint band below the cyclic monomers is attributed to free mannopyranosyluronic acid and gulopyranosyluronic acid. In the loading spot on the TLC, large oligo- and polysaccharides, too large to migrate through the TLC, were observed. Furthermore, digestion with AlyRm4 successfully removed small monomers via dialysis and precipitation, leaving a fraction consisting of a mixture of large M-G poly-and/or big oligosaccharides potentially enriched in G-content and with G-blocks at the non-reducing (Figure 17, lower image to the right).

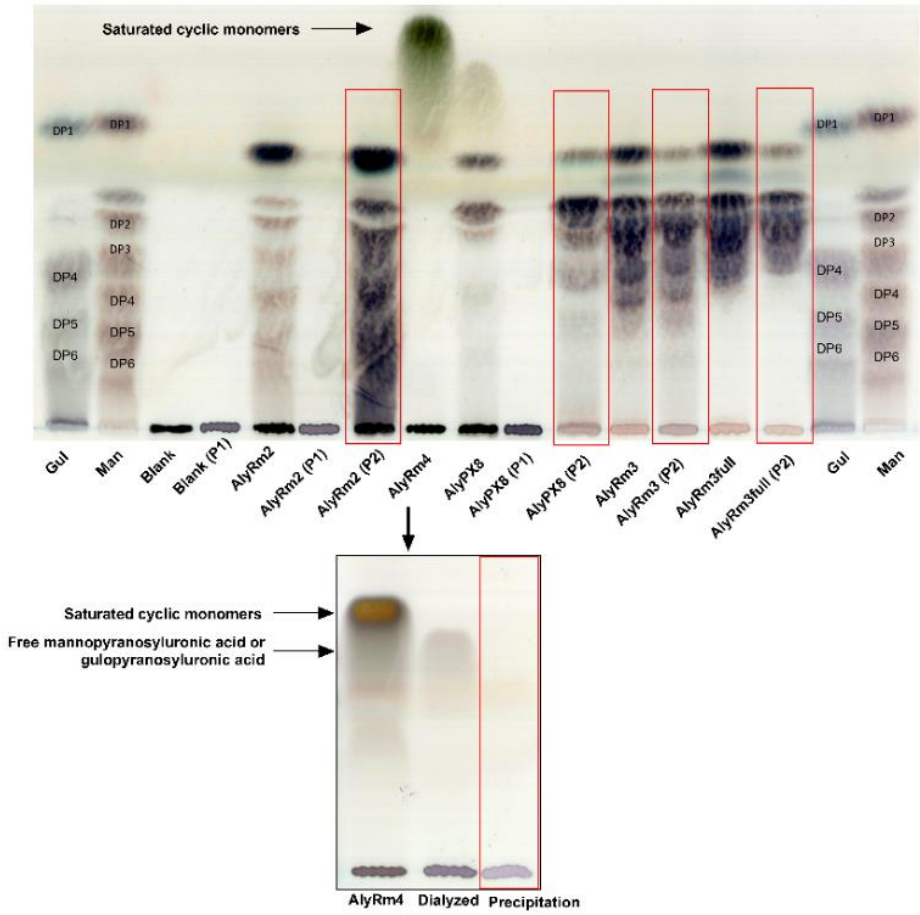

Figure 17: Overview of alginate oligosaccharide sample size distribution on TLC.
'Gul' and 'Man' denote guluronic acid and mannuronic acid, respectively, and serve as ladders with varying degrees of polymerization (DP1-DP6). 'Blank' indicates undigested alginate. P1 and P2 denote precipitation steps using 50% and 76% ethanol, respectively. AlyRm2, AlyRm3, AlyRm4, and AlyPx8 represent enzymatic reactions on alginate. Specifically, AlyRm3 represents the partially digested sample, while AlyRm3full indicates the fully digested sample. The samples used in the dendritic cell model are highlighted in red boxes, which are the 76% ethanol precipitated samples. AlyRm4 samples, highlighted with a bold arrow, show an additional dialysis step that demonstrates the removal of cyclic monomers released from alginate via an exolytic AlyRm4-catalyzed β-elimination reaction, as well as free mannopyranosyluronic acid and gulopyranosyluronic acid (middle lane, lower picture, indicated with thin arrows). Notably, the top bands (except AlyRM4 and partly AlyRM8) corresponding to monomers do not match the expected ladder patterns, likely due to the conversion of the products into their open-chain forms [141], causing them to migrate more slowly in the TLC plate. TLC images were generated by Hörður Guðmundsson (Matís) with minor modification.

Table 9. Alginate fractions used in downstream immunomodulatory studies and their theoretical structure composition after digestion with one of the four alginate lyases.

Alginate oligosaccharide fraction ID	**Theoretical structures of alginate oligosaccharide compositions**
AlyRm2	Mixture of big-small alginate oligosaccharides comprised primarily of: • G-rich Oligosaccharides: Due to the major activity on G-G bonds • MG-rich Oligosaccharides: Due to the major activity on M-G bonds • Few M-rich Oligosaccharides: Due to the minor activity on M-M bonds [142]
AlyRm3 partially digested	Mixture of intermediate-small oligosaccharides • M-rich oligosaccharides: Oligosaccharides consisting only of mannuronic acid units • G-rich oligosaccharides: Oligosaccharides consisting only of guluronic acid units • MG-rich oligosaccharides: Oligosaccharides composed of alternating or mixed mannuronic and guluronic acid units Each with a 4,5-unsaturated non-reducing-end uronic acid [141]
AlyRm3 fully digested	The same as for AlyRm3 partially digested, but primarily smaller oligosaccharides corresponding of di-, tri-, and tetrasaccharides, respectively, each with a 4,5-unsaturated non-reducing-end uronic acid [141]
AlyRm4 dialyzed	A mixture of large M-G poly-and/or big oligosaccharides potentially enriched in G-content and with G-blocks at the non-reducing end [141].
AlyPx8	A mixture of intermediate-sized and smaller alginate oligosaccharides, including M-, G-, and MG-rich varieties. Due to insufficient data on the specific enzymatic activity of AlyPx8, further details cannot be provided [unpublished].

4.4.2 AlyRm3 derived alginate oligosaccharide fractions increase IL-6 and IL-10 secretion by DCs (unpublished data)

Treating DCs with the two AlyRm3-digested oligosaccharide fractions (AlyRm3 partially digested, and AlyRm3 full digestion; 100 µg/mL) significantly increased their secretion of IL-6 (by 39% and 66%, respectively, Figure 18b), IL-10 (by 51% and 88%, respectively, Figure 18d) and IL-12p40 (by 25% and 31%, respectively, Figure 18c), as compared to Neg-DCs, without affecting the TNF-α secretion (Figure 18a). In contrast, treating DCs with any of the other alginate oligosaccharide fractions had no effect on the secretion of the investigated cytokines (TNF-α, IL-6, IL-12p40, and IL-10; Figure 18a-d).

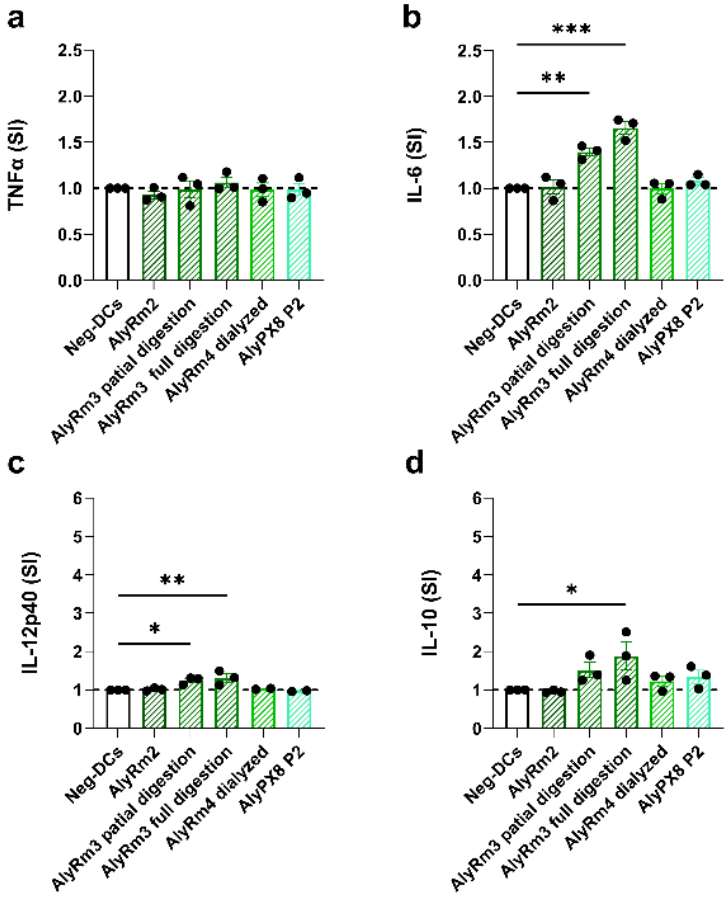

Figure 18: Effect of alginate oligosaccharide fractions on cytokine secretion by dendritic cells. The figure illustrates the impact of alginate oligosaccharide fractions (AlyRm2, AlyRm3 partical digestion, AlyRm3 fully digestion, AlyRm4 dialyzed, and Alg 8) on the secretion of TNFα (a), IL-6 (b), IL-12p40 (c), and IL-10 (d) by DCs matured and activated for 24 hours in the presence or absence of these oligosaccharides. The cytokine concentrations were measured by ELISA, and data are presented as secretion index (SI) with mean ± SEM (n=2-3). Statistical significance was assessed when possible using one-way ANOVA with Dunnett's multiple comparisons test using graphPad Prism (10.1.2 (324)). The * indicate $p \leq 0.033$, ** $p \leq 0.002$ and *** $p<0.001$.

4.4.3 AlyRm3 fully digested oligosaccharide fraction promote a Th1 response (unpublished data)

As the fully AlyRm3-digested oligosaccharide sample caused DCs to secrete raised levels of IL-6, IL-12p40, and IL-10, the effect of the DCs on activation of allogeneic CD4+ T-cells was analyzed in co-culture experiments (Figure 19). This resulted in a significant increase in IFN-γ and IL-10 levels in the co-culture supernatant (Figure 19). A great donor variation was observed in IL-17 levels, resulting in non-significant data, and there was no effect on IL-12p40 levels (Figure 19).

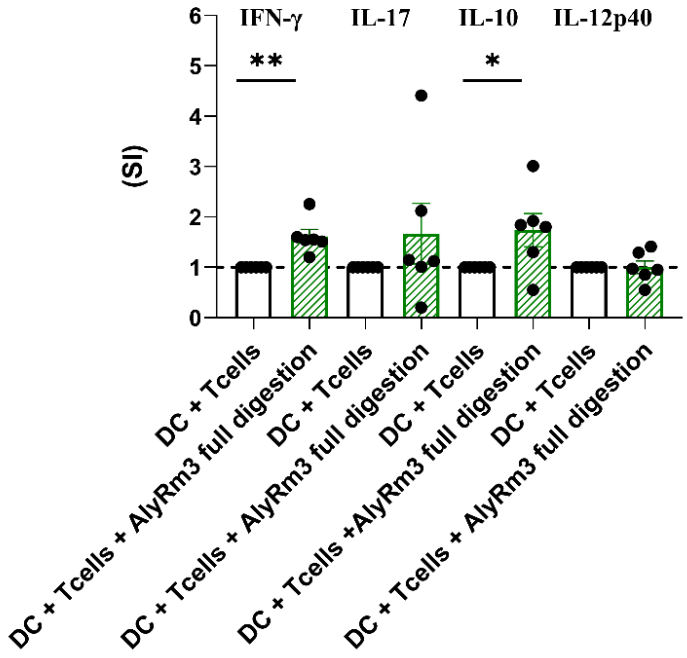

Figure 19: Effect of fully digested alginate oligosaccharide fraction AlyRm3 on dendritic cell and T-cell interaction.
The secretion of IFN-γ, IL-17, IL-10, and IL-12p40 in the supernatant after co-culture of DCs matured without (DC + T-cells) or with AlyRm3 fully digested oligosaccharides at a concentration of 100 µg/mL (DCs + T-cells + AlyRm3 fully digested), and allogenic CD4+ T-cells at a ratio 1:10 was measured by ELISA. Results are presented as mean ± SEM of secretion indexes (SI) of INFγ, IL-17, IL-10, and IL-12p40. Experimental treatments were compared to the DC+ T-cells by unpaired t-test using GraphPad Prism version 10.2.1 (395). Significance markers in the results are denoted as follows: * for $p \leq 0.033$, ** for $p \leq 0.002$, and *** for $p < 0.001$, n=5-6.

5 Discussion

The aim of the present thesis was to identify and characterize the structural complexity and functional diversity of marine-derived polysaccharides and their role in immunomodulation by employing an enzymatic refinement approach to modify and potentially alter immunomodulating activities.

Section I covers the characterization of marine-derived sulfatase from a marine *Arthrobacter* strain. It focuses on the cloning of a marine-derived sulfatase gene *sulA1* and the detailed characterization of the recombinant sulfatase SulA1. It addresses the aim to characterize a newly identified sulfatase's enzymatic activity and substrate specificity, providing insights into its role in marine polysaccharide metabolism and potential applications in modifying polysaccharides for immunomodulatory purposes. The main findings were the discovery of the *sulA1* gene encoding the sulfatase SulA1 from the marine *Arthrobacter* strain MAT3885. SulA1 co-localizes with a chondroitin lyase gene, exhibits specificity for GalNAc4S, and shows optimal activity between pH 5.5 and 7.0 at 40°C.

Section II covers the refinement and immunomodulation of laminarin. It addresses the structural complexity of laminarin extracted from brown seaweed, along with its enzymatic modification. This relates to the aims of refining laminarin from *L. digitata*, *L. hyperborea*, and *S. latissima* and assessing their immunomodulating potential, including detailed structural analysis and production of laminari-oligosaccharide fractions providing a foundation for understanding how structural variations influence bioactivity. Overall, significant differences in sugar composition were observed among laminarin from different brown seaweed species, with high mannitol content in locally sourced *L. digitata* and high glucose content in *L. hyperborea* and *S. latissima*. FT-IR and ^{1}H-NMR spectroscopy analyses revealed species-specific structural differences, including variations in β 1,6-linkages. Additionally, MALDI-TOF MS confirmed the presence of poly- and oligosaccharides predominantly around DP24 or DP25. The immunomodulating effects of laminarin and laminari-oligosaccharides on DCs from *L. digitata*, *L. hyperborea*, and *S. latissima* reveal that laminarin extracts and derivatives had minimal impact on DC maturation and activation. However, specific laminari-oligosaccharides (*Lh*F4, *Lh*F5, and *Sl*F3) reduced TNF-α secretion in a size-dependent manner, indicating immunomodulatory potential. Additionally, laminarin from *L. hyperborea* uniquely increased IL-6 and IL-10 secretion, suggesting anti-inflammatory properties. Furthermore, when examining how these DCs affected T-cell responses, DCs treated with laminarin from *L. hyperborea* increased IL-17 and IL-10 levels in $CD4^{+}$ T-cells, indicating a regulatory role, while *Sl*F3 treatment of the DCs reduced IFN-γ, IL-

12p40, and IL-10 secretion by the T-cells, suggesting a decrease in type 1 immune response.

Section III covers the immunomodulating potential of fucoidan. It explores the immunomodulating effects of fucoidan and fucoidan oligosaccharides, generated using an enzymatic refinement approach. This directly relates to the aim of studying the immunomodulating potential of various molecular-sized fucoidan fractions, offering insights into how different fractions influence immune responses. The main findings were that the molecular size of fucoidan from *S. latissima* influenced the effects on cytokine secretion by DCs. High and MMW fucoidan samples led to a significant increase of the PI (PI>1), indicative of an overall pro-inflammatory response. Conversely, Sl PSf1 LMW significantly decreased IL-12p40 secretion in a dose-dependent manner without affecting IL-10 secretion, resulting in a significant decrease of the PI, suggesting an anti-inflammatory effect. Furthermore, when examining the impact of these DCs on T-cell responses, Sl PSf1 LMW-treated DCs led to reduced IFN-γ secretion by T cells, suggesting a suppression of type 1 immune responses.

Section IV covers the investigation of alginate derivatives. It relates to the aim to investigate the immunomodulating potential of enzymatically produced alginate derivatives, using different alginate lyases. Five alginate oligosaccharide samples with varying sizes and compositions were obtained using four different alginate lyases (AlyRm2, AlyRm3, AlyRm4, and AlyRX8) on alginate from *M. pyrifera*. The AlyRm3-digested samples, possibly enriched in M- and MG-blocks, significantly increased IL-6, IL-12p40, and IL-10 secretion by DCs. These smaller oligosaccharides appeared to promote pro-inflammatory responses, while no effect was observed for any of the other alginate oligosaccharides. Co-culture experiments showed that DCs treated with fully AlyRm3-digested oligosaccharides had elevated IL-12p40 and IFN-γ levels, indicating they were promoting type 1 immune responses.

Overall, the thesis contributes valuable knowledge to the field of marine polysaccharides and their potential therapeutic applications in immunomodulation.

5.1 Section I: Cloning and characterization of SulA1 from a marine *Arthrobacter* strain

The discovery of the FGly-SULF encoding gene, *sulA1*, from the marine *Arthrobacter* strain MAT3885, represent a significant advancement in the field of marine polysaccharide biochemistry. This sulfatase was identified in the cluster with the chondroitin lyase gene *choA1*, isolated previously [143]. Such genetic co-localization suggests a coordinated role of SulA1 in the degradation of complex polysaccharides like CS and harbors the possibility that it may be used as a modifying enzyme in enzymatic refinement approaches. Moreover, the identification of SulA1 adds to the

repertoire of enzymes potentially involved in marine polysaccharide metabolism, contributing to our understanding of microbial adaptation to the marine environment.

The bioinformatic analyses revealed that SulA1 belongs to the family 1 sulfatases, characterized by conserved Type 1 sulfatase motif C/SXPXR, consistent with findings in the literature [57,58,144]. Structural alignments and homology modeling further confirmed these findings, highlighting the evolutionary conservation of its enzymatic structure. Identification of the catalytic residue (Cys57) and the metal-ion-binding site residues (Asp17, Asp18, Asp277, and Asn278) provided central insights into SulA1's enzymatic mechanism and substrate binding specificity aligning with the established understanding that FGly-SULFs typically require divalent cations such as Ca^{2+} (and occasionally Mg^{2+}) to facilitate substrate binding and polarization [145–147]. This was also observed as an increase in the catalytic activity using *p*NCS as a substrate. However, integrating the DSF assay with varying concentrations of calcium and EDTA revealed that calcium did not enhance the thermostability of SulA1. This was evidenced by a slight decrease in T_m with increased calcium concentration and no effect on T_m with EDTA. Thus, the presence of Ca^{2+} may induce conformational changes that compromise the overall stability of SulA1.

Comparing the homology-based model using YASARA and the AlphaFold2 structural prediction for SulA1 reveals notable differences, particularly in loop structures and the orientation of key residues. The homology-based model, which was constructed from five PDB templates, shows discrepancies in loop sizes and orientations due to the dependence on structurally divergent templates that may not accurately capture the flexible regions. In contrast, the AlphaFold2 model, which showed high pLDDT scores and produced an overall better structure, still exhibited variation in loop regions, particularly around Ala360-Val376 and in the C-terminus, and differences in the orientation of Arg61 [130]. These differences can be attributed to the characteristic flexibility and conformational variability of loop regions [148], which are challenging to predict accurately with both methods. Thus, the less precise modeling of flexible loops in the homology approach and the limitations of AlphaFold2's training data and algorithms in handling dynamic regions explain the observed variations.

To validate the accuracy of the amino acid sequence used in these models, PMF was performed using the recombinant protein. The mass fingerprinting data confirmed a 100% identity with the peptide fragments generated in silico using MASCOT, indicating the amino acid sequence used in the structural models is accurate and aligns perfectly with the experimentally derived sequence, thus supporting the validity of the sequence used in structural modeling. However, the partial coverage (40% query coverage) indicated that while the sequence data is reliable, additional validation may be required for regions not covered by this technique. The results support the observed differences in the models, which are most likely due to limitations in modeling methods rather than errors in the sequence data.

The enzymatic properties of SulA1 were initially assessed using the synthetic substrate *p*NCS, demonstrating that SulA1 displayed both pH and temperature sensitivity. The observed temperature sensitivity was consistent with findings from other CS/DS sulfatase studies, which have shown that temperatures exceeding 40°C have a negative impact on the relative activity, while relatively high activity can be obtained at room temperature [149,150]. The narrow pH optimum observed with *p*NCS as substrate contradicted the data obtained with DSF data using different pH levels, and TLC data analysis using GalNAc4S as substrate under different pH conditions. While *p*NCS data suggested a very specific pH optimum at 5.5, both DSF and TLC data indicated that SulA1's optimal working pH range was broader, between pH 5.5 and 7.0. This wider range aligns with the characterization of SulA1 as a cytosolic enzyme. The discrepancy between results obtained with different substrates likely reflects an artifact using the synthetic *p*NCS. Furthermore, estimating kinetic parameters using *p*NCS as substrate proved impractical due to a linear substrate concentration-velocity relationship. This suggested that SulA1 exhibits low affinity for *p*NCS, consistent with earlier research for other sulfatases [151,152]. Therefore, while *p*NCS provides a convenient method for initial activity test of potential FGly-SULFs, its suitability for comprehensive kinetic studies or detailed characterization studies is limited. Consequently, identifying the natural sulfated substrate for the enzyme became crucial.

Among several different sulfated molecules tested, SulA1 demonstrated activity exclusively towards the monosaccharide GalNAc4S. This aligns with the CS sulfation pattern (0.5% CS 4S from Sigma or CS 6S prepared at Matís) used to isolate the marine *Arthrobacter* strain MAT3885 and the genetic position of the *sulA1* gene upstream of the chondroitin lyase gene as characterized by Kale and colleagues [143]. These findings suggested that SulA1 is highly specific and likely plays a role in the final steps of the CS degradation pathway, consistent with suggested pathway by Wang and colleagues [153]. Furthermore, SulA1's strict preference for the sulfated monosaccharide unit contrasts with other CS enzymes like endoVB4SF from *Vibrio* sp. and exoPB4SF from *Photobacterium* sp., which exhibit activity against both poly- and disaccharides of CS with 4-*O*-sulfation [145,150]. Using GalNAc4S as substrate, the specific activity of SulA1 was determined at pH 5.5 and pH 6.5 to be 6.8 mU/mg SulA1 and 14.0 mU/mg SulA1, respectively, using 20 mM and 15 mM GalNAc4S, at 40°C for 30 min. Compared to other CS-sulfatases acting on GalNAc4S, these values are low [145,150] but higher than the exo-acting GalNAc6S acting sulfatase PB_3285 (3.64 mU/mg) [146].

Given the specific activity towards GalNAc4S, it is likely that the neighboring sulfatase gene, *sulA2*, located within the same gene cluster as *sulA1*, encodes an enzyme possessing complementary sulfatase activity, potentially targeting the GalNAc6S unit. This speculation was supported by the characterization of ChoA1 as a chondroitin AC lyase [143] and the high topology conservation of SulA2 with an exolytic CS *N*-acetyl-galactosamine-6-*O*-sulfatase [146], implying functional conservation.

As Michaelis-Menten kinetics provide a foundational framework for understanding enzyme function, efficiency, and regulation, it is a critical tool in biochemical research. We observed a K_m value of 6.94 ± 0.053, at pH 5.5, using GalNAc4S as substrate. At pH 6.5, which is the optimal for this experiment according to the DSF and TLC data, Michalis-Menten behavior was observed, yet additional data points are necessary to obtain a more accurate K_m value. Despite these findings, the high cost of GalNAc4S substrate presents a significant limitation for our study.

The purified SulA1 retained its activity for minimum 5 weeks when stored in 100 mM sodium acetate buffer at pH 5.5, supplemented with 20% glycerol at –80°C. This robust preservation supports its potential for industrial applications, reducing cost, and ensuring reproducibility in e.g., industrial processes. However, due to its limited substrate range, SulA1 may not be the ideal enzyme for refining a broad spectrum of sulfate marine polysaccharides. Nonetheless, it could play a significant role in modifying the immunomodulatory properties of CS and advancing understanding of the structure-function relationship in immunomodulation. In fact, we tested the effects of chondroitin sulfate with a DP4 (CS-AC, DP4) and the GalNAc4S monosaccharide on the cytokine secretion (Appendix A, Table 11) in the DC-model (described in the Materials and Methods). Both compounds were found to decrease IL-12p40 levels, with CS-AC having the most pronounced effect. No effect on IL-10 secretion was observed for either compound. This selective modulation could be attributed to several factors. The longer polysaccharide chain of CS-AC compared to GalNAc4S allows for more effective interaction with cellular receptors and proteins, providing more opportunities for binding and signaling, which can lead to more significant biological effects. Additionally, the extended chains of CS-AC might contribute to greater structural stability, influencing cellular responses more effectively than the shorter GalNAc4S monomer. The higher sulfate content in CS-AC might also play a role in its enhanced effect. However, the lack of a pure desulfated CS sample prevented us from further exploring this hypothesis.

5.2 Section II: Laminarin refinement and immunomodulating potential of laminarin and enzymatically modified laminarin

Seaweed represents a promising source of biomolecules with diverse applications in industries, such as pharmaceuticals and food. To fully benefit from this resource, comprehensive insights into its chemical composition are essential. For laminarin, factors like purity, DP, DB, and linkage profoundly influence its bioactive properties [154]. However, concerns arise from variations in extraction methods and sample preparation, which can lead to structural disruption of the native structure [1,155] high ash content and other contaminants, such as co-extraction of other polysaccharides. These issues contribute to the inconsistency in reported bioactivity across the literature. Furthermore, detailed structural analysis of the specific laminarin under investigation, as

well as species orientation is often lacking, complicating definitive conclusions regarding its bioactivity.

In this study, a significant focus was placed on elucidating the structure-function relationship of native laminarin molecules and their oligosaccharide derivatives. The laminarin molecules were sourced from three different brown seaweed species to ensure structural diversity. However, conducting a detailed structural analysis of laminarins poses challenges due to their complexity and resource-intensive nature. Therefore, careful management of extraction methods, contaminants, and complexities of structural analysis is crucial to ensure the reliability and reproducibility of results. Despite these challenges, the insights gained hold potential to significantly advance the understanding and possible therapeutic application of laminarin.

5.2.1 Extraction and purification of laminarin: Successes, challenges, and structural variability among brown seaweed species

In this study, laminarin was extracted from *L. hyperborea* and *S. latissima* using a two-step water extractions protocol and subsequently purified to homogeneous state. The extraction process involved initial precipitation of trace amounts of alginate with $CaCl_2$, followed by removal of larger molecules such as fucoidan using a 10 kDa filtration step, and finally, the elimination of smaller degradation products and ash with 1 kDa filters. The conductivity was monitored throughout the filtration process, as adding $CaCl_2$ contributed to the ash content. A decrease in conductivity was observed after 1 kDa filtration, indicating the effective removal of ionic contaminants. However, since conductivity only measures the ability of a solution to conduct electricity and does not provide specific information about the exact composition or quantity of ash content, it is crucial to complement this measurement with other analytical methods for a comprehensive assessment. This need for comprehensive analysis was highlighted by the findings in the locally sourced *L. digitata* laminarin extract, which exhibited low conductivity but high ash content (33.5%) in contrast to the laminarin extract from *L. hyperborea* and *S. latissima*.

Monosugar analysis revealed significant differences in the sugar composition of laminarin from different seaweed species. The locally sourced *L. digitata* laminarin showed notably high mannitol content (29.1% *w/dw*) and low glucose content (15.3% *w/dw*). In contrast, laminarin extract from *L. hyperborea* contained 2.25% *w/dw* mannitol and 52.2% *w/dw* glucose, while *S. latissima* extract had 4.7% *w/dw* mannitol and 74.6% *w/dw* glucose. This variability highlights the diverse amounts of laminarin in the biomass from these three seaweed species, a phenomenon also documented for other seaweeds [156]. It also emphasizes the critical role of high-quality biomass in extraction processes. The higher mannitol content compared to glucose content in locally sourced *L. digitata* laminarin extract also posed a threat that using this sample for bioactivity studies would lead to investigating the effect of mannitol rather than

laminarin, possibly leading to misinterpretation of laminarin's effects and inconsistent results. To ensure consistency and reliability in subsequent analyses, commercially available laminarin from *L. digitata* (Sigma Aldrich), characterized by high glucose content (78% *w/dw*) and low mannitol content (0.4% *w/dw*), was used instead.

Fucoidan was detected in the laminarin extract from *L. hyperborea* through monosugar and ^{1}H-NMR analysis. Due to fucoidans' documented bioactivity, including immunomodulation [86,87], which might skew results obtained by the laminarin itself, further purification was necessary. This was achieved using DEAE-cellulose anion-exchange chromatography and was an important step for the subsequent investigation of laminarin structure-function relationship involved in immunomodulatory responses.

FT-IR spectroscopy confirmed the overall structure and purity of laminarin from all three species, displaying characteristic laminarin patterns consistent with those reported in the literature [157,158]. Significant differences were noted in -OH and C-H stretching vibrations. Lower OH stretching vibration in laminarin from *S. latissima* (3314 cm^{-1}) suggested stronger hydrogen bonding and increased branching compared to L. *digitata* (3347 cm^{-1}) and *L. hyperborea* (3361 cm^{-1}). Similarly, C-H stretching vibrations at a lower wavenumber in *S. latissima* laminarin (2887 cm^{-1}) indicated a potentially higher branching content compared to *L. digitata* and *L. hyperborea* (2917 cm^{-1}).

Structural insights from ^{1}H-NMR revealed varying M:G ratios. The M:G ratio represents the proportion of laminarin chains with mannitol at the reducing end compared to those with glucose, offering insight into their distribution within the sample. The laminarin from *L. digitata* and *S. latissima* had a ratio of 2.5:1, indicating that the laminarin from these two species contains approximately 2.5 times more laminarin with mannitol on the reducing end than chains with glucose on the reducing end. In contrast, laminarin from *L. hyperborea* displayed a 1:1 ratio, indicating an equal presence of both chain types. These ratios and the overall mannitol content aligned with existing literature [17,159,160]. Moreover, ^{1}H-NMR data revealed distinct structural features in the laminarin from the three species, showing that laminarin from *S. latissima* and *L. digitata* contained both longer and shorter β–1,6-side chains, either as branches or intrachain links, with *S. latissima* laminarin exhibiting a notable higher content of β–1,6-linkages (21%), compared to *L. digitata* laminarin (6.5%) and *L. hyperborea*, which mainly consisted of the linear β–1,3-linked backbone, only contained minimal β–1,6-linkages (approximately 4%). These findings aligned well with the FT-IR observations, underscoring species-specific structural differences, likely influenced by factors like harvesting season and environmental conditions at which the seaweed was harvested [1,156].

MALDI-TOF MS confirmed that the laminarin samples comprised a mixture of poly- and oligosaccharides, predominantly DP24 or DP25 (~5 kDa), consistent with literature [1,14,15]. Total phenolic content assessed by TPC assay showed undetectable levels of phenolic compounds in laminarin extract from *L. digitata* and *L. hyperborea*. In

contrast, laminarin from *S. latissima* showed low phenolic levels (1.03 ± 0.05 mg PGE/100 g lyophilized laminarin), which is significantly lower compared to findings in other studies, e.g., ~4 g PGE/100 g lyophilized seaweed extract from *S. latissima* and up to 24.2 g PGE/100 g lyophilized seaweed extract from *Fucus vesiculosus* [161] and 20-30 mg PGE/100 g of dried biomass from *L. hyperborea* and *Ascophyllum nodosum* [15]. The undetectable or low polyphenol content observed in this study aligns with the understanding that species like *F. vesiculosus* and *A. nodosum* typically contain significantly higher levels of polyphenols and lower laminarin content compared to *S. latissima* and *Laminaria* species. Moreover, ^{1}H-NMR analysis confirmed the absence of phenolic compounds, validating the homogeneity and high purity of the extracts. Discrepancies between ^{1}H-NMR and TPC-assay for *S. latissima* laminarin may stem from oxidation of non-phenolic compounds like mannitol, impacting the TPC accuracy, as described by Sardari and colleagues [162].

In conclusion, this part of the study elucidates diverse laminarin compositions among species, highlighting structural nuances crucial for bioactivity. Future research should further explore these variations to optimize extraction methods to take full advantage of laminarin's potential in various applications.

5.2.2 The structural complexity of laminari-oligosaccharides for improved immunomodulating elucidation

As highlighted in the introduction section 1.8.4, various bioactivities have been reported for different laminarin molecules. However, there is a lack of detailed information regarding specific structural elements responsible for these activities. To address this knowledge gap, several laminari-oligosaccharide fractions using the laminaripentaose-producing endo-1,3–β-glucanase, LPHase, were successfully produced. This approach enabled the creation of laminari-oligosaccharide fractions with similar DP-sizes, verified by MALDI-TOF MS, but with distinct β–1-6-linkage in the form of branching and intrachain-linkage content, confirmed with 1D/2D ^{1}H-^{13}C NMR analysis.

The laminari-oligosaccharides derived from *L. hyperborea* exhibited an increase in β–1,6-linkage content compared to the native laminarin polymer (4% for the laminarin polymer, 11% for *Lh*F1, 7% for *Lh*F2, 4% for *Lh*F3 and *Lh*F4, and 7% for *Lh*F5). In contrast, laminari-oligosaccharides derived from *S. latissima* and *L. digitata* showed a gradual decrease in β–1,6-linkage content with decreasing DP range. This suggests that the short single residue branches unique for *L. hyperborea* laminarin are well fitted in the active site of LPHase. Conversely, the more complex and potentially irregularly occurring branching points in laminarin from *L. digitata* and *S. latissima* may hinder substrate binding in the enzyme, despite the wide groove observed around the active site of LPHase [163], which could facilitate the accommodation of substrates with a certain degree of branching. Furthermore, the presence of intrachain links observed in

laminarin and laminari-oligosaccharides from *L. digitata* and *S. latissima* suggests a close proximity of these links that may prevent cleavage by LPHase.

^{1}H-NMR data revealed significant citric acid content in all fractions, originating from the hydrolysis of the laminarin using sodium citrate buffer with LPHase. Interestingly, only traces were observed in the laminari-oligosaccharide fractions derived from *L. hyperborea*, potentially due to the less branched structure, minimizing interactions between the sodium citrate buffer and the laminarin. This likely contributed to a more efficient purification on the size exclusion Superdex™ 30 HiLoad 26/600 column.

This study clearly demonstrates that structural variations in laminarin, particularly the degree of β–1,6-linkage and intrachain links, significantly influence their enzymatic degradation by LPHase. Laminari-oligosaccharides derived from *L. hyperborea*, characterized by higher β–1,6-linkage content and no intrachain linkages, are more effectively processed by LPHase compared to those from *S. latissima* and *L. digitata*. These findings underscore the importance of structural elucidation in understanding enzymatic activity and highlight potential applications in biotechnological processes involving laminarin degradation.

5.2.3 The immunomodulating effects of laminarin and laminarin derivatives on dendritic cells

The immunomodulating effects of laminarin and laminari-oligosaccharides from *L. digitata*, *L. hyperborea*, and *S. latissima* using an *in vitro* DC model were thoroughly investigated. Our findings indicated that neither the laminarin extracts nor the laminari-oligosaccharides had a noticeable impact on the maturation and activation status of the DCs, as evidenced by unaffected expression of maturation markers compared to Neg-DCs. These maturation markers included the absence of expression of the monocyte marker CD14 and a high percentage of DCs expressing the antigen-presenting molecule HLA-DR, the co-stimulatory molecules CD40 and CD86, and PD-L1, a molecule involved in preventing excessive inflammation [164].

Interestingly, a higher proportion of the DCs expressed the cDC2 marker CD1c [165] compared to the cDC1 marker CD141 [69]. However, the expression of these markers was unaffected following treatment with laminarin and laminari-oligosaccharides. These findings are consistent with the use of moDCs in this study, as these cells are known to predominantly express CD1c [69,166,167]. CD1c-expressing DCs, primarily associated with cDC2, are crucial for activation and differentiation of $CD4^{+}$ T-cells [167]. This supports the application of the DC model used in this study, as it is advantageous for investigating interactions between DCs and $CD4^{+}$ T-cells, with potential to provide detailed insights into the immunomodulatory effects of laminarin and laminari-oligosaccharides, in order to predict their potential therapeutic applications.

It was observed that the small population of DCs expressing CD141 predominantly co-expressed CD1c. This suggested that some of the DCs possessed the potential to cross-present laminarin and laminari-oligosaccharides, akin to the cDC1 subset essential for cytotoxic $CD8^+$ T-cell activation [69]. This speculation is supported by previous studies, such as that by Haniffa and colleagues, demonstrating the ability of *in vitro* moDCs to cross-present hepatitis B surface antigen [168].

Although the laminarin and laminari-oligosaccharides did not affect expression of surface molecules on the DCs, they affected their cytokine secretion, suggesting distinct immunomodulatory potentials among the samples. While laminarin samples derived from *L. digitata* showed no significant effect, specific laminari-oligosaccharides (*Lh*F4, *Lh*F5, and *Sl*F3) caused a decrease of TNF-α secretion by DCs in a size-dependent manner. The variability in cytokine responses underscored the influence of structural features beyond size, such as β–1,6-linkages and intrachain links, in laminari-oligosaccharides. A plausible explanation for this difference in secretion could be the need for a specific percentage of β–1,6-linkages to affect TNF-α secretion by the DCs. The laminari-oligosaccharide fractions *Ld*F3 and *Ld*F4, which had no effect, comprised only 3% β–1,6-linkages. In contrast, both *Sl*F3 and *Lh*F5 affected TNF-α secretion by the DCs, and both samples contained higher percentages of β–1,6-linkages (11% and 7%, respectively). While *Sl*F3 included both branches and intrachain links, *Lh*F5 lacked the latter, potentially linking the effect on TNF-α secretion to the β–1,6-branching rather than intrachain links in the laminari-oligosaccharides. This can explain the ineffectiveness of the small laminari-oligosaccharide fractions derived from *L. digitata* (*Ld*F3 and *Ld*F4) to affect TNF-α secretion by DCs as compared to Neg-DCs, despite sharing some structural similarities to *Lh*F5 (short side chains and lacking intrachain links).

Under normal immune responses, TNF-α is crucial for increased blood vessel permeability and subsequent influx of other immune cells to the site of infection [169,170]. However, an inappropriate or excessive production of TNF-α can lead to tissue damage and associated inflammatory-mediated diseases, such as inflammatory bowel disease, rheumatoid arthritis, and psoriasis, as reviewed in several articles [171–174]. Thus, the observed effect of *Lh*F4, *Lh*F5, and *Sl*F3s on TNF-α secretion by the DCs suggests a potential for tailoring laminari-oligosaccharides as supplements with anti-inflammatory effects, potentially useful for managing chronic inflammatory diseases.

Interestingly, only laminarin from *L. hyperborea* induced a change in cytokine profile characterized by increased IL-6 and IL-10 secretion compared to Neg-DCs, indicative of anti-inflammatory properties. The increase in IL-10 secretion by DCs treated with laminarin from *L. hyperborea* supports it having an anti-inflammatory effect, as IL-10 plays an important role in limiting excessive immune responses [175]. Notably, *Lh*F5 also caused an increase in IL-6 secretion. IL-6 is typically recognized for its pro-inflammatory role, promoting immune responses and inflammation. However, it can

also exhibit anti-inflammatory effects by inhibiting TNF-α and IL-1 secretion and inducing IL-10 [176,177]. The observed increase in IL-6 secretion together with the decreased secretion of TNF-α observed when DCs were treated with *Lh*F5 could be linked to the anti-inflammatory properties of IL-6. This further suggests that laminari-oligosaccharides can be tailored to achieve specific immune-modulating effects.

Laminarin has been extensively studied for its ability to activate myeloid phagocytes, including DCs, primarily through its binding to the major β-glucan receptor, Dectin-1, in a similar manner as observed for fungal β-glucans [178–180]. However, small water-soluble laminarin compounds have shown lower efficacy in stimulating immune responses compared to large particulate β-glucans, such as those from yeast. Furthermore, soluble β-glucans such as laminarin have also been reported to inhibit Dectin-1-mediated responses to particulate β-glucan in phagocytotic cells [181]. This study revealed that laminarin does not enhance Dectin-1 expression on DCs compared to Neg-DCs, unlike the yeast-derived Nutramunity, which induced increased Dectin-1 expression. This suggests that while laminarin efficiently binds to Dectin-1, it is incapable of activating the receptor, thus possibly acting through alternative receptors, such as complement receptor 3 (CR3) or TLRs [182,183]. However, this study did not explore other receptors beyond Dectin-1, which could have provided additional insights into laminarin's immunomodulatory mechanisms.

5.2.4 The immunomodulating effects of laminarin and laminari-oligosaccharides on DCs and T-cell interactions

The investigation into how laminarin from *L. hyperborea*, and the laminari-oligosaccharides *Lh*F5 and *Sl*F3 influence DCs and subsequently their interactions with $CD4^+$ T cells provides valuable insight into their potential as immunomodulating agents. This study highlighted significant differences in cytokine profiles induced by these laminarin and laminari-oligosaccharides in the DCs model, suggesting that structural variations may critically impact their interaction with immune receptors and their ability to modulate DC-T cell interactions.

Specifically focusing on laminarin from *L. hyperborea*, and the laminari-oligosaccharides *Lh*F5 and *Sl*F3, their effects on cytokine secretion by DCs and subsequent effect on co-cultured allogeneic $CD4^+$ T-cells were examined. Secretion of IFN-γ and IL-17 was monitored as indicators of Th1 and Th17 responses, respectively [184,185]. IL-10 secretion may be an indication for increased activity of Treg cells [97,175], but it must be kept in mind that IL-10 can also be secreted by DCs. This study demonstrated that when DCs matured in the presence of the laminarin from *L. hyperborea* were co-cultured with allogeneic $CD4^+$ T-cells, a significant increase in IL-17 and IL-10 levels was observed. The elevation in IL-17 secretion might be attributed to increased IL-6 secretion observed in the laminarin-treated DC culture, as IL-6 is a known inducer of Th17 differentiation. This implies a potential role for *L. hyperborea* laminarin

in type 3 immune responses, which are mainly directed against extracellular bacteria and fungi [186–188]. Moreover, the increase in IL-10 secretion in the co-culture supernatant might be the result of DCs treated with laminarin from *L. hyperborea*, but it can also be derived from the regulatory $CD4^+$ T-cells. In either case, the high levels of IL-10 secretion are suggestive of a regulatory role of laminarin.

Co-culture of $CD4^+$ T-cells and DCs treated with the laminari-oligosaccharide fraction *Lh*F5 resulted in a non-significant decrease in IFN-γ and IL-12p40 secretion compared to co-culture of $CD4^+$ T-cells and untreated DCs. In contrast, *Sl*F3 treatment of DCs resulted in a significant decrease in IFN-γ, IL-12p40, and IL-10 secretions when co-cultured with $CD4^+$ T-cells. The decrease in IL-12p40 and IFN-γ secretion observed in response to *Sl*F3 treatment suggests a decrease in type 1 immune response, as IL-12 is the main cytokine inducing Th1 differentiation of naïve T-cells [189], which is characterized by immunity against intracellular bacteria [187,188]. Although IL-10 secretion was also decreased in the co-culture supernatant when DCs had been matured in the presence of *Sl*F3, previous results have shown that reduction in IL-10 secretion in the co-cultures may not affect the ability of IL-12p40 to influence IFN-γ secretion [190,191].

These results contribute to a deeper understanding of how size and structural variation of laminarin and laminarin derivatives influence immune responses, providing valuable insights into their mechanisms of action and potential therapeutic applications in immune disorders. Additionally, this study suggests that laminarin and its derivatives can exhibit both pro-inflammatory and anti-inflammatory effects, depending on their specific structure and the immune context in which they are applied. However, further exploration is warranted to elucidate the specific receptor interactions and signaling pathways involved, which could optimize the possible development of laminarin-based therapies. Moreover, evaluating cytokine production over different time points could reveal dynamic changes and better characterize the sample's immunomodulatory potentials.

5.3 Section III: Refinement of fucoidan and immunomodulating potential

Like laminarin, fucoidan has been extensively investigated for its bioactive properties, including immunomodulation [86,87]. However, several challenges and questions related to measuring its bioactivity have been raised. These include the heterogeneous composition of fucoidan in terms of molecular weight, sulfate content, and sugar composition. Additionally, the source variability, such as seaweed species, geographic location of harvest, and extraction methods, can alter the structure of fucoidan and consequently affect its bioactivity. The purity of fucoidan is also critical, as contaminants can interfere with bioactivity assays. Moreover, the choice of bioactivity assays and the

conditions under which they are conducted can significantly influence the results [27,192].

To gain insights into the structure-function relationship of native fucoidan and various sized fucoidan oligosaccharide derivatives on immunomodulation, more than 20 samples were screened in the DC model (Appendix A). The samples that showed the greatest impact on cytokine secretion by DCs were subsequently investigated in detail. This approach aimed to identify specific fucoidan characteristics that contribute to or change their immunomodulatory effects.

5.3.1 Molecular weight profile of *S. latissima* fucoidan and its implications for immunomodulation

In this study, fucoidan from *S. latissima* was successfully isolated using an enzyme-assisted extraction protocol, fractionated into distinct molecular weight oligosaccharides using the endo-fucoidanase Psf1, and subsequently purified. The presence of distinct oligosaccharide bands observed in the C-PAGE gel confirms that Psf1 acts as an endo-active enzyme, efficiently cleaving the α–(1,3)-linkages of the Sl native fucoidan into a range of oligosaccharides of different sizes. This confirms its preference for type 1 fucoidans containing α–(1,3)-linked fucose backbones, consistent with the structural features of *S. latissima*. However, the characterization of Psf1 falls beyond the scope of this thesis and will not be discussed in further detail.

The native Sl fucoidan sample was isolated as a HMW sample, with fucoidan molecules ranging from 400-500 kDa, alongside a smaller population with very HMW between 2000-3000 kDa. The Sl Psf1 MMW fraction, which comprised the majority of the Psf1 enzymatic products, consisted of oligosaccharides in the 10-30 kDa range according to the SEC data. C-PAGE analysis of the MMW fraction revealed that the smallest oligosaccharides present in this sample range from DP10-12. Furthermore, ^{1}H-NMR spectroscopy and monosaccharide analysis confirmed the structural features of the isolated fucoidan fractions, showing that fucose and galactose were abundant in both the MMW and LMW fractions. These results suggest that the materials are galactofucans. In addition, the oligosaccharides were predominantly sulfated on the C4 position, which might be linked to the immunomodulating activity.

The molecular size of fucoidan is a critical determinant of its bioactivity. Previous research has demonstrated that immunomodulatory effects are often linked to both molecular size and sulfate content, with different bioactivities associated with smaller versus larger oligosaccharides. For example, a study on HMW fucoidan from *Undaria pinnatifida* showed significant enhancement of immune function by stimulating natural killer cells and promoting the release of pro-inflammatory cytokines [193]. This suggests that larger molecules, such as the native Sl fucoidan, may exhibit stronger immunostimulatory effects. Similarly, Yang and colleagues (2008) reported that HMW

fucoidan induced the maturation of DCs and promoted a Th1 immune response, further supporting the potent immunomodulatory potential of larger fucoidan fractions.

Conversely, smaller molecular weight fucoidan fractions may also exhibit biological activity, though they typically show weaker effects compared to HMW fractions [193,194]. Nonetheless, these smaller fractions may offer benefits in other biological contexts. These findings underscore the importance of investigating molecular size when determining fucoidan's bioactivity.

Using the endo-fucoidanase, Psf1, to generate distinct molecular weight fucoidan oligosaccharides, this study provides valuable insights into the variables that influence fucoidan's biological activity, particularly in immunomodulatory applications. This work lays the groundwork for future research aimed at optimizing fucoidan-based therapeutics, enabling the targeted use of specific molecular weight fractions to control desired biological effects. Future research should focus on the estimation of the molecular weight of the LMW fraction, as well as fully investigating the effect of the sulfation patterns, particularly the presence and position of the sulfate groups, and how these features influence the biological activity.

5.3.2 Immunomodulating potential of various molecular-sized fucoidan fractions

The immunomodulatory effects of fucoidan and its Psf1 derivatives from *S. latissima* were investigated by treating imDCs with a maturation cocktail containing LPS, TNF-α, and IL-1β in the absence or presence of native high molecular weight fucoidan (Sl Native), Sl PSf1 MMW, or Sl PSf1 LMW.

The results showed that both Sl Native and Sl PSf1 MMW fucoidan samples led to a non-significant increased secretion of IL-12p40 and a non-significant decreased secretion of IL-10 by DCs compared to the Neg-DCs. Although these changes were non-significant, they led to a significant increase in the PI (PI > 1), suggesting a pro-inflammatory response. This finding aligns with previous studies showing that fucoidan from various species of brown seaweed can induce DC maturation *in vitro*, enhance IL-12p40 secretion, and promote Th1 immune responses in both human and mouse models [195,196]. However, it is important to note that high molecular weight fucoidan potentially contains endotoxins, which are known to cause false positive IL-12p40 results [196]. Thus, the high increase of IL-12p40 observed in the DC model by Sl Native and Sl Psf1 MMW cannot be excluded to be due to the presence of endotoxin, as this was not measured in the study.

In contrast, treatment with Sl PSf1 LMW fucoidan resulted in a significantly decreased IL-12p40 secretion by DCs in a dose-dependent manner, while IL-10 secretion was unaffected, a cytokine secretion profile characteristic for tolerogenic DCs [197]. This suggests an anti-inflammatory effect on the DC [199], which was supported by a

decrease in the PI (PI < 1). The decrease in IL-12p40 secretion with LMW fucoidan was comparable to the inhibition of IL-12 secretion observed with 1α,25-Dihydroxyvitamin D3 (1,25(OH)2D3), the active form of vitamin D3, known for its ability to suppress IL-12 production in both DCs and macrophages [198]. This suggests that Sl PSf1 LMW fucoidan might have potential as a bioactive compound for controlling inflammatory responses.

The differences in immunomodulatory effects observed between the various fucoidan fractions are likely linked to their molecular size and sulfate content. As discussed in section 5.3.1, the HMW fucoidan from *S. latissima* exhibited strong immunostimulatory effects, likely due to its larger size and sulfate content, which are known to influence immune responses [191,199]. Conversely, the Sl Psf1 LMW fucoidan fraction demonstrated significant anti-inflammatory effects, suggesting that small oligosaccharides modulate immune responses differently compared to their HMW counterparts. This might be due to the depolymerization of the Sl native fucoidan forms a more homogeneous sample with lower viscosity, as seen in studies with endo-fucoidanases and endo-fucanase [200,201], which might facilitate the interaction with specific PAMPs or DAMPs.

5.3.3 Inhibition of Th1 responses and key signaling pathways by low molecular weight fucoidan

The present study also provided insights into the immunomodulatory effects of Sl Psf1 LMW fucoidan fractions on DCs and their subsequent interactions with $CD4^+$ T-cells. When DCs were treated with Sl PSf1 LMW fucoidan and co-cultured with allogeneic $CD4^+$ T-cells, a significant reduction in IFN-γ secretion was observed, while IL-17 levels remained unaffected. These findings suggested that Sl PSf1 LMW fucoidan inhibited type 1 immune responses, which is consistent with IL-12 being the primary cytokine inducing Th1 differentiation of naïve T-cells, the main producers of the pro-inflammatory cytokine IFN-γ [184,189]. This indicates that Sl Psf1 LMW fucoidan might have a role in suppressing Th1-mediated immune responses and inflammation.

In contrast, higher molecular weight fucoidan, such as Sl Native and Sl PSf1 MMW fucoidan, did not exhibit the same inhibitory effect and may have even supported Th1-mediated responses. This highlights the role of the molecular weight in determining fucoidan's immunomodulatory activity, in line with previous studies associating high molecular weight fucoidan with immune activation [193,194,202]. Additionally, factors such as viscosity and homogeneity of the fucoidan preparations may also influence the observed immunological effects, potentially impacting the bioavailability, cellular interaction, or distribution of bioactive components.

The reduction in IFN-γ secretion likely involved key intracellular signaling pathways, such as NF-κB and STAT1, which are essential for regulating pro-inflammatory cytokine production during immune responses. Several studies have linked the

immunomodulatory activity of high molecular weight fucoidan with the NF-κB signaling pathways in various cell types, including DCs and murine macrophages [202,203]. During the inflammatory immune response, NF-κB binds to the promoter region of the *Il12a* gene, enhancing IL-12p40 production within DCs [204]. In this study, reduced IL-12p40 secretion by DCs treated with Sl PSf1 LMW fucoidan, along with the decreased IFN-γ levels by $CD4^+$ T-cells in co-culture, suggests that Sl PSf1 LMW fucoidan may inhibit key signaling pathways involved in inflammation, such as NF-κB and STAT1 (involved in IFN-γ signaling and Th1 differentiation) [205,206], as well as ERK1/2 phosphorylation in the MAP kinase pathway, which regulates cellular activities like inflammation [207]. This speculation can be further supported by a study of human keratinocytes treated with commercial fucoidan, which demonstrated its anti-inflammatory activity by blocking NF-κB and STAT1 pathway [208]. However, further research is needed to confirm the role of NF-κB inhibition by PSf1 LMW fucoidan.

In summary, these findings support the hypothesis that Sl PSf1 LMW fucoidan exerts anti-inflammatory effects by modulating key immune regulatory pathways. Further research will be necessary to confirm and expand upon these results, particularly in understanding the molecular mechanisms underlying the immunosuppressive activity of LMW fucoidan.

Notably, the position and the amount of sulfate groups on the oligosaccharides in the Sl PSf1 LMW fraction cannot be excluded as contributing factors to its activity. This, along with other structural characteristics—such as distinct branching patterns, linkage types, and the small DP-range—may be responsible for the anti-inflammatory effects observed when treating the DCs with Sl Psf1 LMW sample These findings underscore the importance of determining the full structural composition of Sl PSf1 LMW fucoidan to fully understand the mechanisms of action. Future research should focus on elucidating the detailed structural features of this fraction, as they likely contribute to its unique bioactivity.

5.4 Section IV: Enzymatic refinement of alginate to produce potential immunomodulating alginate oligosaccharides

To gain insights into the structure-function relationship of alginate, alginate oligosaccharide fractions of different sizes and different M, G, and MG-content were obtained by enzymatic digestion of low-viscosity *M. pyrifera* alginate. The size distribution and composition of five alginate oligosaccharide fractions (AlyRm2, AlyRm3 partially digested, AlyRm3 fully digested, AlyRm4 dialyzed, and AlyPx8) obtained through a two-step ethanol precipitation method and TLC analysis were used to estimate their size distributions and possible M-and G composition. The fraction showing the greatest impact on cytokine secretion by DCs was further investigated for its effect on $CD4^+$ allogeneic T-cells.

5.4.1 Purification and characterization of alginate oligosaccharide fractions

The TLC analysis revealed distinct patterns of the purified oligosaccharide sizes resulting from different enzyme treatments. For example, the AlyRm2 enzyme, which functions as an endo-poly-MG lyase with primary activity on M-G and G-G bonds, and minor activity of M-M bonds according to the patent by Hreggviðsson and colleagues (WO2015104723A1), likely produces a heterogeneous mixture of MG-, G-, and M-rich oligosaccharides of various sizes as observed in the TLC, but the TLC data alone does not clarify which type predominates the AlyRm2 fractions. However, previous research indicates that alginate lyases from the CAZy PL6 family subclass 2, to which AlyRm2 belongs, typically generate heterogeneous oligosaccharide mixtures [209]. Thus, the assumed oligosaccharide patterns are consistent with the literature.

In contrast, the other alginate lyases used in this study primarily yielded smaller oligosaccharides. TLC analysis showed that the partially digested fraction obtained with AlyRm3, when using less enzyme concentration, predominantly consisted of intermediate- and small-sized oligosaccharides, whereas using four times as much AlyRm3 resulted in a mixture of small oligosaccharides. According to the study by Dobruchowska and colleagues [141] AlyRm3 digestion of alginate after 24 hours predominantly generated products consisting of unsaturated mixture of M-, G-, and MG-rich oligosaccharides, mainly di-, tri-, and tetra-saccharides.

The AlyRm4 enzyme produced a TLC profile similar to that described by Dobruchowska et al. [141], displaying a prominent band corresponding to saturated cyclic monomers (4-deoxy-L-erythro-hex-4-enopyranosyluronic acid), alongside a fainter band attributed to mannopyranosyluronic acid and gulopyranosyluronic acid. This pattern indicates that AlyRm4 effectively depolymerized both M- and G-blocks of *M. pyrifera* alginate into monomers in an exo-acting manner. However, as demonstrated by Dobruchowska and colleagues (2022), AlyRm4 shows a preference for depolymerizing M-blocks over G-blocks, particularly encountering difficulty with G-blocks at the reducing end. This likely explains why, even after 24 hours of incubation with AlyRm4 on *M. pyrifera* alginate, significant material remains in the loading spot on the TLC, likely consisting of large oligosaccharides and polysaccharides enriched in G-blocks and terminating with a G-block on the non-reducing ends. Nonetheless, the remaining chains would still contain M-blocks upstream of the G-blocks within the alginate structure. Following this, dialysis was used to successfully remove smaller degradation products, resulting in a sample theoretically enriched in G-blocks within large poly- and/or oligosaccharides. Unfortunately, this study did not perform structural confirmation of the resulting sample.

Lastly, digestion of *M. pyrifera* alginate with AlyPx8 resulted in a heterogeneous mixture of larger and smaller oligosaccharides (M-, G-, and MG-rich). This outcome is based on preliminary TLC data and unpublished data, and further structural verification is needed to confirm these findings.

5.4.2 Enhanced immunomodulation by AlyRm3 digested alginate oligosaccharides: Potential for therapeutic applications

Most alginate oligosaccharide fractions showed minor or no impact on the secretion by DCs of the four cytokines investigated in this study (TNF-α, IL-6, IL-12p40, and IL-10), as compared to Neg-DCs. However, treating DCs with two specific fractions, AlyRm3 partially digestion and AlyRm3 fully digestion, led to significantly increased secretion of IL-6, IL-12p40, and IL-10 by the DCs. These findings suggested that the partially and fully AlyRm3-digested alginate oligosaccharides possess unique structural features that can influence immune responses more effectively than the other alginate fractions investigated in this study.

Interestingly, the fully AlyRm3-digested oligosaccharides had a more pronounced impact on the cytokine secretion. This suggests that smaller, more processed alginate oligosaccharides might have higher bioactivity or better accessibility to PRRs on DCs, thus enhancing the pro-inflammatory cytokine responses. Factors, such as the M:G-block ratio and the molecular size of the alginate oligosaccharides, likely play a significant role. The obtained TLC data and the reported endo-acting alginate lyase activity of AlyRm3 on both M and G blocks of alginate [141] suggest that the fully AlyRm3-digested oligosaccharides may contain or expose more M-blocks compared to the 'egg-box' structure formed by G-rich alginate [61]. Supporting this, it has been documented that *M. pyrifera* derived alginate consists of 61% ManA and 39% GulA, resulting in an M:G ratio of 1.56 [210]. Therefore, it can be speculated if the linear, M-rich small alginate oligosaccharides fit more effectively into the binding sites of unidentified PRRs compared to the 'egg-box' structure of G-rich alginate. Furthermore, it has been shown that M-rich alginate increases pro-inflammatory cytokines such as TNF-α, IL-6, and IL-12 in RAW264.7 macrophages and human monocytes [89,211]. This aligns with the cytokine secretion observed in DCs in this study, despite the lack of effect on TNF-α secretion. This discrepancy could be explained by the increased IL-10 secretion by DCs, which might suppress TNF-α production and act as a counter-regulatory mechanism to prevent excessive inflammation [212].

To further investigate the effects of the AlyRm3 fully digested sample on adaptive immune responses, a co-culture experiment was conducted with DCs matured in the presence or absence of fully AlyRm3-digested oligosaccharides and allogeneic $CD4^+$ T-cells. The increased IL-12p40 secretion by DCs corresponded with a statistically significant increase in IFN-γ levels in the co-culture supernatant, strongly suggesting a Th1-skewing effect by the fully AlyRm3-digested fractions, as IL-12 is crucial for Th1 differentiation [189].

The presence of IL-6 secretion by DCs indicated that the DCs were capable of promoting Th17-cell responses by co-cultured allogeneic $CD4^+$ T-cells. However, as there was no effect observed for IL-17 levels, it can be concluded that the fully AlyRm3-digested sample was not affecting DCs to induce Th17 differentiation. This might be

due to the stronger influence of IL-12, which promotes Th1 differentiation and potentially overrides signals for Th17 differentiation.

Thus, the fully AlyRm3-digested oligosaccharide fractions may be beneficial in therapies aimed at enhancing Th1-mediated immune responses, including treatments for infectious diseases, cancer immunotherapy, and vaccine development.

6 Conclusions

In the present study, we aimed to investigate and characterize the structural complexity and functional diversity of marine-derived polysaccharides, specifically their immunomodulatory effects. The research was divided into four major areas: the characterization of marine-derived sulfatase, the refinement and immunomodulation of laminarin and its derivatives, the immunomodulating potential of enzymatically refined fucoidan, and the investigation of the immunomodulating potential of enzymatically refined alginate derivatives. This chapter summarizes the key findings from each area and discusses the implications for future research and potential applications.

6.1 Characterization of a marine-derived sulfatase

The first section of this thesis focused on the cloning of the encoding gene and detailed characterization of the marine-derived sulfatase SulA1 from a marine *Arthrobacter* strain. The discovery of the *sulA1* gene and its enzymatic activity provided insights into its role in marine polysaccharide metabolism. The results suggest that SulA1 exhibited specificity for GalNAc4S, and optimal activity was obtained between pH 5.5 and 7.0 at 40°C. These findings suggested that SulA1 could be utilized to modify sulfation patterns in CS for immunomodulatory purposes, highlighting its potential application in biotechnological processes e.g., in the pharmaceutical or nutraceutical industry to create customized sulfated polysaccharides, aiding in the treatment of inflammatory diseases. However, due to its strict substrate specificity to GalNAc4S, SulA1 may not be ideal for refining a broad spectrum of sulfated marine polysaccharides, which could limit its broader biotechnological utility. Furthermore, the identification of other potential sulfatases, such as the SulA2, within the same gene cluster calls for their characterization, as these enzymes likely play complementary roles in polysaccharide metabolism and offer additional biotechnological applications.

6.2 Refinement and immunomodulation of laminarin

The second section addressed the structural complexity and enzymatic modification of laminarin extracted from *L. digitata*, *L. hyperborea*, and *S. latissima*. Detailed structural analysis revealed significant differences in sugar composition and structural variations among species. The immunomodulating effects of laminarin and laminari-oligosaccharides were assessed on DCs, showing minimal impact on DC maturation but indicating immunomodulatory potential through size-dependent reductions in TNF-α secretion by *Lh*F4, *Lh*F5, and *Sl*F3. Moreover, a species-specific increase in IL-6 and IL-10 secretion by *L. hyperborea* laminarin-treated DCs was observed. Co-culture

experiment between *Sl*F3-treated DCs and allogeneic CD4+ T-cells showed decreased IFN-γ, possibly due to the higher branch content of *Sl*F3, while *L. hyperborea* laminarin-treated DCs co-cultured with allogeneic CD4+ T-cells showed increased IL-17 secretion.

These findings suggest that laminari-oligosaccharides with specific structural features could be employed for targeted therapeutic applications. For example, laminari-oligosaccharides like *Lh*F4, *Lh*F5, and *Sl*F3, which show anti-inflammatory properties, might be developed into treatments for chronic inflammatory or autoimmune diseases. On the other hand, the simple branched laminarin polymer derived from *L. hyperborea*, which induces pro-inflammatory responses, could be explored for enhancing immune responses as an adjuvant in vaccines or as an immunostimulant in cancer treatments. This highlights that specific laminari-oligosaccharides could be developed for anti-inflammatory applications, while the simple branched laminarin polymer derived from *L. hyperborea* induce pro-inflammatory responses.

Thus, understanding the structural impacts on DC and T-cell interactions not only deepens our knowledge of laminarin's biological activities but also paves the way for designing tailored therapies with specific immunomodulatory effects.

6.3 Immunomodulating potential of fucoidan

The third section explored the immunomodulating effects of fucoidan from *S. latissima* and its oligosaccharides produced using the endo-α(1,3)-fucoidanase, designated Psf1. It was found that the molecular size of fucoidan influenced its immunomodulatory effects on DCs. HMW native fucoidan and MMW fucoidan samples induced a pro-inflammatory response by the DCs, whereas LMW fucoidan displayed anti-inflammatory properties by significantly decreasing IL-12p40 secretion by the DCs in a dose-dependent manner without affecting IL-10 levels. Additionally, LMW fucoidan inhibited type 1 immune responses by decreasing IFN-γ secretion in a co-culture experiment between DCs and allogeneic CD4+ T-cells. These results indicated that fucoidan fractions could be tailored for specific immunomodulatory applications, potentially beneficial in chronic inflammatory or autoimmune diseases.

6.4 Immunomodulating investigation of alginate derivatives

The fourth section investigated the immunomodulating potential of alginate derivatives produced using different alginate lyases. Five alginate oligosaccharide fractions with varying sizes and compositions were analyzed. The results demonstrated that alginate oligosaccharides have distinct immunomodulatory effects depending on their size and structural composition. Specifically, the fully digested AlyRm3 fractions, possibly M-rich small oligosaccharides, promoted pro-inflammatory cytokine secretion (IL-6 and IL-12p40) by DCs and Th1-mediated immune responses in co-culture experiment between DCs and allogeneic CD4+ T-cells. These results could be advantageous for therapies targeting infectious diseases, in cancer immunotherapy, and for vaccine development.

6.5 Overall conclusions

The research conducted in this thesis successfully met the overall aims and addressed the research questions asked. The findings contribute to a deeper understanding of how marine-derived polysaccharides can be enzymatically refined to modulate immune responses, offering promising insights for developing novel therapeutic agents derived from a natural sustainable resource.

6.6 Future directions

In this study the main focus was dedicated to laminarin, thus future research should focus on further characterization of both fucoidan and alginate in similar manner, involving detailed analysis of the structural-functional relationships of polysaccharide derivatives to refine their immunomodulatory properties. Additionally, mechanistic studies are essential to investigate the precise molecular processes by which these polysaccharides exert their immunomodulatory effects.

In vivo studies should be conducted to confirm the therapeutic potential of these polysaccharide derivatives. Moreover, exploring the clinical effects of these compounds is crucial, particularly in developing new treatments for inflammatory diseases, cancer, and as vaccine adjuvants. By addressing these future aspects, the potential of marine-derived polysaccharides in biomedicine can be fully realized, paving the way for innovative and effective therapeutics.

References

[1] Rioux LE, Turgeon SL, Beaulieu M. Characterization of polysaccharides extracted from brown seaweeds. Carbohydr Polym 2007;69:530–7. https://doi.org/10.1016/j.carbpol.2007.01.009.

[2] Kurd F, Samavati V. Water soluble polysaccharides from Spirulina platensis: Extraction and in vitro anti-cancer activity. Int J Biol Macromol 2015;74:498–506. https://doi.org/10.1016/j.ijbiomac.2015.01.005.

[3] Sardari RRR, Kulcinskaja E, Ron EYC, Björnsdóttir S, Friðjónsson ÓH, Hreggviðsson GÓ, et al. Evaluation of the production of exopolysaccharides by two strains of the thermophilic bacterium Rhodothermus marinus. Carbohydr Polym 2017;156:1–8. https://doi.org/10.1016/j.carbpol.2016.08.062.

[4] McHugh DJ. A guide to the seaweed industry. FAO Fisheries Technical Paper 2003;441:1–105.

[5] Adams JMM, Ross AB, Anastasakis K, Hodgson EM, Gallagher JA, Jones JM, et al. Seasonal variation in the chemical composition of the bioenergy feedstock Laminaria digitata for thermochemical conversion. Bioresour Technol 2011;102:226–34. https://doi.org/10.1016/j.biortech.2010.06.152.

[6] Ross AB, Jones JM, Kubacki ML, Bridgeman T. Classification of macroalgae as fuel and its thermochemical behaviour. Bioresour Technol 2008;99:6494–504. https://doi.org/10.1016/j.biortech.2007.11.036.

[7] Mucci A, Schenetti L, Volpi N. 1H and 13 C nuclear magnetic resonance identification and characterization of components of chondroitin sulfates of various origin. Carbohydr Polym 2000;41:37–45.

[8] Chi Z, Fang Y. Exopolysaccharides from marine bacteria. Journal of Ocean University of China 2005;4:67–74.

[9] Nwodo UU, Green E, Okoh AI. Bacterial exopolysaccharides: Functionality and prospects. Int J Mol Sci 2012;13:14002–15. https://doi.org/10.3390/ijms131114002.

[10] Randomized A, Gabay C, Medinger-sadowski C, Gascon D, Kolo F, Finckh A. Symptomatic Effects of Chondroitin 4 and Chondroitin 6 Sulfate on Hand Osteoarthritis 2011;63:3383–91. https://doi.org/10.1002/art.30574.

[11] Nadzir MM, Nurhayati RW, Idris FN, Nguyen MH. Biomedical Applications of Bacterial Exopolysaccharides : Polymers (Basel) 2021;13:1–23. https://doi.org/10.3390/polym13040530.

[12] Jung KA, Lim SR, Kim Y, Park JM. Potentials of macroalgae as feedstocks for biorefinery. Bioresour Technol 2013;135:182–90. https://doi.org/10.1016/j.biortech .2012.10.025.

[13] Jönsson M, Allahgholi L, Sardari RRR, Hreggviosson GO, Karlsson EN. Extraction and modification of macroalgal polysaccharides for current and next-generation applications. Molecules 2020;25. https://doi.org/10.3390/molecules 25040930.

[14] Spicer SE, Adams JMM, Thomas DS, Gallagher JA, Winters AL. Novel rapid method for the characterisation of polymeric sugars from macroalgae. J Appl Phycol 2017;29:1507–13. https://doi.org/10.1007/s10811-016-0995-0.

[15] Kadam SU, O'Donnell CP, Rai DK, Hossain MB, Burgess CM, Walsh D, et al. Laminarin from Irish brown seaweeds Ascophyllum nodosum and Laminaria hyperborea: Ultrasound assisted extraction, characterization and bioactivity. Mar Drugs 2015;13:4270–80. https://doi.org/10.3390/md13074270.

[16] Kadam SU, Tiwari BK, O'Donnell CP. Extraction, structure and biofunctional activities of laminarin from brown algae. Int J Food Sci Technol 2015;50:24–31. https://doi.org/10.1111/ijfs.12692.

[17] Read SM, Currie G, Bacic A. Analysis of the structural heterogeneity of laminarin by electrospray-ionisation-mass spectrometry. Carbohydr Res 1996;281:187–201.

[18] Rajauria G, Ravindran R, Garcia-Vaquero M, Rai DK, Sweeney T, O'Doherty J. Molecular characteristics and antioxidant activity of laminarin extracted from the seaweed species Laminaria hyperborea, using hydrothermal-assisted extraction and a multi-step purification procedure. Food Hydrocoll 2021;112:106332. https://doi.org/10.1016/j.foodhyd.2020.106332.

[19] Neyrinck AM, Mouson A, Delzenne NM. Dietary supplementation with laminarin, a fermentable marine β (1–3) glucan, protects against hepatotoxicity induced by LPS in rat by modulating immune response in the hepatic tissue. Int Immunopharmacol 2007;7:1497–506. https://doi.org/10.1016/j.intimp.2007.06.011.

[20] Choi J Il, Kim HJ, Kim JH, Lee JW. Enhanced biological activities of laminarin degraded by gamma-ray irradiation. J Food Biochem 2012;36:465–9. https://doi.org/10.1111/j.1745-4514.2011.00552.x.

[21] Smith AJ, Graves B, Child R, Rice PJ, Ma Z, Lowman DW, et al. Immunoregulatory Activity of the Natural Product Laminarin Varies Widely as a Result of Its Physical Properties. The Journal of Immunology 2018;200:788–99. https://doi.org/10.4049/jimmunol.1701258.

[22] Kim KH, Kim YW, Kim HB, Lee BJ, Lee DS. Anti-apoptotic activity of laminarin polysaccharides and their enzymatically hydrolyzed oligosaccharides from Laminaria japonica. Biotechnol Lett 2006;28:439–46. https://doi.org/10.1007/s10529-005-6177-9.

[23] Menshova R V, Ermakova SP, Anastyuk SD, Isakov V V, Dubrovskaya Y V, Kusaykin MI, et al. Structure , enzymatic transformation and anticancer activity of branched high molecular weight laminaran from brown alga Eisenia bicyclis. Carbohydr Polym 2014;99:101–9. https://doi.org/10.1016/ j.carbpol.2013.08.037.

[24] Liu Z, Xiong Y, Yi L, Dai R, Wang Y, Sun M, et al. Endo-β-1,3-glucanase digestion combined with the HPAEC-PAD-MS/MS analysis reveals the structural differences between two laminarins with different bioactivities. Carbohydr Polym 2018;194:339–49. https://doi.org/10.1016/j.carbpol.2018.04.044.

[25] Kopplin G, Rokstad AM, Mélida H, Bulone V, Skjåk-Bræk G, Aachmann FL. Structural Characterization of Fucoidan from Laminaria hyperborea: Assessment of Coagulation and Inflammatory Properties and Their Structure-Function Relationship. ACS Appl Bio Mater 2018;1:1880–92. https://doi.org/10.1021/acsabm.8b00436.

[26] Carvalho DN, Inácio AR, Sousa RO, Reis RL, Silva TH. Chapter 18: Seaweed polysaccharides as sustainable building blocks for biomaterials in tissue engineering. Sustainable Seaweed Technologies: Cultivation, Biorefinery, and Applications, Elsevier; 2020, p. 543–87. https://doi.org/10.1016/B978-0-12-817943-7.00019-6.

[27] Ale MT, Meyer AS. Fucoidans from brown seaweeds: An update on structures, extraction techniques and use of enzymes as tools for structural elucidation. RSC Adv 2013;3:8131–41. https://doi.org/10.1039/c3ra23373a.

[28] Ale MT, Mikkelsen JD, Meyer AS. Important determinants for fucoidan bioactivity: A critical review of structure-function relations and extraction methods for fucose-containing sulfated polysaccharides from brown seaweeds. Mar Drugs 2011;9:2106–30. https://doi.org/10.3390/md9102106.

[29] Qin Y. Alginate fibres: An overview of the production processes and applications in wound management. Polym Int 2008;57:171–80. https://doi.org/10.1002/pi.2296.

[30] Rashedy SH, Abd El Hafez MSM, Dar MA, Cotas J, Pereira L. Evaluation and characterization of alginate extracted from brown seaweed collected in the red sea. Applied Sciences (Switzerland) 2021;11. https://doi.org/10.3390/app11146290.

[31] Zhang H, Cheng J, Ao Q. Preparation of Alginate-Based Biomaterials and Their Applications in Biomedicine. Marine Drugs 2021;19:1–24. https://doi.org/10.3390/md.

[32] Bojorges H, Martínez-Abad A, Martínez-Sanz M, Rodrigo MD, Vilaplana F, López-Rubio A, et al. Structural and functional properties of alginate obtained by means of high hydrostatic pressure-assisted extraction. Carbohydr Polym 2023;299. https://doi.org/10.1016/j.carbpol.2022.120175.

[33] Puscaselu RG, Lobiuc A, Dimian M, Covasa M. Alginate: From food industry to biomedical applications and management of metabolic disorders. Polymers (Basel) 2020;12:1–30. https://doi.org/10.3390/polym12102417.

[34] Ahmed ABA, Adel M, Karimi P, Peidayesh M. Pharmaceutical, cosmeceutical, and traditional applications of marine carbohydrates. vol. 73. 1st ed. Elsevier Inc.; 2014. https://doi.org/10.1016/B978-0-12-800268-1.00010-X.

[35] Tat SK, Pelletier J, Mineau F, Duval N, Martel-pelletier J. Variable Effects of 3 Different Chondroitin Sulfate Compounds on Human Osteoarthritic Cartilage/Chondrocytes: Relevance of Purity and Production Process. J Rheumatol 2010;37:656–64. https://doi.org/10.3899/JRHEUM.090696.

[36] Abdallah MM, Fernández N, Matias AA, Bronze M do R. Hyaluronic acid and Chondroitin sulfate from marine and terrestrial sources: Extraction and purification methods. Carbohydr Polym 2020;243:116441. https://doi.org/10.1016/j.carbpol.2020.116441.

[37] Chen S, Xue C, Yin L, Tang Q, Yu G, Chai W. Comparison of structures and anticoagulant activities of fucosylated chondroitin sulfates from different sea cucumbers. Carbohydr Polym 2011;83:688–96. https://doi.org/10.1016/j.carbpol.2010.08.040.

[38] du Souich P, García AG, Vergés J, Montell E. Immunomodulatory and anti-inflammatory effects of chondroitin sulphate. J Cell Mol Med 2009;13:1451–63. https://doi.org/10.1111/j.1582-4934.2009.00826.x.

[39] Ustyuzhanina NE, Bilan MI, Dmitrenok AS, Shashkov AS. Two structurally similar fucosylated chondroitin sulfates from the holothurian species Stichopus chloronotus and Stichopus horrens. Carbohydr Polym 2018;189:10–4. https://doi.org/10.1016/j.carbpol.2018.02.008.

[40] Ilieva KM, Cheung A, Mele S, Chiaruttini G, Crescioli S, Griffin M, et al. Chondroitin Sulfate Proteoglycan 4 and its Potential As an Antibody immunotherapy Target across Different Tumor Types. Front Immunol 2018;8:1–15. https://doi.org/10.3389/fimmu.2017.01911.

[41] Bougatef H, Krichen F, Capitani F, Amor I Ben, Maccari F, Mantovani V, et al. Chondroitin sulfate/dermatan sulfate from corb (Sciaena umbra) skin: Purification, structural analysis and anticoagulant effect. Carbohydr Polym 2018;196:272–8. https://doi.org/10.1016/j.carbpol.2018.05.019.

[42] Chettri D, Verma AK, Verma AK. Innovations in CAZyme gene diversity and its modification for biorefinery applications. Biotechnology Reports 2020;28. https://doi.org/10.1016/j.btre.2020.e00525.

[43] Becker S, Scheffel A, Polz MF, Hehemann JH. Accurate quantification of laminarin in marine organic matter with enzymes from marine microbes. Appl Environ Microbiol 2017;83. https://doi.org/10.1128/AEM.03389-16.

[44] Mitsuya D, Sugiyama T, Zhang S, Takeuchi Y, Okai M, Urano N, et al. Enzymatic properties and the gene structure of a cold-adapted laminarinase from Pseudoalteromonas species LA. J Biosci Bioeng 2018;126:169–75. https://doi.org/10.1016/j.jbiosc.2018.02.018.

[45] Spilliaert R, Oli Hreggvidsson' G, Kristjan Kristjansson J, Eggertsson' G, Palsdottir' A. Cloning and sequencing of a Rhodothermus marinus gene, bglA, coding for a thermostable /?-glucanase and its expression in Escherichia coli. vol. 224. 1994.

[46] Bäumgen M, Dutschei T, Bornscheuer UT. Marine Polysaccharides: Occurrence, Enzymatic Degradation and Utilization. ChemBioChem 2021;22:2247–56. https://doi.org/10.1002/cbic.202100078.

[47] Nakabayashi M, Nishijima T, Ehara G, Nikaidou N, Nishihashi H, Watanabe T. Structure of the gene encoding laminaripentaose-producing β-1,3-glucanase (LPHase) of Streptomyces matensis DIC-108. J Ferment Bioeng 1998;85:459–64.

[48] Descamps V, Colin S, Lahaye M, Jam M, Richard C, Potin P, et al. Isolation and culture of a marine bacterium degrading the sulfated fucans from marine brown algae. Marine Biotechnology 2006;8:27–39. https://doi.org/10.1007/s10126-005-5107-0.

[49] Sakai T, Ishizuka K, Shimanaka K, Ikai K, Kato I. Structures of Oligosaccharides Derived from Cladosiphon okamuranus Fucoidan by Digestion with Marine Bacterial Enzymes. Marine Biotechnology 2003;5:536–44. https://doi.org/10.1007/s10126-002-0107-9.

[50] Furukawa SI, Fujikawa T, Koga D, Ide A. Purification and Some Properties of Exo-type Fucoidanases from Vibrio sp. N-5. Biosci Biotechnol Biochem 1992;56:1829–34. https://doi.org/10.1271/bbb.56.1829.

[51] Morya VK, Kim J, Kim EK. Algal fucoidan: Structural and size-dependent bioactivities and their perspectives. Appl Microbiol Biotechnol 2012;93:71–82. https://doi.org/10.1007/s00253-011-3666-8.

[52] Campo VL, Kawano DF, Silva DB da, Carvalho I. Carrageenans: Biological properties, chemical modifications and structural analysis - A review. Carbohydr Polym 2009;77:167–80. https://doi.org/10.1016/j.carbpol.2009.01.020.

[53] Barbeyron T, Brillet-Guéguen L, Carré W, Carrière C, Caron C, Czjzek M, et al. Matching the diversity of sulfated biomolecules: Creation of a classification database for sulfatases reflecting their substrate specificity. PLoS One 2016;11:1–33. https://doi.org/10.1371/journal.pone.0164846.

[54] Helbert W. Marine Polysaccharide Sulfatases. Front Mar Sci 2017;4:1–10. https://doi.org/10.3389/fmars.2017.00006.

[55] Silchenko AS, Rasin AB, Zueva AO, Kusaykin MI, Zvyagintseva TN, Kalinovsky AI, et al. Fucoidan sulfatases from marine bacterium wenyingzhuangia fucanilytica CZ1127T. Biomolecules 2018;8:1–20. https://doi.org/10.3390/biom8040098.

[56] Hettle AG, Vickers C, Robb CS, Liu F, Withers SG, Hehemann JH, et al. The Molecular Basis of Polysaccharide Sulfatase Activity and a Nomenclature for Catalytic Subsites in this Class of Enzyme. Structure 2018;26:747-758.e4. https://doi.org/10.1016/j.str.2018.03.012.

[57] Hanson SR, Best MD, Wong CH. Sulfatases: Structure, mechanism, biological activity, inhibition, and synthetic utility. Angewandte Chemie - International Edition 2004;43:5736–63. https://doi.org/10.1002/anie.200300632.

[58] Schlachter CR, Malley AO, Grimes LL, Tomashek JJ, Chruszcz M, Lee LA. Purification, Characterization, and Structural Studies of a Sulfatase from Pedobacter yulinensis. Molecules 2022;27:1–17. https://doi.org/10.3390/molecules27010087.

[59] Lombard V, Ramulu HG, Drula E, Coutinho PM, Henrissat B. The carbohydrate-active enzymes database (CAZy) in 2013 2014;42:490–5. https://doi.org/10.1093/nar/gkt1178.

[60] Cantarel BI, Coutinho PM, Rancurel C, Bernard T, Lombard V, Henrissat B. The Carbohydrate-Active EnZymes database (CAZy): An expert resource for glycogenomics. Nucleic Acids Res 2009;37. https://doi.org/10.1093/nar/gkn663.

[61] Hreggviðsson GÓ, Nordberg-Karlsson EM, Tøndervik A, Aachmann FL, Dobruchowska JM, Linares-Pastén J, et al. Biocatalytic refining of polysaccharides from brown seaweeds. vol. Chapter 16. 1st ed. Elsevier; 2020. https://doi.org/10.1016/B978-0-12-817943-7.00016-0.

[62] Zhu B, Yin H. Alginate lyase: Review of major sources and classification, properties, structure-function analysis and applications. Bioengineered 2015;6:125–31. https://doi.org/10.1080/21655979.2015.1030543.

[63] Kim HS, Lee CG, Lee EY. Alginate lyase: Structure, property, and application. Biotechnology and Bioprocess Engineering 2011;16:843–51. https://doi.org/10.1007/s12257-011-0352-8.

[64] Medzhitov R. Inflammation 2010: New Adventures of an Old Flame. Cell 2010;140:771–6. https://doi.org/10.1016/j.cell.2010.03.006.

[65] Panigrahy D, Gilligan MM, Serhan CN, Kashfi K. Resolution of inflammation: An organizing principle in biology and medicine. Pharmacol Ther 2021;227. https://doi.org/10.1016/j.pharmthera.2021.107879.

[66] Furman D, Campisi J, Verdin E, Carrera-Bastos P, Targ S, Franceschi C, et al. Chronic inflammation in the etiology of disease across the life span. Nat Med 2019;25:1822–32. https://doi.org/10.1038/s41591-019-0675-0.

[67] Joffre O, Nolte MA, Spörri R, Sousa CRE. Inflammatory signals in dendritic cell activation and the induction of adaptive immunity. Immunol Rev 2009;227:234–47. https://doi.org/10.1111/j.1600-065X.2008.00718.x.

[68] Cabeza-Cabrerizo M, Cardoso A, Minutti CM, Pereira Da Costa M, Reis E Sousa C. Dendritic Cells Revisited. Annu Rev Immunol 2021;39:131–66. https://doi.org/10.1146/annurev-immunol-061020-053707.

[69] Collin M, Bigley V. Human dendritic cell subsets: an update. Immunology 2018;154:3–20. https://doi.org/10.1111/imm.12888.

[70] Clark GJ, Silveira PA, Hogarth PM, Hart DNJ. The cell surface phenotype of human dendritic cells. Semin Cell Dev Biol 2019;86:3–14. https://doi.org/10.1016/j.semcdb.2018.02.013.

[71] Annunziato F, Romagnani C, Romagnani S. The 3 major types of innate and adaptive cell-mediated effector immunity. Journal of Allergy and Clinical Immunology 2015;135:626–35. https://doi.org/10.1016/j.jaci.2014.11.001.

[72] Kaiko GE, Horvat JC, Beagley KW. Immunological decision-making : how does the immune system decide to mount a helper T-cell response ? Immunology 2008;123:326–38. https://doi.org/10.1111/j.1365-2567.2007.02719.x.

[73] Hirohata S, Yanagida T. Human Thl responses driven by IL-12 are associated with enhanced expression of CD40 ligand. Japanese Journal of Clinical Immunology 1998;21:67–76. https://doi.org/10.2177/jsci.21.supplement_67.

[74] Ekkens MJ, Shedlock DJ, Jung E, Troy A, Pearce EL, Shen H, et al. Th1 and Th2 cells help CD8 T-cell responses. Infect Immun 2007;75:2291–6. https://doi.org/10.1128/IAI.01328-06.

[75] Huang H, Hao S, Li F, Ye Z, Yang J, Xiang J. CD4+ Th1 cells promote CD8+ Tc1 cell survival, memory response, tumor localization and therapy by targeted delivery of interleukin 2 via acquired pMHC I complexes. Immunology 2007;120:148–59. https://doi.org/10.1111/j.1365-2567.2006.02452.x.

[76] Chen F, Liu Z, Wu W, Rozo C, Bowdridge S, Millman A, et al. An essential role for T H 2-type responses in limiting acute tissue damage during experimental helminth infection. Nat Med 2012;18:260–6. https://doi.org/10.1038/nm.2628.

[77] Pearce EJ, Kane CM, Sun J, Taylor JJ, McKee AS, Cervi L. Th2 response polarization during infection with die helminth parasite Schistosoma mansoni. Immunol Rev 2004;201:117–26. https://doi.org/10.1111/j.0105-2896.2004.00187.x.

[78] Romagnani S. TH1 and TH2 in Human Diseases. vol. 80. 1996.

[79] Kumar P, Chen K, Kolls JK. Th17 cell based vaccines in mucosal immunity. Curr Opin Immunol 2013;25:373–80. https://doi.org/10.1016/j.coi.2013.03.011.

[80] Mills KHG. Induction, function and regulation of IL-17-producing T cells. Eur J Immunol 2008;38:2636–49. https://doi.org/10.1002/eji.200838535.

[81] Chen L, Ruan G, Cheng Y, Yi A, Chen D, Wei Y. The role of Th17 cells in inflammatory bowel disease and the research progress. Front Immunol 2023;13. https://doi.org/10.3389/fimmu.2022.1055914.

[82] Li B, Huang L, Lv P, Li X, Liu G, Chen Y, et al. The role of Th17 cells in psoriasis Th17 cells 2026. https://doi.org/10.1007/s12026-020-09149-1/Published.

[83] Mittal SK, Roche PA. Suppression of antigen presentation by IL-10. Curr Opin Immunol 2015;34:22–7. https://doi.org/10.1016/j.coi.2014.12.009.

[84] Fujio K, Komai T, Inoue M, Morita K, Okamura T, Yamamoto K. Revisiting the regulatory roles of the TGF-β family of cytokines. Autoimmun Rev 2016;15:917–22. https://doi.org/10.1016/j.autrev.2016.07.007.

[85] Lee JY, Kim YJ, Kim HJ, Kim YS, Park W. Immunostimulatory effect of laminarin on RAW 264.7 mouse macrophages. Molecules 2012;17:5404–11. https://doi.org/10.3390/molecules17055404.

[86] Fang Q, Wang JF, Zha XQ, Cui SH, Cao L, Luo JP. Immunomodulatory activity on macrophage of a purified polysaccharide extracted from Laminaria japonica. Carbohydr Polym 2015;134:66–73. https://doi.org/10.1016/j.carbpol.2015.07.070.

[87] Jiang Z, Okimura T, Yamaguchi K, Oda T. The potent activity of sulfated polysaccharide, ascophyllan, isolated from Ascophyllum nodosum to induce nitric oxide and cytokine production from mouse macrophage RAW264.7 cells: Comparison between ascophyllan and fucoidan. Nitric Oxide 2011;25:407–15. https://doi.org/10.1016/j.niox.2011.10.001.

[88] Xu X, Wu X, Wang Q, Cai N, Zhang H, Jiang Z, et al. Immunomodulatory effects of alginate oligosaccharides on murine macrophage RAW264.7 cells and their structure-activity relationships. J Agric Food Chem 2014;62:3168–76. https://doi.org/10.1021/jf405633n.

[89] Yang D, Jones KS. Effect of alginate on innate immune activation of macrophages. J Biomed Mater Res A 2009;90:411–8. https://doi.org/10.1002/jbm.a.32096.

[90] Park J, Babensee JE. Differential functional effects of biomaterials on dendritic cell maturation. Acta Biomater 2012;8:3606–17. https://doi.org/10.1016/j.actbio.2012.06.006.

[91] Nan Y, Su H, Zhou B, Liu S. The function of natural compounds in important anticancer mechanisms. Front Oncol 2023;12. https://doi.org/10.3389/fonc.2022.1049888.

[92] Rey-Ladino J, Ross AG, Cripps AW, McManus DP, Quinn R. Natural products and the search for novel vaccine adjuvants. Vaccine 2011;29:6464–71. https://doi.org/10.1016/j.vaccine.2011.07.041.

[93] Pulendran B, Ahmed R. Immunological mechanisms of vaccination. Nat Immunol 2011;12:509–17. https://doi.org/10.1038/ni.2039.

[94] Ellis S, Lin EJ, Tartar D. Immunology of Wound Healing. Curr Dermatol Rep 2018;7:350–8. https://doi.org/10.1007/s13671-018-0234-9.

[95] Brockmann L, Giannou AD, Gagliani N, Huber S. Regulation of TH17 cells and associated cytokines in wound healing, tissue regeneration, and carcinogenesis. Int J Mol Sci 2017;18. https://doi.org/10.3390/ijms18051033.

[96] Murray PJ. The primary mechanism of the IL-10-regulated antiinflammatory response is to selectively inhibit transcription. Proceedings of the National Academy of Sciences 2005;102:8686–91. https://doi.org/10.1073/pnas.0500419102.

[97] Saraiva M, O'Garra A. The regulation of IL-10 production by immune cells. Nat Rev Immunol 2010;10:170–81. https://doi.org/10.1038/nri2711.

[98] Song K, Xu L, Zhang W, Cai Y, Jang B, Oh J, et al. Laminarin promotes anti-cancer immunity by the maturation of dendritic cells. Oncotarget 2017;8:38554–67. https://doi.org/10.18632/oncotarget.16170.

[99] Neyrinck AM, Mouson A, Delzenne NM. Dietary supplementation with laminarin, a fermentable marine β (1–3) glucan, protects against hepatotoxicity induced by LPS in rat by modulating immune response in the hepatic tissue. Int Immunopharmacol 2007;7:1497–506. https://doi.org/10.1016/j.intimp.2007.06.011.

[100] Cumashi A, Ushakova NA, Preobrazhenskaya ME, D'Incecco A, Piccoli A, Totani L, et al. A comparative study of the anti-inflammatory, anticoagulant, antiangiogenic, and antiadhesive activities of nine different fucoidans from brown seaweeds. Glycobiology 2007;17:541–52. https://doi.org/10.1093/glycob/cwm014.

[101] Dore CMPG, Faustino Alves MGDC, Pofírio Will LSE, Costa TG, Sabry DA, De Souza Rêgo LAR, et al. A sulfated polysaccharide, fucans, isolated from brown algae Sargassum vulgare with anticoagulant, antithrombotic, antioxidant and anti-inflammatory effects. Carbohydr Polym 2013;91:467–75. https://doi.org/10.1016/j.carbpol.2012.07.075.

[102] Wang T, Gu Q, Zhao J, Mei J, Shao M, Pan Y, et al. up-regulating the ratio of collagen types I/III in diabetic rats. vol. 8. 2015.

[103] Ma Y, Shi R, Li F, Chang H. Emerging strategies for treating autoimmune disease with genetically modified dendritic cells. Cell Communication and Signaling 2024;22:262. https://doi.org/10.1186/s12964-024-01641-7.

[104] Palucka K, Ueno H, Fay J, Banchereau J. Dendritic cells and immunity against cancer. J Intern Med, vol. 269, 2011, p. 64–73. https://doi.org/10.1111/j.1365-2796.2010.02317.x.

[105] Md Fazle Akbar S, Horiike N, Onji Sk Md Fazle Akbar M, Onji M, De- T. Immune therapy including dendritic cell based therapy in chronic hepatitis B virus infection. World J Gastroenterol 2006;12:2876–83.

[106] Ji CF, Ji Y Bin. Laminarin-induced apoptosis in human colon cancer LoVo cells. Oncol Lett 2014;7:1728–32. https://doi.org/10.3892/ol.2014.1952.

[107] Kim KH, Kim YW, Kim HB, Lee BJ, Lee DS. Anti-apoptotic activity of laminarin polysaccharides and their enzymatically hydrolyzed oligosaccharides from Laminaria japonica. Biotechnol Lett 2006;28:439–46. https://doi.org/10.1007/s10529-005-6177-9.

[108] Chamidah A, Prihanto AA, Hardoko H. Edema-reducing activity of Sargassum crassifolium Bglucan (Laminaran) on edema-induced Rattus norvegicus. Asian Journal of Pharmaceutical and Clinical Research 2017;10:311–3. https://doi.org/10.22159/ajpcr.2017.v10i7.18523.

[109] Sellimi S, Maalej H, Rekik DM, Benslima A, Ksouda G, Hamdi M, et al. Antioxidant, antibacterial and in vivo wound healing properties of laminaran purified from Cystoseira barbata seaweed. Int J Biol Macromol 2018;119:633–44. https://doi.org/10.1016/j.ijbiomac.2018.07.171.

[110] Xue M, Liang H, Ji X, Zhou Z, Liu Y, Sun T, et al. Effects of fucoidan on gut flora and tumor prevention in 1,2-dimethylhydrazine-induced colorectal carcinogenesis. Journal of Nutritional Biochemistry 2020;82. https://doi.org/10.1016/j.jnutbio.2020.108396.

[111] Chen H, Cong Q, Du Z, Liao W, Zhang L, Yao Y, et al. Sulfated fucoidan FP08S2 inhibits lung cancer cell growth in vivo by disrupting angiogenesis via targeting VEGFR2/VEGF and blocking VEGFR2/Erk/VEGF signaling. Cancer Lett 2016;382:44–52. https://doi.org/10.1016/j.canlet.2016.08.020.

[112] Rui X, Pan HF, Shao SL, Xu XM. Anti-tumor and anti-angiogenic effects of Fucoidan on prostate cancer: Possible JAK-STAT3 pathway. BMC Complement Altern Med 2017;17. https://doi.org/10.1186/s12906-017-1885-y.

[113] Cong Q, Chen H, Liao W, Xiao F, Wang P, Qin Y, et al. Structural characterization and effect on anti-angiogenic activity of a fucoidan from Sargassum fusiforme. Carbohydr Polym 2016;136:899–907. https://doi.org/10.1016/j.carbpol.2015.09.087.

[114] Xue M, Ge Y, Zhang J, Wang Q, Hou L, Liu Y, et al. Anticancer properties and mechanisms of fucoidan on mouse breast cancer in vitro and in Vivo. PLoS One 2012;7. https://doi.org/10.1371/journal.pone.0043483.

[115] Huang L, Zeng Q, Zhang Y, Yin Q, Zhu X, Zhang P, et al. Effects of fucoidans and alginates from Sargassum graminifolium on allergic symptoms and intestinal microbiota in mice with OVA-induced food allergy. Food Funct 2022;13:6702–15. https://doi.org/10.1039/d2fo00802e.

[116] Mizuno M, Sakaguchi K, Sakane I. Oral administration of fucoidan can exert anti-allergic activity after allergen sensitization by enhancement of galectin-9 secretion in blood. Biomolecules 2020;10. https://doi.org/10.3390/biom10020258.

[117] Wen W, Yang L, Wang X, Zhang H, Wu F, Xu K, et al. Fucoidan promotes angiogenesis and accelerates wound healing through AKT/Nrf2/HIF-1α signalling pathway. Int Wound J 2023;20:3606–18. https://doi.org/10.1111/iwj.14239.

[118] Shanmugapriya K, Kim H, Kang HW. Fucoidan-loaded hydrogels facilitates wound healing using photodynamic therapy by in vitro and in vivo evaluation. Carbohydr Polym 2020;247. https://doi.org/10.1016/j.carbpol.2020.116624.

[119] Zhu L, Ge F, Yang L, Li W, Wei S, Tao Y, et al. Alginate Particles with Ovalbumin (OVA) Peptide Can Serve as a Carrier and Adjuvant for Immune Therapy in B16-OVA Cancer Model. Med Sci Monit Basic Res 2017;23:166–72. https://doi.org/10.12659/msmbr.901576.

[120] Fan Y, Li Y, Zhang J, Ding X, Cui J, Wang G, et al. Alginate Enhances Memory Properties of Antitumor CD8+ T Cells by Promoting Cellular Antioxidation. ACS Biomater Sci Eng 2019;5:4717–25. https://doi.org/10.1021/acsbiomaterials.9b00373.

[121] Tan GK, Tabata Y. Chondroitin-6-sulfate attenuates inflammatory responses in murine macrophages via suppression of NF-κB nuclear translocation. Acta Biomater 2014;10:2684–92. https://doi.org/10.1016/j.actbio.2014.02.025.

[122] Jomphe C, Gabriac M, Hale TM, Héroux L, Trudeau LÉ, Deblois D, et al. Chondroitin sulfate inhibits the nuclear translocation of nuclear factor-κB in interleukin-1β-stimulated chondrocytes. Basic Clin Pharmacol Toxicol 2008;102:59–65. https://doi.org/10.1111/j.1742-7843.2007.00158.x.

[123] Zhou J, Nagarkatti P, Zhong Y, Nagarkatti M. Immune modulation by chondroitin sulfate and its degraded disaccharide product in the development of an experimental model of multiple sclerosis. J Neuroimmunol 2010;223:55–64. https://doi.org/10.1016/j.jneuroim.2010.04.002.

[124] Akiyama H, Sakai S, Linhardt RJ, Goda Y, Toida T, Maitani T. Chondroitin sulphate structure affects its immunological activities on murine splenocytes sensitized with ovalbumin. vol. 382. 2004.

[125] Zhang X, Ma Z, Ke Y, Xia Y, Xu X, Liu J, et al. An injectable serotonin-chondroitin sulfate hydrogel for bio-inspired hemostatic adhesives with high wound healing capability. Mater Adv 2021;2:5150–9. https://doi.org/10.1039/d1ma00137j.

[126] Dower WJ, Miller JF, Ragsdale CW. High efficiency transformation of E.coli by high voltage electroporation. Nucleic Acids Res 1988;16:6127–45.

[127] Motejadded H, Altenbuchner J. Construction of a dual-tag system for gene expression, protein affinity purification and fusion protein processing. Biotechnol Lett 2009;31:543–9. https://doi.org/10.1007/s10529-008-9909-9.

[128] Bradford MM. A rapid and sensitive method for the quantitation of microgram quantities of protein utilizing the principle of protein-dye binding. Anal Biochem 1976;72:248–54. https://doi.org/10.1016/0003-2697(76)90527-3.

[129] Land H, Humble MS. YASARA: A tool to obtain structural guidance in biocatalytic investigations. Methods in Molecular Biology 2018;1685:43–67. https://doi.org/10.1007/978-1-4939-7366-8_4.

[130] Jumper J, Evans R, Pritzel A, Green T, Figurnov M, Ronneberger O, et al. Highly accurate protein structure prediction with AlphaFold. Nature 2021;596:583–9. https://doi.org/10.1038/s41586-021-03819-2.

[131] Mirdita M, Steinegger M, Söding J. MMseqs2 desktop and local web server app for fast, interactive sequence searches. Bioinformatics 2019;35:2856–8. https://doi.org/10.1093/bioinformatics/bty1057.

[132] Laskowski RA, Swindells MB. LigPlot+: Multiple ligand-protein interaction diagrams for drug discovery. J Chem Inf Model 2011;51:2778–86. https://doi.org/10.1021/ci200227u.

[133] Perkins DN, Pappin DJC, Creasy DM, Cottrell JS. Probability-based protein identification by searching sequence databases using mass spectrometry data. Electrophoresis, vol. 20, 1999. https://doi.org/10.1002/(SICI)1522-2683(19991201)20:18<3551::AID-ELPS3551>3.0.CO;2-2.

[134] Shevchenko A, Tomas H, Havliš J, Olsen J V., Mann M. In-gel digestion for mass spectrometric characterization of proteins and proteomes. Nat Protoc 2007;1:2856–60. https://doi.org/10.1038/nprot.2006.468.

[135] Jork H, Funk W, Fischer W, Wimmer H. Thin-Layer Chromatography. vol. 1a. VCH, Weinheim; 1990.

[136] American Society of Enologists. VL, Rossi JA. American journal of enology and viticulture. Am J Enol Vitic, vol. 16, American Society of Enologists; 1965, p. 144–58.

[137] Sluiter A, Hames B, Ruiz R, Scarlata C, Sluiter J, Templeton D. Determination of Ash in Biomass. Laboratory Analytical Procedure (LAP) 2008:8.

[138] Sluiter A, Hames B, Ruiz R, Scarlata C, Sluiter J, Templeton D, et al. Determination of Structural Carbohydrates and Lignin in Biomass. Technical Report NREL/ TP -510 -42618 2008:1–15. https://doi.org/NREL/TP-510-42618.

[139] Nguyen TT, Mikkelsen MD, Nguyen Tran VH, Trang VTD, Rhein-Knudsen N, Holck J, et al. Enzyme-Assisted Fucoidan Extraction from Brown Macroalgae Fucus distichus subsp. evanescens and Saccharina latissima. Mar Drugs 2020;18:1–18. https://doi.org/DOI10.3390/md18060296.

[140] Vuillemin M, Silchenko AS, Cao HTT, Kokoulin MS, Trang VTD, Holck J, et al. Functional Characterization of a New GH107 Endo-α-(1,4)-Fucoidanase from the Marine Bacterium Formosa haliotis. Mar Drugs 2020;18:1–17. https://doi.org/10.3390/md18110562.

[141] Dobruchowska JM, Bjornsdottir B, Fridjonsson OH, Altenbuchner J, Watzlawick H, Gerwig GJ, et al. Enzymatic depolymerization of alginate by two novel thermostable alginate lyases from Rhodothermus marinus. Front Plant Sci 2022;13. https://doi.org/10.3389/fpls.2022.981602.

[142] Hreggvidsson G.O., Jonsson Wheat J.O., Bjornsdottir B., Fridjonsson O.H., Altenbuchner J., Watzlawick H., et al. Thermostable alginate degrading enzymes and their methods of use (WO2015104723A1), 2015.

[143] Kale V, Friðjónsson Ó, Jónsson JÓ, Kristinsson HG, Ómarsdóttir S, Hreggviðsson G. Chondroitin Lyase from a Marine Arthrobacter sp. MAT3885 for the Production of Chondroitin Sulfate Disaccharides. Marine Biotechnology 2015;17:479–92. https://doi.org/10.1007/s10126-015-9629-9.

[144] Sardiello M, Annunziata I, Roma G, Ballabio A. Sulfatases and sulfatase modifying factors: an exclusive and promiscuous relationship. The Journal of the Japanese Forestry Society 2005;14:3203–17. https://doi.org/10.1093/hmg/ddi351.

[145] Wang S, Su T, Zhang Q, Guan J, He J, Gu L, et al. Comparative study of two chondroitin sulfate/dermatan sulfate 4-O-sulfatases with high identity. Front Microbiol 2019;10:1–17. https://doi.org/10.3389/fmicb.2019.01309.

[146] Wei L, Zhang Q, Lu D, Du M, Xu X, Wang W, et al. Identification and Action Patterns of Two Chondroitin Sulfate Sulfatases From a Marine Bacterium Photobacterium sp. QA16. Front Microbiol 2022;12:1–15. https://doi.org/10.3389/fmicb.2021.775124.

[147] Appel MJ, Bertozzi CR. Formylglycine, a post-translationally generated residue with unique catalytic capabilities and biotechnology applications. ACS Chem Biol 2015;10:72–84. https://doi.org/10.1021/cb500897w.

[148] Barozet A, Chacón P, Cortés J. Current approaches to flexible loop modeling. Curr Res Struct Biol 2021;3:187–91. https://doi.org/10.1016/j.crstbi.2021.07.002.

[149] Wang S, Guan J, Zhang Q, Chen X, Li F. Identification and Signature Sequences of Bacterial Delta(4,5)Hexuronate-2-O-Sulfatases. Front Microbiol 2019;10:1–17. https://doi.org/10.3389/fmicb.2019.00704.

[150] Wang W, Han W, Cai X, Zheng X, Sugahara K, Li F. Cloning and characterization of a novel chondroitin sulfate/dermatan sulfate 4-O-Endosulfatase from a marine bacterium. Journal of Biological Chemistry 2015;290:7823–32. https://doi.org/10.1074/jbc.M114.629154.

[151] Matusiewicz M, Krzystek-Korpacka M, Dabrowski K. Characterization of arylsulfatase activity in brine shrimp, Artemia salina. J Exp Mar Biol Ecol 2005;317:175–87. https://doi.org/10.1016/j.jembe.2004.11.019.

[152] Thompson BD, William DL, Janet GH. Comparative studies of rodent anionic arylsulfatases. Comparative Biochemistry and Physiology – Part B: Biochemistry And 1985;82:55–61. https://doi.org/10.1016/0305-0491(85)90127-0.

[153] Wang S, Sugahara K, Li F. Chondroitin sulfate/dermatan sulfate sulfatases from mammals and bacteria. Glycoconj J 2016;33:841–51. https://doi.org/10.1007/s10719-016-9720-0.

[154] Adams EL, Rice PJ, Graves B, Ensley HE, Yu H, Brown GD, et al. Differential high-affinity interaction of Dectin-1 with natural or synthetic glucans is dependent upon primary structure and is influenced by polymer chain length and side-chain branching. Journal of Pharmacology and Experimental Therapeutics 2008;325:115–23. https://doi.org/10.1124/jpet.107.133124.

[155] Karuppusamy S, Rajauria G, Fitzpatrick S, Lyons H, McMahon H, Curtin J, et al. Biological Properties and Health-Promoting Functions of Laminarin: A Comprehensive Review of Preclinical and Clinical Studies. Mar Drugs 2022;20. https://doi.org/10.3390/md20120772.

[156] Rioux LE, Turgeon SL, Beaulieu M. Effect of season on the composition of bioactive polysaccharides from the brown seaweed Saccharina longicruris. Phytochemistry 2009;70:1069–75. https://doi.org/10.1016/j.phytochem.2009.04.020.

[157] Ji CF, Ji Y Bin, Meng DY. Sulfated modification and anti-tumor activity of laminarin. Exp Ther Med 2013;6:1259–64. https://doi.org/10.3892/etm.2013.1277.

[158] Rajauria G, Ravindran R, Garcia-Vaquero M, Rai DK, Sweeney T, O'Doherty J. Molecular characteristics and antioxidant activity of laminarin extracted from the seaweed species Laminaria hyperborea, using hydrothermal-assisted extraction and a multi-step purification procedure. Food Hydrocoll 2021;112:106332. https://doi.org/10.1016/j.foodhyd.2020.106332.

[159] Graiff A, Ruth W, Kragl U, Karsten U. Chemical characterization and quantification of the brown algal storage compound laminarin — A new methodological approach. J Appl Phycol 2016;28:533–43. https://doi.org/10.1007/s10811-015-0563-z.

[160] Allahgholi L, Sardari RRR, Hakvåg S, Ara KZG, Kristjansdottir T, Aasen IM, et al. Composition analysis and minimal treatments to solubilize polysaccharides from the brown seaweed Laminaria digitata for microbial growth of thermophiles. J Appl Phycol 2020;32:1933–47. https://doi.org/10.1007/s10811-020-02103-6.

[161] Scheller J, Chalaris A, Schmidt-Arras D, Rose-John S. Total phenolic compounds, radical scavenging and metal chelation of extracts from Icelandic seaweeds. Food Chem 2009;116:240–8. https://doi.org/10.1016/j.foodchem.2009.02.041.

[162] Sardari RRR, Prothmann J, Gregersen O, Turner C, Karlsson EN. Identification of phlorotannins in the brown algae, saccharina latissima and ascophyllum nodosum by ultra-high-performance liquid chromatography coupled to high-resolution tandem mass spectrometry. Molecules 2021;26. https://doi.org/10.3390/MOLECULES26010043.

[163] Wu HM, Liu SW, Hsu MT, Hung CL, Lai CC, Cheng WC, et al. Structure, mechanistic action, and essential residues of a GH-64 enzyme, laminaripentaose-producing β-1,3-glucanase. Journal of Biological Chemistry 2009;284:26708–15. https://doi.org/10.1074/jbc.M109.010983.

[164] Peng Q, Qiu X, Zhang Z, Zhang S, Zhang Y, Liang Y, et al. PD-L1 on dendritic cells attenuates T cell activation and regulates response to immune checkpoint blockade. Nat Commun 2020;11:1–8. https://doi.org/10.1038/s41467-020-18570-x.

[165] Breton G, Zheng S, Valieris R, Tojal I, Satija R, Nussenzweig MC. Human dendritic cells (DCs) are derived from distinct circulating precursors that are precommitted to become CD1c+ or CD141+ DCs. Journal of Experimental Medicine 2016;213:2861–70. https://doi.org/10.1084/jem.20161135.

[166] Gerlini G, Hans [2], Hefti P, Kleinhans M, Nickoloff BJ, Gu [3], et al. CD1d is Expressed on Dermal Dendritic Cells and Monocyte-Derived Dendritic Cells. n.d.

[167] Schlitzer A, McGovern N, Ginhoux F. Dendritic cells and monocyte-derived cells: Two complementary and integrated functional systems. Semin Cell Dev Biol 2015;41:9–22. https://doi.org/10.1016/j.semcdb.2015.03.011.

[168] Haniffa M, Shin A, Bigley V, McGovern N, Teo P, See P, et al. Human Tissues Contain CD141 hi Cross-Presenting Dendritic Cells with Functional Homology to Mouse CD103 + Nonlymphoid Dendritic Cells. Immunity 2012;37:60–73. https://doi.org/10.1016/j.immuni.2012.04.012.

[169] Kumar KP, Nicholls AJ, Wong CHY. Partners in crime: neutrophils and monocytes/macrophages in inflammation and disease. Cell Tissue Res 2018;371:551–65. https://doi.org/10.1007/s00441-017-2753-2.

[170] Germolec DR, Shipkowski KA, Frawley RP, Evans E. Markers of inflammation. Methods in Molecular Biology, vol. 1803, Humana Press Inc.; 2018, p. 57–79. https://doi.org/10.1007/978-1-4939-8549-4_5.

[171] Celis R, Cuervo A, Ramírez J, Cañete JD. Psoriatic synovitis: Singularity and potential clinical implications. Front Med (Lausanne) 2019;6. https://doi.org/10.3389/fmed.2019.00014.

[172] Adegbola SO, Sahnan K, Warusavitarne J, Hart A, Tozer P. Anti-TNF therapy in Crohn's disease. Int J Mol Sci 2018;19. https://doi.org/10.3390/ijms19082244.

[173] Müller-Ladner U, Pap T, Gay RE, Neidhart M, Gay S. Mechanisms of disease: the molecular and cellular basis of joint destruction in rheumatoid arthritis. Nat Clin Pract Rheumatol 2005;1:102–10. https://doi.org/10.1038/ncprheum0047.

[174] Jang DI, Lee AH, Shin HY, Song HR, Park JH, Kang TB, et al. The role of tumor necrosis factor alpha (Tnf-α) in autoimmune disease and current tnf-α inhibitors in therapeutics. Int J Mol Sci 2021;22:1–16. https://doi.org/10.3390/ijms22052719.

[175] Kassianos AJ, Hardy MY, Ju X, Vijayan D, Ding Y, Vulink AJE, et al. Human CD1c (BDCA-1) + myeloid dendritic cells secrete IL-10 and display an immuno-regulatory phenotype and function in response to Escherichia coli. Eur J Immunol 2012;42:1512–22. https://doi.org/10.1002/eji.201142098.

[176] Scheller J, Chalaris A, Schmidt-Arras D, Rose-John S. The pro- and anti-inflammatory properties of the cytokine interleukin-6. Biochim Biophys Acta Mol Cell Res 2011;1813:878–88. https://doi.org/10.1016/j.bbamcr.2011.01.034.

[177] Tilg H, Trehu E, Atkins MB, Dinarello CA, Mier JW. Interleukin-6 (IL-6) as an Anti-inflammatory Cytokine: Induction of Circulating IL-1 Receptor Antagonist and Soluble Tumor Necrosis Factor Receptor p55. Blood 1994;83:113–8.

[178] Brown GD, Herre J, Williams DL, Willment JA, Marshall ASJ, Gordon S. Dectin-1 mediates the biological effects of β-glucans. Journal of Experimental Medicine 2003;197:1119–24. https://doi.org/10.1084/jem.20021890.

[179] Sahasrabudhe NM, Dokter-Fokkens J, de Vos P. Particulate β-glucans synergistically activate TLR4 and Dectin-1 in human dendritic cells. Mol Nutr Food Res 2016;60:2514–22. https://doi.org/10.1002/mnfr.201600356.

[180] Elder MJ, Webster SJ, Chee R, Williams DL, Hill Gaston JS, Goodall JC. β-glucan size controls dectin-1-mediated immune responses in human dendritic cells by regulating IL-1β production. Front Immunol 2017;8:14–6. https://doi.org/10.3389/fimmu.2017.00791.

[181] Goodridge HS, Reyes CN, Becker CA, Katsumoto TR, Ma J, Wolf AJ, et al. Activation of the innate immune receptor Dectin-1 upon formation of a -˜ Phagocytic synapse-™. Nature 2011;472:471–5. https://doi.org/10.1038/nature10071.

[182] Bose N, Chan ASH, Guerrero F, Maristany CM, Qiu X, Walsh RM, et al. Binding of soluble yeast β-glucan to human neutrophils and monocytes is complement-dependent. Front Immunol 2013;4. https://doi.org/10.3389/fimmu.2013.00230.

[183] Dalonso N, Goldman GH, Gern RMM. β-(1→3),(1→6)-Glucans: medicinal activities, characterization, biosynthesis and new horizons. Appl Microbiol Biotechnol 2015;99:7893–906. https://doi.org/10.1007/s00253-015-6849-x.

[184] Manetti R, Gerosa F, Giudizi MG, Biagiotti R, Parronchi P, Piccinni MP, et al. Interleukin 12 induces stable priming for interferon 3′(ifn-3″) production during differentiation of human t helper (th) cells and transient ifn-3′ production in established th2 cell clones. Journal of Experimental Medicine 1994;179:1273–83. https://doi.org/10.1084/jem.179.4.1273.

[185] Harrington LE, Hatton RD, Mangan PR, Turner H, Murphy TL, Murphy KM, et al. Interleukin 17-producing CD4+ effector T cells develop via a lineage distinct from the T helper type 1 and 2 lineages. Nat Immunol 2005;6:1123–32. https://doi.org/10.1038/ni1254.

[186] Guglani L, Khader SA. Th17 cytokines in mucosal immunity and inflammation. Curr Opin HIV AIDS 2010;5:120–7. https://doi.org/10.1097/COH.0b013e328335c2f6.

[187] Ishigame H, Kakuta S, Nagai T, Kadoki M, Nambu A, Komiyama Y, et al. Differential Roles of Interleukin-17A and -17F in Host Defense against Mucoepithelial Bacterial Infection and Allergic Responses. Immunity 2009;30:108–19. https://doi.org/10.1016/j.immuni.2008.11.009.

[188] Lin L, Ibrahim AS, Xu X, Farber JM, Avanesian V, Baquir B, et al. Th1-Th17 cells mediate protective adaptive immunity against Staphylococcus aureus and Candida albicans infection in mice. PLoS Pathog 2009;5. https://doi.org/10.1371/journal.ppat.1000703.

[189] Gately MK, Renzetti LM, Magram J, Stern AS, Adorini L, Gubler U, et al. THE INTERLEUKIN-12/ INTERLEUKIN-12-RECEPTOR SYSTEM: Role in Normal and Pathologic Immune Responses. vol. 16. 1998.

[190] Freysdottir J, Sigurpalsson MB, Omarsdottir S, Olafsdottir ES, Vikingsson A, Hardardottir I. Ethanol extract from birch bark (Betula pubescens) suppresses human dendritic cell mediated Th1 responses and directs it towards a Th17 regulatory response in vitro. Immunol Lett 2011;136:90–6. https://doi.org/10.1016/j.imlet.2010.12.009.

[191] Kale V, Freysdottir J, Paulsen BS, Friojónsson ÓH, Óli Hreggviosson G, Omarsdottir S. Sulphated polysaccharide from the sea cucumber Cucumaria frondosa affect maturation of human dendritic cells and their activation of allogeneic CD4(+) T cells in vitro. Bioactive Carbohydrates and Dietary Fibre 2013;2:108–17. https://doi.org/10.1016/j.bcdf.2013.09.009.

[192] Wang Y, Xing M, Cao Q, Ji A, Liang H, Song S. Biological activities of fucoidan and the factors mediating its therapeutic effects: A review of recent studies. Mar Drugs 2019;17. https://doi.org/10.3390/md17030183.

[193] Hu X, Goff HD. Fractionation of polysaccharides by gradient non-solvent precipitation: A review. Trends Food Sci Technol 2018;81:108–15. https://doi.org/10.1016/j.tifs.2018.09.011.

[194] Xu J, Yue RQ, Liu J, Ho HM, Yi T, Chen HB, et al. Structural diversity requires individual optimization of ethanol concentration in polysaccharide precipitation. Int J Biol Macromol 2014;67:205–9. https://doi.org/10.1016/j.ijbiomac.2014.03.036.

[195] Yoo HJ, You DJ, Lee KW. Characterization and Immunomodulatory Effects of High Molecular Weight Fucoidan Fraction from the Sporophyll of Undaria pinnatifida in Cyclophosphamide-Induced Immunosuppressed Mice. Mar Drugs 2019;17. https://doi.org/10.3390/md17080447.

[196] Yang M, Ma C, Sun J, Shao Q, Gao W, Zhang Y, et al. Fucoidan stimulation induces a functional maturation of human monocyte-derived dendritic cells. Int Immunopharmacol 2008;8:1754–60. https://doi.org/10.1016/j.intimp.2008.08.007.

[197] Yang M, Ma C, Sun J, Shao Q, Gao W, Zhang Y, et al. Fucoidan stimulation induces a functional maturation of human monocyte-derived dendritic cells. Int Immunopharmacol 2008;8:1754–60. https://doi.org/10.1016/j.intimp.2008.08.007.

[198] Liu L, Yang X, Yuan P, Cai S, Bao J, Zhao Y, et al. In Vitro and In Vivo Dendritic Cell Immune Stimulation Effect of Low Molecular Weight Fucoidan from New Zealand Undaria pinnatifida. Mar Drugs 2022;20. https://doi.org/10.3390/md20030197.

[199] Rutella S, Danese S, Leone G. Tolerogenic dendritic cells: Cytokine modulation comes of age. Blood 2006;108:1435–40. https://doi.org/10.1182/blood-2006-03-006403.

[200] D'Ambrosio D, Cippitelli M, Cocciolo MG, Mazzeo D, Di Lucia P, Lang R, et al. Inhibition of IL-12 production by 1,25-dihydroxyvitamin D3. Involvement of NF-κB downregulation in transcriptional repression of the p40 gene. Journal of Clinical Investigation 1998;101:252–62. https://doi.org/10.1172/JCI1050.

[201] Wu GJ, Shiu SM, Hsieh MC, Tsai GJ. Anti-inflammatory activity of a sulfated polysaccharide from the brown alga Sargassum cristaefolium. Food Hydrocoll 2016;53:16–23. https://doi.org/10.1016/j.foodhyd.2015.01.019.

[202] Liu L, Yang X, Yuan P, Cai S, Bao J, Zhao Y, et al. In Vitro and In Vivo Dendritic Cell Immune Stimulation Effect of Low Molecular Weight Fucoidan from New Zealand Undaria pinnatifida. Mar Drugs 2022;20. https://doi.org/10.3390/md20030197.

[203] Tabarsa M, Dabaghian EH, You SG, Yelithao K, Cao RA, Rezaei M, et al. The activation of NF-κB and MAPKs signaling pathways of RAW264.7 murine macrophages and natural killer cells by fucoidan from Nizamuddinia zanardinii. Int J Biol Macromol 2020;148:56–67. https://doi.org/10.1016/j.ijbiomac.2020.01.125.

[204] Murphy TL, Cleveland MG, Kulesza P, Magram J, Murphy KM. Regulation of Interleukin 12 p40 Expression through an NF-κB Half-Site. Mol Cell Biol 1995;15:5258–67. https://doi.org/10.1128/mcb.15.10.5258.

[205] Schultz AB, Kugler DG, Nivelo L, Vitari N, Doyle LP, Ristin S, et al. T cell intrinsic STAT1 signaling prevents aberrant Th1 responses during acute toxoplasmosis. Front Immunol 2023;14. https://doi.org/10.3389/fimmu.2023.1212190.

[206] Hu X, Ivashkiv LB. Cross-regulation of Signaling Pathways by Interferon-γ: Implications for Immune Responses and Autoimmune Diseases. Immunity 2009;31:539–50. https://doi.org/10.1016/j.immuni.2009.09.002.

[207] Roskoski R. ERK1/2 MAP kinases: Structure, function, and regulation. Pharmacol Res 2012;66:105–43. https://doi.org/10.1016/j.phrs.2012.04.005.

[208] Ryu MJ, Chung HS. Anti-inflammatory Activity of Fucoidan with Blocking NF-κB and STAT1 in Human Keratinocytes Cells. Natural Product Sciences 2015;21:205–9.

[209] Mathieu S, Henrissat B, Labre F, Skjåk-Bræk G, Helbert W. Functional exploration of the polysaccharide lyase family PL6. PLoS One 2016;11. https://doi.org/10.1371/journal.pone.0159415.

[210] Saji S, Hebden A, Goswami P, Du C. A Brief Review on the Development of Alginate Extraction Process and Its Sustainability. Sustainability (Switzerland) 2022;14. https://doi.org/10.3390/su14095181.

[211] Otterlei M, Østergaard K, Skjåk-Bræk G, Smidsrød O, Soon-shiong P, Espevik T. Induction of Cytokine Production from Human Monocytes Stimulated with Alginate. Journal of Immunotherapy 1991;10:286–91.

[212] Clarke CJP, Hales A, Hunt A, Foxwell BMJ. IL-10-mediated suppression of TNF-α production is independent of its ability to inhibit NFκB activity. Eur J Immunol 1998;28:1719–26. https://doi.org/10.1002/(SICI)1521-4141(199805)28:05<1719::AID-IMMU1719>3.0.CO;2-Q.

[213] Wang W, Shi L, Qin Y, Li F. Research and Application of Chondroitin Sulfate/Dermatan Sulfate-Degrading Enzymes. Front Cell Dev Biol 2020;8. https://doi.org/10.3389/fcell.2020.560442.

[214] Pulendran B, Tang H, Manicassamy S. Programming dendritic cells to induce T H 2 and tolerogenic responses. Nat Immunol 2010;11:647–55. https://doi.org/10.1038/ni.1894.

Original Publications

Paper I

marine drugs

MDPI

Article

Cloning and Characterization of a Novel *N*-Acetyl-D-galactosamine-4-*O*-sulfate Sulfatase, SulA1, from a Marine *Arthrobacter* Strain

Monica Daugbjerg Christensen [1,2,*], Leila Allahgholi [3], Javier A. Linares-Pastén [3], Ólafur Friðjónsson [1], Hörður Guðmundsson [1], Varsha Kale [1], Roya R. R. Sardari [3], Guðmundur Ó. Hreggviðsson [1,4] and Eva Nordberg Karlsson [3]

[1] Matís, Vínlandsleið 12, 113 Reykjavik, Iceland; olafur@matis.is (Ó.F.); hordurg@matis.is (H.G.); matis@matis.is (V.K.); gudmundo@matis.is (G.Ó.H.)
[2] Faculty Food Science and Nutrition, University of Iceland, 101 Reykjavik, Iceland
[3] Division of Biotechnology, Department of Chemistry, Lund University, P.O. Box 124, 22100 Lund, Sweden; leila.allahgholi@biotek.lu.se (L.A.); javier.linares-pasten@biotek.lu.se (J.A.L.-P.); roya.sardari@biotek.lu.se (R.R.R.S.); eva.nordberg_karlsson@biotek.lu.se (E.N.K.)
[4] Faculty of Life and Environmental Sciences, University of Iceland, 101 Reykjavik, Iceland
* Correspondence: monica@matis.is

Abstract: Sulfation is gaining increased interest due to the role of sulfate in the bioactivity of many polysaccharides of marine origin. Hence, sulfatases, enzymes that control the degree of sulfation, are being more extensively researched. In this work, a novel sulfatase (SulA1) encoded by the gene *sulA1* was characterized. The *sulA1*-gene is located upstream of a chondroitin lyase encoding gene in the genome of the marine Arthrobacter strain (MAT3885). The sulfatase was produced in *Escherichia coli*. Based on the primary sequence, the enzyme is classified under sulfatase family 1 and the two catalytic residues typical of the sulfatase 1 family—Cys57 (post-translationally modified to formyl glycine for function) and His190—were conserved. The enzyme showed increased activity, but not improved stability, in the presence of Ca^{2+}, and conserved residues for Ca^{2+} binding were identified (Asp17, Asp18, Asp277, and Asn278) in a structural model of the enzyme. The temperature and pH activity profiles (screened using *p*-nitrocatechol sulfate) were narrow, with an activity optimum at 40–50 °C and a pH optimum at pH 5.5. The T_m was significantly higher (67 °C) than the activity optimum. Desulfation activity was not detected on polymeric substrates, but was found on GalNAc4S, which is a sulfated monomer in the repeated disaccharide unit (GlcA–GalNAc4S) of, e.g., chondroitin sulfate A. The position of the sulA1 gene upstream of a chondroitin lyase gene and combined with the activity on GalNAc4S suggests that there is an involvement of the enzyme in the chondroitin-degrading cascade reaction, which specifically removes sulfate from monomeric GalNAc4S from chondroitin sulfate degradation products.

Keywords: marine bacterium; chondroitin sulfate; *N*-acetylgalactosamine-4-*O*-sulfate; sulfatase

Citation: Christensen, M.D.; Allahgholi, L.; Linares-Pastén, J.A.; Friðjónsson, Ó.; Guðmundsson, H.; Kale, V.; Sardari, R.R.R.; Hreggviðsson, G.Ó.; Karlsson, E.N. Cloning and Characterization of a Novel *N*-Acetyl-D-galactosamine-4-*O*-sulfate Sulfatase, SulA1, from a Marine *Arthrobacter* Strain. *Mar. Drugs* **2024**, *22*, 104. https://doi.org/10.3390/md22030104

Academic Editors: Yuya Kumagai, Hideki Kishimura and Benwei Zhu

Received: 23 January 2024
Revised: 17 February 2024
Accepted: 20 February 2024
Published: 23 February 2024

1. Introduction

Chondroitin sulfate/dermatan sulfate sulfatases (CS/DS-sulfatases) are specialized enzymes. They hydrolyze and remove sulfate ester groups from mono-, di-, oligo-, and polysaccharides of chondroitin sulfate (CS) or dermatan sulfate (DS). These enzymes can exhibit either endo- or exo-acting activities. This enables them to either remove sulfate groups located along the poly-/oligosaccharide chain or cleave sulfate groups from the reducing and/or the non-reducing ones [1,2].

The majority of sulfatases, including CS/DS-sulfatases, belong to Type 1 sulfatases, also known as arylsulfatases, or more accurately, formylglycine-dependent sulfatases (FGly-SULFs [3,4]; http://abims.sb-roscoff.fr/sulfatlas/ (accessed on 18 February 2024)). They

are given this name due to the post-translational formation of the active site residue Cα-formylglycine (FGly), derived from a conserved cysteine (or serine) residue found in the signature motif C/S-X-P-X-R [5]. CS/DS-sulfatases have been further categorized based on their substrate specificity, namely $\Delta^{4,5}$hexuronate-2-*O*-sulfatase, *N*-acetylgalactosamine-4-*O*-sulfatase (GalNAc-4-*O*-sulfatase), and *N*-acetylgalactosamine-6-*O*-sulfatase (GalNAc-6-*O*-sulfatase). These sulfatases target specific sulfate groups within CS/DS molecules, enabling the modification and degradation of these biomolecules [6,7]. However, despite the discovery of new enzymes and a large amount of genomic data, sulfatases remain, to a large extent, underexplored concerning substrate specificity and kinetic properties [8,9]. So far, only three $\Delta^{4,5}$hexuronate-2-*O*-sulfatase [10–12], three endo-type and two exo-type GalNAc-4-*O*-sulfatases [2,7,12–14], and three exo-type GalNAc-6-*O*-sulfatases [7,12,14], have been identified and characterized.

CS and DS are types of glycosaminoglycans (GAG) present in the cartilage tissue of both land and marine animals [15]. Their overall structures are characterized by repeated disaccharide units consisting of the glucuronic acid (GlcA) and *N*-acetyl-galactosamine (GalNAc) or L-iduronic acid (IdoUA) and GalNAc, respectively, linked by β-1,4-glycosidic bonds. These polysaccharides can be classified into different classes based on their heterogeneous length and degree of sulfation, and are influenced by the species of origin of the CS [16]. The two major classes of CS are CS-A and CS-C, which are distinguished by the position of the sulfate group on the GalNAc unit. In CS-A, the sulfate group is located at C4, while, in CS-C, it is positioned at C6 on the GalNAc molecule. However, more distinct and complex CS structures exist, like CS-AC, characterized by alternating C4 and C6 sulfation on the GalNAc unit and fucosylated CS from sea cucumber [17]. CS is widely recognized for its functional properties and diverse bioactivities, including anti-inflammatory properties [18,19], anti-cancer properties [20], anti-coagulating properties [21], and it is used as osteoarthritis treatment [22]. These characteristics make CS molecules intriguing for pharmaceutical and nutraceutical applications. The bioactivities of CS are primarily attributed to its sulfate content, the positions of the sulfate groups, and the size of the polymer.

In the recent years, researchers at Matís successfully isolated and sequenced the marine chondroitin-degrading *Arthrobacter* strain MAT3885. This discovery was made using microbial traps coated with CS [23]. The gene encoding the sulfatase described here, designated SulA1, originates from this strain and is classified under the Type 1 sulfatase family based on sequence characteristics. The substrate specificity was investigated and specific activity on a natural substrate was only found on monosulfated GalNAc4S, which is a building block in both CS and DS. Modelling of the structure and substrate docking revealed that binding of GalNAc4S was energetically favored, while the position of the substrate molecule was somewhat unexpected in relation to the calcium ligand bound in the active site. This study contributes insights into the substrate specificity of one of the relatively underexplored sulfatases from marine bacteria. Furthermore, these findings have the potential to serve as a valuable resource for further investigations into the structural features and practical applications of CS sulfatases.

2. Results

2.1. Phylogenetic Identification, Identification of SulA1, and Modelling of the Enzyme

A BlastN analysis of the MAT3885 16S rDNA sequence confirmed its affiliation with *Arthrobacter*. The closest relative was found to be *Arthrobacter cryoconiti* strain GS9 (99.79% id). Potential sulfatase genes were observed in the vicinity of the chondroitin lyase gene, ChoA1. ChoA1 belongs to the polysaccharide lyase family 8, as described by Kale et al. [23]. This family of lyases, known to act on CS with sulfation on both C4 and C6, is referred to as CS-AC (www.cazy.org (accessed on 18 February 2024)). A small chondroitin lyase gene cluster including two potential sulfatase-encoding genes (*sulA1* and *sulA2*) was identified (Figure 1). The *sulA1* gene was located immediately upstream of the chondroitin lyase gene, *choA1*, making it an interesting target for further investigation. The SulA1 sequence

(484 amino acids) did not contain a signal peptide, according to the SignalP v5.0 analysis, indicating that the protein is expressed intracellularly.

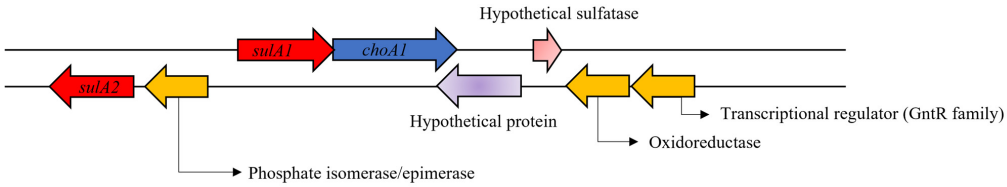

Figure 1. Schematic representation of the chondroitin lyase gene cluster with annotations. Within the cluster, two sulfatase-encoding genes (highlighted in red), *sulA1* and *sulA2*, were identified. The *sulA1* gene was located upstream of the chondroitin lyase gene, *choA1* (marked in blue), while *sulA2* was positioned downstream. An adjacent gene was predicted to encode a sulfatase (shaded red). Additionally, other genes within the cluster encoded proteins implicated in sugar metabolism (marked in yellow). Furthermore, a hypothetical protein (shaded purple) was found within the cluster.

The deduced amino acid sequence of SulA1 shared 28.5% sequence identity with SulA2 and was encoded in the same gene cluster. BlastP analysis of SulA1 against the PDB database revealed that the closest related structure determined candidates shared relatively low sequence homology with SulA1, but the query coverage was high (Table 1). The closest matches were enzymes from *Bacteroides thetaiotaomicron* VPI-5482 (PDB 5G2V), *Pseudoalteromonas* sp. (PDB 6B0K), *Bacteroides fragilis* YCH46 (PDB 2QZU), *Pseudoalteromonas fuliginea* (PDB 6BIA), and *Hungatella hathewayi* (PDB 6UST). Nevertheless, analysis of the deduced amino acid sequence of SulA1 in Interpro (https://www.ebi.ac.uk/interpro/ (accessed on 25 January 2024)) confirmed some conserved motifs and residues throughout the aligned sequences (Figure 2). All sequences contained the FGly-SULF signature motif C/S-X-P-X-R, essential for the formation of the FGly residue, and the two catalytic residues (Cys57 (converted to FGly) and His190). In addition, four residues were identified as being calcium-binding (Asp17, Asp18, Asp277, and Asn278), and they were conserved in the enzymes and located close to the active site.

Table 1. Crystallographic structures used as templates for the modeling SulA1.

Template (PDB Code)	Source	Sequence Coverage (%)	Amino Acid Sequence Identity (%)	Transferred Region to the Model (Residue Numbering)
5G2V	*Bacteroides thetaiotaomicron* VPI-5482	76	32.09	1–459
6B0K	*Pseudoalteromonas* sp.	89	27.27	168–180, 435–483
2QZU	*Bacteroides fragilis* YCH46	90	24.79	1–9, 283–282, 433–441
6BIA	*Pseudoalteromonas fuliginea*	90	27.20	452–484
6UST	*Hungatella hathewayi*	94	30.60	86–89

The high query coverage (Table 1) indicated an overall conserved topology. However, it should be noted that aligning SulA1 with the potential sulfatase SulA2, illustrated within the cluster in Figure 1, as well as with two recently characterized GalNAc4S-acting CS/DS sulfatases from marine *Photobacteria* sp. QA16 (GenBank UFQ91287.1 and QAB47431.1), a notably higher query coverage of 90% was observed. In contrast, the CS sulfatase that acts on GalNAc6S, from another *Photobacterium* strain (GenBank UFQ91288.1), showed a lower coverage of 67%. As observed for the PDB sequences (Table 1), sequence identity remained low, ranging from 26.6 to 28.01%. Interestingly, the SulA2 demonstrated higher query coverage with the CS sulfatase acting on GalNAc6S (GenBank UFQ91288.1, 96% coverage). The SulA2 sequence contained the FGly-SULF signature motif, two catalytic residues, and four calcium-binding residues, as observed for the other sulfatase amino acid sequences.

Figure 2. Multiple sequence alignment of SulA1 with characterized sulfatases, from *Bacteroides theraiotaomicron* VPI-5482 (PDB 5G2V), *Pseudoalteromonas* sp. (PDB 6B0K), *Bacteroides fragilis* YCH46 (PDB 2QZU), *Pseudoalteromonas fuliginea* (PDB 6BIA), and *Hungatella hathewayi* (PDB 6UST). Catalytic residues are marked in blue/yellow; the sulfatase signature motif (C/S-X-P-X-R) is marked within gray and is boxed; and Ca^{2+} binding residues are marked in pink. (*) denotes identical amino acid, (:) denotes conservative or amino acid with similar biochemical property, and (.) denotes semiconservative amino acid. The alignment was made using Clustal Omega (CLUSTAL O (1.2.4) at EMBL-EBI (https://www.ebi.ac.uk/ (accessed on 25 January 2024))).

To further investigate structure–function relationships, three-dimensional models of the SulA1 enzyme were constructed via two alternative approaches: homology-based structural modelling using YASARA and structural prediction using AlphaFold2. The respective approach resulted in a monomeric 3D molecular model, with Ca^{2+} included as a ligand.

In the homology model, five templates from PDB (Table 1) were used to obtain a hybrid model, which was assessed as "satisfactory" according to the overall Z-score (Z = −1.786) (Table 2), regardless of the low sequence similarity with the crystallographic structures.

Table 2. Hybrid model assessment according to Z-scores obtained in the YASARA program. The Z-score indicates how many standard deviations the model quality is away from the average high-resolution X-ray structure, where higher values are better, and negative values indicate a model worse than a high-resolution X-ray structure. Despite the low value for the Packaging 3D, the overall model was acceptable.

Check Type	Quality Z-Score	Comment
Dihedrals	−0.660	Good
Packing 1D	−1.453	Satisfactory
Packing 3D	−2.417	Poor
Overall	−1.786	Satisfactory

A significant portion of the predicted three-dimensional model of the enzyme generated using AlphaFold2 was of good quality and showed a high predicted local distance difference test (pLDDT) score above 90% (Figure 3A). Low PLDDT was only observed for the loop Ala360-Val376 (ADDGTGDAAGRAENAVV) and for the C-terminal part of the model (Figure 3A).

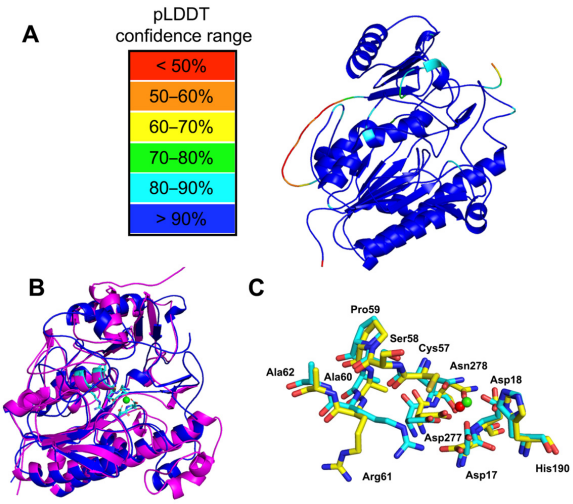

Figure 3. Predicted molecular structure of the sulfatase SulA1 from *Arthrobacter* strain MAT3885. (**A**) SulA1 modeled by AlphaFold2 with pLDDT confidence levels mapped onto the structure. (**B**) Comparison of the generated YASARA (Magenta) and AlphaFold2 (blue) models of SulA1; the active site residues are shown in stick and the Ca^{2+} is shown in green. (**C**) Comparison of the active site residues of the models generated using YASARA (yellow sticks, Ca^{2+} in red) and AlphaFold2 (blue sticks, Ca^{2+} in green).

In both cases, the modelled 3D structure revealed a typical sulfatase fold consisting of a large N-terminal domain and a smaller C-terminal domain, each one centered on a β-sheet. Detailed comparison of the models, however, revealed discrepancies, particularly in the size and orientation of loops (Figure 3B and Supplementary Figure S1), and in the orientation of the active site residue Arg61 (Figure 3C). Considering the relatively low

sequence identity to the structure-determined candidates (Table 1), the prediction from AlphaFold2 was used for a further evaluation.

The N-terminal domain (Domain I) encompassed the β-strands β1, β2, and β4-β8, β11, β14, and β15 surrounded by the α-helixes α1, α2, α5, α6, α7, α8, α10, and α13 (Figure 4). The C-terminal domain (Domain II) consisted of a β–sheet formed by β17–β20 strands, surrounded by α-helices α17–α21 (Figure 4). The catalytic site was located in the interdomain region, which also contained the Ca^{+2} binding site with the conserved residues Asp17, Asp18, Asp277, and Asn278 (Figure 4B).

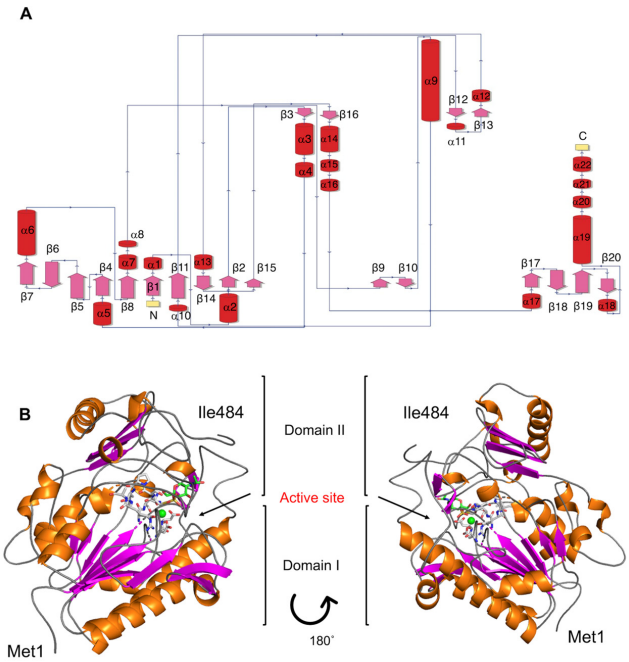

Figure 4. Predicted molecular structure of the sulfatase SulA1 from *Arthrobacter* strain MAT3885. (**A**) Topology map. Purple arrows represent β-sheets, while α-helices are indicated with red cylinders. (**B**) Overall structure. The ligand, highlighted in the active site in B, is N-Acetyl-D-galactosamine-4S. The green sphere represents a Ca^{2+} ion. The structure is predicted using AlphaFold2.

Based on the location of *sulA1* in the genome, potential activity on CS-AC degradation products produced with ChoA1 was suspected. Hence, the sulfated monosaccharides GalNAc4S and GalNAc6S were docked into the active site (Supplementary Figure S2). However, it was challenging to predict which substrate would undergo desulfation from the docking results. The sulfate groups of GalNAc4S and GalNAc6S were orientated in opposite directions in the active site in the model. The 4S-group did not interact with the calcium-binding site (Supplementary Figure S2), but the binding energy was more favorable for GalNAc4S. The distance between the sulfate group and the catalytic residues was, however, longer for GalNAc4S compared to GalNAc6S (and the distance to the catalytic residues was not significantly different when changing the Cys57 into the FGly residue). However, as seen below, GalNAc4S was the only biochemically identified substrate. This indicated that fine-tuned conformational changes may be crucial for sulfatase specificity. Such conformational flexibility, which may be influenced by solvent effects, substrate dynamics, as well as specific interactions critical for catalysis, is difficult to consider in docking models. Discrepancies may also increase by the oversimplification of experimental conditions (such as pH, temperature, and ionic strength) in modeling and docking, which can significantly influence enzyme specificity in vivo [24].

2.2. Recombinant Production in *E. coli*, and Purification of SulA1

The gene designated *sulA1* was cloned and expressed in an *E. coli* system (pVK13/*E. coli* Bl21(C43)). The recombinant SulA1 (484 amino acids) was produced in a soluble form, exhibited sulfatase activity using *para*-nitrocatechol-sulfate (*p*NCS) (Table 3), and was subsequently purified for further characterization. The molecular weight of the recombinant protein was estimated with SDS-PAGE and was aligned with the calculated weight of 51.9 kDa (Figure 5). Purification of the recombinant protein was efficiently achieved using his-tag affinity beads (Figure 5A,B). The specific activity of purified SulA1 increased approximately 4-fold compared to the corresponding activity in the crude extract under standard conditions (Table 3). The SulA1 amino acid sequence was also subjected to peptide mass fingerprinting, validating 100% sequence identity in peptide fragments (generated in silico from the software MASCOT, https://www.matrixscience.com/), corresponding to 40% query coverage of the SulA1 amino acid sequence (Figure 6).

Table 3. Relative activity of crude SulA1 and purified SulA1 tested on *p*NCS.

Sample	Relative Activity (%)
Crude SulA1	24.4 ± 1.08
Pure SulA1	100.0 ± 0.0

Data are expressed as mean ± SD of two independent reactions.

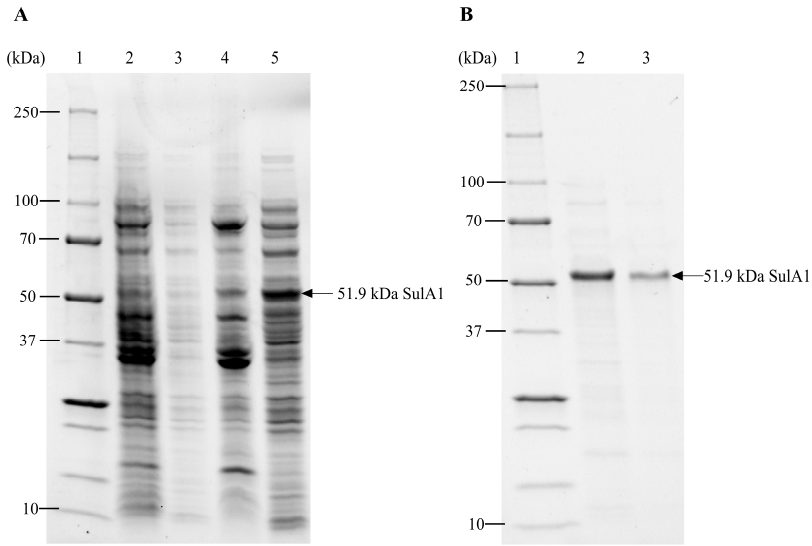

Figure 5. SDS-PAGE analysis of *SulA1* gene overexpression in *E. coli* BL21(C43). Gene expression was induced with 10% (*w/v*) L-rhamnose when the OD_{600} at 37 °C was between 0.8 and 0.9, and the culture was grown overnight at room temperature. Proteins were separated into a 4–20% Mini-PROTEAN® TGX Stain-Free™ Precast gel. Both pellets (insoluble protein) and supernatants (soluble proteins) are shown. (**A**) Lane 1, Precision Plus Protein™ Standards. Lane 2, uninduced *E. coli* BL21(C43) culture, pellet. Lane 3, uninduced *E. coli* BL21(C43) culture, supernatant. Lane 4, L-rhamnose-induced *E. coli* BL21(C43) culture, pellet. Lane 5, L-rhamnose-induced *E. coli* BL21(C43) culture, supernatant. (**B**) Lane 1, Precision Plus Protein™ Standards. Lane 2, first elution from PureCube INDIGO Ni-MagBead purification. Lane 3, second elution from PureCube INDIGO Ni-MagBead purification. The SulA1 protein is marked with an arrow at 51.9 kDa.

```
  1 MVSSSPAAPN IVFILSDDQG PWALGCAGND EIHTPVLDTL AAGGTRLENF
 51 FCVSPVCSPA RASLMTGQIP SRHGVHDYLT GVEVGAQAPD YLAGQAIFTD
101 VLAEHGYRMG LAGKWHLGAN DAPRKGFVHW YGLEGGGSPY LGATMYRNGE
151 REDVTDYLTD IITDDAHAFL DREAAREEPF FLAVNYTAPH KPWKGQHPQK
201 FEDLYADCAF DSCPQEEPHP WQPTVDGVAI GGEPDVRAAL VGYFAAVSAM
251 DAAIGSLLEH LEKLGIAENT LVIFSSDNGF NCGHHGVWGK GNGTFPQNMY
301 DSSVKVPAIF HWPGRIAAGQ VREELLSAYD VAATILELTG LDPAPFETGP
351 GSSFAPLLRA DDGTGDAAGR AENAVVVYDE YGPVRMIRTP EFKYVHRHPH
401 GPHELYHLAA DPGERHNLMD DAVPHPALVG LRAQLAGWFS RHGVPDFDGA
451 ALPVAGAGQH SPLRPPGGQT DPLGAFTAPN WDGI
```

Figure 6. Peptide fingerprint mapping of the purified SulA1. Matched peptides are shown in bold red. The amino acid sequence coverage was 40%.

2.3. The pH and Temperature Profile of SulA1

The activity of SulA1 on *p*NCS was pH-sensitive, with maximum relative activity observed at pH 5.5 (Supplementary Figure S3). The activity significantly reduced to 21% and 54% of its optimum at pH 5.0 and pH 6.0, respectively (Supplementary Figure S3A), highlighting the sensitivity of the activity to minor pH fluctuations.

The apparent optimum temperature for *p*NCS activity at pH 5.5 was observed between 40 °C and 50 °C (Supplementary Figure S3B), while, at 60 °C, the SulA1 had lost 83% of the activity. This temperature range was lower than the observed unfolding temperature (T_m) of the enzyme, as determined with differential scanning fluorimetry (DSF), which was 67 °C at pH 6.0 and increased with increasing pH up to pH 7 with a T_m = 72.4 °C (Figure 7). This showed that the substrate affinity in the active site was lost prior to the unfolding of the enzyme.

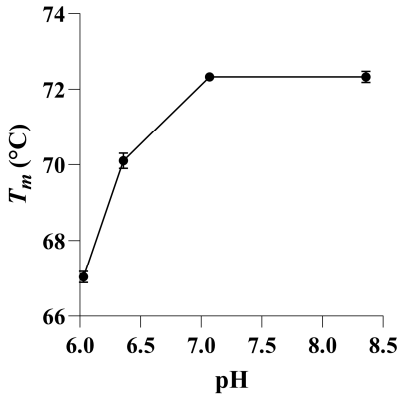

Figure 7. The effect of different pH on the unfolding temperature (T_m) using differential scanning fluorimetry (DSF) analysis. The highest thermostability was observed at near-neutral pH conditions, resulting in a maximum T_m = 72.4 °C. Scatters were unclear at a pH below 5. Data are expressed as mean ± SD of three measurements for each pH.

The $T_{½}$, defined as the temperature at which 50% of the relative activity is lost after 30 min of incubation, was determined to be 55 °C (Supplementary Figure S3C). The activity was less susceptible to lower temperatures, as at room temperature approximately 50% of the optimal *p*-activity was observed (Supplementary Figure S3C). Analysis of kinetic parameters of SulA1 was attempted using *p*NCS under standard conditions. However, there appeared to be a linear relationship between substrate concentration and reaction rate, suggesting that there was a high K_m and a low affinity of SulA1 for this substrate.

2.4. Storage Stability

It was noted that purified SulA1 precipitated during storage at 4 °C and −20 °C, leading to a loss of activity. Therefore, storage optimization was investigated using *p*NCS as the substrate. It was found that when the SulA1 was stored in a 100 mM sodium acetate buffer supplemented with 20% glycerol at pH 5.5, the enzymatic activity remained stable for at least 5 weeks at −80 °C. In contrast, storing purified SulA1 in the same buffer at −20 °C led to a small decrease in activity. After one week of storage, the remaining relative activity was measured to be 86%, which remained unchanged after 5 weeks of storage. Conversely, when SulA1 was stored in 100 mM sodium acetate buffer pH 5.5 at 4 °C, a substantial reduction in activity was observed. After 1 week of storage, the relative activity dropped to 26%, and after 5 weeks, it declined to 13% of the initial activity.

2.5. Cation Dependence

Due to the presence of ligands for a potential calcium-binding site (Figures 2 and 3), the effect of mono- and divalent cations on the activity was tested (Supplementary Figure S4). It was found that different concentrations of the divalent cation Ca^{2+} (ranging from 0 to 30 mM) had an impact on the activity, increasing the relative activity on *p*NCS 3.5-fold at concentrations from 15 to 30 mM $CaCl_2$ (Supplementary Figure S3D). This fits with the presence of the conserved residues (Asp17, Asp18, Asp277, and Asn278), and corresponding residues have, in previous studies of related enzymes, been identified as ligands for calcium binding (and in a few cases magnesium binding) in structure-determined candidates [4,25]. Moreover, it was observed that EDTA, which effectively chelated the Ca^{2+} ions, decreased SulA1 activity by ~90% (Supplementary Figure S4), showing that the Ca^{2+} ion is needed for the binding of the substrate in the SulA1 active site.

DSF analysis, however, showed that increasing concentrations of $CaCl_2$ slightly reduced the unfolding temperature of SulA1, while increasing concentrations of EDTA did not result in any reduction of the unfolding temperature (Table 4). Thus, calcium did not play any crucial role in stabilizing the structure of SulA1 but had a large effect on substrate affinity.

Table 4. The effect of different concentrations of $CaCl_2$ or EDTA on the unfolding temperature (T_m). A decrease in T_m suggests destabilization, and an increase in T_m is interpreted as an increase in protein thermostability.

$CaCl_2$ (mM)	T_m (°C)	EDTA (mM)	T_m (°C)
0	67.2 ± 0.15	0	67.5 ± 0.09
7	64.0 ± 0.06	0.5	67.3 ± 0.21
14	62.3 ± 0.10	1	67.3 ± 0.67
		2	67.1 ± 0.54
		5	67.0 ± 0.15

2.6. Sulfatase Activity against Natural Substrates

To investigate the substrate specificity of SulA1, various types of CS sulfated mono-, di-, and oligo/polysaccharides, with different sulfation patterns (Table 5), were used in a substrate screening. Given SulA1′s location upstream of the chondroitin lyase, ChoA1 (Figure 1), it was reasonable to expect activity related to CS. However, activity was only confirmed in reactions containing the monomeric sulfated amino/sugar unit with sulfation on C4, i.e., *N*-acetyl-D-galactosamine-4-sulfate (GalNAc4S), derived from CS-A. This was observed as a shift of mobility in the TLC, corroborating the formation of *N*-acetyl-D-galactosamine (GalNAc). No such change was detectable for the monomeric sulfated amino/sugar unit with sulfation on C6, or on CS-disaccharides with different sulfation patterns (Δdi0S, Δdi4S and Δdi6s), respectively (Figure 8A). As indicated by the DSF data, the pH condition that conferred the highest stability to SulA1 was found near pH 7 (Figure 8). Subsequently, an investigation of the pH optimum for SulA1, utilizing GalNAc4S as the substrate, was carried out, and the outcomes were visualized through TLC analysis

(Figure 9A). These findings confirmed that the optimal pH range for this substrate was higher (pH 6.0–6.5) than initially expected (pH 5.5 for *p*NCS). Consequently, the same CS sulfated mono-, di-, and oligo/polysaccharides were reevaluated as substrates, but this time at a pH of 6.5 instead. However, enzymatic activity was still only confirmed on GalNAc4S, underscoring that SulA1 was only active on the 4-*O*-sulfate ester bond on the monosaccharide. Furthermore, complementary data from HPAEC-PAD analysis confirms the production of GalNAc following incubation with SulA1. A minor peak at 41 min (Figure 8B) was observed when the GalNAc4S had not undergone SulA1 digestion. After 30 min of digestion with SulA1 a peak appeared at 9.5 min in the HPAC-PAD spectrum, indicative of the formation of GalNAc (Figure 8C). The assumption is based on control experiments where a GalNac and galactose (Gal) were separately analyzed, resulting in the detection of a peak earlier (7.75 min) than for the GalNAc standard peak (9.5 min; Supplementary Figure S5A,B). Other sulfated natural substrates, such as heparin, κ-carrageenan, and seaweed derived fucose-containing sulfated polysaccharides (FCSPs), were also investigated as substrates for SulA1, but no activity was detected. Interestingly, despite the structural similarity to D-galactose-4-sulfate (Gal-4S), which is the sulfated monosaccharide found in κ-carrageenan, SulA1 was unable to cleave the sulfate ester group from it. This suggests that SulA1 exhibited a highly specific substrate preference towards GalNAc4S, potentially requiring the amine group for precise positioning within the active site. These results strongly implied that SulA1 is involved in the complete degradation of CS-A, in combination with the previously characterized ChoA1.

Table 5. Overview of SulA1's effect on different substrates.

Substrates	Activity
Chondroitin sulfate AC dp4 (contain both 4S and 6S)	−
Chondroitin without sulfation (Δdi0S)	−
Chondroitin sulfate (Δdi4S)	−
Chondroitin sulfate (Δdi6S)	−
N-Acetyl-D-galactosamine-4-sulfate (GalNAc4S)	+
N-Acetyl-D-galactosamine-6-sulfate (GalNAc6S)	−
Heparin disaccharide I-H	−
N-Acetyl-D-glucosamine-6-sulfate (GlcNac-6S)	−
D-galactose-4-sulfate (Gal-4S)	−
Neocarrabiose-4-*O*-sulfate	−
Neocarratetraose-41,43-di-*O*-sulfate	−
L-fucose from Chorda filum cut-off <10 kDa Fuc310)	−
Fucoidan	−

+ and − indicate if activity has been observed or not in the TLC plate, respectively.

Relatively high activity at both pH 5.5 and pH 6.5, investigated with TLC (Figure 9A), indicated a broader activity range for the natural substrate compared to the artificial substrate *p*NCS, which showed a narrow pH optimum profile (Supplementary Figure S3A).

Furthermore, the specific activity of pure SulA1 was determined to be 6.8 mU/mg SulA1 at pH 5.5 with 20 mM GalNAc4S and 14.0 mU/mg SulA1 at pH 6.5 with 15 mM GalNAc4S, (Table 6), respectively.

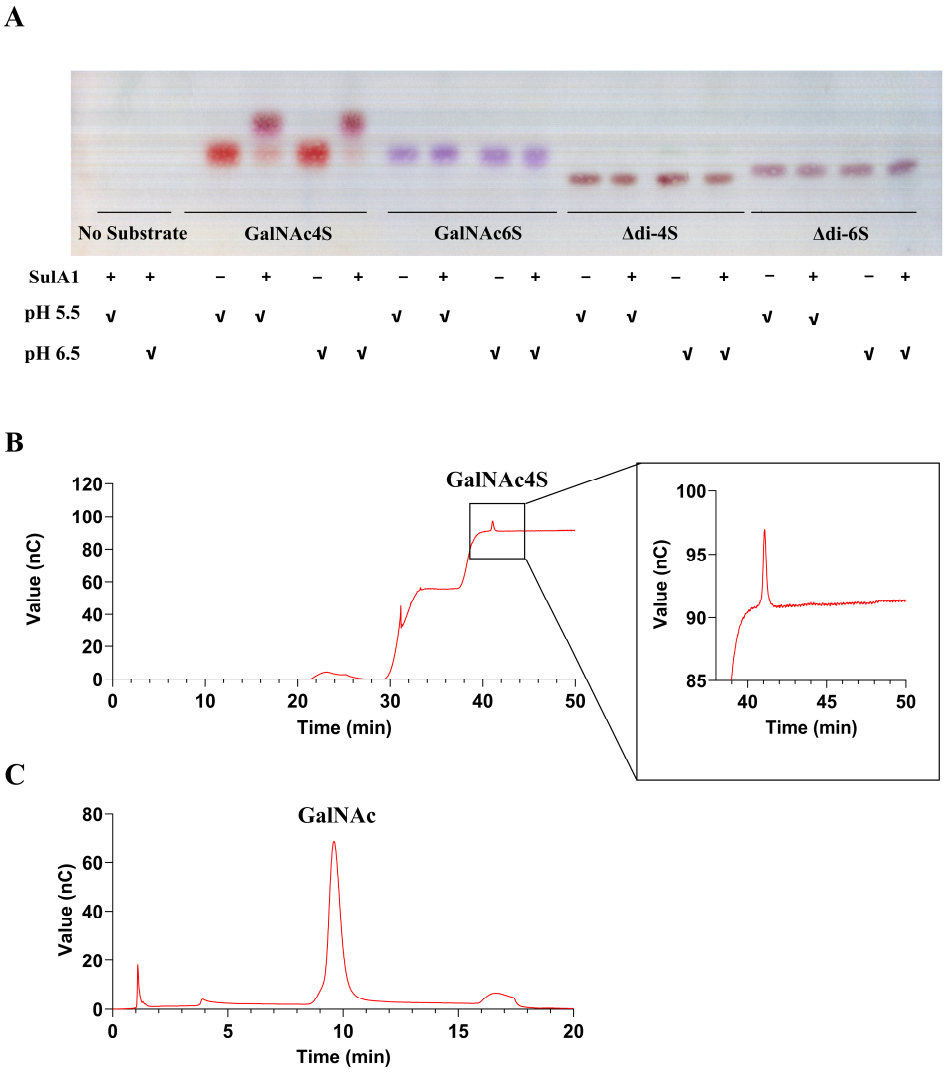

Figure 8. The impact of SulA1 on different chondroitin sulfate products analyzed using TLC and HPAEC-PAD. (**A**) Thin-layer chromatography (TLC) of reaction mixtures containing the monosaccharides *N*-Acetyl-D-galactosamine-4S (GalNAc4S; lane 3–6) and *N*-Acetyl-D-galactosamine-6S (GalNAc6S; lane 7–10) from chondroitin sulfate (CS) and CS-disaccharide; Δdi-4S (lane 11–14) and Δdi-6S (lane 15–18), incubate with (+) or without (−) SulA1 for 30 min at pH 5.5 or pH 6.5 indicated with ✓ using 100 mM acetate buffers. Lane 1 and 2 serve as controls where SulA1 was incubated in absence of a substrate at pH 5.5 or pH 6.5. The reactions were carried out as described in the Materials and Methods section. The mobile phase comprised 1-butanol, acetic acid, and Milli-Q water (2:1:1) and was run for 1.5 h. The TLC plate was dried and developed using a mixture of diphenylamine–aniline–phosphoric acid in acetone. (**B**) Representative chromatograms of the substrate GalNAc4S including a magnified view of the elution peak at 41 min, and the resulting formation of GalNAc (Elution peak 9.5 min; (**C**)) generated from GalNAc4S following a 30 min reaction with SulA1 and detected with HPAEC-PAD.

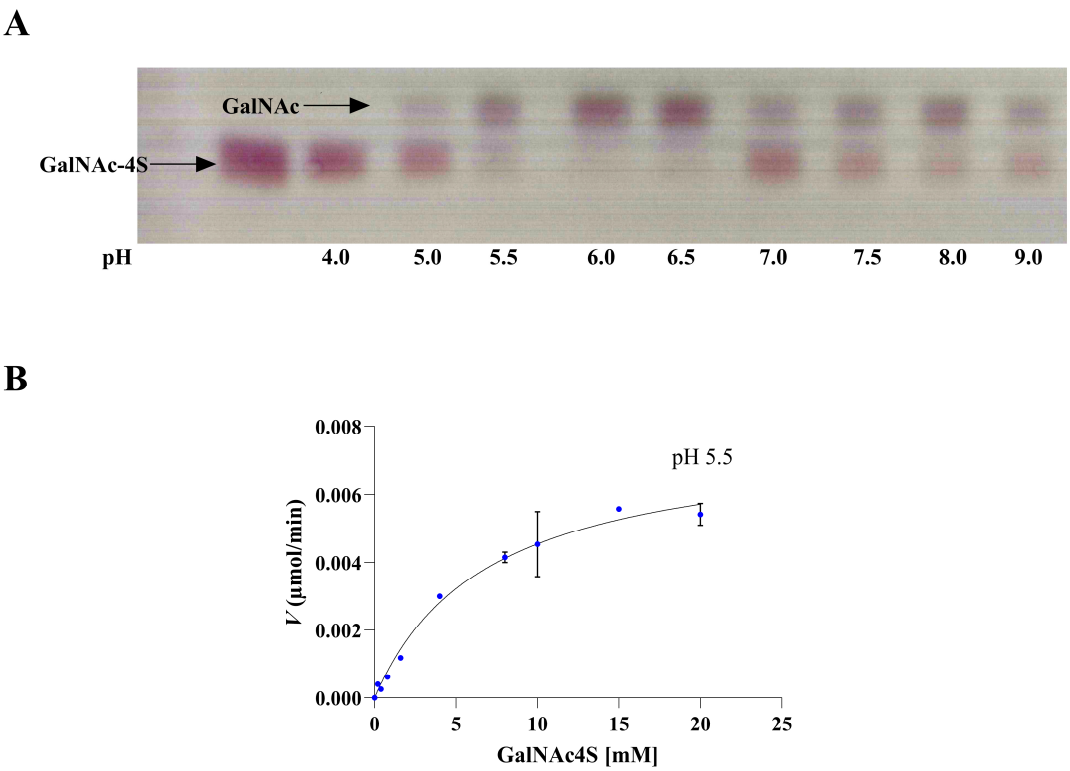

Figure 9. pH optimum and Michaelis–Menten curve of SulA1 using the substrate *N*-Acetyl-D-galactosamine-4-sulfate (GalNAc4S). (**A**) TLC showing reaction mixtures of SulA1 acting on GalNAc-4S at varying pH using 100 mM acetate buffer for pH 4.0-6.5 and 100 mM phosphate buffer for pH 7.0-9.0. Reactions was assayed for 30 min at 40°C and stopped by heating the reaction to 95 °C for 3 min. The mobile phase was 1-butanol, acetic acid, and Milli-Q water (2:1:1), and the plates were run for 1.5 h. Thereafter, the TLC plates were dried and developed using a mixture of diphenylamine–aniline–phosphoric acid in acetone. (**B**) The reaction rate *V* (µmol/min) was plotted against the concentration of GalNAc4S (mM) at pH 5.5. The graph shows the GalNAc formation after the SulA1 reaction with Michaelis–Menten nonlinear curve fitting (black line); data are represented as mean ± SD of two individual experiments.

Activity assays using different concentrations of substrate (GalNAc4S) were carried out to investigate if the SulA1 followed Michaelis–Menten kinetics. In contrast to *p*NCS, SulA1 followed Michaelis–Menten behavior using GalNAc4S at pH 5.5 (Figure 9B). The Michaelis–Menten behavior was also observed at pH 6.5, but was not as clear. At pH 5.5, K_m was determined to be 6.94 ± 0.053 using the Michaelis–Menten nonlinear fitted curve. As 16.5 µg of enzyme was used in the kinetic experiment, the Vmax at saturation corresponded to the specific activity of 6.8 mU/mg SulA1 at pH 5.5 and 40 °C.

Table 6. Comparison of properties of recombinant SulA1 with selected sulfatases.

Enzyme	Type	Size (kDa)	pH Optimum	Temperature Optimum	Ligand	Substrate	Specific Activity	Reference
SulA1	*N*-acetyl-galactosamine-4-*O*-sulfatase	51.9	6.0–6.5	40–50 °C	Ca^{2+}	GalNAc4S	pH 5.5 6.8 mU/mg (at 20 mM GalNAc4S) pH 6.5 14.0 mU/mg (at 15 mM GalNAc4S)	This work
endoVB4SF (*Vibrio* sp. FC509)–pdb:6J66_A	CS/DS 4-*O*-endosulfatase	59.5	8.0	30 °C	none	ΔA [1] CS-A	5020 and 820 mU/mg	[13]
exoPB4SF (*Photobacterium* sp.)–QAB47431.1	Exolytic *N*-acetyl-galactosamine-4-*O*-sulfatase	56.1	8.0	30 °C	Na^{+}, Li^{+}, K^{+}, Mg^{2+}, and Ca^{2+}	ΔA	2857 mU/mg (for the purified protein)	[2]
PB_3262 (*Photobacterium* sp. QA16)–UF91287.1	Endo-CS-4-*O*-Sulfatase	56.7	7.0	50 °C	Ca^{2+} Ba^{2+}	ΔA	165.750 U/mg	[7]
PB_3285 (*Photobacterium* sp. QA16)–UF91288.1	Exolytic CS *N*-acetyl-galactosamine-6-*O*-sulfatase	57.3	7.0	30 °C	Ca^{2+} K^{+}	ΔC [2]	3.64 mU/mg	[7]

CS: chondroitin sulfate. DS: dermatan sulfate. [1] ΔA CS disaccharides ΔHexUA1-3GalNAc4S. [2] ΔC CS disaccharide ΔHexUA1–3GalNAc6S.

3. Discussion

Certain bacteria possess remarkable abilities to efficiently utilize complex sulfated polysaccharides, including glycosaminoglycans (GAGs) such as chondroitin sulfate (CS), for their survival [26]. Consequently, there has been considerable interest in exploring modifications of sulfation patterns in CS and DS to unravel the intricate structure–function relationships associated with CS bioactivities. Despite the abundance of genomic data (with over 41,000 sulfatase entries documented in SulfAtlas), only a few sulfatases have been crystallized, and knowledge regarding substrate specificity is limited. Currently, only 11 other CS/DS sulfatases have been expressed as recombinant proteins and extensively characterized. Early research solely used synthetic aryl substrates to characterize sulfatases, such as *p*NCS, (e.g., [27,28] or *p*-nitrophenyl sulfate (*p*NP-S; [29]). Consequently, this has led to naming the enzymes as arylsulfatases instead of relating the enzymes to their natural function. A more accurate name could be related to their structural modification of the catalytic residue to formyl glycine (FGly), resulting in a structure-based classification of FGly-SULFs. Additionally, our study demonstrated that the use of *p*NCS does not necessarily correspond to the profile of the natural substrate, resulting in misleading pH information. This emphasizes the importance of identifying the enzyme's natural substrate for a comprehensive understanding of its characteristics.

In this study, a FGly-SULF encoding gene was successfully isolated, cloned, and expressed from the marine *Arthrobacter* strain MAT3885, producing the enzyme referred to as SulA1. This sulfatase originated from a microorganism isolated with the aim to identify novel polysaccharides processing chondroitin lyases [23]. The selected sulfatase was found to be encoded in the same gene cluster as the chondroitin lyase, ChoA1, isolated in a previous work. Bioinformatic analysis revealed that the deduced amino acid sequences of the family 1 sulfatase are often similar in length, indicating a conserved topology. This observation was further strengthened by structure-based alignments and homology modeling. Notably, the conserved sulfatase Type 1 signature motif C/SXPXR was identified in SulA1 as well as in all the aligned homologous sequences, in line with the previous findings in the literature [8,9,30]. Notably, characterized CS/DS sulfatases [2,7,13] showed less than 30% identity compared to SulA1 in BLASTp analysis on NCBI, highlighting the novelty of SulA1 and the challenges in predicting substrate specificity based on its structure.

The sequence alignment and the model showed that Cys57 was the catalytic residue that required a post-translational modification to obtain the catalytically active FGly residue.

Additionally, SulA1's active site included conserved residues (Asp17, Asp18, Asp277, and Asn278), forming a metal-ion-binding site. These findings were supported by increased relative activity observed with varying concentrations of calcium. This aligns with the established understanding that FGly-SULFs typically require divalent cations, such as Ca^{2+} (and in a few cases Mg^{2+}), to facilitate substrate binding and polarization [2,7,25]. However, when integrating the DSF assay with varying concentrations of calcium and EDTA, it was revealed that calcium did not constitute to any improvement in the thermostability of SulA1. This was observed by a slight decrease in T_m with an increased calcium concentration and a lack of effect on T_m with EDTA. Conversely, calcium enhanced catalytic activity, and may simultaneously induce conformational changes that compromise the overall stability of SulA1.

The activity of SulA1 was initially assessed in a screening trial using the synthetic substrate *p*NCS. This trial produced a measurable and colorimetric change compared to the blank control. Notably, SulA1 demonstrated sensitivity to both pH and temperature. Particularly, temperatures exceeding 40°C have been reported to significantly impact the relative activity of CS/DS sulfatases, whereas relatively high activity can be observed at room temperature [10,13]. However, the narrow pH was especially low using *p*NCS as the substrate. On the other hand, DSF data at different pH levels, along with confirmed activity on GalNAc4S, affirmed that SulA1's working pH range is between 5.5 and 7.0. This aligns with SulA1's characterization as a cytosolic enzyme.

Estimation of kinetic parameters using *p*NCS as the substrate was not feasible due to a linear relationship between substrate concentration and velocity. This suggested that SulA1 has a low affinity for *p*NCS. A similar linear relationship was reported in previous studies [27,31]. Thus, while *p*NCS serves as a convenient and rapid method for testing the activity of potential FGly-SULFs, it is important to note its limitations. It is not suitable for conducting comprehensive kinetic studies or detailed characterization studies. For such investigations, the identification of natural sulfated substrates is necessary. Among mono-, di-, and oligosaccharides, it was found that SulA1 showed high specific activity towards the amino monosaccharide, GalNAc4S. These findings are in line with the sulfation pattern on the substrate used to isolate the marine *Arthrobacter* strain MAT3885 and with the localization of the *sulA1* gene upstream of the gene encoding the chondroitin lyase, which was previously characterized by Kale and coworkers [23]. No activity was detected using *N*-Acetyl-D-galactosamine-6-sulfate (GalNAc6S) as the substrate. Additionally, SulA1 showed no activity towards any of the CS-oligosaccharides with C4 and/or C6 sulfation. These results suggested that SulA1 is highly specific and is likely involved in the final steps of the CS degradation pathway in a similar manner, as proposed by Wang and coworkers [6]. Furthermore, it can be hypothesized that the neighboring sulfatase (SulA2) located in the same cluster may exhibit complementing sulfatase activity, e.g., towards the GalNAc6S unit. This speculation was supported by the characterization of ChoA1 as a chondroitin AC lyase [23], exhibiting activity towards CS-4S and CS-6S. Additionally, the amino acid sequence of SulA2 shares high topology conservation with the exolytic CS *N*-acetyl-galactosamine-6-*O*-sulfatase [7], with 96% coverage, which could be indicative for functional conservation. No activity was detected for either heparin or κ-carrageenan-derived saccharides, nor for the fucose-containing sulfated polysaccharides (FCSPs) from brown seaweed. This confirms the strict substrate preference of SulA1.

The specific activity of SulA1 was determined at pH 5.5 and pH 6.5 using 20 mM and 15 mM GalNAc4S, respectively, at 40 °C for 30 min, which resulted in specific activities of 6.8 mU/mg and 14.0 mU/mg SulA1. In comparison to other CS-sulfatases acting on the GalNAc4S unit in CS [2,13], these values are low but higher than the exo-acting enzyme termed PB_3285 (3.64 mU/mg, acting on the CS disaccharide 6 sulfate). SulA1 also appeared to strictly prefer the sulfated monosaccharide unit, whereas enzymes such as the endoVBSF from *Vibrio* sp. and exoPB4SF from *Photobacterium* sp. demonstrated activity against both poly and di-saccharides of CS with 4-*O*-sulfation.

Overall, the isolation and characterization of SulA1 provide new insights into the structure, function, and substrate specificity of *N*-acetyl-D-galactosamine-4-*O*-sulfate sulfa-

tase, which is involved in the CS metabolism in the marine *Arthrobacter* strain MAT3885. The addition of 20% glycerol to the purified SulA1 in a 100 mM sodium acetate buffer at pH 5.5, followed by storage at −80 °C, successfully prevented precipitation and maintained SulA1's activity for a minimum of 5 weeks. This preservation of activity not only ensures reproducibility, but also reduces cost and supports its potential in industrial applications.

4. Materials and Methods

4.1. Bacterial Strain and Plasmids

The expression vector pJOE3075 [32] and the bacterial host *Escherichia coli* BL21 C43 [F^- *ompT hsdS*$_B$ (r_B^- m_B^-) *gal dcm* (DE3)] [33] were used for the recombinant production of the sulfatase, SulA1, from the marine *Arthrobacter* strain MAT3885, and the plasmid pJOE3075 was used as vector for the heterologous expression in *E. coli* [32].

4.2. Sequencing, Bioinformatic Analysis, and Structure Modeling

The genome sequencing and annotation of the marine *Arthrobacter* strain MAT3885, using the RAST Server (Rapid Annotation using Subsystem Technology) (rast.nmpdr.org/ (accessed on 2 December 2023)) [34], was performed as previously described by Kale and coworkers [23]. The annotated 16S rDNA gene was subjected to similarity analysis using BlastN to identify the phylogenetically closest related microbial strains. Potential gene clusters in the vicinity of the CS-lyase (identified by Kale et al. [23]) were analyzed based on the RAST-data, allowing us to complete identification of the gene encoding the putative sulfatase (SulA1). The presence of any potential signal peptide was analyzed with Signal IP v5.0 [35].

Sequence similarities between the deduced amino acid sequence of SulA1 and structure determined sulfatases were analyzed using BlastP against the PDB database in NCBI. Conserved residues and motifs were analyzed by submitting the sequence to Interpro (https://www.ebi.ac.uk/interpro/ (accessed on 18 February 2024)). The output was displayed in a multiple sequence alignment, with the identified FGly-SULFs amino acid sequences (detailed below) using the Clustal Omega Multiple Sequence Alignment tool at ENBI-EBI (https://www.ebi.ac.uk/ (accessed on 25 January 2024)).

The SulA1 amino acid sequence was aligned with five best matching sulfatases of known three-dimensional structures from Protein Data Bank (PDB), originating from *Bacteroides thetaiotaomicron* VPI-5482 (PDB 5G2V), *Pseudoalteromonas* sp. (PDB 6B0K), *Bacteroides fragilis* YCH46 (PDB 2QZU), *Pseudoalteromonas fuliginea* (6BIA), and *Hungatella hathewayi* (PDB 6UST). Likewise, the SulA1 amino acid sequence was aligned and used for a comparison against four characterized CS/DS sulfatases derived from *Vibrio* sp. FC509 (PDB 6J66-A), *Photobacterium* sp. (PDB QA16) (GenBank UFQ91287.1 and QAB47431.1), and from *Photobacterium* sp. (GenBank UFQ91288.1), and the SulA2 amino acid sequence found within the chondroitin lyase cluster.

Based on these data, the 3D structure of SulA1 from marine *Arthrobacter* strain MAT3885 was built using YASARA software (http://www.yasara.org/) [36] with the templates highlighted in Table 1 at default settings (Table 7) to obtain a hybrid model. The structure was analyzed and depicted with Chimera [37]. The enzyme–ligand interaction was analyzed with LigPlot+ [38]. In addition, the SulfAtlas database (https://sulfatlas.sb-roscoff.fr/ (accessed on 18 February 2024)) was consulted to confirm the novelty of SulA1.

Table 7. Homology modeling settings.

Parameter	Description
Modeling speed	Slow
PSI-BLAST iterations in template search	3
Maximum allowed (PSI-)BLAST E-value to consider template (EValue Max)	0.5
Maximum number of templates to be used	5
Maximum number of templates with same sequence	1
Maximum oligomerization state	4
Maximum number of alignment variations per template	5
Maximum number of conformations tried per loop	50
Maximum number of residues added to the termini	10

Substrate Docking and MD Simulation

The three-dimensional model of the enzyme was also obtained using AlphaFold2 via ColabFold v1.5.2: AlphaFold2 (colab.research.google.com/github/sokrypton/ColabFold/blob/main/AlphaFold2.ipynb (accessed on 2 February 2024) which was hosted on Colab notebook. The model confidence was assessed via the pLDDT score, and the top ranked model was used for docking experiments. The figures were illustrated using the PyMOL v2.5.4 program (Schrödinger, [39,40]).

Docking of the enzyme with the different sulfated sugars, Gal4S, GalNAc4S, and GalNAc6S, was conducted with the local docking program implemented in YASARA. The ligands were built with the oligosaccharides building tool from YASARA. Each structure was energetically minimized using the AMBER14 forcefield. The three-dimensional model of the enzyme–ligand complexes and the active sites were graphically presented using the PyMOL v2.5.4 program (Schrödinger). The model of the enzyme and the enzyme–ligand complexes were subjected to MD simulations at 293 K and pH 6.0 for 50 ns using a YASARA macro in a simulation cell 20 Å larger than the protein. Snapshots were stored every 100 ps, and the AMBER14 forcefield was used to calculate the energies.

4.3. Cloning of the Sulfatase Gene sulA1

The *sulA1* gene from the marine *Arthrobacter* strain (MAT3885) was amplified via PCR using forward primer SulA1-Nde-f (5′-CGAATTCCATATGGTCAGCTCGTCCCCTGCG-3′) targeting the 5′ end of the orf including the deduced ATG start codon and the reverse primer, SulA1- BamHi-r-his (5′-CGCGGATCCGATTCCATCCCAGTTCGGCG-3′), targeting the 3′ end of the orf excluding the stop codon. The PCR product was digested with *Nde*I and *Bam*HI and ligated into *Nde* I and *Bam*HI-digested pJOE3075 vector. The resulting plasmid with *sulA1* was designated pVK13. As the reverse primer did not include a stop codon, the *sulA1* gene was cloned upstream of and in frame with 6 × 3′ histidine codons.

E. coli BL21(C43) was transformed with the expression vector containing the inserted gene by electroporation [41]. The transformed cells were screened for the *sulA1* gene by performing PCR using the above-described primers. Correct sequence and fusion in the plasmid were verified with sequence analysis.

4.4. Production, Purification, and Storage of the Recombinant Sulfatase

The *E. coli* BL21(C43) strain transformed with pVK13 was inoculated in LB broth containing ampicillin (100 µg/mL) overnight at 37 °C. The overnight culture was further diluted in fresh LB-amp broth (1:100) and cultivated at 37 °C and 200 rpm until an OD_{600} between 0.7 and 0.9 was reached. Gene expression was induced with 10% (*w/v*) L-rhamnose (final concentration of 0.1%). The culture was then grown overnight at room temperature. Cells were harvested via centrifugation (35,700× *g* for 10 min at 4 °C) and resuspended in a lysis buffer and further disrupted via sonication. The cells were kept on ice and centrifugated at 16,000× *g* for 30 min at 4 °C to separate the supernatant from the insoluble debris.

Thereafter, SulA1 was purified using PureCube His Affinity MagBeads (Cube Biotech; https://cube-biotech.com/solubilization-database (accessed on 2 February 2024), Mon-

heim, Germany) using the protocol provided by the manufacturer. In brief, protein purifications were made with PureCube 100 INDOGO Ni-MagBeads (Cube Biotech), using the recommended lysis, wash, and elution buffers. Lysis, binding, and elution buffers consisted of 50 mM NaH_2PO_4 and 300 mM NaCl (pH 8.0) with varying concentrations of imidazole (10, 20, and 500 mM, respectively). After purification, the elution buffer was exchanged with 100 mM acetate buffer pH 5.5 using Amicon Ultra-0.5 centrifugal filter unit with a 30 K cut-off (Merck Millipore, Darmstadt, Germany). The expression level and purification of SulA1 were verified with SDS-PAGE, as described below.

The purified SulA1 enzyme was prepared for storage experiments as follows: First, the enzyme was added to a 30 kD Amicon ® 0.5 mL centrifugal filter, and the elution buffer was exchanged with 0.1M sodium acetate buffer pH 5.5, following the manufacturer's protocol. Afterwards, the solution was supplemented with 80% glycerol to achieve a final concentration of 20%.

4.5. Total Protein Content and Protein Distribution

Total protein content, including the protein content in the purified SulA1 fraction, was determined with the Bradford method [42], with bovine serum albumin as standard. Furthermore, the size distribution of proteins produced in all expression trials and the purity of SulA1 were displayed using sodium dodecyl-sulfate polyacrylamide gel electrophoresis (SDS-PAGE), using Mini-PROTEAN® TGX Stain-Free™ Precast Gels (4–20%, 15–well), in a Tris-glycine-SDS (TGS) running buffer.

4.6. Sulfatase Activity—Standard Assay

To investigate the sulfatase activity, a standard assay based on the synthetic substrate *p*-nitrocatechol sulfate dipotassium salt (*p*NCS; 2.05 mg/mL; Merck, Darmstadt, Germany) was used. In short, 5 µL enzyme extract was mixed with 20 µL 6.5 mM substrate, 10 µL 100 mM acetate buffer, pH 5.5, and 15 µL water, and the reaction was carried out at 40 °C 30 min. The reaction was stopped by adding 100 µL 1 M NaOH. The activity was determined spectrophotometrically at 515 nm. All activity tests on *p*NCS were performed in triplicate and expressed as mean ± SD.

4.7. Temperature Optimum, Thermal Deactivation, and Storage Capacity

The optimal temperature was determined using *p*NCS (see protocol above) assayed at varying temperatures between 20 °C and 90 °C for 30 min.

Thermal deactivation was determined as half-life ($T_{½}$), defined as the temperature at which the enzyme lost 50% of its activity. This was completed by pre-incubating the enzyme at various temperatures (25 °C, 30 °C, 40 °C, 50 °C, 60 °C, and 70 °C) for 30 min, followed by the *p*NCS activity assay under optimal conditions (pH 5.5 and at 40 °C) for 30 min. Residual activity was calculated and plotted against the temperature.

The storage capacity of purified SulA1 in 20% (*v*/*v*) glycerol was tested at three different temperatures: −80 °C, −20 °C, and 4 °C, respectively. The activity was measured by using the standard assay (see above) before storage, and after 1 and 5 weeks of storage, respectively, for each storage condition.

4.8. pH Optimum

The sulfatase activity against *p*NCS was measured at pH ranging from 4.0 to 9.0 by using 100 mM acetate buffers (4.0 to 6.5) and 100 mM phosphate buffers (7.0 to 9.0). Reactions were conducted at 40 °C for 30 min. Similarly, the pH optimum for SulA1 was investigated using GalNAc4S as the substrate. In short, 20 µL GalNAc4S (2 mg/mL) was mixed with 15 µL pure SulA1 (16.5 µg), 10 µL 100 mM acetate buffer (ranging from 5.0 to 6.5) or 10 µL 100 mM phosphate buffers (7.0 to 9.0), and 5 µL Milli-Q water. Reactions were carried out at 40 °C for 30 min and further investigated with TLC (thin-layer chromatography; see protocol below).

4.9. The Effect of Cations and EDTA on Activity

To screen for the effect of different cations effect on SulA1 activity stock solutions of 100 mM $MgCl_2$, $CaCl_2$, KCl, and NaCl were prepared in Milli-Q water and diluted to different concentrations (20 mM, 40 mM, 60 mM, 80 mM, and 100 mM). EDTA was made at 10 mM concentration. Purified SulA1 (3.3 mg/mL) was diluted 3× (1.10 mg/mL), whereas 5 µL SulA1 was pre-incubated for 2 min at 37 °C with 10 µL of 100 mM acetate buffer, pH 5.5, and 15 µL of one of the cation's solutions (at the concentrations defined above), leading to the final concentrations in the assay to become 6 mM, 12 mM, 18 mM, 24 mM, and 30 mM. Moreover, 20 µL substrate *p*NCS (2.05 mg/mL)) was added, and the enzyme activity was assayed at optimum conditions. Given the significant impact of calcium ions, a comprehensive evaluation of calcium concentrations was conducted. The tested concentrations included 0 mM, 5 mM, 10 mM, 20 mM, 40 mM, 60 mM, 70 mM, 80 mM, and 100 mM, corresponding to the final concentrations in the assay, as follows: 0.0 mM, 1.5 mM, 3.0 mM, 6mM, 12 mM, 18.0 mM, 21.0 mM, 24.0 mM, 27.0 mM, and 30 mM.

4.10. Differential Scanning Fluorimetry (DSF) in Presence and Absence of Calcium Ions and EDTA

Thermal stability SulA1 (0.56 g/L in McIlvaine buffer system) was examined under various pH conditions (ranging from 4 to 8.3) using differential scanning fluorimetry (DSF), conducted with the Prometheus NT 48 nanoDSF instrument (NanoTemper Technologies, GmbH, Munich Germany).

The effect of $CaCl_2$ concentrations on the SulA1 thermostability was investigated in the same instrument using 50 µL 100 mM citrate phosphate, buffer (pH 6.03) with different concentrations of $CaCl_2$ (0, 7, and 14 mM, at pH 6.03). In addition, all Ca-ions were chelated using EDTA concentrations from 0 to 5 mM. For each experiment, 10 µL of each sample was loaded in the instrument capillaries subjected to a temperature ramp from 20 °C to 90 °C, with a gradual increase of 1 °C per min. To monitor the unfolding of the protein intrinsic fluorescence at emission, wavelengths of 330 and 350 nm were used.

4.11. Peptide Mass Fingerprinting

Peptide mass fingerprinting was performed using ESI-Orbitrap MS/MS and MASCOT [43] to validate the amino acid sequence of the purified SulA1. The gel fragment with the correct molecular weight was cut from an SDS-PAGE and digested with trypsin in-gel [44]. After in-gel digestion, peptide fragments were determined using MS/MS analysis and compared with the deduced amino acid sequence.

4.12. Preparation of Sulfated Mono-, Di-, and Oligosaccharide Solutions from Various Resources

Different sulfated mono-, di-, and oligosaccharides were tested as substrates for SulA1: chondroitin sulfate dp4 (1 mg; in reaction 0.4 mg/µL, shark origin; Iduron, Alderley Edge, United Kingdom), three chondroitin-based disaccharides with different sulfation patterns; chondroitin disaccharide sodium salts without sulfation (Δdi0S), with sulfation on C4 on the *N*-Acetyl-D-galactosamine (GalNAc) unit (Δdi4S) and with sulfation of C6 on the GalNAc unit (Δdi6) (all 5 mg; in reaction 2 mg/µL; and from Dextra laboratories Ltd, Reading, United Kingdom.), the major monosaccharides units from chondroitin *N*-Acetyl-D-galactosamine-4-sulfate (GalNAc4S) sodium salt and *N*-Acetyl-D-galactosamine-6-sulfate sodium (GalNAc6S) salt (both from Dextra laboratories Ltd.; 5 mg and 1 mg, respectively; in reaction 2 mg/µL and 0.4 mg/µL, respectively), a heparin disaccharide I-H sodium salt (1mg; in reaction 0.4 mg/µL; Sigma-Aldrich), and two sulfated monosaccharides; *N*-Acetyl-D-glucosamine 6-sulfate sodium salt (major unit from heparin sulfate; 25 mg; in reaction 10 mg/µL; Sigma-Aldrich), D-galactose 4-sulfate sodium salt (the sulfated monosaccharide from κ carrageenan; 1 mg; in reaction 0.4 mg/µL; Dextra laboratories Ltd.), two κ carrageenan oligosaccharides; Neocarrabiose-4-*O*-sulfate sodium salt (25 mg; in reaction 10 mg/µL) and Neocarratetraose-41,43-di-*O*-sulfate sodium salt (5 mg; in reaction 2 mg/µL), both from Dextra laboratories Ltd., and finally two seaweed related sugars the L-fucose oligomers from *Chorda filum* cut-off <10 kDa (Fuc310; 6.25 mg/mL, in

reaction 2.5 mg/µL), a sulfated polysaccharide, a Fucoidan sample from ProSea (Batch no. HFI206002, Fmc BioPolymer, 12.5 mg/mL, in reaction 5 mg/µL). Each was mixed with 15 µL 1/3 diluted pure SulA1 (1.1 mg/mL; 0.0165 mg in reaction), 10 µL 100 mM acetate buffer, pH 5.5, and 5 µL Milli-Q water. Enzyme activity was assayed after 30 min, at 40 °C. As controls, for each reaction, 20 µL of the substrate was mixed with 10 µL 100 mM acetate buffer pH 5.5 and 20 µL Milli-Q water without the addition of SulA1.

4.13. Analysis of the Degradation Product by Thin-Layer Chromatography

To verify the activity of SulA1 on the different substrates, TLCs were generated. Samples (2 µL) were taken from each reaction and spotted near the bottom of the TLC Silica gel 60 F_{254} (10 × 20; Merck, Darmstadt, Germany). As the mobile phase, a mixture of 1-butanol, acetic acid, and Milli-Q water (2:1:1) was run for 2 h. Thereafter, the TLC plate was dried and developed using a mixture of diphenylamine–aniline–phosphoric acid in acetone in accordance with the published procedure [45]. Then, the plates were dried and heated at 120 °C, using the TLC Plate Heater III (CAMAG®) until bands became visible.

4.14. Determination of the Kinetic Properties and the Specific Activity of SulA1

The kinetic parameters of SulA1 were attempted to be estimated by quantifying the amount of GalNAc formed after 30 min of incubation at 40 °C with different molarities (0–20 mM) of GalNAc4S, using purified SulA1 (16.5 µg). Similarly, specific activity was determined by quantifying the amount of GalNAc formed after 30 min incubation at 40 °C using 20 mM GalNAc4S, with purified SulA1 (16.5 µg). The reactions were analyzed on a Dionex ICS 5000+ (Thermo Scientific, Waltham, Massachusetts) using high-performance anion exchange chromatography with pulsed amperometric detection (HPAEC-PAD). The column used was the Dionex CarboPac 20 analytical column (3 × 150 mm) and guard column (Thermos fisher scientific, USA). Prior to analysis, the reaction mixtures were filtered through 0.45 µm syringe filter and diluted 4–60-fold in MiliQ water. A standard solution containing GalNAc ranging from 3 mg/L to 53 mg/L was prepared. For the analysis, 10 µL reaction mixture or standard was injected into the system under isocratic conditions at a flow rate of 0.5 mL/min. Both the column and compartments were maintained at a constant temperature of 30 °C. The eluents were (A) 200 mM sodium hydroxide and (C) MiliQ water; to equilibrate the system, 5.0% (A) and 95.0% (C) concentrations were used. The samples were eluted after injection under the same conditions for 14 min. Subsequently, the column was washed with 100% (A) for 7 min.

The elution peak of GalNAc4S was investigated using the same system as above but with a gradient elution protocol. Eluent composition was A: 200 mM NaOH, B: 1 M Sodium Acetate in 200 mM NaOH, and C: Milli-Q water, and the flow rate was 0.4 mL/min. To balance the system, 1.2% (A) and 98.8% (C) concentrations were used. The sample was eluted as follows: 0–20 min 1.2% (A) and 98.8% (C); 18-30 min 50% (A) and 50% (C); 30–36.1 min 20% (A); 30% (B); and 50% (C). Subsequently, the column was washed with 50% (B) and 50% (C) for ~14 min.

The experiment was performed in duplicate, and mean values along with the standard deviations were calculated, as well as specific activity. Likewise, the reaction rates were plotted against the substrate concentrations of GalNAc4S in an attempt to determine the catalytic value K_m using Michaelis–Menten nonlinear equation in GraphPad Prism (10.1.2 (324)).

4.15. Graphs and Statistics

All graphs were generated using GraphPad Prism 10.1.2 (324). All activity tests as well as DFS were performed in triplicate and data were displayed as mean ± SD. The specific activity experiment was completed in duplicate and displayed as mean ± SD.

5. Conclusions

This study included the characterization of a novel sulfatase, SulA1, derived from the marine Arthrobacter strain MAT3885. Through bioinformatic analyses and comprehensive

structural insights from 3D modeling, SulA1 was firmly established as a member of the sulfatase family 1. The successful expression and purification of the recombinant SulA1 facilitated a detailed examination of its biochemical properties. While SulA1 was partly characterized using the synthetic substrate *p*NCS, limitations were encountered regarding pH sensitivity and the determination of the kinetic parameters.

The investigation into natural substrate specificity revealed that SulA1 exhibited high activity against the CS monosaccharide GalNAc4S, underscoring its pivotal role in chondroitin sulfate-A degradation. Notably, the pH range was found to be broader than initially anticipated using *p*NCS as the substrate, and SulA1 displayed Michaelis–Menten behavior at pH 5.5 when GalNAc4s was used as the substrate. These findings highlight the importance of exploring natural substrates to discover the relevant conditions for enzyme catalysis. In essence, this research enhances our understanding of the catalytic mechanism of CS/DS sulfatases, providing valuable insights into their functional roles and paving the way for further investigations in this field.

Supplementary Materials: The following supporting information can be downloaded at: https://www.mdpi.com/article/10.3390/md22030104/s1. Figure S1: Comparison of generated AlphaFold2 and YASARA models of SulA1; Figure S2. Complexes of SulA1 with ligands using molecular docking; Figure S3: Determination pH optimum, temperature optimum, $T_{1/2}$, and calcium ion effects using *p*-nitrocatechol sulfate dipotassium salt as substrate; Figure S4: The effect of four metal ions on SulA1 activity using p-nitrocatechol sulfate dipotassium salt as substrate.

Author Contributions: M.D.C., G.Ó.H. and Ó.F. designed the research; V.K. and R.R.R.S. obtained preliminary data, which was important for the completion of the remaining research; M.D.C., L.A., J.A.L.-P. and H.G. conducted the research and obtained the data used for this manuscript; M.D.C., L.A., J.A.L.-P., Ó.F. and E.N.K. analyzed the data; G.Ó.H., Ó.F. and E.N.K. supervised this study; M.D.C., G.Ó.H., Ó.F. and E.N.K. drafted this manuscript. All authors have read and agreed to the published version of the manuscript.

Funding: This research was funded by the MARIKAT JPI Cofund Blue BioEconomy project (grant number 9082-00021B) and European Union's Horizon Europe program SeaMark (Seaweed-based market applications) project (grant number 101060379).

Institutional Review Board Statement: Not applicable.

Data Availability Statement: The data presented in this study are available upon request from the corresponding author.

Acknowledgments: Katja Bernfur is thanked for MS analysis. DSF analysis was performed at the Lund Protein Production Platform, Lund University, Sweden (http://www.lu.se/lp3 (accessed on 18 February 2024)).

Conflicts of Interest: The authors declare that the research was conducted in the absence of any commercial or financial relationships that could be construed as potential conflicts of interest.

References

1. Silchenko, A.S.; Rasin, A.B.; Zueva, A.O.; Kusaykin, M.I.; Zvyagintseva, T.N.; Kalinovsky, A.I.; Kurilenko, V.V.; Ermakova, S.P. Fucoidan Sulfatases from Marine Bacterium Wenyingzhuangia Fucanilytica CZ1127T. *Biomolecules* **2018**, *8*, 98. [CrossRef]
2. Wang, S.; Su, T.; Zhang, Q.; Guan, J.; He, J.; Gu, L.; Li, F. Comparative Study of Two Chondroitin Sulfate/Dermatan Sulfate 4-O-Sulfatases with High Identity. *Front. Microbiol.* **2019**, *10*, 1309. [CrossRef]
3. Stam, M.; Lelièvre, P.; Hoebeke, M.; Corre, E.; Barbeyron, T.; Michel, G. SulfAtlas, the Sulfatase Database: State of the Art and New Developments. *Nucleic Acids Res.* **2023**, *51*, D647–D653. [CrossRef] [PubMed]
4. Barbeyron, T.; Brillet-Guéguen, L.; Carré, W.; Carrière, C.; Caron, C.; Czjzek, M.; Hoebeke, M.; Michel, G. Matching the Diversity of Sulfated Biomolecules: Creation of a Classification Database for Sulfatases Reflecting Their Substrate Specificity. *PLoS ONE* **2016**, *11*, e0164846. [CrossRef]
5. Helbert, W. Marine Polysaccharide Sulfatases. *Front. Mar. Sci.* **2017**, *4*, 6. [CrossRef]
6. Wang, S.; Sugahara, K.; Li, F. Chondroitin Sulfate/Dermatan Sulfate Sulfatases from Mammals and Bacteria. *Glycoconj. J.* **2016**, *33*, 841–851. [CrossRef]

7. Wei, L.; Zhang, Q.; Lu, D.; Du, M.; Xu, X.; Wang, W.; Zhang, Y.Z.; Yuan, X.; Li, F. Identification and Action Patterns of Two Chondroitin Sulfate Sulfatases From a Marine Bacterium *Photobacterium* Sp. QA16. *Front. Microbiol.* **2022**, *12*, 775124. [CrossRef] [PubMed]
8. Hanson, S.R.; Best, M.D.; Wong, C.H. Sulfatases: Structure, Mechanism, Biological Activity, Inhibition, and Synthetic Utility. *Angew. Chem. Int. Ed.* **2004**, *43*, 5736–5763. [CrossRef]
9. Schlachter, C.R.; Malley, A.O.; Grimes, L.L.; Tomashek, J.J.; Chruszcz, M.; Lee, L.A. Purification, Characterization, and Structural Studies of a Sulfatase from Pedobacter Yulinensis. *Molecules* **2022**, *27*, 87. [CrossRef]
10. Wang, S.; Guan, J.; Zhang, Q.; Chen, X.; Li, F. Identification and Signature Sequences of Bacterial Delta(4,5)Hexuronate-2-O-Sulfatases. *Front. Microbiol.* **2019**, *10*, 704. [CrossRef]
11. Myette, J.R.; Shriver, Z.; Claycamp, C.; Mclean, M.W.; Venkataraman, G.; Sasisekharan, R. The Heparin/Heparan Sulfate 2-O-Sulfatase from Flavobacterium Heparinum. *J. Biol. Chem.* **2003**, *278*, 12157–12166. [CrossRef] [PubMed]
12. Ulmer, J.E.; Vilén, E.M.; Namburi, R.B.; Benjdia, A.; Beneteau, J.; Malleron, A.; Bonnaffé, D.; Driguez, P.A.; Descroix, K.; Lassalle, G.; et al. Characterization of Glycosaminoglycan (GAG) Sulfatases from the Human Gut Symbiont Bacteroides Thetaiotaomicron Reveals the First GAG-Specific Bacterial Endosulfatase. *J. Biol. Chem.* **2014**, *289*, 24289–24303. [CrossRef]
13. Wang, W.; Han, W.; Cai, X.; Zheng, X.; Sugahara, K.; Li, F. Cloning and Characterization of a Novel Chondroitin Sulfate/Dermatan Sulfate 4-O-Endosulfatase from a Marine Bacterium. *J. Biol. Chem.* **2015**, *290*, 7823–7832. [CrossRef] [PubMed]
14. Yamagata, T.; Saito, H.; Habuchi, O.; Suzuki, S. Purification and Properties of Bacterial Chondroitinases and Chondrosulfatases. *J. Biol. Chem.* **1968**, *243*, 1523–1535. [CrossRef]
15. Mucci, A.; Schenetti, L.; Volpi, N. 1H and 13 C Nuclear Magnetic Resonance Identification and Characterization of Components of Chondroitin Sulfates of Various Origin. *Carbohydr. Polym.* **2000**, *41*, 37–45. [CrossRef]
16. Abdallah, M.M.; Fernández, N.; Matias, A.A.; Bronze, M. do R. Hyaluronic Acid and Chondroitin Sulfate from Marine and Terrestrial Sources: Extraction and Purification Methods. *Carbohydr. Polym.* **2020**, *243*, 116441. [CrossRef]
17. Chen, S.; Xue, C.; Yin, L.; Tang, Q.; Yu, G.; Chai, W. Comparison of Structures and Anticoagulant Activities of Fucosylated Chondroitin Sulfates from Different Sea Cucumbers. *Carbohydr. Polym.* **2011**, *83*, 688–696. [CrossRef]
18. García, A.G.; Vergés, J.; Montell, E. Immunomodulatory and Anti-Inflammatory Effects of Chondroitin Sulphate. *J. Cell Mol. Med.* **2009**, *13*, 1451–1463. [CrossRef]
19. Ustyuzhanina, N.E.; Bilan, M.I.; Dmitrenok, A.S.; Shashkov, A.S. Two Structurally Similar Fucosylated Chondroitin Sulfates from the Holothurian Species Stichopus Chloronotus and Stichopus Horrens. *Carbohydr. Polym.* **2018**, *189*, 10–14. [CrossRef]
20. Ilieva, K.M.; Cheung, A.; Mele, S.; Chiaruttini, G.; Crescioli, S.; Griffin, M.; Nakamura, M.; Spicer, J.F.; Tsoka, S.; Lacy, K.E.; et al. Chondroitin Sulfate Proteoglycan 4 and Its Potential As an Antibody Immunotherapy Target across Different Tumor Types. *Front. Immunol.* **2018**, *8*, 1911. [CrossRef]
21. Bougatef, H.; Krichen, F.; Capitani, F.; Amor, I.B.; Maccari, F.; Mantovani, V.; Galeotti, F.; Volpi, N.; Bougatef, A.; Sila, A. Chondroitin Sulfate/Dermatan Sulfate from Corb (*Sciaena Umbra*) Skin: Purification, Structural Analysis and Anticoagulant Effect. *Carbohydr. Polym.* **2018**, *196*, 272–278. [CrossRef] [PubMed]
22. Randomized, A.; Gabay, C.; Medinger-sadowski, C.; Gascon, D.; Kolo, F.; Finckh, A. Symptomatic Effects of Chondroitin 4 and Chondroitin 6 Sulfate on Hand Osteoarthritis. *Arthritis Rheum.* **2011**, *63*, 3383–3391. [CrossRef]
23. Kale, V.; Friðjónsson, Ó.; Jónsson, J.Ó.; Kristinsson, H.G.; Ómarsdóttir, S.; Hreggviðsson, G. Chondroitin Lyase from a Marine Arthrobacter Sp. MAT3885 for the Production of Chondroitin Sulfate Disaccharides. *Mar. Biotechnol.* **2015**, *17*, 479–492. [CrossRef] [PubMed]
24. Huang, S.Y.; Zou, X. Advances and Challenges in Protein-Ligand Docking. *Int. J. Mol. Sci.* **2010**, *11*, 3016–3034. [CrossRef] [PubMed]
25. Appel, M.J.; Bertozzi, C.R. Formylglycine, a Post-Translationally Generated Residue with Unique Catalytic Capabilities and Biotechnology Applications. *ACS Chem. Biol.* **2015**, *10*, 72–84. [CrossRef] [PubMed]
26. Ndeh, D.; Baslé, A.; Strahl, H.; Yates, E.A.; McClurgg, U.L.; Henrissat, B.; Terrapon, N.; Cartmell, A. Metabolism of Multiple Glycosaminoglycans by Bacteroides Thetaiotaomicron Is Orchestrated by a Versatile Core Genetic Locus. *Nat. Commun.* **2020**, *11*, 646. [CrossRef]
27. Matusiewicz, M.; Krzystek-Korpacka, M.; Dabrowski, K. Characterization of Arylsulfatase Activity in Brine Shrimp, Artemia Salina. *J. Exp. Mar. Biol. Ecol.* **2005**, *317*, 175–187. [CrossRef]
28. Bhattacharyya, S.; Look, D.; Tobacman, J.K. Increased Arylsulfatase B Activity in Cystic Fibrosis Cells Following Correction of CFTR. *Clin. Chim. Acta* **2007**, *380*, 122–127. [CrossRef]
29. Berteau, O.; Guillot, A.; Benjdia, A.; Rabot, S. A New Type of Bacterial Sulfatase Reveals a Novel Maturation Pathway in Prokaryotes. *J. Biol. Chem.* **2006**, *281*, 22464–22470. [CrossRef] [PubMed]
30. Sardiello, M.; Annunziata, I.; Roma, G.; Ballabio, A. Sulfatases and Sulfatase Modifying Factors: An Exclusive and Promiscuous Relationship. *J. Jpn. For. Soc.* **2005**, *14*, 3203–3217. [CrossRef] [PubMed]
31. Thompson, B.D.; William, D.L.; Janet, G.H. Comparative Studies of Rodent Anionic Arylsulfatases. *Comp. Biochem. Physiol. Part B Biochem.* **1985**, *82*, 55–61. [CrossRef]
32. Wegerer, A.; Sun, T.; Altenbuchner, J. Optimization of an *E. coli* L-Rhamnose-Inducible Expression Vector: Test of Various Genetic Module Combinations. *BMC Biotechnol.* **2008**, *8*, 2. [CrossRef]

33. Dumon-Seignovert, L.; Cariot, G.; Vuillard, L. The Toxicity of Recombinant Proteins in *Escherichia coli*: A Comparison of Overexpression in BL21(DE3), C41(DE3), and C43(DE3). *Protein Expr. Purif.* **2004**, *37*, 203–206. [CrossRef]
34. Aziz, R.K.; Bartels, D.; Best, A.; DeJongh, M.; Disz, T.; Edwards, R.A.; Formsma, K.; Gerdes, S.; Glass, E.M.; Kubal, M.; et al. The RAST Server: Rapid Annotations Using Subsystems Technology. *BMC Genom.* **2008**, *9*, 75. [CrossRef]
35. Armenteros, J.J.A.; Tsirigos, K.D.; Sønderby, C.K.; Petersen, T.N.; Winther, O.; Brunak, S.; von Heijne, G.; Nielsen, H. SignalP 5.0 Improves Signal Peptide Predictions Using Deep Neural Networks. *Nat. Biotechnol.* **2019**, *37*, 420–423. [CrossRef]
36. Land, H.; Humble, M.S. YASARA: A Tool to Obtain Structural Guidance in Biocatalytic Investigations. *Methods Mol. Biol.* **2018**, *1685*, 43–67. [CrossRef] [PubMed]
37. Pettersen, E.F.; Goddard, T.D.; Huang, C.C.; Couch, G.S.; Greenblatt, D.M.; Meng, E.C.; Ferrin, T.E. UCSF Chimera—A Visualization System for Exploratory Research and Analysis. *J. Comput. Chem.* **2004**, *25*, 1605–1612. [CrossRef] [PubMed]
38. Laskowski, R.A.; Swindells, M.B. LigPlot+: Multiple Ligand-Protein Interaction Diagrams for Drug Discovery. *J. Chem. Inf. Model.* **2011**, *51*, 2778–2786. [CrossRef] [PubMed]
39. Mirdita, M.; Steinegger, M.; Söding, J. MMseqs2 Desktop and Local Web Server App for Fast, Interactive Sequence Searches. *Bioinformatics* **2019**, *35*, 2856–2858. [CrossRef] [PubMed]
40. Jumper, J.; Evans, R.; Pritzel, A.; Green, T.; Figurnov, M.; Ronneberger, O.; Tunyasuvunakool, K.; Bates, R.; Žídek, A.; Potapenko, A.; et al. Highly Accurate Protein Structure Prediction with AlphaFold. *Nature* **2021**, *596*, 583–589. [CrossRef] [PubMed]
41. Dower, W.J.; Miller, J.F.; Ragsdale, C.W. High Efficiency Transformation of *E. coli* by High Voltage Electroporation. *Nucleic Acids Res.* **1988**, *16*, 6127–6145. [CrossRef] [PubMed]
42. Bradford, M.M. A Rapid and Sensitive Method for the Quantitation of Microgram Quantities of Protein Utilizing the Principle of Protein-Dye Binding. *Anal. Biochem.* **1976**, *72*, 248–254. [CrossRef] [PubMed]
43. Perkins, D.N.; Pappin, D.J.C.; Creasy, D.M.; Cottrell, J.S. Probability-Based Protein Identification by Searching Sequence Databases Using Mass Spectrometry Data. *Electrophor. Int. J.* **1999**, *20*, 3551–3567. [CrossRef]
44. Shevchenko, A.; Tomas, H.; Havliš, J.; Olsen, J.V.; Mann, M. In-Gel Digestion for Mass Spectrometric Characterization of Proteins and Proteomes. *Nat. Protoc.* **2007**, *1*, 2856–2860. [CrossRef] [PubMed]
45. Jork, H.; Funk, W.; Fischer, W.; Wimmer, H. *Thin-Layer Chromatography*; VCH: Weinheim, Germany, 1990; Volume 1a, ISBN 3527278346.

Paper II

International Journal of Biological Macromolecules 306 (2025) 141287

Contents lists available at ScienceDirect

International Journal of Biological Macromolecules

journal homepage: www.elsevier.com/locate/ijbiomac

Laminarins and their derivatives affect dendritic cell activation and their crosstalk with T cells

Monica Daugbjerg Christensen [a,b,c,*], Leila Allahgholi [d], Justyna M. Dobruchowska [e], Antoine Moenaert [a,f], Hörður Guðmundsson [a], Ólafur Friðjónsson [a], Eva Nordberg Karlsson [d], Guðmundur Ó. Hreggviðsson [a,f], Jona Freysdottir [c,g]

[a] Department of Biotechnology and Biomedicine, Matís ohf, Vínlandsleið 12, IS-113 Reykjavík, Iceland
[b] Faculty of Food Science and Nutrition, University of Iceland, Sæmundargata12, IS-102 Reykjavík, Iceland
[c] Department of Immunology, Landspitali—The National University Hospital of Iceland, IS-101 Reykjavik, Iceland
[d] Division of Biotechnology, Department of Chemistry, Lund University, PO Box 124, SE-221 00 Lund, Sweden
[e] Department of Chemical Biology and Drug Discovery, Utrecht Institute for Pharmaceutical Sciences, Bijvoet Center for Biomolecular Research, Utrecht University, Universiteitsweg 99, 3584 CG Utrecht, the Netherlands
[f] Faculty of Life and Environmental Sciences, University of Iceland, Sturlugata 7, IS-102 Reykjavík, Iceland
[g] Faculty of Medicine, Biomedical Center, University of Iceland, Vatnsmyrarvegur 16, IS-101 Reykjavik, Iceland

ARTICLE INFO

Keywords:
Laminarin structure
Dendritic cells
Allogeneic T-cells
Immunomodulating effects
Brown macroalgae

ABSTRACT

This research explores the impact of structural variations in laminarins derived from seaweed on their immunomodulatory properties. Laminarins from *Laminaria digitata*, *L. hyperborea*, and *Saccharina latissima,* were obtained using a two-step water extraction protocol, followed by structural characterization by FT-IR spectroscopy, ^{1}H NMR, and MALDI-TOF MS. The laminarin backbones were confirmed as β–1,3-linked glucans with species-specific percentages of β–1,6-linkages (~10 %, ~4 %, and ~21 %, respectively). Each polymer chain consists of approximately 24 to 25 monomer units, while oligosaccharide fractions, produced using the enzyme LPHase, displayed distinct DP-ranges, degrees of β–1,6-branching and intrachain linkages. Laminarin from *L. hyperborea* and specific oligosaccharide fractions from *L. hyperborea* and *S. latissima* influenced cytokine secretion by dendritic cells (DCs). *L. hyperborea* laminarin and the fraction *Lh*F5 (DP5–DP8) stimulated increased IL-6 and IL-10 secretion by DCs, suggesting a dual role in promoting inflammation and regulating the immune response. In contrast, *Lh*F5, *Lh*F4 (DP6–DP10), and *S. latissima* laminari-oligosaccharide fraction *Sl*F3 (DP6–DP9) caused decreased TNFα secretion, reflecting anti-inflammatory potential. Co-culturing of treated DCs and CD4^{+} T-cells showed that *L. hyperborea* laminarin caused increased IL-17 and IL-10 secretion, whereas *Sl*F3 caused reduced IL-12p40 and IFN-γ secretion. These findings show that DC maturation and T-cell activation are affected by laminarins of certain size-distribution and branching, implying therapeutic potential for the treatment of inflammatory diseases or vaccine enhancement.

1. Introduction

Brown seaweed, encompassing around 2000 different species, is a potentially rich source of health promoting compounds [1]. This has raised significant interest in studying their potential for medical purposes or as functional foods. One of the compounds of interest is laminarin, a low-molecular-weight storage polysaccharide (2–7 kDa), with a degree of polymerization (DP) in the range of 25–40 [2–4]. Laminarin is a water-soluble β-glucan, consisting of a β–1,3–D-glucose backbone, interspersed with β–1,6-linked glucose moieties [5]. The content and positioning of β–1,6 linkages in laminarins varies depending on the species, season, and environmental conditions [6]. The β–1,6-linkages can be internal in the linear β–1,3-backbone (intrachain) or form branch-points (branched β-glucan oligosaccharides) [3,7]. Furthermore, the laminarin glucan chains are capped at the reducing end with either mannitol or glucose moieties, referred to as M-chains and G-chains, respectively. The content and distribution of these two variants also varies among species [7,8].

* Corresponding author at: Department of Biotechnology and Biomedicine, Matís ohf, Vínlandsleið 12, IS-113 Reykjavík, Iceland.
E-mail address: monica@matis.is (M.D. Christensen).

https://doi.org/10.1016/j.ijbiomac.2025.141287
Received 11 December 2024; Received in revised form 28 January 2025; Accepted 17 February 2025
Available online 19 February 2025

Laminarin polysaccharides have been associated with a range of bioactive properties including: antioxidant, anti-inflammatory, anti-apoptotic, immunomodulation, and potential anti-cancer properties [4,9–13]. Due to their bioactivities, they are promising candidates for nutraceutical and pharmaceutical applications. However, the relation between structural features and biological functions of laminarin is not yet fully understood. Addressing this knowledge gap is critical for developing laminarin-based interventions, particularly for functional foods or therapies targeting immune-related disorders, such as inflammatory diseases, or enhancing vaccine efficacy. The bioactive properties of laminarin polysaccharides have been proposed to be associated with their structural features, such as DP, degree of branching (DB), and the ratio of β–1,3 to β–1,6-glycosidic linkages, but also affected by purity [4,5,11,14]. Conventional extraction methods for laminarin have often used acidic conditions, which can alter the compound's structure and potentially lead to inconsistent bioactivity results [15]. For example, treatment with 0.1 M hydrochloric acid has been shown to lower the DP of oat-derived β-glucan by breaking 1,3– and 1,4–β-linkages, thereby increasing the amounts of glucose and smaller oligosaccharides [16]. Additionally, mildly acidic conditions have been intentionally used to produce high-value oligosaccharides from *L. digitata*, leading to laminarin oligosaccharides with modified antioxidant and prebiotic properties [17]. Methods that introduce structural changes, also introduce challenges in relating structure to function, making it essential to determine detailed structures in the same batch as used for the documentation of the bioactivity. Further knowledge on the native laminarins, is also essential for rational choices of raw-material, to improve our understanding of which species produce relevant laminarins for specific applications. Moreover, existence of impurities and high ash content can result in misleading conclusions regarding bioactivities. This was documented in a study by Smith and colleagues (2018), where a laminarin sample was initially acting as a Dectin-1 antagonist, but after removing low molecular weight impurities it became a Dectin-1 agonist [4,5,11,14].

Recently, enzymatic digestion methods, using laminaripentaose-producing β–1,3-glucanases suitable for hydrolyzing laminarin into oligosaccharides, have been employed to elucidate more structural details in biomacromolecules like laminarin [5]. Liu and colleagues [5] applied this method combined with HPAEC-PAD-MS/MS analysis to, e.g., reveal the presence of β–1,6-linkages in laminarins from *L. digitata* and *Eisenia bicyclis*. This method can not only provide insight into the structural intricacies of laminarin but can also help to explore structure-function relationships of the produced oligosaccharides. Laminarin-degrading enzymes have, therefore been used to generate laminari-oligosaccharides to study bioactivities, including antioxidant, antidiabetic, and to a certain extent, immuno-modulating effects [7,12,18]. However, the relation between oligosaccharide structures and immunomodulating activities is still underexplored, and thus far no definite conclusions are drawn.

DCs are the key initiators of the adaptive immune response, by activating and polarizing naïve T-cell responses. In their immature state, they reside in tissues, functioning as sentinels scanning for danger signals [19,20]. When encountering foreign antigens, such as pathogen- or damage-associated molecular patterns (PAMPs or DAMPs), DCs activate and undergo phenotypic and functional changes transforming them into their mature stage. This maturation involves the up-regulation of surface molecules vital for antigen presentation, such as major histocompatibility complex (MHC) molecules, as well as the co-stimulatory molecules CD80 and CD86 [20]. Subsequently, mature DCs migrate to draining lymph nodes where they prime naïve T-cells, steering them toward becoming effector cells, including T-helper (Th)1, Th2, and Th17 subsets, or cytotoxic T-cells [21,22]. The repertoire of cytokines secreted by the mature DCs during this process depends on the PAMPs or DAMPs encountered [19,20].

Notably, the cytokines secreted by DCs orchestrate the downstream immune responses, such as IL-12 and IL-6, which direct the polarization of naïve $CD4^+$ T-cells into Th1 or Th17 effector cells, respectively [23,24]. However, IL-6 has a complex role in immune modulation, as reviewed in [25]. It is a pro-inflammatory cytokine critical for activating Th17 responses against extracellular pathogens and initiating acute inflammation, whereas it can also promote production of IL-10 by T cells, thus restricting inflammatory processes [25]. Simultaneous upregulation of IL-6 and IL-10 cytokine secretion can, therefore, be linked to anti-inflammatory responses. TNFα, is a potent pro-inflammatory cytokine, which plays a pivotal role in driving inflammation and the activation of immune cells [26,27]. However, its sustained production can contribute to chronic inflammation and tissue damage. This is observed in numerous autoimmune disorders, such as rheumatoid arthritis, inflammatory bowel disease, psoriatic arthritis and multiple sclerosis (reviewed [28], which respond well to anti-TNF therapy. IL-10 acts as a potent anti-inflammatory cytokine that suppresses the production of pro-inflammatory mediators (e.g., TNFα, IL-1β, IL-6) and reduces the expression of MHC and co-stimulatory molecules on DCs [29]. While extended production of IL-6 and TNFα initiates the recruitment and activation of immune effector cells, IL-10 counter-regulates these processes to mitigate excessive immune activation and restore homeostasis [29,30]. These mechanisms are in line with the complex effects of laminarin and its oligosaccharides on cytokine secretion observed in this study, reflecting both pro-inflammatory and regulatory capacities. Such immunomodulatory properties highlight their multiple potential in therapeutic applications, including the treatment of inflammatory diseases and immune-mediated disorders.

In this study, a mild two-step water extraction protocol was used for laminarin extraction. A temperature escalation approach was applied for effective isolation of laminarin. This method was chosen for its simplicity, eco-friendliness, and ability to avoid the use of residual solvents or chemical modifications, which is critical for applications in functional foods, pharmaceuticals, or nutraceuticals, where regulatory compliance and consumer safety are paramount. This approach not only preserves the structural integrity of laminarin but also simplifies the purification process, avoiding the need for additional reagents or complex downstream procedures. As mentioned, mildly acidic extraction conditions can alter laminarin's structure by breaking β-linkages, reducing the DP, resulting in production of altered structures with smaller oligosaccharides. In contrast, our protocol avoids such extremes, ensuring that the laminarin's structural and functional characteristics remain intact. Although alternative methods, such as enzymatic hydrolysis or ultrasound-assisted extraction, may offer higher yields or efficiency, these techniques often require additional reagents or specialized equipment, increasing both complexity and cost. High purity of the laminarins was ensured by including precipitation, filtration, and dialysis of the extracts from *L. digitata*, *L. hyperborea,* and *S. latissima*. The output, purity, DP and DB of the extracted laminarins were subsequently evaluated by high-performance anion exchange chromatography with pulsed amperometric detection (HPAEC-PAD), Fourier-transform infrared spectroscopy (FT-IR), proton nuclear magnetic resonance (^{1}H NMR), and Matrix-Assisted Laser Desorption/Ionization Time-of-Flight Mass Spectrometry (MALDI-TOF MS). Furthermore, the laminarins extracted from the aforementioned species were subjected to enzymatic hydrolysis to produce laminari-oligosaccharides of different sizes and DB. The hydrolysis process was executed using the laminaripentaose-producing endo-1,3–β-glucanase (LPHase) from *Streptomyces matensis* DIC-108 [31], in an attempt to create laminari-oligosaccharides with varied immunomodulating effect and facilitating a systematic exploration of their structure-function relationships. Given laminarin's structural complexity and species-specific variations, we hypothesize that its immunomodulatory effects are associated with distinct structural features, including DP, branching patterns, and β–1,6-linkage content, which may influence its interactions with immune cells. By utilizing a mild, non-degradative extraction method and precise enzymatic hydrolysis to produce laminari-oligosaccharides, this study aims to correlate these structural characteristics systematically with

immunomodulatory activities by exploring their impact on the maturation and activation of human monocyte-derived DCs, as well as the ability of laminarin- or laminari-oligosaccharide treated monocyte-derived DCs to activate and differentiate allogeneic $CD4^+$ T-cells. This is an innovative approach to bridging the existing knowledge gap concerning the structure-function relationships in laminarins, offering potential applications in developing laminarin-based nutraceuticals or therapeutic agents, for the context of treating inflammatory diseases or enhancing vaccine efficacy.

2. Material and method

2.1. Materials

Dried *S. latissima* was kindly provided by Annette Bruhn (Department of Bioscience at Aarhus University, AlgeCenter, Denmark). Similarly, dried *L. hyperborea* and *L. digitata* were provided by Íslensk Bláskel og Sjávargróður, Iceland. The samples were harvested during summer (2018) to assure high laminarin yields. Voucher specimens for *L. hyperborea* and *L. digitata* were deposited and are available for reference. Unfortunately, it was not possible to deposit a voucher specimen for *S. latissima*. The dried raw materials were stored in sealed bags, at room temperature, in the dark. Purified laminarin from *L. digitata* (harvested in Iceland) was also obtained from Merck (Darmstadt, Germany, Lot #SLCG6449), and was stored according to the manufacturer's instructions. The *S. latissima*, *L. hyperborea*, and the commercial *L. digitata* biomasses were used to generate the laminari-oligosaccharides fractions described in Section 2.4.2.

2.2. Laminarin extractions and purification

2.2.1. Extractions and filtration

Dried *L. hyperborea* and *S. latissima* were ground to a fine powder (~1 mm particle size) using an IKA® A10 mill. Crude laminarin was extracted with a two-step water protocol: 100 g of seaweed powder was mixed with 1.5 L distilled water, initially extracted at 30 °C for 2 h with continuous shaking (75 rpm), followed by extraction at 70 °C for 3 h. The cooled extracts (4 °C overnight) were centrifuged (~12,000*g* for 20 min) to separate pellets and supernatants. The pellets were recentrifuged to maximize yield.

Calcium chloride ($CaCl_2$) of 1 % was used at 4 °C overnight to precipitate alginate, a well-established method for isolating polysaccharides [32], followed by centrifugation (~12,000*g* for 20 min) to separate and discard the precipitated alginate pellet from the extract. For further purification, the clear laminarin extracts underwent filtration using the Cogent®10 M1 tangential flow filtration (TFF) system (Merck Millipore) equipped with 10 kDa filters. Subsequently, the extracts were further purified by dialysis on the TFF-system using 1 kDa filters. The extracts were lyophilized and stored at −20 °C until further use.

2.2.2. Separation of *L. hyperborea*-derived laminarin from fucoidan polysaccharides by anion-exchange chromatography

The extract from *L. hyperborea* (extracted as described in Section 2.2.1) required further purification to separate laminarin from fucoidan. A 10 mg dried extract sample was dissolved in 1 mL of distilled water and loaded onto a DEAE-cellulose column (1 × 20 cm; Sigma-Aldrich, St. Louis, MO, USA), equilibrated with distilled water. Laminarin fractions were eluted with water and lyophilized. The remaining material in the column was fucoidan (containing sulfate as anionic functional group), which was eluted with 1 M ammonium bicarbonate buffer.

2.3. Composition analyses and profiling of the laminarin polysaccharides

2.3.1. Total phenolic content (TPC)

Portions (100 mg) of lyophilized laminarin extracts were dissolved in 10 mL ultrapure water (Milli-Q grade) and vortexed until all the powder was dissolved. The total phenolic content was determined using the method published by Singleton and Rossi [33], adapted to a microplate format with some modifications. Briefly, 20 μL of the sample was mixed with 100 μL of 0.2 N Folin & Ciocalteu's phenol reagent (Sigma-Aldrich) and incubated at room temperature for 5 min. Then, 80 μL of 7.5 % Na_2CO_3 (Sigma-Aldrich) were added, and the mixture was heated for 10 s in microwave oven at 550 W. After heating, the mixture was incubated at room temperature for 30 min under constant agitation. Absorbance was read at 730 nm using a microplate reader (Thermo Scientific MultiSkan Sky with SkanIt software 6.0.1). A standard curve with seven concentrations of phloroglucinol was used, and results were expressed as mg of phloroglucinol equivalents (PGE) per 100 g of lyophilized laminarin extract, obtained through interpolation from regression analysis.

2.3.2. Ash content

Ash content was measured after combusting the moisture free powder at 550 °C for 10 h in a furnace [34]. All measurements were carried out in duplicates, and quantification was done gravimetrically.

2.3.3. Carbohydrate composition quantification and laminarin profiling

The carbohydrate composition of the water-extracted laminarin samples and the commercial sample was quantified using a two-step sulfuric acid hydrolysis, adjusted for algal biomass [35]. An amount of 25 mg of freeze-dried extracts was mixed with 250 μL of 72 % sulfuric acid in Pyrex tubes, and the samples were incubated at 30 °C for 1 h with shaking (150 rpm). Then, the acid was diluted to 4 % (*w/w*) by adding 7 mL of distilled water to the tubes and then the samples were autoclaved for 1 h at 121 °C (1 atm). The hydrolysates were cooled to room temperature and centrifuged at 3000 ×*g* for 5 min (Sigma 3–16PK centrifuge, Sigma), followed by neutralization of the supernatants with Ba $(OH)_2{\cdot}H_2O$ (0.1 M). Removal of precipitated residues was done by centrifugation at 3000 ×*g* for 5 min (Sigma 3–16PK centrifuge, Sigma). The neutralized hydrolysates were diluted and filtered through 0.2 μm PTFE syringe filters (Pall) and analyzed using HPAEC-PAD (Thermo Fisher Scientific), with a Dionex CarboPac PA-20 analytical column and a corresponding guard column (Thermo Fisher Scientific) for monosaccharide separation. The separation of monosaccharides and uronic acid was performed under isocratic conditions at a flow rate of 0.5 mL/min. Eluents for separation of monosaccharides and mannitol were (A) milliQ-water, (B) 2 mM NaOH, and (C) 200 mM NaOH. Separation was done using an eluent mixture of 62.5 % (A) and 37.5 % (B) for 30 min. For separation of uronic acids, eluent (B) was 1 M sodium acetate in 200 mM NaOH while eluents (A) and (C) were the same as for monosaccharide separation. The uronic acids were eluted by an eluent mixture of 55 % (A), 15 % (B) and 30 % (C) for 18 min. The column and the compartment temperature were kept at 30 °C. All the experiments were performed in duplicate, and the mean value and standard deviation were calculated. Total carbohydrates were estimated as the sum of all individual monomeric sugars.

2.4. Enzymatic generation of laminari-oligosaccharides

2.4.1. Expression of the lph gene and production of recombinant LPHase in *Escherichia coli*

The sequence for LPHase (encoding 376 amino acids) was obtained from *Streptomyces matensis* DIC-108, as previously described [31], and was extended with a maltose-binding protein domain (MalE) in the cloning design to enhance solubility. The gene was amplified using the forward primer f(CCATCGTGAACAGATTGGTGGCGCCGCCGTTCCAGCGACCATTC) and the reverse primer, r(TTAATGATGATGATGATGATGGG*GATCC*ATCGAACGGGTCCAGAGTCAG). The expression vector pHWG1106 [36] was linearized with *Kas*I and *Bam*HI and subsequently, the gene was inserted into the vector using the NEBuilder® HiFi DNA Assembly Cloning Kit (New England Biolabs Inc.). The resulting plasmid,

pHG247, was introduced into *E. coli* NEB10 beta competent cells by transformation. Expression was achieved by cultivating pHG247/NEB10 in 30 mL LB broth supplemented with ampicillin (100 μg/mL) at 37 °C until reaching an OD_{600} 0.7. The culture was then moved to room temperature and allowed to grow until reaching an OD_{600} of approximately 0.9. Gene expression was induced by adding 10 % (*w/v*) L-rhamnose, resulting in a final concentration of 0.15 %. The culture was incubated overnight at room temperature. Cells were harvested by centrifugation at 3,400*g* for 10 min at 4 °C (~0.3 g) and resuspended in four times the volume of lysis buffer (~1.2 mL; 50 mM sodium citrate, pH 6, 150 mM NaCl, 15 % glycerol). Cell disruption was achieved by sonication on ice. The cell lysate was centrifuged at 16,000*g* for 30 min at 4 °C to separate the supernatant from the insoluble debris. Expression of LPHase was confirmed by sodium dodecyl-sulfate polyacrylamide gel electrophoresis (SDS-PAGE), using Mini-PROTEAN® TGX Stain-Free™ Precast Gels (4–20 %, 15-well), in Tris-glycine-SDS (TGS) running buffer. The supernatant was stored as a crude extract at −80 °C until use in laminarin hydrolysis experiments.

2.4.2. Enzymatic laminarin hydrolysis and purification of laminari-oligosaccharide extracts

The enzymatic hydrolysis was conducted at 50 °C and pH 5.7, as optimized for LPHase activity. Simultaneously, dialysis was performed to separate the laminari-oligosaccharides from the substrate. The procedure was as follows: A 50 mL 4 % solution of lyophilized laminarin from *L. digitata*, *L. hyperborea* and *S. latissima* was prepared by mixing it with 20 mM sodium citrate buffer (pH 5.7). LPHase crude extract was added to the laminarin solutions at a volume of 200 μL, corresponding to approximately 1.2 mg per reaction. The mixtures were transferred into Slide-A-Lyzer® 3.5 K Dialysis cassettes G2 (Thermo Scientific) and placed in 1 L beakers. The beakers were filled to the 550 mL mark with 20 mM sodium citrate buffer (pH 5.7) and securely covered with plastic wrap and aluminum foil to prevent evaporation. The sealed beakers were incubated in a 50 °C in a heating cabinet for two days, with manual shaking 4 to 5 times daily throughout the incubation period. Upon completion, the surrounding buffer, containing the produced oligosaccharides, was collected for each reaction, frozen, and subsequently lyophilized to yield the desired product.

For the purification of the laminari-oligosaccharide mixtures, a 12 % (*w/v*) solution of lyophilized laminari-oligosaccharides from each species was prepared by mixing the extracted laminarins with milli-Q water. The solutions were filtered through non-sterile Phenex RC membrane (0.45 μm, 26 mm syringe filters; Phenomenex). Purification of the laminari-oligosaccharide mixtures was executed using an ÄKTA system with a size-exclusion Superdex™ 30 HiLoad 26/600 column (Cytiva). The column was equilibrated with a low ionic strength buffer (50 mM NaCl), and the running buffer was degassed milli-Q water. A total of 12 mL of the 12 % oligosaccharides solution, plus additional 5 mL of milli-Q water, was loaded onto the column. Separation was initiated by allowing 0.37 column volumes to flow into 50 mL tubes, utilizing the running buffer at a flow rate at 2 mL/min. Subsequently, 1.7 mL fractions of laminari-oligosaccharide mixtures were collected in a 2.2 mL V-shaped, 96 squared deep well microplate (4titude, Azenta Life Science) using a flow rate at 2 mL/min. The sizes of the laminari-oligosaccharides were analyzed with thin-layer chromatography (TLC). Distinct oligosaccharide fractions were carefully collected, lyophilized and stored at −20 °C for future utilization. The fractions were named according to their source species as follows: *L. digitata* (*Ld*), *L. hyperborea* (*Lh*) or *S. latissima* (*Sl*), with fraction indicated by a "F" and a number (e.g., *Ld*F1).

2.4.3. Thin-layer chromatography (TLC)

For a comprehensive assessment of laminari-oligosaccharides distribution and approximate sizes, 0.8 μL samples from wells 1, 4, 7, and 10 of the rows A-H of each 96 square deep well microplate containing the laminari-oligosaccharide fractions of one of three seaweed species (Figs. S1 and S2) were spotted near the bottom of the TLC silica gel (10 × 20; Merck). Close-up views were generated by spotting 2 μL on the TLC plate from the end wells in row C to E12. As a mobile phase, a mixture of 1-butanol, acetic acid, and Milli-Q water (2:1:1) was run for 1.5 h. Thereafter, the TLC plates were dried and developed using 100 mg orcinol in 95 mL methanol and 5 mL sulfuric acid. Then, the plates were dried and heated at 120 °C using the TLC Plate Heater III (CAMAG®) until bands became visible.

2.5. Structural analyses of laminarin and laminari-oligosaccharide fractions

2.5.1. Nuclear magnetic resonance (NMR) spectroscopy

1D and 2D NMR spectra were recorded on a 600 MHz Bruker Avance Neo NMR spectrometer equipped with a 5 mm TCI Prodigy CryoProbe (Bruker). Samples were dissolved in D_2O (0.5 mL, 99.9 %; Cambridge Isotope Laboratories, Tewksbury, MA, USA) and transferred to 5 mm NMR tubes. All spectra were obtained using standard Bruker pulse programs with water suppression. The 2D TOCSY spectra were recorded using an MLEV-17 mixing sequence with spin-lock times of 150 ms. The 2D NOESY spectra were recorded with a mixing time of 300 ms. Natural abundance 2D ^{13}C–^{1}H HSQC experiments were recorded without decoupling during the acquisition of the ^{1}H free induction decay. Chemical shifts were expressed in parts per million (ppm) relative to solvent HOD signal (4.84 ppm for ^{1}H NMR, 292 K). Data were processed using TopSpin™ software (Bruker). Line fitting (deconvolution) was used to estimate the average degree of polymerization, branching and G:M ratio. The expanded region (5.3–4.0 ppm) with selected peaks on the 1D ^{1}H NMR spectrum was fitted with Lorentz/Gaussian functions, to obtain the position of overlapping peaks, line widths, and integrals.

2.5.2. Matrix-assisted laser desorption/ionization time-of-flight mass spectrometry (MALDI-TOF/TOF MS)

MALDI-TOF/TOF MS experiments were performed using a Bruker ultrafleXtreme (Bruker Daltonics) mass spectrometer. All spectra were recorded in reflector positive-ion mode, and the acquisition mass range was 200–6000 Da. Samples were prepared by mixing on the target 0.5 μL sample solutions with 0.5 μL aqueous 10 % 2,5-dihydroxybenzoic acid as matrix solution.

2.5.3. Fourier transform infrared spectroscopy (FT-IR) analysis

Freeze-dried laminarin was analyzed to identify its functional groups using an FT-IR spectrometer (Nicolet iS5, Thermo Scientific) with a spectral range of 400–4000 cm^{-1}.

2.6. Laminarin and laminari-oligosaccharides effect on dendritic cells and T-cell activation

2.6.1. Sample preparation for DC-model

Lyophilized laminarin and the laminari-oligosaccharide fractions were diluted in RPMI cell culture medium (Gibco, Invitrogen, Paisley, UK), supplemented with 10 % (*v/v*) fetal calf serum (FCS; Gibco) and 1 % (*v/v*) penicillin/streptomycin (Gibco) to a stock concentration at 5 mg/mL.

2.6.2. Maturation and activation of monocyte-derived DCs

Peripheral blood mononuclear cells (PBMCs) were isolated from buffy coats of healthy donors by Ficoll Histopaque density-gradient (Sigma-Aldrich). $CD14^{+}$ monocytes were isolated using CD14 Microbeads (Miltenyi Biotec, Bergisch Gladbach, Germany). The $CD14^{+}$ monocytes were cultured in 48-well plates (Nunc) at concentration of 0.5×10^{6} cells/mL for seven days in RPMI medium supplemented with FCS and antibiotics. The differentiation into immature DCs was induced with IL-4 at 12.5 ng/mL, and GM-CSF at 25 ng/mL (both from R&D Systems, Bio-Techne, Abingdon, England). Maturation of the immature DCs into mature DCs was achieved by culturing the immature DCs for 24

h in RPMI medium supplemented with FCS and antibiotics in 48-well plates at concentration of 2.5×10^5 cells/mL in the presence of IL-1β (10 ng/mL), TNFα (50 ng/mL; both from R&D Systems) and lipopolysaccharide (LPS) from *E. coli*, serotype 055:B5 (0.5 μg/mL, Sigma-Aldrich). The stock solution of 5 mg/mL of each laminarin sample was diluted in RPMI medium and added to the maturing DCs at a concentration of 100 μg/mL together with cytokines and LPS. Cells cultured with cytokines and LPS but in the absence of sample were used as negative control (Neg-DCs). After 24 h, the matured DCs were harvested and the effect of laminarin and the laminari-oligosaccharide fractions on their maturation was evaluated by measuring cytokine secretion by ELISA and expression of surface molecules by flow cytometry.

2.6.3. Co-culture of DCs and allogeneic $CD4^+$ T-cells

Allogeneic $CD4^+$ T cells were obtained from PBMCs using CD4 microbeads (Miltenyi Biotec) following the same procedure as for the isolation of $CD14^+$ monocytes described above. DCs which were matured and activated with LPS, TNFα, and IL-1β [in presence or absence of either laminarin from *L. hyperborea*, *L. hyperborea* oligosaccharide fraction *Lh*F5 or *S. latissima* oligosaccharide fraction *Sl*F3 (all at 100 μg/mL)] were co-cultured at 2×10^5 cell/mL with allogeneic $CD4^+$ T-cells at 2×10^6 cells/mL in 96-well round bottom culture plates for six days. The effects of the fractions on the ability of DCs to activate and differentiate the $CD4^+$ T-cells were determined by measuring cytokine concentrations in the co-cultures by ELISA.

2.6.4. Determination of cytokine concentrations by ELISA

The concentrations of TNFα, IL-6, IL-12p40 and IL-10 in culture supernatants from DCs and IFNγ, IL-17, IL-12p40, and IL-10 in culture supernatants from co-cultured DCs and $CD4^+$ T-cells were measured by sandwich ELISA using DuoSets from R&D Systems according to the manufacturer's protocols. To minimize the effect of variance between individuals in cytokine secretion by cultured DCs and by DCs and $CD4^+$ T-cells in co-cultures, the results are expressed as secretion index (SI). The calculations were performed by dividing the cytokine concentration (pg/mL) in the supernatant from DCs matured in the presence of a laminarin sample or in co-cultures of these DCs with $CD4^+$ T-cells, by the cytokine concentration (pg/mL) in supernatants from Neg-DCs or in co-cultures of the Neg-DCs with $CD4^+$ T-cells. Proportional index (PI) was used to evaluate the overall effect of the samples on the IL-12p40 and IL-10 cytokine secretion, calculated by dividing the SI for IL-12p40 with SI for IL-10, where $PI > 1$ was indicative of a pro-inflammatory effect and $PI<1$ of an anti-inflammatory effect.

2.6.5. Expression of surface molecules by flow cytometry

To investigate whether laminarin and the laminari-oligosaccharide had an impact on the activation status and functional capacity of the DCs, DCs were stained with mouse monoclonal antibodies against Human Leukocyte Antigen-DR (HLA-DR; clone L243), Cluster of Differentiation (CD)40 (clone 5C3), CD14 (clone M5E2), programmed death-ligand 1 (PD-L1; CD274) (clone 5C3), and CD1c (clone L161) (all from BioLegend, Nordic Biosite, Sweden), CD141 (clone 501733; from R&D Systems), and CD86 (clone Bu63; from Bio-Rad, Watford, United Kingdom). Approximately 10,000 events gated as DCs were collected using a Sony SH800S flow cytometer (Sony Biotechnologies, UK), and the data were analyzed using Kaluza analysis software (Beckman Coulter, California, USA). Appropriate isotypic antibodies were used to evaluate background staining and set positive gates. The results are presented as percentage positive cells.

2.6.6. Viability assessment of dendritic cells

The viability of DCs exposed and not exposed to laminarin samples was analyzed by Trypan blue staining and counted by C-Chip Neubauer improved counting chamber. The percentage of viable cells was calculated by the formula provided in Eq. (1)

$$\text{Cell viability}\,(\%) = (\text{Number of viable cells})/(\text{Total number of cells}) \times 100 \quad (1)$$

2.7. Statistical analysis

Data were expressed as mean ± standard error of the mean (SEM), and statistical analysis was performed using GraphPad Prism version 10.2.1 (395) (GraphPad Software, San Diego, California, USA, www.graphpad.com). One-way ANOVA was used to compare the treated DCs with DC-Neg ($n \geq 3$) and unpaired *t*-test was used to compare co-culture experiments ($n = 6$). An asterisk indicates $p \leq 0.033$ (*), $p \leq 0.002$ (**), and $p < 0.001$ (***).

3. Results and discussion

3.1. Extraction, purification, composition analysis and capping

Laminarins from *S. latissima* and *L. hyperborea* were successfully extracted by a two-step water extraction protocol and were subsequently purified to apparent homogeneity. Firstly, the extract was treated with $CaCl_2$ to precipitate traces of alginate, then filtered through a 10 kDa membrane to remove larger molecules like fucoidan, and finally passed through a 1 kDa filter to remove smaller (degradation) products and minerals (Table 1). The laminarin % yield was 10 % and 12 % of the *L. hyperborea* and *S. latissima* biomass, respectively. In contrast, laminarin extracted from a locally sourced *L. digitata*, resulted in a low yield, likely due to a low laminarin-content present in the raw material (Table S1), while mannitol and ash content remained high after purification. To obtain *L. digitata* laminarin of good purity, commercially available laminarin (Merck) was used instead for structural analyses and

Table 1
Composition analyses of pure laminarin from *L. digitata*, *L. hyperborea* and *S. latissima*.

	L. digitata	*L. hyperborea*	*S. latissima*
Ash [% *dw*[a]]	3.90 ± 0.60	15.33 ± 0.18	15.45 ± 0.55[*]
TPC[b] [mg PGE/100 g lyophilized laminarin extract]	– nd[c] with NMR	– nd with NMR	1.03 ± 0.50 nd with NMR
Monosaccharide composition [% *dw*]			
Mannitol	0.42 ± 0.06	2.25 ± 0.20	4.68 ± 0.26
Fucose	0.24 ± 0.02	2.51 ± 0.02	nd
Arabinose	nd	nd	nd
Galactose	nd	0.95 ± 0.02	nd
Glucose	78.36 ± 2.17	52.86 ± 0.11	74.63 ± 4.29
Xylose	0.88 ± 0.02	0.54	nd
Mannose	1.73 ± 0.03	0.33 ± 0.07	nd
Mannuronic acid	nd	5.57 ± 0.57	nd
Guluronic acid	nd	2.19 ± 0.25	nd
Glucuronic acid	nd	0.63 ± 0.08	nd
Total uronic acids	nd	8.39 ± 0.90	nd
Total carbohydrates[d]	81.63 ± 2.30	67.83 ± 2.22	79.31 ± 4.55

The data are presented as mean value ± standard deviation (for TPC, $n = 3$ for ash, $n = 2$, and for monosaccharides, $n = 2$).
[*] The sample size of *S. latissima* was very low causing high standard deviation.
[a] dw means dry weight.
[b] TPC means Total Polyphenol Content.
[c] nd means not detected.
[d] Total carbohydrate is the combined amounts of neutral sugars and uronic acids.

immunomodulation tests. This laminarin product from *L. digitata* contained 78 % glucose (*w/dw*), and low levels of mannitol and ash (Table 1).

Monosugar analysis of the extracted *L. hyperborea* and *S. latissima* laminarins showed that both extracts primarily contained glucose and mannitol (Table 1). In the *S. latissima* extract, glucose constituted 75 % of the dry weight (*dw*), and mannitol made up 5 % of the *dw*, resulting in a total carbohydrate content of 80 %, with a high purity of the extracted laminarin. The extract from *L. hyperborea* was also predominantly composed of glucose (53 % *w/dw*) and mannitol (2 % *w/dw*), with minor amounts of fucose, galactose, and xylose (Table 1), implying fucoidan contamination, which was confirmed by ^{1}H NMR analysis (Fig. S3). Fucoidan was successfully removed from this sample using DEAE-cellulose anion-exchange chromatography (Fig. S3), facilitating further characterization by ^{1}H NMR and enzymatic preparation of laminari-oligosaccharides (Section 3.3).

^{1}H NMR characterization of the three chosen laminarin samples revealed coexistence of M- and G-type laminarin, with variations in the M:G ratio between the seaweed species (Fig. 1 and Table 2), consistent with existing literature [8,37]. This was observed as a chemical shift at 4.18 ppm for mannitol connected to glucose or as glucose in its α or β configuration at the reducing end (Gα/β) [(1 → 3) –β–D–Glc*p*] at δ 5.22/4.67 ppm (Fig. 1). The ratio was estimated to be 2.5:1 for the laminarins from both *L. digitata* and *S. latissima* and to be 1:1 for laminarin from *L. hyperborea* (Table 2). The M:G ratio, along with the observed mannitol content, harmonizes with literature data [8,38,39]. Comparison with the composition analysis (above) indicates that free mannitol is present in the *S. latissima* sample. Such coexistence of free mannitol has been previously reported [3,7,8], and cannot be ruled out for this study.

The total phenolic content was quantified using the TPC-assay. Phenolic content in the *L. digitata* and the *L. hyperborea* laminarin extracts was below detection levels, while *S. latissima* laminarin extract had a phenolic content of 1.03 ± 0.05 mg PGE/100 g lyophilized extract (Table 1). Although detectable, the quantity of phenolic compounds in the *S. latissima* sample was low compared to findings in other studies (5–8 g PGE/100 g lyophilized extract) [4,40].

3.2. Degree of polymerization, linkage types and branching

3.2.1. FT-IR spectroscopy for estimation of components and bond-types

FT-IR spectra of laminarin extracted from each of the three species (Fig. 2) consistently displayed characteristic absorption peaks associated with the stretching vibration of —OH groups, appearing at 3347 cm^{-1} for *L. digitata*, 3361 cm^{-1} for *L. hyperborea*, and 3314 cm^{-1} for *S. latissima*, respectively. The C—H stretching vibrations in —CH_3 or —CH_2 groups, characteristic of sugars, were observed at 2917 cm^{-1} for *L. digitata* and *L. hyperborea*, and at 2887 cm^{-1} for *S. latissima*, probably a result of variations in the laminarin structure across the species (as further described below). The pyranose absorption peak, associated with the C—H weak scissor vibration around 890 cm^{-1}, confirmed the existence of β-type glycosidic bonds for all three species. The peaks observed between 1000 and 1200 cm^{-1} were attributed to the stretching vibrations of C—C and C—O bonds in the pyranose rings, indicating polysaccharides as dominant components in the extracts. These observations agree with previously reported data [13,41].

3.2.2. Estimation of the degree of polymerization

MALDI-TOF MS analysis of the laminarins from *L. digitata*, *L. hyperborea* and *S. latissima* showed that the extracts constituted a mixture of poly- and oligosaccharides of varying sizes (Fig. 3 and Table 2). The laminarin from *L. digitata* displayed a range from DP10 to DP36, with DP25 being the dominant signal (Fig. 3). Laminarin from *L. hyperborea* exhibited a size range from DP8 to DP33, with DP24 being the dominant signal (Fig. 3), and *S. latissima* laminarin had a DP range from DP7 to DP36, with DP24 being the dominant signal (Fig. 3). This suggests an average molecular weight of approximately 5 kDa, in line with previous reported data [2–4].

3.2.3. Structural analysis of the laminarins by 1D/2D ^{1}H NMR spectroscopy

In the 1D ^{1}H NMR spectra of laminarin from *L. digitata*, *L. hyperborea*, and *S. latissima* (Fig. 1), the anomeric signals are detected at positions that correspond to the occurrence of β–1,3 and β–1,6 linkages. For the assignment of the various signals, our previously developed library of

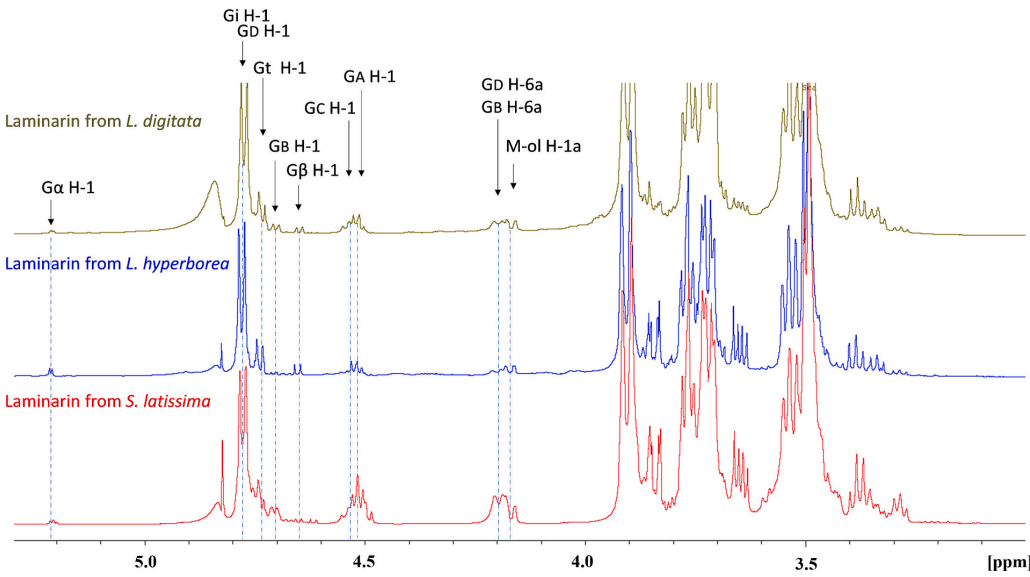

Fig. 1. ^{1}H NMR spectra of laminarin from *L. digitata*, *L. hyperborea*, and *S. latissima* highlighting possible linkages. The spectra were recorded in D_2O at 292 K. The possible linkages are shown as Gt [β-D-Glc*p*-(1 → 3)-]; Gi [–(1 → 3)-β-D-Glc*p*-(1 → 3)-]; GD [–(1 → 3,6)-β-D-Glc*p*-(1 → 3)-]; GB [–(1 → 6)-β-D-Glc*p*-(1 → 3)-]; GC [–(1 → 3)-β-D-Glc*p*-(1 → 6)-]; GA [β-D-Glc*p*-(1 → 6)-]; Gα/β (reducing end) [–(1 → 3)-β-D-Glc*p*] and M-ol [–(1 → 1)-M-ol].

Table 2
Sample overview of laminarin and laminari-oligosaccharide samples including degree of polymerization range determined by MALDI-TOF-MS, branching content, and mannitol:glucose (M:G) ratio determined with ^{1}H NMR.

Sample	Degree of polymerization	Branching	M:G chains
L. digitata laminarin	DP10–DP36, highest signal DP25	~10 % β–1,6-linkages (6.5 % branching, 3.5 % intrachain) Residues ratio GD:GB* ~2:1	~2.5:1
*Ld*F1 (well: C10-D2)[a]	DP-12–DP15	10 % β–1,6-linkage Residues ratio GD:GB 2:1	
*Ld*F2 (well: D3-D8)	DP9–DP12	7 % β–1,6-linkage Residues ratio GD:GB 2:1	
*Ld*F3 (well: D9-E1)	DP8–DP10	3 % β–1,6-branching GB residue not detected	
*Ld*F4 (well: E2-E5)	DP6–DP8	3 % β–1,6-branching GB residue not detected	
L. hyperborea laminarin	DP8–DP33, highest signal at DP24	~4 % β–1,6-branching, GB traces	~1:1
*Lh*F1 (well: C10-C12)	DP12–DP15	11 % β–1,6-branching **NB:** contamination with fucoidan	
*Lh*F2 (well: D1-D5)	DP10–DP13	7 % β–1,6-branching **NB:** contamination with fucoidan	
*Lh*F3 (well: D6-D10)	DP8–DP11	3 % β–1,6-branching	
*Lh*F4 (well: D11-E5)	DP6–DP10	3 % β–1,6-branching	
*Lh*F5 (well: E6-E7)	DP5–DP8	7 % β–1,6-branching	
S. latissima laminarin	DP7–DP36 highest signal detected at DP24	~21 % β–1,6-linkages (~15 % branching, ~6 % intrachain) Residues ratio GD:GB ~ 2:1	~2.5:1
*Sl*F1 (well: C10-D2)	DP10–DP14	20 % β–1,6-linkages (~15 % branching, ~5 % interchain) Residues ratio GD:GB ~2:1	
*Sl*F2 (well: D9-E1)	DP9–DP11	16 % β–1,6-linkages (~11 % branching, ~5 % interchain) Residues ratio GD:GB ~2:1	
*Sl*F3 (well: E2-E5)	DP6–DP9	11 % β–1,6-linkages (~7 % branching, ~4 % interchain) Residues ratio GD:GB ~2:1	

[a] Wells merged in Fig. S2.
* The GD:GB ratio reflects the β1,6-branch to β1,6-intrachain ratio.

NMR data for laminari-oligosaccharides was used (Table 3) [42,43]. Additionally, 2D ^{13}C – ^{1}H HSQC spectra were recorded confirming the assignment of chemical shifts, particularly in the bulk region, where significant overlap of signals was observed in the 1D spectrum (Fig. S4). In the 1D ^{1}H NMR spectrum, terminal *β*-D-Glc*p*-(1 → 3)-units are reflected by Gt H-1 at *δ* 4.75, internal -(1 → 3)-*β*-D-Glc*p*-(1 → 3)- units by Gi H-1 at *δ* 4.79, branching -(1 → 3,6)-*β*-D-Glc*p*-(1 → 3)- units by GD H-1 at *δ* 4.77, –(1 → 6)-*β*-D-Glc*p*-(1 → 3)- units by GB at *δ* 4.72, –(1 → 3)-*β*-D-Glc*p*-(1 → 6)- units by GC H-1 at *δ* 4.55, terminal *β*-D-Glc*p*-(1 → 6)-units by GA H-1 at *δ* 4.52, G*α/β* (reducing end) [–(1 → 3)-*β*-D-Glc*p*] at *δ* 5.22/4.67, respectively, and mannitol itself, which gives a M-ol H-1a signal outside the bulk region at *δ* 4.18 (Fig. 1). Due to strong overlap of the signals, line fitting (deconvolution) was used to estimate the average DP, branching and mannitol to glucose (M:G) ratio (Table 3). The percentage of the *β*–1,6-intrachain/branching in laminarin samples was estimated after integration of the GB/GD H-6a at *δ* 4.21; reducing ends: G*α/β* H-1 at *δ* 5.22/4.67, respectively, M-ol H-1a at *δ* 4.18 and remaining overlapping anomeric signals: Gt, Gi, GD, GC, GB, GA, respectively. The peak area of well-resolved GB H-1 signal was subtracted from the GB/GD H-6a signal, giving the percentage of GB:GD ratio. Average DP was determined by comparing the integrals of reducing ends: G*α/β*, M-ol signals and the integrals of overlapping anomeric signals: Gt, Gi, GD, GC, GB, GA, respectively.

The analysis highlighted distinct structural features in the laminarins from the three species. Specifically, laminarin from *S. latissima* exhibited a notable degree of branching, constituting 21 % of *β*–1,6-linkages, of which 15 % was assigned to branching and 6 % formed intrachain links, including a 1,6-branch point on the non-reducing glucose forming a kinked-linear structure (Fig. 1 and Table 2). In contrast, laminarin from *L. digitata* displayed fewer *β*–1,6-linkages compared with laminarin from *S. latissima*, with 6.5 % allocated to branching, and 3.5 % to intrachain links (Fig. 1 and Table 2). Importantly, both types of laminarin contained both longer and shorter sidechains of glucose. In contrast, laminarin from *L. hyperborea* predominantly featured a linear *β*–1,3–linked backbone with minimal branching, approximately 4 %, and lacked intrachain links (Fig. 1 and Table 2). The existing branches in *L. hyperborea* laminarin consisted solely of single glucose units, a feature that may also be influenced by various factors such as the habitats and environmental factors of the seaweed species. These results collectively affirm structural distinctions of laminarins from different brown seaweed species.

3.3. Enzymatically produced laminari-oligosaccharides

3.3.1. Structural analysis of laminari-oligosaccharides generated by LPHase

The relatively diverse bioactivities previously reported for laminarin may, partially, be attributed to distinct structural differences across brown seaweed species. These differences include elements such as branch points, intrachain links, and the distribution of *β*–1,6-linkages [44]. However, the specific structural elements responsible driving specific activities remain unclear. To address this knowledge gap, several laminari-oligosaccharide fractions from the three laminarin types, extracted and characterized above, were produced using the laminaripentaose-producing endo–1,3–*β*-glucanase, LPHase, a glycoside hydrolase family 64 enzyme. This approach enabled the creation of laminari-oligosaccharides with similar DP but with varying branching and intrachain linkage content. MALDI-TOF MS was used to determine the DP range of the laminari-oligosaccharides (Table 2), while 1D/2D ^{1}H-^{13}C NMR analyses were used to explore structural differences (Tables 2 and 3).

Laminari-oligosaccharide fractions derived from *L. hyperborea* showed an increase in *β*–1,6-branching compared to the laminarin polymer. Specifically, the oligosaccharide fraction *Lh*F1, eluting with a retention time corresponding to a higher apparent molecular weight and lower mobility on TLC (Fig. S2), contained 11 % *β*–1,6-branching, compared to 4 % in undigested laminarin. Fraction *Lh*F2 contained oligosaccharides with a somewhat lower apparent molecular weight, and showed 7 % *β*–1,6-branching (Table 2). Unfortunately, both *Lh*F1 and *Lh*F2 were contaminated with fucoidan, leading to their exclusion from immunological analysis. The two fractions, which, based on mobility, comprised intermediate-sized (*Lh*F3) and intermediate to small-sized oligosaccharides (*Lh*F4), exhibited 3 % *β*–1,6-branching, while the apparent smaller oligosaccharide fraction (*Lh*F5) contained 7 % *β*–1,6-branching, indicating an uneven distribution of the branches (Table 2). No intrachain links were observed in any of the above fractions, nor were they present in the laminarin polymer (above). The increase in branching in the oligosaccharides indicates that the short single-residue branches in *L. hyperborea* laminarin may be well accommodated in the active site of the LPHase. The enzyme is shown to have an unusually

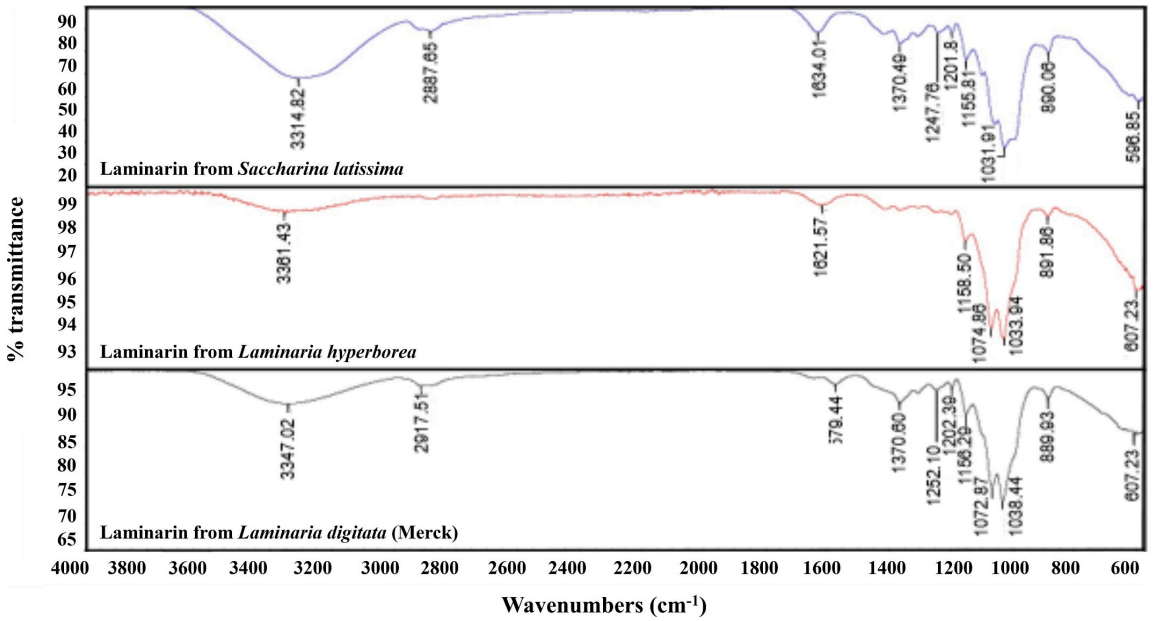

Fig. 2. FT-IR spectra of purified laminarin from *L. digitata*, *L. hyperborea* and *S. latissima.* The infrared spectra were recorded in the 400–4000 cm^{-1} region using a FT-IR system. The spectra for laminarin from *L. digitata*, *L. hyperborea* and *S. latissima* are highlighted in black, red and blue, respectively.

wide groove around the active site [45], a feature that may allow accommodation of substrates with a certain degree of branching.

In contrast, the laminarin fractions from *L. digitata* and *S. latissima* showed a gradual reduction in the percentage of β–1,6-linkages as the oligosaccharide mixtures decreased in their DP range (Table 2). This could suggest that the branching points occur irregularly in the polymer and that the longer branches in the polymers from these species are less accessible for substrate binding by the enzyme. For *L. digitata* laminarin, the larger oligosaccharide fractions (*Ld*F1 and *Ld*F2) contained 10 % and 7 % of the β–1,6-linkages, including both intrachain links and branched structures. In contrast, the intermediate and smaller oligosaccharide fractions (*Ld*F3 and *Ld*F4) each contained 3 % β–1,6-linkages with short side chains but without the intrachain links, indicating that these may have been hydrolyzed during the enzymatic treatment.

The *S. latissima* oligosaccharide fractions (*Sl*F1, *Sl*F2 and *Sl*F3) displayed a higher percentage of β–1,6-linkages (20 %, 16 %, and 11 %, respectively), reflecting the greater branching and intrachain links (21 %) of the *S. latissima* laminarin, and in *Sl*F1, maintaining the proportion found in the laminarin polymer (Table 2). Interestingly, all fractions derived from *S. latissima* contained intrachain links, indicating a higher abundance in this species [this feature was not found in the smaller oligosaccharide fractions of similar DP from *L. digitata* (*Ld*F3 and *Ld*F4)]. This indicates that the intrachain links are located closer to each other in *S. latissima*, prohibiting cleavage in the active site of LPHase.

Notably, similar to the ^{1}H NMR data from the laminarin polymer sample of *L. digitata*, citric acid was observed in all fractions from the three different species, originating from the hydrolysis with LPHase carried out using a sodium citrate buffer (data not shown). However, only traces were observed in the laminari-oligosaccharide fractions derived from *L. hyperborea*, likely due to the less branched structure of its laminarin, which results in reduced interaction with the sodium citrate buffer and the laminarin, leading to more efficient purification on the size-exclusion Superdex™ 30 HiLoad 26/600 column.

3.4. Effect of laminarin and laminari-oligosaccharide fractions on immunomodulation

3.4.1. Effect on DC maturation, cell viability and cytokine secretion

No impact on the appearance or viability of the DCs treated with laminarin or laminari-oligosaccharides for 24 h was observed compared to the non-treated control (Neg-DCs), as evidenced by their unchanged appearance under a light microscope (Fig. 4a) and viability counts exceeding 80 % in most cases (Table S2).

Maturation of the immature DCs into mature DCs was confirmed by the absence of expression of the CD14 monocyte marker and by the higher percentage of DCs expressing the antigen-presenting molecule HLA-DR, along with the co-stimulatory molecules CD40 and CD86. The expression of these molecules was not affected by treatment with any of the laminarins (Fig. 4b). In addition, laminarin treatment did not affect the expression of CD1c and CD141 on the DCs, molecules commonly used to distinguish between the DC1 and DC2 subsets [46,47], with a higher percentage of DCs expressing CD1c than CD141 (Fig. 4b). Moreover, a high percentage of DCs that expressed PD-L1 was observed, a ligand known to be upregulated upon activation (e.g., by LPS) to prevent excessive inflammation [48] (Fig. 4b), but this was not different from Neg-DCs. In summary, these results demonstrate that none of the laminarin extracts affected the maturation of the immature DCs into mature DCs.

No impact on the secretion of any of the investigated cytokines was observed when the DCs were treated with samples derived from *L. digitata* (Fig. 5a–e, light grey graphs), implying that laminarin and laminari-oligosaccharides from *L. digitata* do not promote pro- or anti-inflammatory responses in this model.

The *L. hyperborea* laminarin polymer did not affect the TNFα secretion by DCs compared to Neg-DCs, whereas DCs treated with the laminari-oligosaccharide fractions *Lh*F4 and *Lh*F5 secreted decreased levels of TNFα (35 % and 32 %, respectively; Fig. 5a, middle grey). This suggests size-dependent effect on decrease in TNFα secretion by the *L. hyperborea* laminari-oligosaccharide fractions. DCs treated with

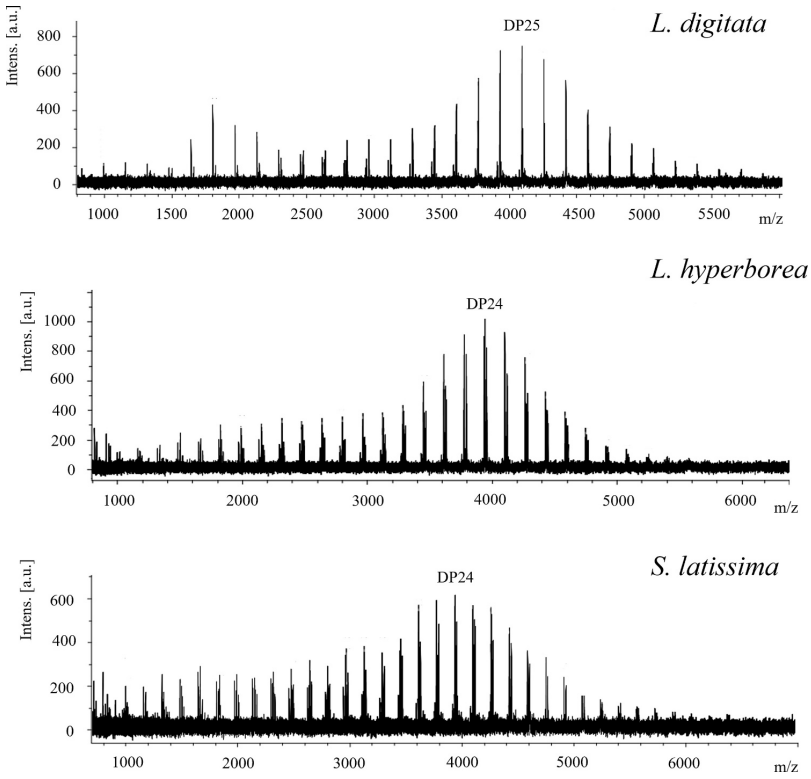

Fig. 3. MALDI-TOF MS spectra of laminarin from *L. digitata*, *L. hyperborea* and *S. latissima*. The MALDI-TOF MS spectra display the degree of polymerization composition of each extract. The dominant peaks correspond to DP25 for *L. digitata*, and DP24 for *L. hyperborea* and *S. latissima* are highlighted. These findings are consistent with the reported ranges of DP25–DP40, corresponding to molecular weights of 4.2–7.2 kDa.

laminarin from *L. hyperborea* secreted higher levels of IL-6 compared to Neg-DCs (24 %) and this was also observed for DCs treated with *Lh*F5 (34 %) (Fig. 5b, middle grey). Laminarin and laminari-oligosaccharides from *L. hyperborea* did not affect secretion of IL-12p40 (Fig. 5c, middle grey), while DCs treated with the *L. hyperborea* laminarin polymer secreted significantly higher levels of the anti-inflammatory cytokine IL-10 as compared to Neg-DCs (Fig. 5d, middle grey), resulting in a non-significant decrease in the PI by 26 % (PI < 1; Fig. 5e middle grey). Although IL-6 can induce inflammatory responses, it can, in combination with IL-10 secretion, induce anti-inflammatory response, suggesting an overall anti-inflammatory effect associated with *L. hyperborea* laminarin polymer treatment of DCs.

An 18 % decrease in TNFα secretion was observed when the DCs were treated with *Sl*F3, the smallest laminari-oligosaccharide fraction from *S. latissima* (Fig. 5a, dark grey). Treatment of DCs with laminarin and laminari-oligosaccharides from *S. latissima* did not affect the secretion of other cytokines analyzed, i.e. IL-6, IL-12p40, and IL-10, by the DCs (Fig. 5a, c and d, dark grey).

The decreased TNFα secretion by DCs is associated with the smaller fractions of laminari-oligosaccharides derived from *L. hyperborea* (*Lh*F4 and *Lh*F5) and *S. latissima* (*Sl*F3). However, it is evident that factors beyond size (DP range) may also play a role in down-regulating TNFα secretion by the DCs. This is highlighted by the observation that neither of the small laminari-oligosaccharide fractions derived from *L. digitata* (*Ld*F3 and *Ld*F4) exhibited any effect on the TNFα secretion by the DCs compared to Neg-DCs.

Results from ^{1}H NMR (Table 2) provided more detailed insights into the structural composition of the laminari-oligosaccharides. Specifically, the *Sl*F3 oligosaccharide displayed a mixture of branched and linear structures, including linear intrachain links located at the non-reducing end (Fig. S5), exhibiting a total of 11 % *β*–1,6-linkages. Conversely, the *Lh*F5 oligosaccharide primarily had linear structures with short side chains and lacked intrachain links, with an overall *β*–1,6-linkage content of 7 %. Structures similar to *Lh*F5 were found in *Ld*F3 and *Ld*F4; however, only *Lh*F5 affected TNFα secretion by the DCs. A plausible explanation for this difference in secretion is that a specific percentage of *β*–1,6-linkages may be necessary to influence TNFα secretion by the DCs, as the laminari-oligosaccharide fractions *Ld*F3 and *Ld*F4, which had no effect, only contained 3 % *β*–1,6-linkages. Both *Sl*F3 and *Lh*F5 affected TNFα secretion by the DCs, but while *Sl*F3 included both branches and intrachain links, *Lh*F5 was lacking the latter, potentially linking the effect on TNFα secretion to the *β*–1,6-branching rather than intrachain links in the laminari-oligosaccharides.

The absence of intrachain links, combined with the presence of small branches may also affect the IL-10 secretion by DCs. The *L. hyperborea* laminarin polymer, characterized by approximately 4 % *β*–1,6-linkages (Table 2), is devoid of intrachain links, but caused an increase in IL-10 secretion by the DCs, a phenomenon not observed with the other two laminarin polymers that contain the intrachain structures (Fig. S5). Thus, the simple branching pattern, primarily consisting of short side chains, of laminarin from *L. hyperborea* may play a significant role in its effect on IL-10 secretion by DCs.

The ^{1}H NMR data revealed the presence of citric acid in all fraction samples, likely originating from the LPHase digestion method. Therefore, the effect of sodium citrate buffer on cytokine secretion by DCs was assessed. No significant effects were observed on TNFα, IL-6, IL-12p40,

Table 3
^{1}H and ^{13}C NMR chemical shifts (δ) of *L. digitata*, *L. hyperborea*, S. *latissima*, recorded in D_2O at 292 K.

	Residue	H-1a/ 1b C-1	H-2 C-2	H-3 C-3	H-4 C-4	H-5 C-5	H-6a/ 6b C-6
Gα	-(1 → 3)-α-D-Glc*p*	5.22 93.0	3.73 72.0	3.92 83.3	3.52 70.0	3.86 72.2	3.83/ 3.79 61.6
Gβ	-(1 → 3)-β-D-Glc*p*	4.67 96.6	3.44 74.9	3.74 85.7	3.52 69.2	3.49 76.6	3.90/ 3.74 61.6
G2α	-(1 → 3)-β-D-Glc*p*- (1 → 3)- α-D-Glc*p*	4.76 103.7	3.56 74.3	3.78 85.3	3.54 69.1	3.52 76.7	3.93/ 3.74 61.7
G2β	-(1 → 3)-β-D-Glc*p*- (1 → 3)- β-D-Glc*p*	4.77 103.7	3.56 74.3	3.78 85.3	3.53 69.1	3.53 76.7	3.93/ 3.74 61.7
G2	-(1 → 3)-β-D-Glc*p*- (1 → 1)- D-Man-ol	4.54 103.6	3.56 73.9	3.74 85.3	3.54 69.1	3.52 76.6	3.92/ 3.76 61.7
Gi	-(1 → 3)-β-D-Glc*p*- (1 → 3)-	4.79 103.4	3.56 73.9	3.77 85.5	3.54 69.1	3.52 76.6	3.92/ 3.76 61.7
Gt	β-D-Glc*p*-(1 → 3)-	4.75 103.7	3.37 74.4	3.53 76.6	3.42 70.6	3.48 76.8	3.92/ 3.72 61.7
GA	β-D-Glc*p*-(1 → 6)-	4.52 103.7	3.32 74.0	3.51 76.0	3.41 70.6	3.46 76.7	3.92/ 3.74 61.6
GB	-(1 → 6)-β-D-Glc*p*- (1 → 3)-	4.72 103.8	3.38 74.4	3.53 76.5	3.48 70.5	3.67 75.6	4.21/ 3.87 69.7
GC	-(1 → 3)-β-D-Glc*p*- (1 → 6)-	4.55 103.6	3.52 73.6	3.74 85.6	3.51 69.1	3.50 76.6	3.92/ 3.75 61.6
GD	-(1 → 3,6)-β-D- Glc*p*-(1 → 3)-	4.77 103.8	3.60 74.0	3.79 85.4	3.58 69.1	3.69 75.4	4.21/ 3.89 69.7
M-ol	-(1 → 1)-D-Man-ol	4.18/ 3.84 72.6	3.87 70.6	3.85 n.d.	3.75 71.7	3.79 70.0	3.86/ 3.67 64.0

n.d. = not determine.

or IL-10 (Fig. S6), confirming that the alterations in cytokine secretion by DCs treated with laminarins can be attributed to the polymer or oligomers of the laminarins rather than by the buffer.

As TNFα is a key pro-inflammatory cytokine involved in the initiation and progression of acute inflammatory responses, important in protecting the body against harmful effects of pathogens and damaged tissues [26]. However, in autoimmune diseases, such as inflammatory bowel disease, rheumatoid arthritis, and psoriasis [49,50], dysregulated TNFα production becomes a hallmark of pathogenesis, driving chronic inflammation and exacerbating tissue injury [27,51]. Thus, treatments that decrease TNFα secretion by DCs, such as by *Lh*F5 and *Sl*F3, could potentially ameliorate inflammatory conditions and autoimmune diseases by reducing TNFα secretion, minimizing tissue damage and inflammation [53]. Similarly, the increase in IL-10 secretion by DCs treated with the laminarin polymer from *L. hyperborea* indicates anti-inflammatory properties, as IL-10 plays an important role in limiting excessive immune responses [52]. In summary, these data suggest that the laminarin polymer from *L. hyperborea* and the small oligosaccharide fractions *Lh*F5 and *Sl*F3 may be beneficial as treatment of excessive inflammation as observed in many chronic inflammatory diseases.

3.4.2. Effect on DCs and T-cell crosstalk

Given the key role of DCs in not only activating naïve T cells but also in directing their differentiation, the impact of DCs matured for 24 h in the presence of laminarin from *L. hyperborea*, and the laminari-oligosaccharides *Lh*F5 or *Sl*F3 on cytokine secretion when co-cultured with allogeneic $CD4^+$ T-cells was investigated. Secretion of IFN-γ and IL-17 was examined as indicators of Th1 and Th17 responses, respectively, while IL-10 can be secreted by both the DCs, to stimulate T-regulatory (Treg) cells [52,53], or by the $CD4^+$ T-cells themselves, suggesting a Treg cell response (as reviewed [54,55]). IL-12p40 is reported to be secreted only by DCs in the co-culture [56].

When DCs were matured in the presence of laminarin from *L. hyperborea* and subsequently co-cultured with allogeneic $CD4^+$ T-cells, a significant increase in both IL-17 and IL-10 secretion was observed (Fig. 6a). This indicates a complex interplay between *L. hyperborea* laminarin-treated DCs and allogeneic $CD4^+$ T-cells in modulating the immune response. The increased IL-17 concentration in the co-culture supernatant may result from the increased IL-6 secretion by laminarin-treated DCs (Fig. 5b), as IL-6 is one of the main cytokines inducing Th17 differentiation of naïve T cells [57]. This suggests that laminarin from *L. hyperborea* may play a role in type 3 immune response, which is characteristic of immunity against extracellular bacteria and fungi [58,59]. The increase in IL-10 was similar to what was observed when DCs were cultured in the presence of laminarin from *L. hyperborea* (Fig. 5d, middle grey). The increase in IL-10 secretion in the co-culture supernatant might result from DC secretion, as DCs treated with laminarin from *L. hyperborea* secreted elevated levels of IL-10; however, it can also be derived from the $CD4^+$ T-cells. In either case, the high levels of IL-10 secretion suggest a regulatory role of laminarin, most likely within the adaptive immune system.

When *Lh*F5-treated DCs were co-cultured with allogeneic $CD4^+$ T-cells, a non-significant decrease in IFN-γ secretion and IL-12p40 secretion was observed compared to untreated DCs co-cultured with allogeneic $CD4^+$ T-cells (Fig. 6b). In contrast, when DCs matured in the presence of *Sl*F3 were co-cultured with allogeneic $CD4^+$ T-cells, a significant decrease in IFN-γ, IL-12p40, and IL-10 secretions by 26 %, 16 %, and 38 %, respectively, was observed (Fig. 6c). The decrease in IL-12p40 and IFN-γ secretion observed in response to *Sl*F3 treatment suggests a decrease in type 1 immune response, as IL-12 is the main cytokine inducing Th1 differentiation of naïve T cells [60], which is characteristic of immunity against intracellular bacteria [58,59]. Although decreased IL-10 secretion on its own may point toward a pro-inflammatory response, the data was in line with previous results that have shown that reduction in IL-10 secretion in combination with decreased IL-12p40 secretion leads to lower IFN-γ secretion [61,62].

4. Conclusions

In this study, laminarins were isolated and purified from two species of brown seaweed, *L. hyperborea* and *S. latissima*, using a two-step water extraction process, while laminarin from *L. digitata* was sourced commercially. Laminari-oligosaccharides were generated from the purified laminarins through digestion with LPHase, enabling structural analysis that revealed differences and similarities among the laminarins and their laminari-oligosaccharide fractions in *β–1,3(1,6)*-linkages and DP.

Treating DCs with laminarin from *L. hyperborea* increased IL-6 secretion and resulted in elevated IL-17 secretion when the treated DCs were co-cultured with allogeneic $CD4^+$ T-cells, suggesting a promotion of type 3 immune responses, which may be beneficial against extracellular pathogens. Furthermore, DCs treated with small, simply branched oligosaccharides without intrachain links from *L. hyperborea* (*Lh*F4 and *Lh*F5) and the more complex-structured small oligosaccharides fraction from *S. latissima* (*Sl*F3) secreted reduced levels of TNFα without affecting their IL-12p40 secretion. When the DCs treated with *Lh*F5 or *Sl*F3 were co-cultured with allogeneic $CD4^+$ T-cells effects were observed on type 1 immune response. The effects were marked for *Sl*F3. As type 1 immune response is linked to chronic inflammation, these data suggest that the small oligosaccharides fractions from *L. hyperborea* (*Lh*F5) and *S. latissima* (*Sl*F3) might be useful as therapeutics against chronic inflammatory diseases.

However, these promising data also highlight challenges to be

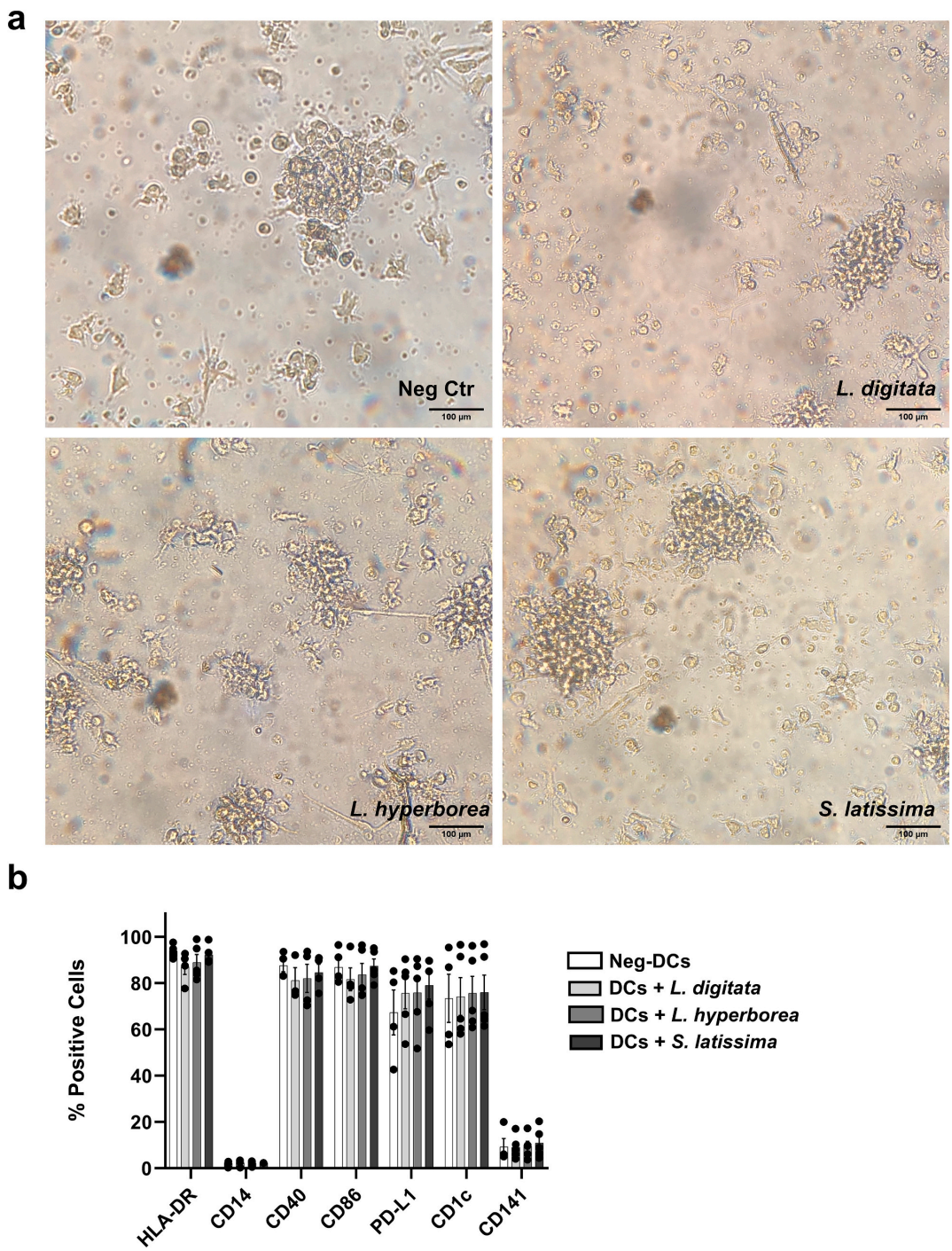

Fig. 4. The impact of laminarin on dendritic cell (DC) maturation and activation. The maturation and activation of DCs were assessed through light microscopy and flow cytometry analysis. (a) Representative images of mature DCs in the absence (Neg Ctr) or presence of laminarin from *L. digitata*, *L. hyperborea* or *S. latissima* after 24 h incubation. Arrows indicate mature DCs. Images were captured using a Leica DMLS light microscope equipped with a Cplan 10×/0.22 objective. (b) Expression of surface molecules crucial for mature DC function following laminarin supplementation is displayed. Results are presented as mean ± SEM of percentage positive cells, with individual data points shown ($n = 4$). The DCs were treated for 24 h without (Neg-DCs) or with laminarin from *L. digitata*, *L. hyperborea* and *S. latissimi*.

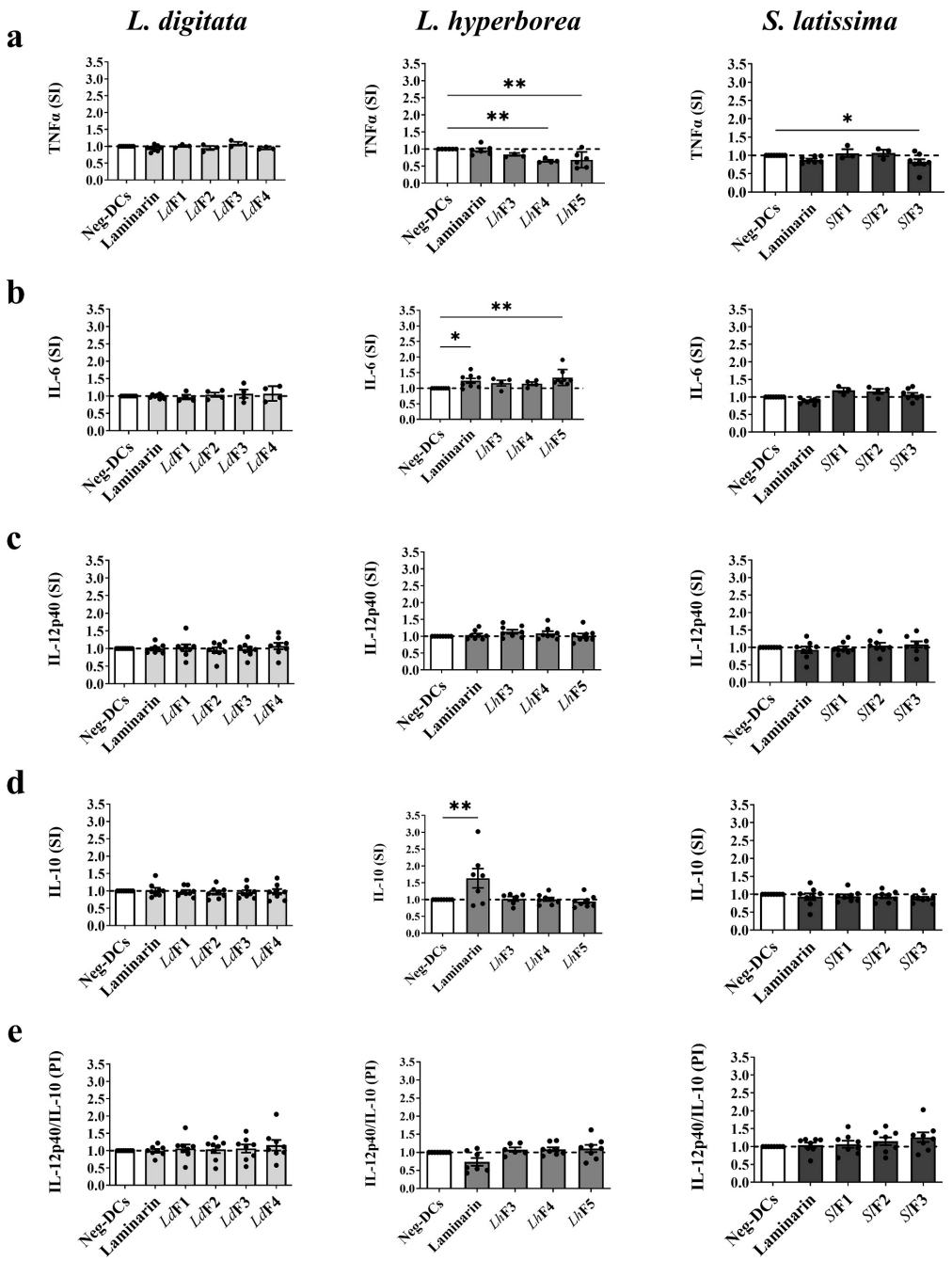

Fig. 5. Effect of laminarin and laminari-oligosaccharides on cytokine secretion by mature dendritic cells (DCs). Cytokine secretion indexes (SI) of TNFα (a), IL-6 (b), IL-12p40 (c), and IL-10 (d), as well as the proportional indexes (PI) between IL-12p40 and IL-10 (e), are shown for mature DCs treated with of laminarin or laminari-oligosaccharides fractions from *L. digitata* (Light grey), *L. hyperborea* (middle grey) and *S. latissima* (dark grey), respectively, compared to the mature DCs without experimental treatment (Neg-DCs). In each graph, treatments labeled as "laminarin" represent laminarin derived from the species specified on top of the images, while the respective oligosaccharide fractions are marked with an "F" followed by a number. All samples were given in a concentration at 100 μg/mL. Experimental treatments were compared to the Neg-DCs using one-way ANOVA with Dunnett's post hoc test in GraphPad Prism version 10.2.1 (395) Significance markers in the results are denoted as follows: * for $p \leq 0.033$, ** for $p \leq 0.002$, and *** for $p < 0.001$. Sample sizes ranged from $n = 3$–8.

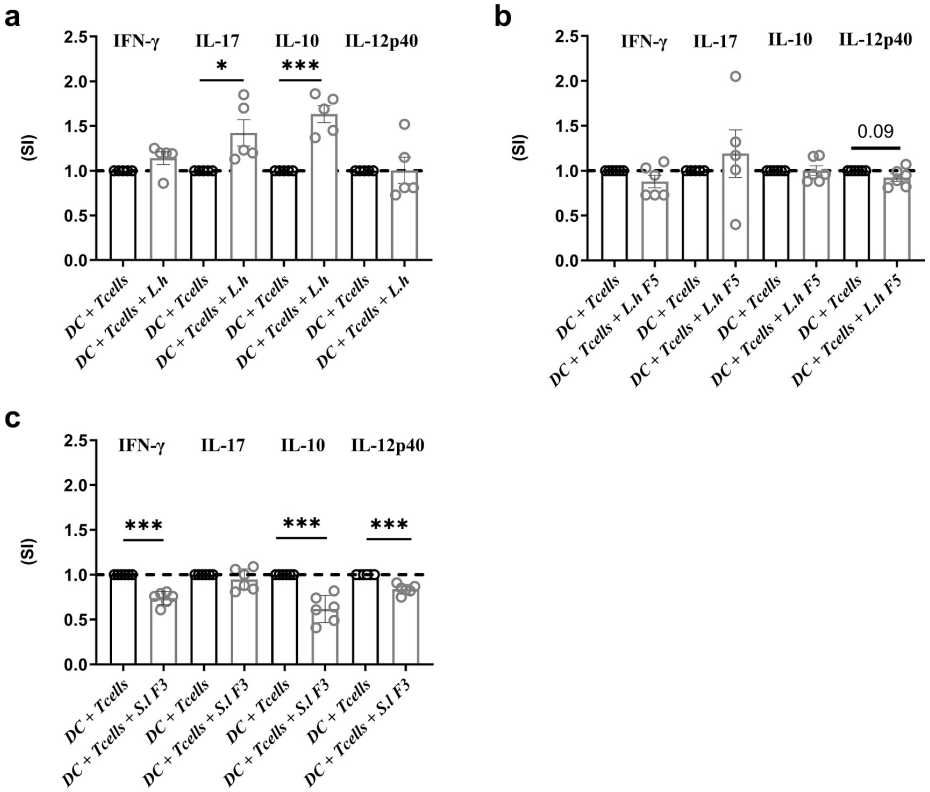

Fig. 6. Cytokine secretion indexes in cultures of dendritic cell (DCs) co-cultured with allogeneic $CD4^+$ T-cells after treatment with laminarin or laminari-oligosaccharides. The cytokine secretion of IFNγ, IL-17, IL-10 and IL-12p40 in supernatants of DCs co-cultured with allogeneic $CD4^+$ T-cells ($CD4^+$T) were measured and presented in as secretion indexes (SI). The DCs were matured either without or with laminarin from *L. hyperborea*, or with the fractions *Lh*F5 or *Sl*F3, at a concentration of 100 μg/mL for 24 h, before being co-cultured with allogeneic $CD4^+$ T cells. The label DC + $CD4^+$ T refers to DCs without treatment co-cultured with allogeneic $CD4^+$ T cells and DC + Laminarin (a), *Lh*F5 (b), or *Sl*F3 (c) indicate DCs treated with one of the samples for 24 h. The DC:$CD4^+$ T cell ratio was 1:10. Cytokine secretion was quantified by ELISA. Results are presented as mean ± SEM of secretion indexes (SI) of IFNγ, IL-17, IL-10 and IL-12p40 (n = 5–6). Experimental treatments were compared to the DC + $CD4^+$ T by unpaired t-test in GraphPad Prism version 10.2.1 (395). Significance markers in the results are denoted as follows: * for $p \leq 0.033$, ** for $p \leq 0.002$, and *** for $p < 0.001$, n = 5–6.

addressed in future research. The variability in laminarin yield and purity from different seaweed species underscores the need for standardized extraction and purification protocols, as the structural features resulting in biological activity may need fine-tuning, as was found for *S. latissima* laminarin, where only certain oligosaccharides resulted in bioactivity. This calls for further work, to fully elucidate the bioactivity mechanisms. This study also provided detailed data on structural analysis and immunomodulatory effects of laminarins and their oligosaccharides, with the observed effects on DCs and T-cell interactions assessed in a controlled in vitro environment. This may, however, not completely reflect the complexities of in vivo immune responses, or the influence of other biological factors present in a living organism. Thus, investigations of the bioavailability, metabolism, and safety of laminarins and their oligosaccharide derivatives in animal models are also necessary to confirm their therapeutic potential and address possible adverse effects.

This work shows that laminarins from brown seaweeds have potential as immune-modulating compounds, both in fighting infections and treating chronic inflammation but that detailed selection of the structure is necessary to obtain the desired effect.

Supplementary data to this article can be found online at https://doi.org/10.1016/j.ijbiomac.2025.141287.

CRediT authorship contribution statement

Monica Daugbjerg Christensen: Writing – review & editing, Writing – original draft, Visualization, Methodology, Investigation, Formal analysis, Data curation. **Leila Allahgholi:** Writing – review & editing, Visualization, Formal analysis, Data curation. **Justyna M. Dobruchowska:** Writing – review & editing, Investigation, Formal analysis, Data curation. **Antoine Moenaert:** Data curation. **Hörður Guðmundsson:** Writing – review & editing, Formal analysis, Data curation. **Ólafur Friðjónsson:** Writing – review & editing, Supervision. **Eva Nordberg Karlsson:** Writing – review & editing, Supervision, Funding acquisition. **Guðmundur Ó. Hreggviðsson:** Writing – review & editing, Supervision, Funding acquisition, Conceptualization. **Jona Freysdottir:** Writing – review & editing, Supervision, Funding acquisition.

Institutional review board statement

Not applicable.

Funding

This research was funded by the MARIKAT JPI Cofund Blue Bio-Economy project (grant number 9082-00021B), European Union's Horizon Europe program SeaMark (Seaweed-based market applications) project (grant number 101060379), and Landspitali Science Fund (grants number A-2020-034, A-2021-027 and A-2022-025).

Declaration of competing interest

The authors declare that they have no known competing financial interests or personal relationships that could have appeared to influence the work reported in this paper.

Acknowledgments

Not applicable.

Data availability

The data presented in this study are available upon request from the corresponding author.

References

[1] T.M. Thompson, B.R. Young, S. Baroutian, Advances in the pretreatment of brown macroalgae for biogas production, Fuel Process. Technol. 195 (2019) 106–151, https://doi.org/10.1016/j.fuproc.2019.106151.
[2] S.E. Spicer, J.M.M. Adams, D.S. Thomas, J.A. Gallagher, A.L. Winters, Novel rapid method for the characterisation of polymeric sugars from macroalgae, J. Appl. Phycol. 29 (2017) 1507–1513, https://doi.org/10.1007/s10811-016-0995-0.
[3] L.E. Rioux, S.L. Turgeon, M. Beaulieu, Characterization of polysaccharides extracted from brown seaweeds, Carbohydr. Polym. 69 (2007) 530–537, https://doi.org/10.1016/j.carbpol.2007.01.009.
[4] S.U. Kadam, C.P. O'Donnell, D.K. Rai, M.B. Hossain, C.M. Burgess, D. Walsh, B. K. Tiwari, Laminarin from Irish brown seaweeds Ascophyllum nodosum and Laminaria hyperborea: ultrasound assisted extraction, characterization and bioactivity, Mar. Drugs 13 (2015) 4270–4280, https://doi.org/10.3390/md13074270.
[5] Z. Liu, Y. Xiong, L. Yi, R. Dai, Y. Wang, M. Sun, X. Shao, Z. Zhang, S. Yuan, Endo-β-1,3-glucanase digestion combined with the HPAEC-PAD-MS/MS analysis reveals the structural differences between two laminarins with different bioactivities, Carbohydr. Polym. 194 (2018) 339–349, https://doi.org/10.1016/j.carbpol.2018.04.044.
[6] D. Wang, D.H. Kim, E.J. Yun, Y.C. Park, J.H. Seo, K.H. Kim, The first bacterial β-1,6-endoglucanase from Saccharophagus degradans 2-40T for the hydrolysis of pustulan and laminarin, Appl. Microbiol. Biotechnol. 101 (2017) 197–204, https://doi.org/10.1007/s00253-016-7753-8.
[7] S.U. Kadam, B.K. Tiwari, C.P. O'Donnell, Extraction, structure and biofunctional activities of laminarin from brown algae, Int. J. Food Sci. Technol. 50 (2015) 24–31, https://doi.org/10.1111/ijfs.12692.
[8] S.M. Read, G. Currie, A. Bacic, Analysis of the structural heterogeneity of laminarin by electrospray-ionisation-mass spectrometry, Carbohydr. Res. 281 (1996) 187–201.
[9] A.M. Neyrinck, A. Mouson, N.M. Delzenne, Dietary supplementation with laminarin, a fermentable marine β (1–3) glucan, protects against hepatotoxicity induced by LPS in rat by modulating immune response in the hepatic tissue, Int. Immunopharmacol. 7 (2007) 1497–1506, https://doi.org/10.1016/j.intimp.2007.06.011.
[10] J. Il Choi, H.J. Kim, J.H. Kim, J.W. Lee, Enhanced biological activities of laminarin degraded by gamma-ray irradiation, J. Food Biochem. 36 (2012) 465–469, https://doi.org/10.1111/j.1745-4514.2011.00552.x.
[11] A.J. Smith, B. Graves, R. Child, P.J. Rice, Z. Ma, D.W. Lowman, H.E. Ensley, T. Ryter, J.T. Evans, D.L. Williams, Immunoregulatory activity of the natural product laminarin varies widely as a result of its physical properties, J. Immunol. 200 (2018) 788–799, https://doi.org/10.4049/jimmunol.1701258.
[12] K.H. Kim, Y.W. Kim, H.B. Kim, B.J. Lee, D.S. Lee, Anti-apoptotic activity of laminarin polysaccharides and their enzymatically hydrolyzed oligosaccharides from Laminaria japonica, Biotechnol. Lett. 28 (2006) 439–446, https://doi.org/10.1007/s10529-005-6177-9.
[13] G. Rajauria, R. Ravindran, M. Garcia-Vaquero, D.K. Rai, T. Sweeney, J. O'Doherty, Molecular characteristics and antioxidant activity of laminarin extracted from the seaweed species Laminaria hyperborea, using hydrothermal-assisted extraction and a multi-step purification procedure, Food Hydrocoll. 112 (2021) 106332, https://doi.org/10.1016/j.foodhyd.2020.106332.
[14] R.V. Menshova, S.P. Ermakova, S.D. Anastyuk, V.V. Isakov, Y.V. Dubrovskaya, M. I. Kusaykin, B. Um, T.N. Zvyagintseva, Structure, enzymatic transformation and anticancer activity of branched high molecular weight laminaran from brown alga Eisenia bicyclis, Carbohydr. Polym. 99 (2014) 101–109, https://doi.org/10.1016/j.carbpol.2013.08.037.
[15] Y. Huang, H. Jiang, X. Mao, F. Ci, Laminarin and laminarin oligosaccharides originating from brown algae: preparation, biological activities, and potential applications, J. Ocean Univ. China 20 (2021) 641–653, https://doi.org/10.1007/s11802-021-4584-8.
[16] S.M. Tosh, P.J. Wood, Q. Wang, J. Weisz, Structural characteristics and rheological properties of partially hydrolyzed oat β-glucan: the effects of molecular weight and hydrolysis method, Carbohydr. Polym. 55 (2004) 425–436, https://doi.org/10.1016/j.carbpol.2003.11.004.
[17] K.L. Cheong, J.K. Li, S. Zhong, Preparation and structure characterization of high-value Laminaria digitata oligosaccharides, Front. Nutr. 9 (2022), https://doi.org/10.3389/fnut.2022.945804.
[18] N. Jayapala, V. Toragall, G.K. Gnanesh, S.R. Chaudhari, V. Baskaran, Preparation, characterization, radical scavenging property and antidiabetic potential of laminarioligosaccharides derived from laminarin, Algal Res. 63 (2022) 102642, https://doi.org/10.1016/j.algal.2022.102642.
[19] O. Joffre, M.A. Nolte, R. Spörri, C.R.E. Sousa, Inflammatory signals in dendritic cell activation and the induction of adaptive immunity, Immunol. Rev. 227 (2009) 234–247, https://doi.org/10.1111/j.1600-065X.2008.00718.x.
[20] M. Cabeza-Cabrerizo, A. Cardoso, C.M. Minutti, M. Pereira Da Costa, C. Reis E. Sousa, Dendritic cells revisited, Annu. Rev. Immunol. 39 (2021) 131–166, https://doi.org/10.1146/annurev-immunol-061020-053707.
[21] F. Annunziato, C. Romagnani, S. Romagnani, The 3 major types of innate and adaptive cell-mediated effector immunity, J. Allergy Clin. Immunol. 135 (2015) 626–635, https://doi.org/10.1016/j.jaci.2014.11.001.
[22] G.E. Kaiko, J.C. Horvat, K.W. Beagley, Immunological decision-making : how does the immune system decide to mount a helper T-cell response ? Immunology 123 (2008) 326–338, https://doi.org/10.1111/j.1365-2567.2007.02719.x.
[23] L. Zhou, I.I. Ivanov, R. Spolski, R. Min, K. Shenderov, T. Egawa, D.E. Levy, W. J. Leonard, D.R. Littman, IL-6 programs TH-17 cell differentiation by promoting sequential engagement of the IL-21 and IL-23 pathways, Nat. Immunol. 8 (2007) 967–974, https://doi.org/10.1038/ni1488.
[24] S. Hirohata, T. Yanagida, Human Thl responses driven by IL-12 are associated with enhanced expression of CD40 ligand, Jpn. J. Clin. Immunol. 21 (1998) 67–76, https://doi.org/10.2177/jsci.21.supplement_67.
[25] C.A. Hunter, S.A. Jones, IL-6 as a keystone cytokine in health and disease, Nat. Immunol. 16 (2015) 448–457, https://doi.org/10.1038/ni.3153.
[26] D.I. Jang, A.H. Lee, H.Y. Shin, H.R. Song, J.H. Park, T.B. Kang, S.R. Lee, S.H. Yang, The role of tumor necrosis factor alpha (Tnf-α) in autoimmune disease and current tnf-α inhibitors in therapeutics, Int. J. Mol. Sci. 22 (2021) 1–16, https://doi.org/10.3390/ijms22052719.
[27] D.R. Germolec, K.A. Shipkowski, R.P. Frawley, E. Evans, Markers of inflammation, in: Methods in Molecular Biology, Humana Press Inc., 2018, pp. 57–79, https://doi.org/10.1007/978-1-4939-8549-4_5.
[28] F. Ghorbaninezhad, P. Leone, H. Alemohammad, B. Najafzadeh, N.S. Nourbakhsh, M. Prete, E. Malerba, H. Saeedi, N.J. Tabrizi, V. Racanelli, B. Baradaran, Tumor necrosis factor-α in systemic lupus erythematosus: structure, function and therapeutic implications (review), Int. J. Mol. Med. 49 (2022), https://doi.org/10.3892/IJMM.2022.5098.
[29] S.K. Mittal, P.A. Roche, Suppression of antigen presentation by IL-10, Curr. Opin. Immunol. 34 (2015) 22–27, https://doi.org/10.1016/j.coi.2014.12.009.
[30] P.J. Murray, The primary mechanism of the IL-10-regulated antiinflammatory response is to selectively inhibit transcription, Proc. Natl. Acad. Sci. 102 (2005) 8686–8691, https://doi.org/10.1073/pnas.0500419102.
[31] M. Nakabayashi, T. Nishijima, G. Ehara, N. Nikaidou, H. Nishihashi, T. Watanabe, Structure of the gene encoding laminaripentaose-producing β-1,3-glucanase (LPHase) of Streptomyces matensis DIC-108, J. Ferment. Bioeng. 85 (1998) 459–464.
[32] A.D. Premarathna, T.A.E. Ahmed, A. Sooäär, V. Rjabovs, A.T. Critchley, M. T. Hincke, R. Tuvikene, Extraction and functional characterization of fucoidans and alginates from Ecklonia maxima: a focus on skin, immune, and intestinal health, Food Hydrocoll. 159 (2025), https://doi.org/10.1016/j.foodhyd.2024.110668.
[33] V.L. American Society of Enologists, J.A. Rossi, American Journal of Enology and Viticulture, in: Am J Enol Vitic, American Society of Enologists, 1965, pp. 144–158.
[34] A. Sluiter, B. Hames, R. Ruiz, C. Scarlata, J. Sluiter, D. Templeton, Determination of Ash in Biomass, Laboratory Analytical Procedure (LAP), 2008, p. 8.
[35] A. Sluiter, B. Hames, R. Ruiz, C. Scarlata, J. Sluiter, D. Templeton, D. Crocker, Determination of Structural Carbohydrates and Lignin in Biomass, Technical Report NREL/ TP -510 -42618, 2008, pp. 1–15, doi:NREL/TP-510-42618.
[36] H. Motejadded, J. Altenbuchner, Construction of a dual-tag system for gene expression, protein affinity purification and fusion protein processing, Biotechnol. Lett. 31 (2009) 543–549, https://doi.org/10.1007/s10529-008-9909-9.
[37] A.O. Chizhov, A. Dell, H.R. Morris, A.J. Reason, S.M. Haslam, R.A. Mcdowell, O.S. Chizhov, A.I. Usov, Structural Analysis of Laminarans by MALDI and FAB Mass Spectrometry, (n.d.).
[38] A. Graiff, W. Ruth, U. Kragl, U. Karsten, Chemical characterization and quantification of the brown algal storage compound laminarin — a new methodological approach, J. Appl. Phycol. 28 (2016) 533–543, https://doi.org/10.1007/s10811-015-0563-z.
[39] L. Allahgholi, R.R.R. Sardari, S. Hakvåg, K.Z.G. Ara, T. Kristjansdottir, I.M. Aasen, O.H. Fridjonsson, T. Brautaset, G.O. Hreggvidsson, E.N. Karlsson, Composition analysis and minimal treatments to solubilize polysaccharides from the brown

seaweed Laminaria digitata for microbial growth of thermophiles, J. Appl. Phycol. 32 (2020) 1933–1947, https://doi.org/10.1007/s10811-020-02103-6.
[40] T. Wang, R. Jónsdóttir, G. Ólafsdóttir, Total phenolic compounds, radical scavenging and metal chelation of extracts from Icelandic seaweeds, Food Chem. 116 (2009) 240–248, https://doi.org/10.1016/j.foodchem.2009.02.041.
[41] C.F. Ji, Y. Bin Ji, D.Y. Meng, Sulfated modification and anti-tumor activity of laminarin, Exp. Ther. Med. 6 (2013) 1259–1264, https://doi.org/10.3892/etm.2013.1277.
[42] J.M.M. Dobruchowska, Jon O. Jonsson, Olafur H. Fridjonsson, Arnthor Aevarsson, Jakob K. Kristjansson, Josef Altenbuchner, Hildegard Watzlawick, Gerrit J. Gerwig, Lubbert Dijkhuizen, Johannis P. Kamerling, Gudmundur O. Hreggvidsson, Modification of linear (β1→3)-linked gluco-oligosaccharides with a novel recombinant 2 β-glucosyltransferase (trans-β-glucosidase) enzyme from Bradyrhizobium diazoefficiens, Glycobiology 26 (2016) 1157–1170.
[43] G.O. Hreggvidsson, J.M. Dobruchowska, O.H. Fridjonsson, J.O. Jonsson, G. J. Gerwig, A. Aevarsson, J.K. Kristjansson, D. Curti, R.R. Redgwell, C.E. Hansen, J. P. Kamerling, T. Debeche-Boukhit, Exploring novel non-Leloir β-glucosyltransferases from proteobacteria for modifying linear (β1→3)-linked gluco-oligosaccharide chains, Glycobiology 21 (2011) 304–328, https://doi.org/10.1093/glycob/cwq165.
[44] E.L. Adams, P.J. Rice, B. Graves, H.E. Ensley, H. Yu, G.D. Brown, S. Gordon, M. A. Monteiro, E. Papp-Szabo, D.W. Lowman, T.D. Power, M.F. Wempe, D. L. Williams, Differential high-affinity interaction of Dectin-1 with natural or synthetic glucans is dependent upon primary structure and is influenced by polymer chain length and side-chain branching, J. Pharmacol. Exp. Ther. 325 (2008) 115–123, https://doi.org/10.1124/jpet.107.133124.
[45] H.M. Wu, S.W. Liu, M.T. Hsu, C.L. Hung, C.C. Lai, W.C. Cheng, H.J. Wang, Y.K. Li, W.C. Wang, Structure, mechanistic action, and essential residues of a GH-64 enzyme, laminaripentaose-producing β-1,3-glucanase, J. Biol. Chem. 284 (2009) 26708–26715, https://doi.org/10.1074/jbc.M109.010983.
[46] M. Collin, V. Bigley, Human dendritic cell subsets: an update, Immunology 154 (2018) 3–20, https://doi.org/10.1111/imm.12888.
[47] G. Breton, S. Zheng, R. Valieris, I. Tojal, R. Satija, M.C. Nussenzweig, Human dendritic cells (DCs) are derived from distinct circulating precursors that are precommitted to become CD1c+ or CD141+ DCs, J. Exp. Med. 213 (2016) 2861–2870, https://doi.org/10.1084/jem.20161135.
[48] Q. Peng, X. Qiu, Z. Zhang, S. Zhang, Y. Zhang, Y. Liang, J. Guo, H. Peng, M. Chen, Y. Fu, H. Tang, PD-L1 on dendritic cells attenuates T cell activation and regulates response to immune checkpoint blockade, Nat. Commun. 11 (2020) 1–8, https://doi.org/10.1038/s41467-020-18570-x.
[49] S.O. Adegbola, K. Sahnan, J. Warusavitarne, A. Hart, P. Tozer, Anti-TNF therapy in Crohn's disease, Int. J. Mol. Sci. 19 (2018), https://doi.org/10.3390/ijms19082244.
[50] U. Müller-Ladner, T. Pap, R.E. Gay, M. Neidhart, S. Gay, Mechanisms of disease: the molecular and cellular basis of joint destruction in rheumatoid arthritis, Nat. Clin. Pract. Rheumatol. 1 (2005) 102–110, https://doi.org/10.1038/ncprheum0047.
[51] K.P. Kumar, A.J. Nicholls, C.H.Y. Wong, Partners in crime: neutrophils and monocytes/macrophages in inflammation and disease, Cell Tissue Res. 371 (2018) 551–565, https://doi.org/10.1007/s00441-017-2753-2.
[52] A.J. Kassianos, M.Y. Hardy, X. Ju, D. Vijayan, Y. Ding, A.J.E. Vulink, K. J. Mcdonald, S.L. Jongbloed, R.B. Wadley, C. Wells, D.N.J. Hart, K.J. Radford, Human CD1c (BDCA-1) + myeloid dendritic cells secrete IL-10 and display an immuno-regulatory phenotype and function in response to Escherichia coli, Eur. J. Immunol. 42 (2012) 1512–1522, https://doi.org/10.1002/eji.201142098.
[53] M. Saraiva, A. O'Garra, The regulation of IL-10 production by immune cells, Nat. Rev. Immunol. 10 (2010) 170–181, https://doi.org/10.1038/nri2711.
[54] M.G. Roncarolo, S. Gregori, M. Battaglia, R. Bacchetta, K. Fleischhauer, M. K. Levings, Interleukin-10-secreting type 1 regulatory T cells in rodents and humans, Immunol. Rev. 212 (2006) 28–50, https://doi.org/10.1111/j.0105-2896.2006.00420.x.
[55] C.M. Hawrylowicz, A. O'Garra, Potential role of interleukin-10-secreting regulatory T cells in allergy and asthma, Nat. Rev. Immunol. 5 (2005) 271–283, https://doi.org/10.1038/nri1589.
[56] X. Ma, W. Yan, H. Zheng, Q. Du, L. Zhang, Y. Ban, N. Li, F. Wei, Regulation of IL-10 and IL-12 production and function in macrophages and dendritic cells, F1000Res 4 (2015) 1–13, https://doi.org/10.12688/f1000research.7010.1.
[57] L. Guglani, S.A. Khader, Th17 cytokines in mucosal immunity and inflammation, Curr. Opin. HIV AIDS 5 (2010) 120–127, https://doi.org/10.1097/COH.0b013e328335c2f6.
[58] H. Ishigame, S. Kakuta, T. Nagai, M. Kadoki, A. Nambu, Y. Komiyama, N. Fujikado, Y. Tanahashi, A. Akitsu, H. Kotaki, K. Sudo, S. Nakae, C. Sasakawa, Y. Iwakura, Differential roles of interleukin-17A and -17F in host defense against mucoepithelial bacterial infection and allergic responses, Immunity 30 (2009) 108–119, https://doi.org/10.1016/j.immuni.2008.11.009.
[59] L. Lin, A.S. Ibrahim, X. Xu, J.M. Farber, V. Avanesian, B. Baquir, Y. Fu, S. W. French, J.E. Edwards, B. Spellberg, Th1-Th17 cells mediate protective adaptive immunity against Staphylococcus aureus and Candida albicans infection in mice, PLoS Pathog. 5 (2009), https://doi.org/10.1371/journal.ppat.1000703.
[60] M.K. Gately, L.M. Renzetti, J. Magram, A.S. Stern, L. Adorini, U. Gubler, D. H. Presky, The Interleukin-12/ Interleukin-12-receptor System: Role in Normal and Pathologic Immune Responses, 1998.
[61] J. Freysdottir, M.B. Sigurpalsson, S. Omarsdottir, E.S. Olafsdottir, A. Vikingsson, I. Hardardottir, Ethanol extract from birch bark (Betula pubescens) suppresses human dendritic cell mediated Th1 responses and directs it towards a Th17 regulatory response in vitro, Immunol. Lett. 136 (2011) 90–96, https://doi.org/10.1016/j.imlet.2010.12.009.
[62] V. Kale, J. Freysdottir, B.S. Paulsen, Ó.H. Friojónsson, G. Óli Hreggviosson, S. Omarsdottir, Sulphated polysaccharide from the sea cucumber Cucumaria frondosa affect maturation of human dendritic cells and their activation of allogeneic CD4(+) T cells in vitro, Bioact. Carbohydr. Diet. Fibre 2 (2013) 108–117, https://doi.org/10.1016/j.bcdf.2013.09.009.

Paper III

International Journal of Biological Macromolecules 320 (2025) 145930

Contents lists available at ScienceDirect

International Journal of Biological Macromolecules

journal homepage: www.elsevier.com/locate/ijbiomac

A cold-adapted *endo*-fucoidanase Psf1 from *Pseudoalteromonas* sp. that catalyzes production of T-cell activating fucoidan oligosaccharides from *Saccharina latissima* fucoidan

Vo Thi Dieu Trang [a,b], Maria Dalgaard Mikkelsen [a], Monica Daugbjerg Christensen [d,e,g], Sebastian Meier [c], Cameron James Hunt [a], Jesper Holck [a], Guðmundur Óli Hreggviðsson [d,f], Jona Freysdottir [g,h], Hang Thi Thuy Cao [b], Huynh Hoang Nhu Khanh [b], Anne S. Meyer [a,*]

[a] *Protein Chemistry and Enzyme Technology Section, Dept. of Biotechnology and Biomedicine, Technical University of Denmark, 2800 Kgs. Lyngby, Denmark*
[b] *Institute of Oceanography, Vietnam Academy of Science and Technology, 01 Cau Da Street, Nha Trang 650000, Viet Nam*
[c] *Department of Chemistry, Technical University of Denmark, 2800 Kgs. Lyngby, Denmark*
[d] *Department of Biotechnology and biomolecules, Matís, Reykjavík, Iceland*
[e] *Faculty of Food Science and Nutrition, University of Iceland, Reykjavík, Iceland*
[f] *Faculty of Life and Environmental Sciences, University of Iceland, Reykjavík, Iceland*
[g] *Department of Immunology, The National University Hospital of Iceland, Reykjavik, Iceland*
[h] *Faculty of Medicine, University of Iceland, Reykjavík, Iceland*

ARTICLE INFO

Keywords:
Psychrophilic *endo*-α-1,3-fucoidanase
GH107
Immune modulation

ABSTRACT

Bioactive sulfated fucoidans have high fucose content and are derived from brown seaweeds. Here we report the discovery of the first cold-adapted *endo*-α(1 → 3)-fucoidanase (EC 3.2.1.211), Psf1. The *psf1* gene was found in the genome of *Pseudoalteromonas* sp. S3178, a bacterium isolated from a shrimp near Antarctica. Phylogenetic analyses designated Psf1 as a putative member of glycoside hydrolase family 107 (GH107). Substrate selectivity analysis confirmed Psf1 as being *endo*-acting and indicated that the enzyme catalyzes hydrolysis of α(1 → 3)-glycosidic fucoidan linkages. Psf1 had temperature optimum of 10–30 °C but retained activity at 1 °C. Structural modeling indicated similarity to the crystal structure of P5A_FcnA (*Psychromonas* sp. SW5A), yet distinct high variability regions were identified by RMSF. Psf1 released low molecular weight fucoidan oligosaccharides from *Saccharina latissima* fucoidan that dose-dependently reduced IL-12p40 secretion in dendritic cells, and lowered IFN-γ and IL-10 levels in dendritic cells co-cultured with allogeneic $CD4^+$ T-cells, without affecting IL-17 secretion, indicating a suppression of Th1-mediated immune response. Treatment of dendritic cells with native fucoidan from *S. latissima* did not affect cell viability or cytokine secretion. These findings have potential to enable new enzyme-assisted production, at low temperatures, of bioactive fucoidan oligosaccharides from *S. latissima* grown in the Northern Hemisphere.

1. Introduction

Approximately 75–80 % of the Earth's biosphere, including the polar regions, deep-sea waters, and glaciers, is constantly cold with temperatures below 5 °C [1]. In spite of the low temperatures and limited nutrients, a wide variety of microorganisms have been identified and isolated from these environments [1,2]. A particular feature of these psychrotolerant or psychrophilic microorganisms is that they have evolved cold-adapted enzymes to survive. Cold-adapted enzymes are of interest in a wide range of industrial processes [2]. Catalytic activity at low temperatures can save energy, which is relevant in various processes where, for example, heat-sensitive compounds must be conserved during the process [3].

Fucoidans are fucose-rich, sulfated polysaccharides primarily found in the cell walls of brown seaweeds, but which are also present in e.g. sea cucumbers [4]. Fucoidans are classified into three main groups dependent on the backbone linkages, group 1: α(1 → 3)-fucosyl linkages; group 2: alternating α(1 → 3) and α(1 → 4)-linked fucosyl units and group 3 α(1 → 3)-, α(1 → 4)-linked fucosyls and β-D-galactose units [5].

The structural variability of fucoidans is vast and the degree and

* Corresponding author.
E-mail address: asme@dtu.dk (A.S. Meyer).

https://doi.org/10.1016/j.ijbiomac.2025.145930
Received 9 April 2025; Received in revised form 9 July 2025; Accepted 10 July 2025
Available online 11 July 2025

patterns of for instance sulfation differ between different fucoidans [6,7]. Fucoidans are known to exert a range of bioactivities including anti-inflammatory, anticoagulant and antitumor effects [8–14], although the structural heterogeneity and enhanced viscosity in solution limits the therapeutic applications. A prerequisite for unlocking the full potential of the fucoidan bioactivity is a mild and preserving extraction technique followed by separation of native fucoidan populations [15]. Then, a selective depolymerization process to obtain homogeneous bioactive fucoidans with low viscosity can be achieved using specific fucoidanases [11–13].

Currently, *endo*-fucoidanases that cleave the α(1 → 4) linkages are classified to Glycoside Hydrolase (GH) family 107 (EC 3.2.1.212) in the CAZy database [17]. Although three α(1 → 3) specific fucoidanases are also found in GH107, including Mef2 [16], the *endo*-fucoidanases that attack α(1 → 3) linkages in fucoidans are otherwise categorized into GH168 (EC 3.2.1.211), GH174, or GH187 [9]. Most fucoidanases characterized to date, belong to the GH107 family [16,18–25]. So far, these fucoidanases have been reported to have optimal temperatures from 25 to 37 °C, and reduced activity at lower temperatures [16,18–25].

One particularly unique activity is the potential immune-regulatory effect of fucoidans as well as presumably fucoidan oligosaccharides [9,10], which can be investigated by analyzing DCs and T-cell responses in an in vitro dendritic cell system. Dendritic cells (DCs) are specialized in antigen presentation and can directly activate naïve T-cells. They reside in tissues in their immature state, where they act as sentinels on the lookout for foreign antigens [26,27]. Upon encountering a foreign antigen, DCs activate by undergoing phenotypic and functional changes to develop into their mature stage, resulting in up-regulation of surface molecules specific for antigen presentation [27]. Mature DCs then migrate to the lymph nodes where they prime naïve T-cells, directing them to become effector cells. The cytokines that DCs secrete during this process depend on the antigen encountered (e.g., microbial, viral or parasitic) and tissue-environmental factors, which determine the appropriate T-cell response [28]. For example, during the generation of Th1 or Th17 responses, DCs secrete either IL-12 or IL-6, respectively, which polarize naïve T-cells into Th1 of Th17 effector cells [29,30].

As part of our quest for identifying *endo*-fucoidanases that modify fucoidan to novel bioactive products we investigated the *psf1* gene encoding a putative GH107 protein, Psf1, which had been identified in the genome of the arctic bacterial strain *Pseudoalteromonas* sp. 3178. This strain of bacteria was extracted from a surface swab of a shrimp retrieved from the Arctic Ocean vicinity by the Danish marine expedition known as Galathea 3 [31,32].

Dendritic cell signalling studies in vitro using Psf1 degraded fucoidan, suggest that this enzyme exhibits unique properties for production of potentially immune regulative fucoidan oligosaccharides in low temperature processes.

2. Materials and methods

2.1. Fucoidan substrates

Fucoidans from *Fucus evanescens* (Fe) and *Saccharina latissima* (Sl) were extracted using an enzyme-assisted extraction method followed by purification by ion-exchange chromatography (IEX) as described in [15] using an anion exchange DEAE-Macroprep resin material (Bio-Rad, CA, USA). The Sl fucoidan used in this study, was the third elution fraction obtained after IEX and is referred to here as Sl native.

Crude fucoidans were extracted as previously described from the Vietnamese brown seaweeds *Turbinaria ornata* (To) [33], *Sargassum mcclurei* (Sm) [34], *Sargassum oligocystum* (So) [35], and *Sargassum polycystum* (Sp) [36], and further separated by anion-exchange chromatography. Fucoidan from *Undaria pinnatifida* (Up) was isolated by the Pacific Institute of Bioorganic Chemistry (PIBOC, Russia) as described previously [37].

Fucoidan from *Fucus vesiculosus* F8190 (Fv) was purchased from Sigma-Aldrich (Steinheim, Germany).

Table S1 details the reported branches, glycosidic linkages, and degree of sulfation of the structural moieties of the fucoidan substrates.

2.2. Identification of the psf1 gene and sequence analysis

The putative fucoidanase-encoding *psf1* gene (Genbank WP_138682449.1) was discovered in the genome of *Pseudoalteromonas* sp. *S3178* (GenBank assembly accession GCA_005886985.1) by sequence alignment. An N-terminal signal peptide was predicted in the Psf1 protein using SignalP 5.0 (https://services.healthtech.dtu.dk/service.php/SignalP-5.0). Conserved domains in Psf1 were predicted using InterProScan (https://www.ebi.ac.uk/interpro/search/sequence/). Multiple sequence alignment was carried out by using CLUSTALW (https://www.genome.jp/tools-bin/clustalw). A phylogenetic tree was constructed by maximum likelihood using Phylogeny.fr (http://www.phylogeny.fr/index.cgi). ESPript 3.0 https://espript.ibcp.fr/ESPript/ESPript/ was used to visualize the alignment [38].

Selected and previously characterized GH107 fucoidanases in the CAZy database (http://www.cazy.org) were used for sequence comparisons and include Fhf1 (Genbank: WP_006217780.1), Fhf2 (WP_006217784.1) from *Formosa haliotis*; FFA1 (WP_057784217.1), FFA2 (WP057784219.1) from *Formosa algae* KMM 3553^T; MfFcnA (CAI47003.1) from *Mariniflexile fucanivorans* SW5; P5A_FcnA (AYF59291.1) from *Psychromonas* sp. SW5A; P19D_FcnA (AYF59292.1) from *Psychromonas* sp. SW19D; Fda1 (AAO00508.1), Fda2 (AAO00509.1) from *Alteromonas* sp. SN-1009; FWf1 (ANW96097.1), FWf2 (ANW96098.1), FWf3 (ANW96115.1) and FWf4 (ANW96116.1) from *Wenyingzhuangia fucanilytica* CZ1127^T; SVI_0379 (BAJ00350.1) from *Shewanella violacea* DSS12; Fp273 (AYC81240.1), Fp277 (AYC81238.1), Fp279 (AYC81239.1) from an uncultured bacterium; Mef1 (OQ831695), Mef2 (URS64324.1) from *Muricauda eckloniae*.

2.3. Cloning of the psf1 gene

The *psf1* gene without the predicted N-terminal signal peptide but with an N-terminal 10× histidine tag was codon optimized for *Escherichia coli* expression, synthesized by GenScript (Piscataway, NJ, USA), and cloned into the pET-28b(+) using the *Nco*I and *Xho*I restriction sites (Thermo Fisher Scientific, Waltham, MA, USA). The *psf1* construct was confirmed by DNA sequencing (Macrogen Europe, Amsterdam, Netherlands).

The plasmid was transformed into *E. coli* DH5α for plasmid amplification and into *E. coli* BL21 (DE3) for protein expression (Invitrogen® Life Technologies, Thermo Fisher Scientific, Waltham, MA, USA). The theoretical molecular weight (MW) of the recombinant Psf1 protein was calculated using the protein molecular weight tool (https://www.bioinformatics.org/sms/prot_mw.html).

2.4. Expression and purification of the recombinant Psf1 fucoidanase

The recombinant Psf1 protein was expressed under isopropylβ-D-1-thiogalactopyranoside (IPTG) induction. A colony was used to inoculate 5 mL of lysogeny broth (LB) medium containing kanamycin (50 μg/mL) followed by incubation at 37 °C with shaking (180 rpm) overnight. The culture was then transferred to 500 mL LB medium with kanamycin (50 μg/mL) and incubated similarly at 37 °C (180 rpm). When OD_{600} of the culture reached 0.8–1.0, IPTG was added to a final concentration of 1 mM to induce expression, and the culture was incubated for 20 h at 20 °C (180 rpm). The cells were harvested by centrifugation at 5000 *g* and 4 °C for 30 min and stored at −80 °C. Purification of Psf1 was performed by immunoaffinity his-tag purification following resuspension and sonication of the cells, cell debris removal by centrifugation, and the filtering of the supernatant as previously described [20].

2.5. General protein analysis

Protein concentration was quantified by the Bradford method with bovine serum albumin (BSA) (Thermo Scientific™ Pierce™ pre-diluted standard set (calibrated to purified BSA fraction V), Product #23208, Thermo Scientific, Rockford, IL, USA) as the standard in concentrations from 0.1 to 1.0 μg/mL [39]. Molecular weight and purity of purified proteins were estimated by sodium dodecyl sulfate-polyacrylamide gel electrophoresis (SDS-PAGE) and western blotting, using monoclonal anti-poly histidine-peroxidase conjugated antibodies (Sigma-Aldrich, Steinheim, Germany) as previously described [20]. The protein markers used were precision plus protein standard for SDS-PAGE, and precision plus protein dual colour standard for the western blots (Bio-Rad, Hercules, CA, USA).

2.6. Carbohydrate polyacrylamide gel electrophoresis (C-PAGE)

Fucoidanase activity of Psf1 was detected using Carbohydrate Polyacrylamide Gel Electrophoresis (C-PAGE) as described previously [19,20]. In short, one volume of assay reaction was mixed with one volume of loading buffer (0.02 % phenol red in 20 % glycerol). Samples were then loaded on a 20 % (*w/v*) 1 mm thick polyacrylamide gel and oligosaccharides were separated at 30 mA for 90 min, in running buffer (100 mM Tris-borate buffer pH 8.3). The gel was stained with 0.5 % alcian blue 8 GX (Panreac, Barcelona, Spain) in 2 % acetic acid and 0.02 % O-toluidine (Sigma-Aldrich, Steinheim, Germany) in ethanol, for 1 h at room temperature. The gel was washed with distilled water until bands were visible.

The oligosaccharide standard (St) was obtained after enzymatic reaction of 0.9 % (w/v) native *F. evanescens* fucoidan and 0.3 mg/mL Fhf1 fucoidanase from *Formosa haliotis*, 10 mM Tris-HCl buffer pH 7.4, 125 mM NaCl, 10 mM $CaCl_2$. The furthest migrating band of the standard corresponds to a tetra-saccharide sulfated at C2 of all fucose residues and acetylated at C3 on the fucose residue adjacent to the reducing end α-L-Fucp2S-(1 → 3)-α-L-Fucp2S-(1 → 4)-α-L-Fucp2S,3OAc-(1 → 3)-α-L-Fucp2S.

2.7. Psf1 assay and thermal stability assessment

For substrate specificity assessments, enzymatic hydrolysis was conducted using 0.9 % (w/v) substrate (the concentration of fucoidan substrate is limited to this concentration to enable visualization and proper separation in the C-PAGE-gel), 0.3 mg/mL enzyme, 10 mM Tris-HCl buffer pH 7.4, 125 mM NaCl, 10 mM $CaCl_2$. These assays were performed at 25 °C for 18 h. The reactions were halted by heating at 85 °C for 10 min. Fucoidanase activity was determined by C-PAGE (as outlined in section 2.6.). For determination of optimal conditions for the Psf1 fucoidanase, assays were performed as above unless stated otherwise. The optimal temperature of Psf1 was evaluated at temperatures from 1 to 37 °C. The reaction time was determined for the different time-durations 0, 10, 30, 60 min and 2, 4, 8, 12, 24 and 48 h.

The optimal pH was investigated in 10 mM of different buffers with varying pH ranges including Universal buffer-UB4 buffer pH 2–8, Tris-HCl buffer pH 7–9, and borate buffer pH 7–11. Psf1 was treated with 10 mM EDTA to remove all divalent cations in the protein solution, followed by PD10 desalting and the effects of various divalent metal ions were investigated by adding 10 mM $CaCl_2$, $NiCl_2$, $MgCl_2$, $CuSO_4$, $MnSO_4$, $ZnCl_2$, $FeCl_2$, or $CoCl_2$ solution to the reaction. The optimal $CaCl_2$ and NaCl concentrations were investigated using concentrations ranging from 1 to 100 mM, and from 0 to 400 mM, respectively.

Determination of thermostability of Psf1 was investigated by pre-incubation of enzyme without substrate at different temperatures (4, 20, 25, 30, 35 and 37 °C) before assaying by addition of substrate under optimal assay conditions: 0.9 % fucoidan from *S. latissima*, 0.3 mg/mL enzyme, 10 mM Tris buffer at pH 7, 10 mM $CaCl_2$, and 80 mM NaCl at 25 °C for 8 h.

2.8. Preparation and isolation of fucoidan oligosaccharides

The enzymatic reaction using 0.3 mg/mL Psf1 fucoidanase and 0.9 % fucoidan from *S. latissima* (total weight 180 mg fucoidan) was incubated in 10 mM Tris-HCl pH 7, 100 mM NaCl, 10 mM $CaCl_2$ at 25 °C for 24 h. The medium molecular weight products (MMW) and low molecular weight products (LMW) were separated by ethanol precipitation as reported previously [20]. The reaction mixture and the separated fractions were analyzed by C-PAGE.

2.9. NMR spectroscopy

Fucoidan samples were freeze dried and analyzed with NMR spectroscopy. The samples consisted of 6.6 mg of intact fucoidan from *S. latissima*, 6.5 mg of deacetylated fucoidan from *S. latissima* and 17.0 mg of a reaction of Psf1 on intact substrate in 10 mM Tris-HCl, 50 mM NaCl, 10 mM $CaCl_2$. These samples were dissolved in D_2O and were transferred to 3 mm NMR sample tubes. All NMR spectra were collected at 323 K on an 800 MHz Bruker Avance III instrument equipped with an Oxford magnet and a TCI cryoprobe. The NMR spectra included one-dimensional ^1H NMR spectra (acquiring 16,384 complex data point that sampled 1.7 s in the FID), and 2D ^1H—^1H TOCSY (2048 × 256 complex data points that sampled 128 ms and 16 ms in the direct and indirect dimension of the 2D spectrum, respectively), ^1H—^1H COSY (2048 × 256 complex data points that sampled 128 ms and 16 ms in the direct and indirect dimensions, respectively), ^1H—^{13}C HMBC (2048 × 128 complex data points sampling 256 ms and 6.3 ms, respectively) and ^1H—^{13}C HSQC (2048 × 512 complex data points sampling 160 ms and 21.2 ms, respectively) spectra. These NMR spectra were processed with zero filling to twice the number of acquired data pointed in all dimensions. All NMR spectra were baseline corrected and analyzed using Bruker Topspin 3.5 pl7 software.

2.10. Assessment of molecular weight distribution of fucoidan structures

The molecular weight distribution of native and hydrolyzed fucoidan was estimated by High Performance Size Exclusion Chromatography (HPSEC) using an Ultimate iso-3100 SD pump with a WPS-3000 sampler (Thermo Scientific, Waltham, MA, USA) connected to an ERC RefractoMax 520 refractive index detector (Thermo Scientific, Waltham, MA, USA). 100 μL of sample was loaded on a Shodex SB-806 HQ column (300 × 8 mm) equipped with a Shodex SB-G guard column (50 mm × 6 mm) (Showa Denko K.K., Tokyo, Japan).

Elution was performed with 100 mM sodium acetate pH 6 at a flow rate of 0.5 mL/min at 40 °C. External pullulan standards (PSS Polymer Standards Service GmbH, Maiz, Germany) were applied to establish a polynomial relationship between the logarithmic molecular weight and the corresponding retention time to convert the retention times of the samples to molecular weights. Molecular weights above and below the applied standard range are estimates based on extrapolation of the polynomial expression [40].

2.11. 3D structural AlphaFold model of Psf1

A 3D structural model of the Psf1 was generated by AlphaFold and structurally aligned with P5A_FcnA (PDB:6M8N), originating from *Psychromonas* species SW5A based on the crystal structure of the GH107 *endo*-fucoidanase [24]. The predicted structure of Psf1 was generated via AlphaFold (v2.1.0) [41].

MSA generation was done against the reduced database (db_preset = reduced_dbs). All 5 relaxed structures were manually inspected for defects and the highest scoring structure (ranked_0.pdb, pLDDT = 92.95) was chosen for further analysis.

2.12. Molecular dynamics simulation

A molecular dynamics (MD) simulation of both Psf1 and P5A_FcnA (PDB:6M8N) was conducted using GROMACS using the CHARM36-jul2021 FF. A Calcium ion was inserted into Psf1 at the proposed Ca^{2+} binding site of 6M8N. Each structure was surrounded in a periodic dodecahedral system of ~130 Å and solvated with TIP3P water molecules. The system was equilibrated with Na^+ or Cl^- as needed. MD simulations were performed with 2 fs time step for a total of 50 ns at 300 K and 1 bar with additional equilibration and heating steps. Simulations were visualized using PyMol and analyzed using GROMACS functions rms and rmsf for calculation of root mean square deviation (RMSD) and root mean square fluctuation (RMSF). A mid simulation (25 ns) structure for both Psf1 and P5A_FcnA was selected for structural analysis. Hydrophobic centers, salt bridges and hydrogen bonding networks were investigated using ProteinTools and visualized using PyMol. The electrostatic potential was calculated using the APBS plugin in PyMol with the monovalent salt concentration set to 0.5 M. The backbone RMSD of Psf1 and P5A_FcnA was assessed during the full 50 ns simulation. P5A_FcnA (PDB:6M8N) appeared very stable after ~15 ns, while Psf1 appeared stable between 10 and 40 ns, followed by a decrease in RMSD from 0.21 to 0.15 nm. The stable region between 15 and 40 ns was used in the calculation of RMSF.

2.13. Maturation and activation of DCs

Buffy coats were obtained from healthy blood donors (ethical approval #06–68-V1 by the National Bioethics Committee). Peripheral blood mononuclear cells (PBMCs) were isolated from the buffy coats by Ficoll Histopaque density-gradient (Sigma-Aldrich). $CD14^+$ monocytes were isolated using CD14 Microbeads (Miltenyi Biotec, Bergisch Gladbach, Germany). The $CD14^+$ monocytes were cultured in 48-well plates (Nunc, Thermo Fisher Scientific, Paisley, UK) at a concentration of 0.5×10^6 cells/mL for seven days in complete cell medium (RPMI medium (Gibco®, Thermo Fisher Scientific), supplemented with 10 % fetal calf serum (Gibco®) and 1 % penicillin/streptomycin (Gibco®)). The differentiation into immature DCs was induced with IL-4 at 12.5 ng/mL, and granulocyte-macrophage colony-stimulating factor at 25 ng/mL (both from R&D Systems, Bio-Techne, Abingdon, England). Maturation of immature DCs was performed by culturing them for 24 h in complete cell medium in 48-well plates at a concentration of 2.5×10^5 cells/mL in the presence of IL-1β (10 ng/mL), TNF-α (50 ng/mL) (both from R&D Systems) and lipopolysaccharide (LPS) from *E. coli*, serotype 055:B5 (0.5 μg/mL, Sigma-Aldrich). A stock solution of 5 mg/mL of each fucoidan sample was diluted in complete cell medium and added to the maturing DCs to a final concentration of 100 μg/mL, except for the Sl Psf1 LMW sample, which was investigated at 1, 10 and 100 μg/mL. Cells cultured with cytokines and LPS alone or in the presence of 1α,25 dihydroxyvitamin D3 (VitD3; Biomol International, Plymouth Meeting, PA) at final concentration of 4×10^{-8} M, were used as the negative (Neg-DCs) and positive (VitD3-DCs) controls. After 24 h, the matured DCs were harvested and the effect of the fucoidan samples on their maturation was evaluated by measuring cytokine secretion by ELISA and expression of surface molecules by flow cytometry (for the Sl Psf1 LMW sample only). Additionally, the effect of reaction buffer, in the presence or absence of deactivated Psf1, on cytokine secretion using ELISA was determined.

2.14. Co-culture of DCs and allogeneic $CD4^+$ T-cells

Allogeneic $CD4^+$ T-cells were obtained from PBMCs using CD4 microbeads (Miltenyi Biotec, Bergisch Gladbach, Germany) using the same procedure as for the isolation of $CD14^+$ monocytes described above. DCs matured and activated with LPS, TNF-α, and IL-1β in the presence or absence of the Sl Psf1 LMW sample (100 μg/mL) were co-cultured at 2×10^5 cell/mL with allogeneic $CD4^+$ T-cells at 2×10^6 cells/mL in 96-well round bottom culture plates (Nunc) for 6 days. The effect of the Sl Psf1 LMW sample on the ability of DCs to activate the allogeneic $CD4^+$ T-cells was determined by measuring cytokine concentrations in the co-culture supernatants by ELISA.

2.15. Determination of cytokine concentrations by ELISA

The concentrations of pro-inflammatory cytokine IL-12p40 and anti-inflammatory cytokine IL-10 in the supernatants from DCs matured in the presence or absence of fucoidan samples and IFN-γ, IL-17 and IL-10 in supernatants from co-cultured DCs and allogeneic $CD4^+$ T-cells were measured by sandwich ELISA using DuoSets from R&D Systems according to the protocol from the manufacturer. To minimize the effect of variance in cytokine secretion by DCs obtained from different individuals, the results are expressed as secretion index (SI), calculated by dividing the concentration of cytokines (pg/mL) in the supernatant from DCs matured in the absence of a sample (and co-cultured with allogeneic $CD4^+$ T-cells) into the concentration of cytokines (pg/mL) in the supernatant of DCs matured in the presence of the sample or VitD3 (and co-cultured with allogeneic $CD4^+$ T-cells). Proportional index (PI) was used to evaluate the overall effect of the samples on the IL-12p40 and IL-10 cytokine secretion from the DCs matured in the presence or absence of fucoidan samples, calculated by dividing the SI for IL-12p40 with SI for IL-10. PI >1.0 indicates an increased secretion of IL-12p40 and/or decreased secretion of IL-10, which is more likely to promote an inflammatory response. Conversely, PI <1.0 indicates a decreased secretion of IL-12p40 and/or increased secretion of IL-10, which is more likely to induce an anti-inflammatory response.

2.16. Expression of surface molecules by flow cytometry

In this study, mature monocyte-derived DCs were defined by their phenotype as HLA-DR, CD40, CD86, CD1c, CD141 and PD-L1 positive, and CD14 negative by flow cytometry. The DCs were stained with fluorochrome-labelled mouse monoclonal antibodies against human HLA-DR (clone L243), CD40 (clone 5C3), CD14 (clone M5E2), PD-L1 (CD274) (clone 5C3), and CD1c (clone L161) (all from BioLegend), CD141 (clone 501,733) (R&D Systems), and CD86 (clone Bu63) (Bio-Rad). The data were collected using Sony SH800S flow cytometer (Sony Biotechnologies, UK), using a 10,000 events gate of mDCs. The data were analyzed using Kaluza analysis software (Beckman Coulter, California, USA). Appropriate isotypic antibodies were used to evaluate background staining. The results are given as percentage of positive cells and mean fluorescent intensity.

The gating strategy (Fig. S1) involved initial selection of singlet cells based on FSC-A against FSC-H to exclude doublets. Viable, intact cells were subsequently gated using FSC-A versus SSC-A to eliminate debris and dead cells. Appropriate isotypic antibodies were used to evaluate background staining, and staining with specific antibodies was used to define the percentage of positive cells.

2.17. Statistical analysis

Results are presented as means ± standard error of the mean (SEM). Reported n-values indicate the number of individual donors. As the same donors were used across all treatment conditions, a repeated-measures design was applied. Prior to analysis, normality of data distribution was assessed using the Shapiro-Wilk test. For comparisons involving three or more treatments, a repeated-measures one-way ANOVA was conducted (employing the Geisser-Greenhouse correction function in GraphPad Prism when sphericity was not met), followed by Dunnett's multiple comparisons post-hoc test to compare each treatment group to the negative control. All statistical analyses were performed using GraphPad Prism (10.3.1(509)) (GraphPad Software, San Diego, California, USA).

3. Results

3.1. Gene identification and amino acid sequence analysis

From a surface swap of a shrimp caught in the Arctic Ocean region by The Danish marine expedition, Galathea 3, a *Pseudoalteromonas* sp. S3178 bacterium was isolated and the whole genome was sequenced (GenBank: PNCW00000000.1) [31]. In a general search for glycosyl hydrolases, a putative GH107 fucoidanase encoding gene (Genbank WP_138682449.1; protein ID: TMP05905.1) was identified in the *Pseudoalteromonas* sp. S3178 genome and named *psf1* for *Pseudoalteromonas* sp. fucoidanase 1. Psf1 is a 402 amino acid long predicted protein containing an N-terminal signal peptide of 22 amino acids and a 380 amino acid long catalytic D1 domain, predicted through alignment with other fucoidanases, but without any additional predicted domains when using InterProScan (Fig. 1A and Fig. S2).

Most GH107 fucoidanases contain various predicted domains of unknown functions in their C-termini [16,18–25]. Truncation of the C-termini is often required for heterologous expression without degradation [42], as exemplified for the Fhf2 fucoidanase [19]. However, the modular construction of Psf1, consisting almost exclusively of the D1 domain, has previously been observed for other characterized marine bacterial fucoidanases including Mef1 [18] from *Muricauda eckloniae* as well as P19D_FcnA and P5A_FcnA from *Psychromonas* sp. [24].

The highest identity to Psf1 when using BLASTp was a hypothetical protein from *Pseudoalteromonas fuliginea* (WP_149613817.1), with 90 % identity on 99 % of the query sequence, while the most similar characterized fucoidanase was P5A_FcnA with 63 % identity on 90 % of the query sequence. The enzyme specificity of P5A_FcnA and P19D_FcnA has not yet been determined, but the crystal structure was previously solved for P5A_FcnA [24].

A phylogenetic tree was constructed from the multiple alignment of the D1 catalytic domain of Psf1 and 19 GH107 fucoidanases (Fig. S2 and Fig. 1B). Psf1 clustered closely to P5A_FcnA and P19D_FcnA, as expected

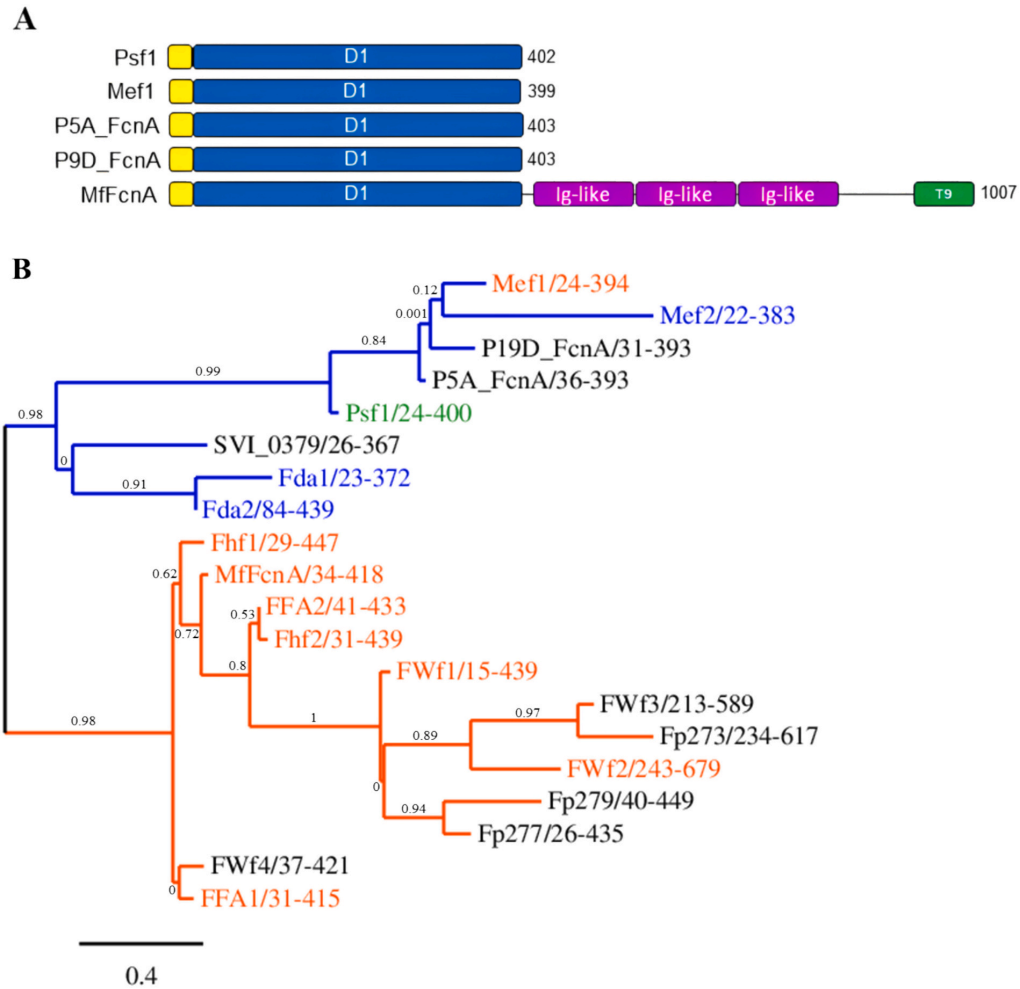

Fig. 1. The modular structures and phylogenetic tree of Psf1 and other characterized GH107 *endo*-fucoidanases. (A) The domain prediction of Psf1, Mef1, P5A_FcnA, P19D_FcnA and MfFcnA; Yellow: signal peptide; Blue: D1 catalytic domain; Purple: Ig-like domain (IPR03343); Green: C-terminal module of secretion system IX (IPR026444). (B) A phylogenetic tree of Psf1 (green) and 19 fucoidanases with known amino acids sequences belonging to GH107 family based on the D1 multiple alignment sequences with maximum likelihood numbers indicated branch support values. The specific α-(1 → 3) fucoidanases are shown in blue, while the specific α-(1 → 4) fucoidanases are shown in orange. Fucoidanases without determined specificity are shown in black. Accession numbers are listed in the Methods section.

but also clustered closely to the *endo*-α(1 → 3)-fucoidanases Mef2 [16], Fda1 and Fda2 [43,44], suggesting that Psf1 could be an *endo*-α(1 → 3)-specific fucoidanase.

The previously identified catalytic amino acids in MfFcnA, predicted to act as nucleophile (D226) and as acid base catalyst (H294), were identified in the Psf1 sequence at positions D203 and H278, respectively (Table 1).

Furthermore, three of the four amino acids residues predicted to be important for the catalytic −1 subsite of MfFcnA, including Y147, N149, and W351, were predicted at positions Y142, N144, and W327 in Psf1 in the alignment. However, the last −1 subsite amino acid of MfFcnA is an N270, which is changed to a S231 in Psf1.

Notably, two asparagine residues of the −1 subsite at position N149 and N270 in MfFcnA were not conserved in all sequences analyzed (Table 1 and Fig. S2). N149 in MfFcnA was an alanine in Mef1, Fda1, and Fda2 and a serine in Mef2, while N270 in MfFcnA was changed to Ser231 in Psf1 and Q267 in FWf1 (Table 1). Whether these changes in the −1 subsite in GH107 enzymes are important for the substrate linkage specificity or sulfate positioning, remains however to be elucidated.

3.2. AlphaFold 3D prediction revealed high structural conservation of Psf1

An AlphaFold prediction of the Psf1 structure was generated, revealing, as expected, an irregular $(\beta/\alpha)_8$-barrel structure (Fig. 2) as previously determined for the solved crystal structures of the three GH107 fucoidanases MfFcnA, P5A_FcnA [24] and Mef1 [18]. The AlphaFold prediction was of overall good quality, including 354 amino acids out of the 402 amino acids with a pLDDT score > 90. The N-terminal 30 amino acids were, as anticipated, not well predicted. Furthermore, a stretch of four amino acids (D310, G311, K312, and N313) and three amino acids (N253, D254 and K232) were predicted with a lower score (>84). This prediction corresponds to an overall good AlphaFold prediction of the 3D structure of Psf1. The AlphaFold prediction was aligned with the crystal structure of P5A_FcnA (PDB 6M8N), showing that the two enzymes had highly similar structures (Fig. 2A). The active site amino acids predicted from the multiple sequence alignment superimposed well to the active site amino acids of P5A_FcnA (Fig. 2A and B). In agreement with the sequence alignment the −1 subsite N229 in P5A_FcnA was the S231 Psf1 in the structural alignment.

A number of factors were investigated to determine and explain a possible cold adaptation of Psf1. This included comparisons of surface charge, RMSF and RMSD of Psf1 and P5A_FcnA via an MD simulation, analysis of hydrogen bonding networks, hydrophobic clusters and solvent accessible electrostatic potential. All factors that have been accredited to psychrophilic enzymes [45]. A surface charge plot was generated for Psf1 and compared with a surface plot for P5A_FcnA (Fig. 2C). A pronounced shift to a more neutral/positive electrostatic surface charge, particularly around the active site cleft was evident. In total, there were approximately 14 mutations of a polar side group to a positive side group, 10 from negative to polar side groups and 8 from hydrophobic to polar. The surface of P5A_FcnA was highly negatively

Table 1
Conserved motifs around the D1 catalytic domain and the − 1 subsite of GH107 fucoidanases. The two active site amino acids are shown in red. The two conserved aspartic acids residues and a conserved glycine in the active site are shown in purple. The four suggested amino acids of the −1 subsite are shown in blue (not conserved residues are underlined). Accession numbers are listed in the Methods section.

		The catalytic site					The -1 subsite								
GH107	Specificity	I			II		1			2			3		
Psf1	α-(1→3)	198	DGYWLD	273	DFTGGH		142	YLNAA	223	DSTLAISVS	327	WT			
P5A_FcnA	-	196	DGYWLD	271	DFTNGH		143	YLNSA	221	DPELTIAVN	325	WS			
P19D_FcnA	-	193	DGFWLD	271	DFTNGH		140	YLNTA	221	DPSFAIGVN	325	WS			
SVI_0379	-	197	DGWWFD	244	DYTSGH		125	YAATQ	220	NPAVILAFN	298	WN			
Mef2	α-(1→3)	177	DGYWLD	255	DFTNGH		127	YISTQ	199	DPTAVVTTN	307	WH			
Fda1	α-(1→3)	221	DGWWFD	268	DYTFGH		135	YIATQ	244	NNDAAVAFN	323	WN			
Fda2	α-(1→3)	290	DGWWFD	337	DFTGGH		198	YIATQ	313	NSNAAVSLN	392	WN			
MfFcnA	α-(1→4)	221	DAWCFD	289	DYTFGH		147	YVNSY	262	NPNAAIAFN	351	WN			
Mef1	α-(1→4)	182	DGYWLD	265	DFTSGH		128	YIATD	207	DPSVMIASN	318	WT			
Fhf1	α-(1→4)	218	DAWCFD	285	DYTFGH		142	YVNSY	258	NPNAAISFN	364	WN			
Fhf2	α-(1→4)	222	DAWCFD	292	DYKFGH		144	YVNSA	262	NPNAAITFN	355	WN			
FFA1	α-(1→4)	218	DAWCFD	286	DYTFGH		144	YVNSY	259	NPKAAISFN	348	WN			
FFA2	α-(1→4)	232	DAWCFD	302	DYKFGH		154	YVNSA	272	NPDAAITFN	365	WN			
FWf1	α-(1→4)	220	DAWCFD	288	DFMFGH		129	YVNSS	259	NPDAALSFQ	357	WN			
FWf2	α-(1→4)	459	DAWVFD	532	DFMFGH		365	YVNSS	498	NENAAVAFN	611	WQ			
FWf3	-	396	DSWIFD	464	DFTFGH		311	YTNSE	435	NPDIAIAFN	528	WK			
FWf4	-	224	DAWCFD	292	DYTFGH		150	YVNSY	265	NPNAAVAFN	354	WN			
Fp273	-	424	DSWIFD	492	DFTFGH		339	YLNSE	463	NPEIPIAFN	556	WT			
Fp277	-	229	DGWLFD	297	DYMFGH		139	YVNSS	268	NPNAPVSFN	368	WN			
Fp279	-	244	DGWLFD	312	DYMFGH		154	YVNSS	283	NPMAAISFN	383	WN			
Conservation			*.: :*		*: **			* :		: : .		*			

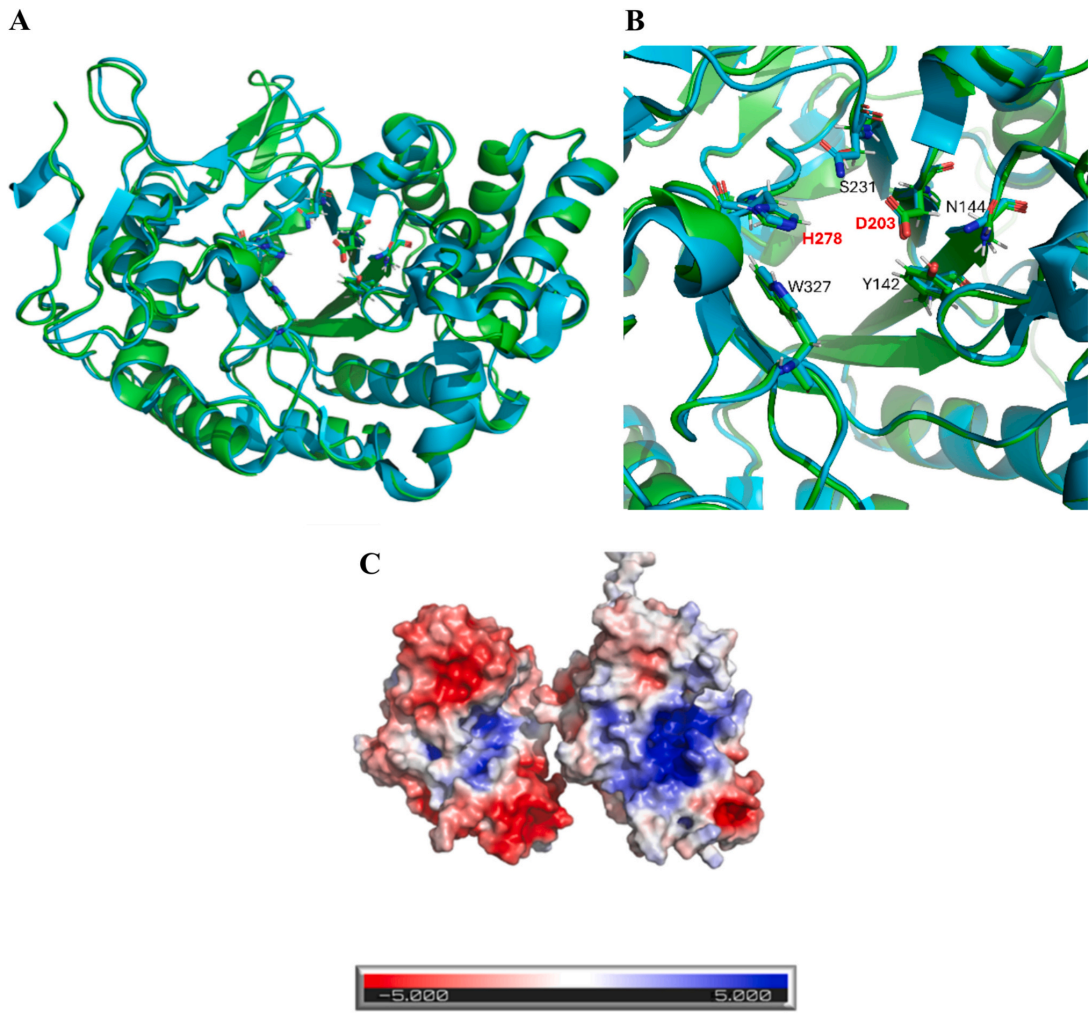

Fig. 2. AlphaFold 3D structure prediction of Psf1. A) AlphaFold 3D model prediction of Psf1 (green) overlaid with the crystal structure of P5A_FcnA (PDB: 6M8N) (cyan). Amino acids in the active site region of Psf1 (D203, H278, Y142, N144, S231, and W327) are indicated as sticks. B) Close-up view of the active site region with the catalytically active amino acids D203 and H278 highlighted in red. C) Comparison of the surface charge plot of the crystal fucoidanase P5A_FcnA (left) and the predicted structure of Psf1 (right).

charged, except near the active site, which was positively charged (Fig. 2C). The active site groove, expanding from the active site, was otherwise largely non-charged. In contrast, the surface charge of Psf1 was mostly neutral, except in the active site and active site groove, which was highly positively charged (Fig. 2C).

Analysis of the RMSF for Psf1 and P5A_FcnA revealed 5 regions where the RMSF showed a significant difference of >0.05 nm (Fig. S3). Psf1 exhibited higher RMSF than P5A_FcnA in 4 regions (1–3 and 5), while P5A_FcnA had significantly higher RMSF than Psf1 in region 4 (difference of ~0.15 nm) (Fig. S3). The largest increase in RMSF for Psf1 was in region 2, which affected region 1. Several prominent salt-bridges were either introduced or removed in Psf1 compared to P5A_FcnA, including in the helix in the variable region 2 and in region 3. While region 4 seemed more stable in Psf1 than in P5A_FcnA, region 5 showed increased flexibility (Fig. S3).

3.3. Substrate specificity and mode of action of the fucoidanase Psf1

The full length putative fucoidanase Psf1 was expressed (without the signal peptide) and purified giving a single band in SDS-PAGE and western blot analysis, corresponding to the expected molecular weight of 45 kDa (Fig. 3A and B).

Eight fucoidans, covering the three different fucoidan groups, were used as substrates for investigations of substrate specificity of Psf1 (Fig. 3C). The fucoidans include group 1 fucoidans from *S. latissima* (Sl), *Undaria pinnatifida* (Up) and *Turbinaria ornata* (To) mainly containing α(1 → 3)-linked fucosyl residues, group 2 fucoidans from *Fucus evanescens* (Fe) and *Fucus vesiculosus* (Fv) mainly containing alternating α(1 → 3)- and α(1 → 4)-linked fucosyl residues and group 3 galactofucans from *Sargassum mcclurei* (Sm), *Sargassum oligocystum* (So) and *Sargassum polycystum* (Sp) containing various monosaccharides and glycosidic linkages (Table S1). The Psf1 fucoidanase assay reactions were run for 18 h at 25 °C to obtain maximal fucoidan degradation, and the activity

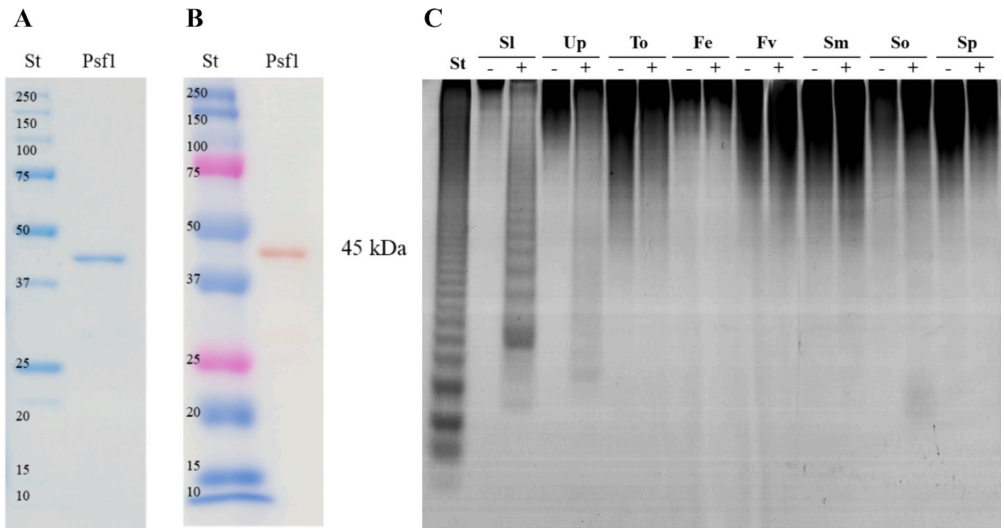

Fig. 3. Purification of the Psf1 fucoidanase and C-PAGE analysis of Psf1 activity on fucoidans isolated from different seaweed species. (A) SDS-PAGE, and (B) western blot of Psf1 with the expected molecular weight of 45 kDa. (St) in SDS-PAGE: Precision plus protein standard (St) for western blot: precision plus protein dual colour standard. (C) C-PAGE of (−) control substrate, (+) enzymatic reaction of Psf1 on fucoidans from *S. latissima* (Sl: Sl native), *U. pinnatifida* (Up), *T. ornata* (To), *F. evanescens* (Fe), *F. vesiculosus* (Fv), *S. mcclurei* (Sm), *S. oligocystum* (So), *S. polycystum* (Sp). (St) oligosaccharides standard produced from the enzymatic reaction of Fhf1 on fucoidan from *F. evanescens* [20].

of the recombinant Psf1 fucoidanase towards the fucoidans was evaluated by C-PAGE using the enzymatic reaction of *Formosa haliotis* Fhf1 on *F. evanescens* fucoidan as oligosaccharide standard [20]. The C-PAGE assay was used as a semi-quantitative assay for fucoidanase activity determination, like most previously published fucoidanase characterizations [16,18–21,23,24]. Quantitative glycosyl-hydrolase activity assays usually used for other types of glycosyl-hydrolases, including reducing sugar assays, are unfortunately not usable for fucoidanase activity assessments. The C-PAGE visualization of activity should be taken with precaution, since it is only semi-quantitative and not quantitative.

Psf1 only showed activity on some of the substrates including low activity on fucoidans from *U. pinnatifida* (group 1 fucoidan) and *S. oligocystum* (group 3 fucoidan) as a light smear in the gel, while the highest activity was observed on fucoidan from *S. latissima* (group 1 fucoidan), showing clear and distinct oligosaccharide bands in the C-PAGE gel **(**Fig. 3**)**. The number of oligosaccharide bands formed during reaction on *S. latissima* fucoidan, indicated that Psf1 is an *endo*-acting fucoidanase. Fucoidans from *S. latissima* and *U. pinnatifida* belong to group 1, with a backbone mainly consisting of α(1 → 3)-linked fucosyls and Psf1 showed highest activity on these fucoidans, in particular on fucoidans from *S. latissima*, compared to all other fucoidans tested. The Psf1 substrate specificity is likely reflecting the bond linkage specificity but also the sulfation degree and position as well at the branching in the different fucoidan molecules. The data suggest that Psf1 catalyzes hydrolysis of α(1 → 3)-linkages between fucosyls residues in group 1 fucoidans. Fucoidan from *S. latissima* was selected as substrate for further biochemical studies of the Psf1 fucoidanase.

3.4. Optimal conditions for catalytic activity of Psf1

Due to the Arctic origin, Psf1 activity was investigated at lower temperatures (1, 4, 10, 20, 25, 30, 35 and 37 °C) (Fig. 4A**).** The temperature optimum for the Psf1 fucoidanase was found between 10 and 30 °C, reaching maximum activity at 25 °C. The activity was almost undetectable when the incubation temperature reached 35 °C and it was completely absent at 37 °C. Interestingly, Psf1 exhibited activity at 10 °C which only decreased slightly at 4 °C. In fact, Psf1 showed activity at temperatures as low as 1 °C, suggesting that Psf1 is a psychrotolerant enzyme. All further experiments were carried out at 25 °C, since this temperature seemed to be in the middle of the optimal temperature range (20–30 °C) of the enzyme.

Like the temperature effects, varying buffers and pH conditions strongly affected Psf1 fucoidanase activity. The optimal pH of Psf1 was investigated in different buffers including UB4, Tris, and borate buffer. Psf1 displayed fucoidanase activity at pH values from 6 to 9. Tris and UB4 buffers were more suitable for activity assessments of Psf1 than borate buffer **(**Fig. 4B**)**.

Many fucoidanases are metal dependent as supported by previous crystal structures of GH107 fucoidanases, which were found to contain calcium sites [18,24]. Fucoidanases are often affected differently by different divalent cations [16,18–21]. Addition of EDTA completely abolished the activity of Psf1, suggesting that metal ions were required for Psf1 activity. The addition of different metal ions to the EDTA pretreated Psf1 enzyme, showed that Psf1 was most significantly reactivated by Ca^{2+} and Mn^{2+}, whereas Ni^{2+}, Mg^{2+}, Cu^{2+}, Zn^{2+}, Fe^{2+}, and Co^{2+} did not induce recovery of Psf1 activity **(**Fig. 4C**)**.

Addition of different Ca^{2+} concentrations indicated that Psf1 activity was activated in the presence of 2 mM Ca^{2+}, and slightly higher activity was found up to 10 mM **(**Fig. 4D**)**. The effect of NaCl on Psf1 activity showed low activity at 0–40 mM NaCl, while the activity was highest at NaCl concentrations from 80 to 400 mM **(**Fig. 4E**)**.

3.5. The Psf1 fucoidanase shows prolonged stability at low temperatures

Psf1 was pre-incubated at different temperatures from 4 to 37 °C for varying time periods without substrate, followed by addition of substrate and assaying under optimal conditions, to determine the enzyme stability **(**Fig. 5**)**.

While Psf1 completely lost activity after incubation at 35 and 37 °C for only 2 min, Psf1 remained stable for 2 h at 30 °C, but remained stable and highly active for several days at 4 °C. These results corroborated the cold-adapted nature of Psf1 activity.

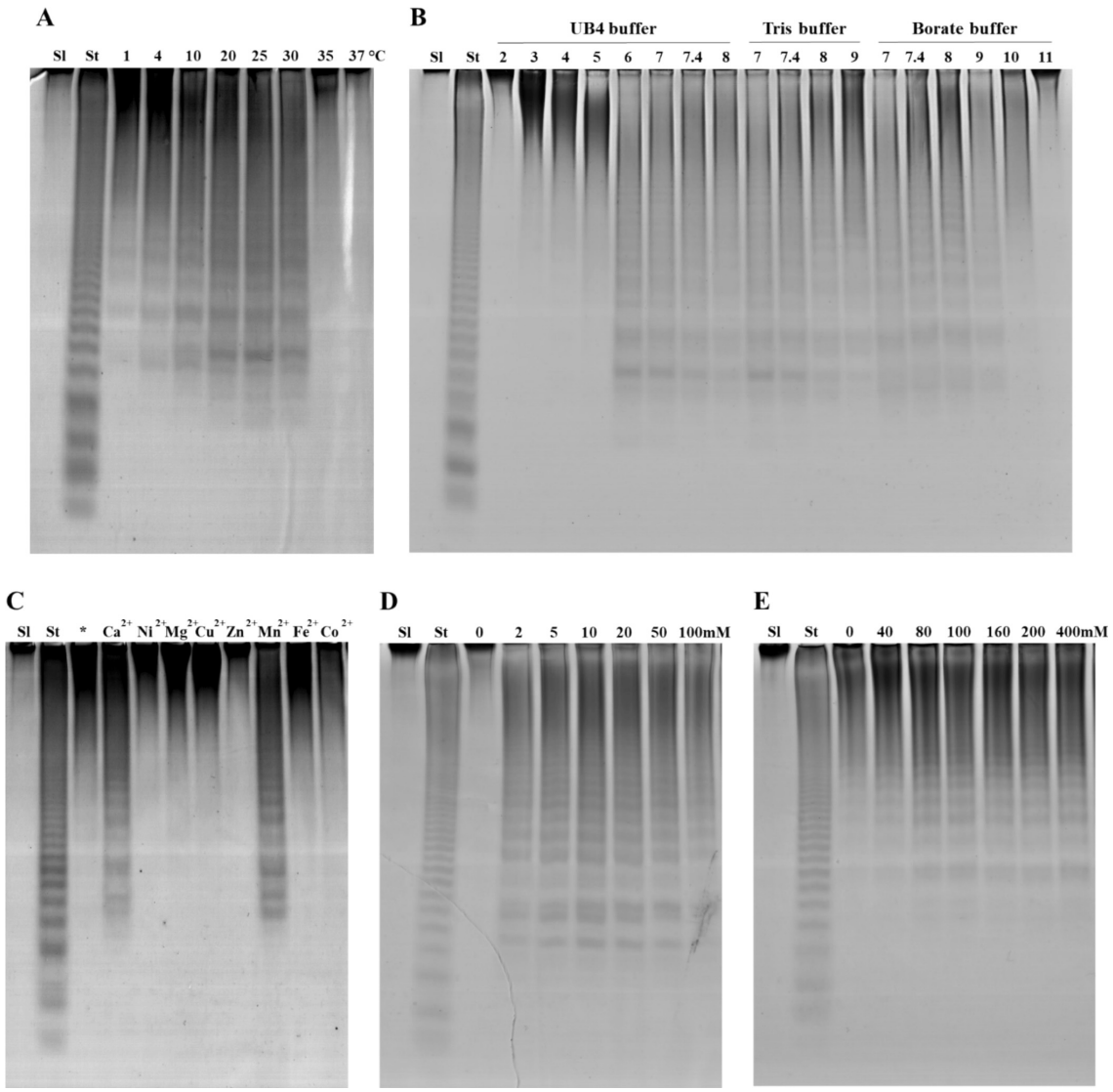

Fig. 4. Fucoidanase activity of Psf1 on fucoidan from *S. latissima* under different reaction conditions. C-PAGE of enzymatic hydrolysis of *S. latissima* fucoidan (Sl) by Psf1 (A) at different temperatures from 1 to 37 °C, and (B) different pH and buffer conditions. The numbers at each well indicate pH values for specific buffers: UB4 buffer pH 2–8, Tris-buffer pH 7–9, and borate buffer pH 7–11. Reaction conditions were 0.9 % substrate, 0.3 mg/mL enzyme, 10 mM $CaCl_2$ and 125 mM NaCl at 25 °C for 8 h at 10 mM of the various buffers. (C) C-PAGE of Psf1 activity with addition of different divalent cations at a concentration of 10 mM, (*) indicates Psf1 activity after EDTA treatment and without addition of divalent ions, (D) with addition of $CaCl_2$ at concentrations of 0–100 mM, (E) with addition of NaCl at concentrations of 0–400 mM. Reaction conditions were 0.9 % fucoidan (Sl), 0.3 mg/mL enzyme, 10 mM Tris-buffer pH 7, incubation at 25 °C for 8 h. (Sl) *S. latissima* fucoidan control substrate. (St) oligosaccharides standard produced from the enzymatic reaction of Fhf1 on fucoidan from *F. evanescens* [20].

3.6. Enzymatic degradation analysis

To determine the enzymatic degradation progress catalyzed by the Psf1 fucoidanase, the enzymatic reaction of Psf1 on *S. latissima* fucoidan was followed in time and the product profile visualized by C-PAGE and size-exclusion chromatography (SEC) (Fig. 6A and B). Large changes were observed in SEC after 30 min compared to the substrate, due to the *endo*-acting activity of the enzyme. The highest molecular weight fucoidan peak at around 2–3 × 10^6 Da decreased significantly, already after 30 min. Meanwhile, the peak around 300–400 kDa was slightly reduced from approximately 21–17 μRIU and an increase in compounds ranging from ~10–80 kDa was observed. After 1 h of reaction, smaller oligosaccharide products of DP 10–12 and above were visible in C-PAGE as distinct bands. No further smaller-sized products were visible as distinct bands in the C-PAGE after extended reaction time beyond 4–8 h, which was in accordance with the SEC data, although a gradual increase in the population of fucoidan products in the range 10–40 kDa was evident with longer reaction time and the 300–400 kDa peak was further decreased to approximately 12 μRIU (Fig. 6B).

In addition, with the extended reaction time, the SEC profile showed

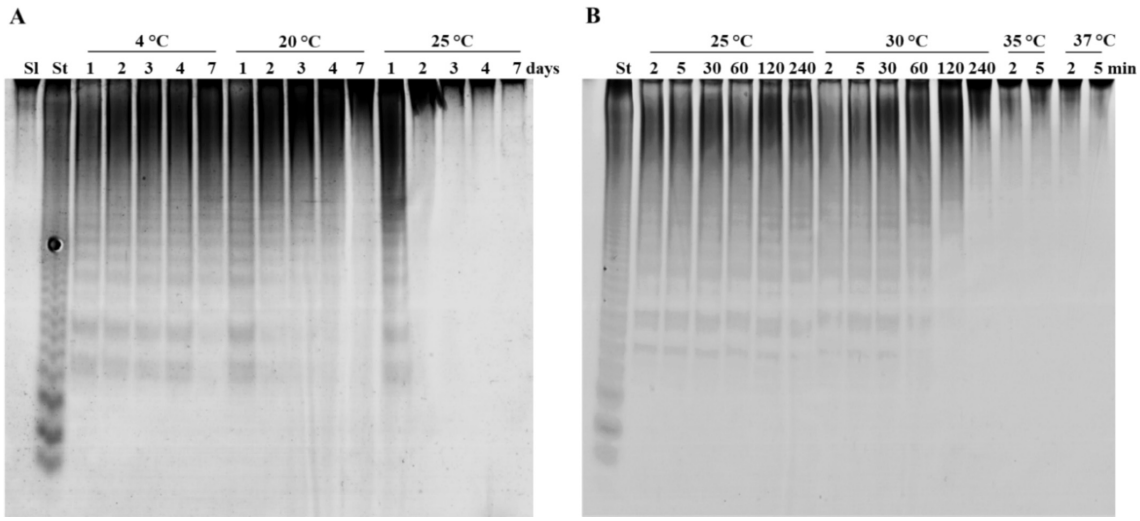

Fig. 5. Thermostability of the Psf1 fucoidanase. Psf1 was pre-treated at different temperatures at the indicated time durations, followed by fucoidanase activity assays on fucoidan from *S. latissima* (Sl native) under optimal conditions. C-PAGE of fucoidanase activity of Psf1 after pre-treatment (A) for 1–7 days at 4, 20, and 25 °C, and (B) for 2 to 240 min at 25, 30, 35, and 37 °C. (St) oligosaccharides standard produced from the enzymatic reaction of Fhf1 on fucoidan from *F. evanescens* [20]. Reaction conditions were 0.9 % fucoidan Sl, 0.3 mg/mL enzyme, 10 mM Tris buffer at pH 7, 10 mM $CaCl_2$, and 80 mM NaCl at 25 °C for 8 h.

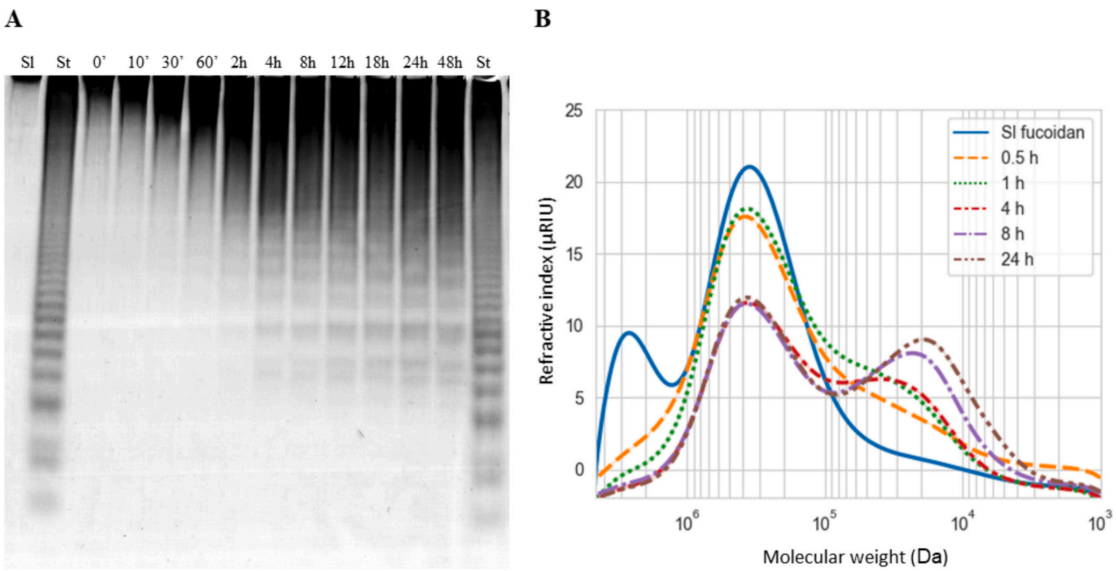

Fig. 6. Time-course assessments of Psf1 activity on the native fucoidan from *S. latissima* (Sl fucoidan) (A) Time-course of enzymatic hydrolysis (at 25 °C, 80 mM NaCl, 10 mM $CaCl_2$, pH 7) in minutes (') or in hours (h) is indicated at each well. (St) oligosaccharides standard producing from the enzymatic reaction of Fhf1 on fucoidan from *F. evanescens* [20]. (B) Size-exclusion chromatography of time-dependent Psf1 action on fucoidan from *S. latissima*.

an increase in smaller oligosaccharide products that were in the molecular weight range of 3–10 kDa, and the higher molecular weight bands on C-PAGE became gradually more evident.

These observations suggest that Psf1 quickly degraded the very high molecular weight fucoidan of 2–3 × 10^6 Da as well as the high molecular weight fucoidans (300–400 kDa), but according to C-PAGE, the enzyme was apparently unable to degrade the Sl fucoidan oligomers that had a DP 10–12, which indicates that the Psf1 cleavable sites in the fucoidan were exhausted. Compared to the results obtained with the fucoidanase Mef2 the resulting fucoidan oligosaccharide products were in essence larger than anticipated from the Fhf1 hydrolyzed *F. evanescens* standard oligomeric products in the C-PAGE. The C-PAGE data are thus consistent with the observed size distribution in the SEC meaning that the lowest visible bands in the C-PAGE are likely larger in molar weight than DP 10–12.

3.7. Separation of Psf1 hydrolysis products on fucoidan from S. latissima

The products from the Psf1 catalyzed hydrolysis of fucoidan from *S. latissima* were separated into two fractions using ethanol precipitation (Fig. S4), a technique which has been shown previously to separate LMW from MMW after fucoidanase hydrolysis [16,20]. The monosaccharide composition confirmed the high prevalence of fucose and galactose indicative of galactofucans in both the LMW and MMW fraction (Table S4).

3.8. NMR spectroscopy

NMR spectroscopy of the intact *S. latissima* fucoidan (Sl native, which was still acetylated and sulfated) showed three predominant spin systems likely deriving from a repetitive structural motif (Fig. 7A, Table 2). Two of the major $^{1}H—^{13}C$ HSQC-detectable spin systems could be assigned to galactose units. This assignment was based on a distinct coupling pattern in galactose yielding efficient magnetization transfer between H1 and H4, but not between H4 and H5. The third major spin system was identified as fucose. Doubling of $^{1}H—^{13}C$ HSQC signals and the presence of weaker signals in the spectral region that is characteristic of alpha-pyranosyl residues corrobated the heterogeneous nature of the fucoidan. This interpretation is supported by literature data highlighting the complexity of the *S. latissima* fucoidan [6] and by the fact that the monomer composition of the Sl native fraction is dominated by fucose [16]. Chemical shifts and sequential assignments of the repetitive major motif (shown in Fig. S5) are given in Table 2.

Linkage patterns were established based on HMBC and NOE correlations across the glycosidic bonds. The linkage in this structural motif was consistent with a previously reported structural motif detected in the reinvestigation of desulfated *S. latissima* fractions [6] and with the presence of galactose and fucose in the polysaccharide as determined by monosaccharide analysis.

NMR spectroscopy on the native, acetylated fraction showed a strong and characteristic deshielding of $^{1}H3$ in the terminal [α-Fucp3OAc,4OSO$_3$-(1→] unit to chemical shifts of 5.166 ppm/71.9 ppm for the C3H3 group (Table 2). An equivalent deshielding at $^{1}H2$ in the adjacent [→3)-β-Galp2OAc,4OSO$_3$-(1→] unit to 5.118 ppm/70.9 ppm for the C2H2 group (Table 2) witnesses that the preparation was predominantly acetylated at O3 of the terminal α-fucosyl residue and at O2 of the adjacent β-galactosyl residue. Sulfation could be determined by characteristic deshielding of ^{1}H and ^{13}C chemical shifts.

Upon treatment with Psf1, this polymeric structural motif containing a terminal [α-Fucp3OAc,4OSO$_3^-$(1→] residue remained intact, thus showing that the terminal fucosyl residue was not cleaved off by Psf1. Neither did chromatography indicate the release of monomeric fucose

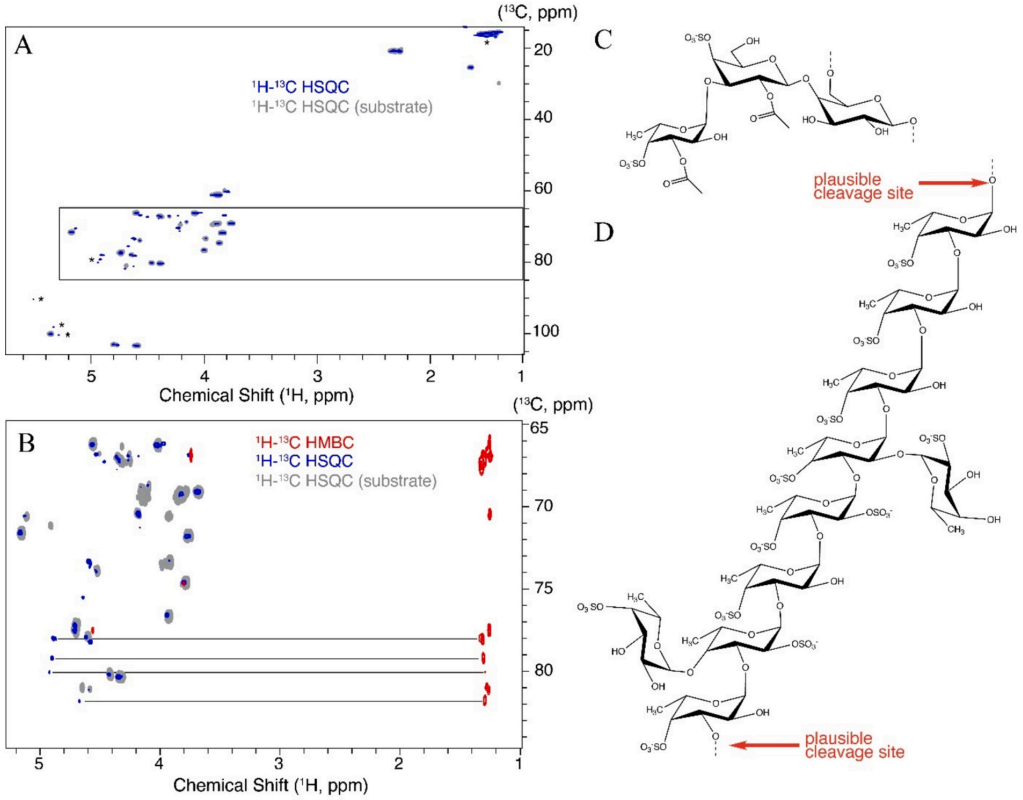

Fig. 7. NMR analysis of the hydrolyzed products obtained from degradation of fucoidan from *S. latissima* by Psf1. (A) $^{1}H^{13}C$ HSQC spectra after cleavage of *S. latissima* Sl native fucoidan (blue) with Psf1 and comparison to the substrate $^{1}H^{13}C$ HSQC (grey). Some additional signals are highlighted by asterisks as a guide to the eye. (B) $^{1}H^{13}C$ HSQC (blue) and HMBC (red) spectra after cleavage of *S. latissima* Sl native fucoidan with Psf1 and comparison to the substrate $^{1}H^{13}C$ HSQC (grey). Additional signals arise from released fucoidan and are consistent with predominant 4-sulfation of the emerging fucose signals, as judged from long-range correlations between ^{1}H-6 and ^{13}C-4, and from characteristic chemical shifts above 4.8 ppm for ^{1}H and near 80 ppm for ^{13}C in the C4H4. (C) Structure of the repetitive structural element in the *S. latissima* Sl native fucoidan that is preserved upon treatment with Psf1. (D) Structural elements that get liberated by Psf1 include 2- and 4-sulfation of fucosyl residues, low acetylation and some carbohydrate branching.

Table 2
^{1}H (first line) and ^{13}C (second line) NMR chemical shift values (in ppm) for the Sl native polysaccharide fraction of *S. latissima* fucoidan. The same regular polysaccharide is preserved in the high molecular weight fraction after Psf1 cleavage.

Residue\Atom	1	2	3	4	5	6
α-Fucp3OAc, 4OSO$_3^-$(1→	5.355	4.032	5.166	4.711	4.570	1.263
	100.3	66.5	71.9	77.7	66.5	16.2
→3)-β-Galp2OAc, 4OSO$_3^-$(1→	4.770	5.118	3.939	4.605	3.798	3.802
	103.4	70.9	77.0	78.1	74.9	61.4
→4,6)-β- Galp3OSO$_3^-$(1→	4.551	3.699	4.341	4.540	3.93	3.852/4.165
	103.6	69.5	80.7	74.1	73.8	69.6

through an *exo*-acting activity. The Psf1 treatment thus released long oligosaccharides and opposite to the substrate, signals for diverse fucosyl-residues become more prominent, as these residues appear to become more mobile upon Psf1-treatment and release from polymeric and heterogeneous regions. Considering that *S. latissima* fucoidan only contains 1 → 3 fucosyl stretches that are decorated with monomeric, single-sulfate substituted 1 → 4 fucosyls in this substrate [16], and contain 1 → 2 attached single fucosyl residues branches [6], the increased mobility in fucoidan oligosaccharides is indicative of *endo*-1,3 cleavage by Psf1, especially as the 1,4 linkages appear to remain intact. These additional oligo−/polymeric fucoidans that are released by Psf1 are predominantly 4-sulfated, judging from a strong H4 deshielding that is characteristic of sulfation. The C4H4 chemical shifts could be identified by correlating the H6 in ^{1}H—^{13}C HMBC spectra to the C4 carbon and the C4 carbon to H4 in ^{1}H—^{13}C HSQC. These correlations are shown by the horizontal lines in Fig. 7B connecting HMBC signals (red) between H6 and C4 spins with their corresponding C4H4 signals in the HSQC (blue) for the newly liberated species. The O4-sulfation validates with the liberated fucosyl-rich regions are not glycosylated at O4. In addition, the anomeric NMR signals are indicative of liberation of fucoidan from 1 to 3 linked α-fucosyl-rich stretches, including a spin system of a structural motif with a 2,3-branched fucosyl residue reported in a 1–3 linked α-fucosyl-rich stretch [6].

3.9. Impact of fucoidan and fucoidan oligosaccharide fractions obtained from S. latissima on the cytokine secretion of IL-12p40 and IL-10 and maturation of DCs

DCs were selected due to their central role as antigen-presenting cells (APCs), particularly in initiating and directing adaptive immune

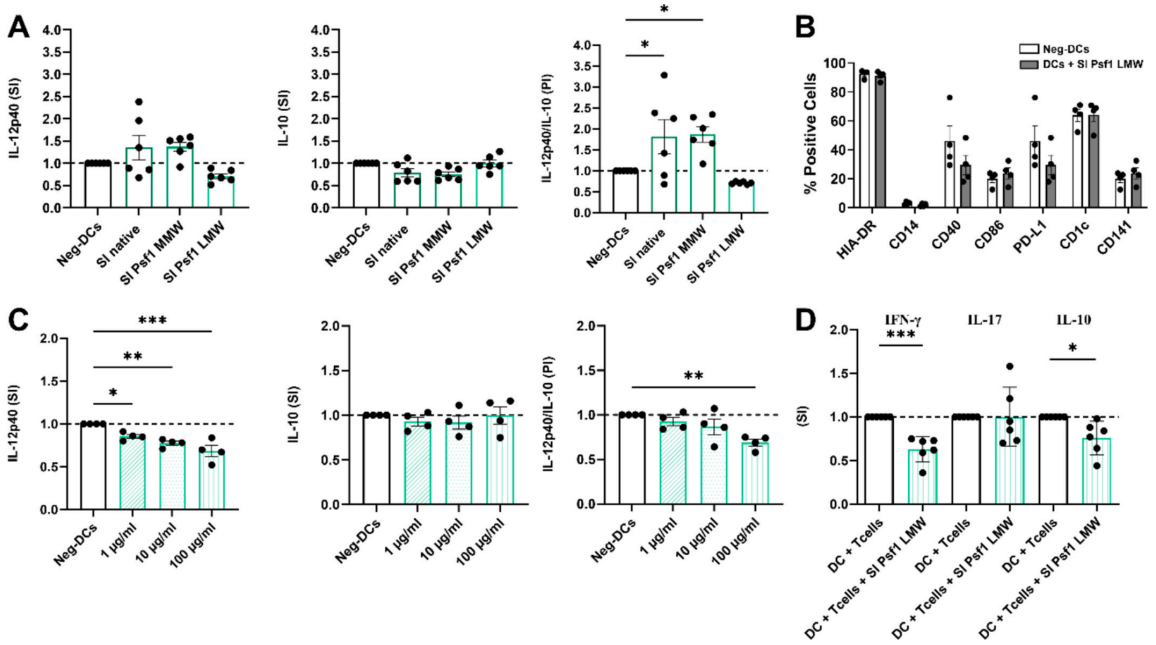

Fig. 8. The impact of fucoidan and fucoidan oligosaccharide fractions from *S. latissima* and digested with Psf1 on the cytokine secretion of IL-12p40 and IL-10 by DCs and their expression of cell surface molecules, as well as the effect of Sl Psf1 LMW on DCs and T-cell crosstalk. DCs were matured and activated for 24 h by TNF-α, IL-1β and LPS in the absence (Neg-DCs) or presence of Sl native, Sl Psf1 MMW or Sl Psf1 LMW. The experimental treatment was given as 100 μg/mL, except if otherwise stated. The supernatants were collected and the concentration of IL-12p40 and IL-10 were determined by ELISA. The data are presented as secretion index (SI) of IL-12p40 and IL-10 and proportional index (PI) between IL-12p40 and IL-10 in bar plots showing mean ± SEM (A, C and D; $n = 4$–6). The PI was calculated as the SI from IL-12p40 divided by SI from IL-10 (A). The effect of Sl Psf1 LMW on surface molecule expression was measured by flow cytometry using Sony SH800S flow cytometry with results expressed as percentage of positive cells (n = 4). The dose-dependent effect of Sl Psf1 LMW response was investigated at 1, 10 and 100 μg/mL (n = 4) (D). The secretion of IFN-γ, IL-17 and IL-10 in the supernatant after co-culture of DCs matured without (DC + T-cells) or with the Sl Psf1 LMW sample at 100 μg/mL and allogeneic CD4^{+} T-cells (DCs + T-cells + Sl Psf1 LMW) at a ratio1:10 was measured by ELISA and results given as mean ± SEM of SI of IFN-γ, IL-17 and IL-10 ($n = 6$) (D). Experimental treatments were compared with the Neg-DCs with one-way ANOVA utilizing Dunnett comparison test (A & C) or by unpaired *t*-test in (B & D) using graphPad Prism (10.3.1 (509)). The * indicate $p \leq 0.033$, ** $p \leq 0.002$ and *** $p < 0.001$.

responses. Unlike macrophages and B-cells, DCs are uniquely capable of activating naïve T-cells and are thus critical in shaping T-cell-mediated immunity - a key focus in immunomodulatory research [46,47]. Human monocyte-derived DCs offer a physiologically relevant in vitro model that closely reflects human immune function. Their responsiveness to pattern recognition receptor (PRR) ligands, such as polysaccharides, makes them particularly suitable for studying structure-function relationships of bioactive carbohydrates like fucoidans [48]. Treating DCs with 100 μg/mL of the native fucoidan substrate (Sl native) and the two fucoidan derivatives (Sl Psf1 MMW and Sl Psf1 LMW) did not affect their viability as compared with Neg-DCs (Table S2). However, DCs treated with 100 μg/mL of Sl native, Sl Psf1 MMW and Sl Psf1 LMW secreted different levels of IL-12p40 and IL-10 compared with Neg-DCs (Fig. 8A). Stimulation of DCs with Sl native or Sl Psf1 MMW led to a trend towards increased secretion of IL-12p40 and decreased IL-10 secretion (by 22 and 25 %, respectively) as compared with Neg-DCs (Fig. 8A). In contrast, when DCs were stimulated with Sl Psf1 LMW a reduction in secretion of IL-12p40 (by 29 %) was observed, which was comparable to the reduction obtained in IL-12p40 secretion by VitD3-DCs (~30 %; **Fig. S6**). In contrast, DCs stimulated with Sl Psf1 LMW did not affect the IL-10 secretion compared with Neg-DCs (Fig. 8A). PI was calculated to assess the polarization of cytokine secretion induced by the fucoidan compounds. The PI values were higher for Sl native (significantly) and Sl Psf1 MMW (significantly) compared with the Neg-DCs, suggesting pro-inflammatory effect, while PI for Sl Psf1 LMW was decreased (by 29 %), suggesting an anti-inflammatory effect (Fig. 8A). Further investigation was carried out to examine the Sl Psf1 LMW effect on cytokine secretion using different concentrations (1, 10 and 100 μg/mL). IL-12p40 secretion by DCs was significantly reduced in a dose-depended manner when treated with Sl Psf1 LMW at 1, 10 and 100 μg/mL (by 15, 22 and 32 %, respectively) (Fig. 8C). Similarly, a decrease in IL-10 secretion by 7 and 8 %, respectively, was observed for DCs treated with Sl Psf1 LMW at 1 and 10 μg/mL, but not at 100 μg/mL (Fig. 8C). This resulted in significant reduction in PI when DCs were treated with Sl Psf1 LMW at 100 μg/mL, indicating a possible anti-inflammatory effect (Fig. 8C), making it interesting for further allogeneic $CD4^+$ T-cells co-culture experiments (see the section below). Neither buffer, consisting of 50 mM NaCl and 10 mM $CaCl_2$, nor the enzyme within the same buffer influenced the cytokine secretion or the cell viability in the DC model (Fig. S7 and Table S3).

Mature DCs lack expression of the monocytic marker CD14 but upregulate their expression of the antigen-presenting molecule HLA-DR and the co-stimulatory molecules CD40 and CD86. In addition, monocyte-derived DCs express CD1c and CD141, as reviewed by Colin and Bigley (2018) [49], and upregulate PD-L1 expression upon stimulation [50]. Maturation of $CD14^+$ monocytes and subsequent activation into mature DCs was confirmed by lack of CD14 expression and high percentage of DCs expressing HLA-DR, which was not affected by treatment of the DCs with Sl Psf1 LMW (Fig. 8B). The percentage of DCs expressing other molecules analyzed was also unaffected by treating DCs Sl Psf1 LMW (Fig. 8B). In addition, when analyzing the levels of expression by mean fluorescent intensity there was no difference between DCs treated with Sl Psf1 LMW treated and Neg-DCs (data not shown). These results indicate that fucoidan LMW fraction does not hinder the DC maturation and activation, although it affects their cytokine secretion.

3.10. Stimulation of allogeneic $CD4^+$ T-cells by Psf1 released Sl LMW treated DCs

Since DCs are important in directing immune responses by differentiating naïve T-cells, we investigated the effect of DCs matured in the presence of Sl Psf1 LMW for 24 h on the cytokine secretion of co-cultured allogeneic $CD4^+$ T-cells.

Our findings show a significant reduction of IFN-γ secretion (by 37 %) and IL-10 secretion (by 24 %) by allogeneic $CD4^+$ T-cells co-cultured with DCs stimulated with Sl Psf1 LMW compared with those co-cultured with DCs stimulated in the absences of Sl Psf1 LMW, whereas IL-17 secretion was not affected (Fig. 8D).

4. Discussion

The analysis of substrate specificity of Psf1 indicated a preference for α(1 → 3) linkages, since activity was observed on fucoidans from *S. latissima*, *U. pinnatifida* and *S. oligocystum*, all of which mainly contains α(1 → 3)-linked fucosyl residues [6,35,37,51]. The data suggest that Psf1 has distinct recognition of the structural presentation of the fucoidan structure near the scissile bond, as the highest activity of Psf1 was observed on fucoidan from *S. latissima*, which is mainly sulfated at C4 and to lesser extent at C2 [6], while lower activity was observed on fucoidans from *U. pinnatifida* [37,51] and no activity on fucoidan from *T. ornata* [52], which contains higher degree of sulfated fucose residues at C2 than on C4, suggesting that Psf1 might have a preference for C4 sulfated fucoidans. However, C4 sulfations are also occurring in fucoidans from *F. evanescens* and *F. vesiculosus* fucoidans, which are sulfated at C2, C4, C2/C4, and C3 [53,54], but no activity was observed on these fucoidans containing a backbone of alternating α(1 → 3)- and α(1 → 4)-linkages, suggesting that other structural features in the fucoidans are important for Psf1 activity.

Most fucoidanases show a high specificity towards the structural motifs near the fucoidan cleavage site. *Endo*-α(1 → 3) fucoidanase activity in the GH107 family has only been described previously for Mef2 [16], Fda1, and Fda2 [43,44]. Other characterized GH107 fucoidanases were identified as *endo*-α(1 → 4) fucoidanases [18–21,23]. Therefore, the discovery of Psf1 as a new GH107 *endo*-α(1 → 3) fucoidanase demonstrates the diversity of the fucoidanases.

Interestingly, Psf1 exhibited activity at significantly lower temperatures than other fucoidanases, with activity detected at 10, 4 and even 1 °C. In addition, Psf1 was able to remain active for a long time at 4 °C, which has not previously been reported for other fucoidanases. Hence, Psf1 is the first cold-adapted fucoidanase described. In a biological perspective, the psychrophilic fucoidanase Psf1, is likely an adaptation required for *Pseudoalteromonas* sp. S3178 to feed on brown seaweed fucoidans under the extreme environments this bacterium is inhabiting, in the Arctic Ocean [31]. Other fucoidanases characterized to date have low activity at temperatures below 20 °C [16,18,20,25,44].

Protein factors that determine cold adaption are not clearly known but may include elements that increase flexibility of the enzyme structure, reducing the activation enthalpy for the reaction but at the cost of stability. These include; increased flexibility of surface exposed loops that mediate interactions with other secondary elements of the structure; a larger active site accommodating a more relaxed binding pocket; differences in electrostatic potential to help align the substrate into the pocket, a reduction in hydrophobic clusters; the clustering of glycine residues providing mobility; the disappearance of proline residues in loops; a reduction in arginine residues which are capable of forming salt bridges and H-bonds; insertions and deletions to modify surface charge and or secondary structure; and an increase in nonpolar side chains into the surrounding medium [45]. Psf1 does have a number of these indicator when compared to P5A_FcnA, likely contributing to the cold adaptation of Psf1.

Psf1 contains several more flexible (higher RMSF) regions that are also associated with the absence of key salt bridges connecting secondary structure elements of the enzyme. There is also a remarkable positive electrostatic potential around the active site. There appears to be little change to the hydrophobic clusters within the enzyme, though there is an increase in the number of outwards facing hydrophobic side groups, clustered in surface exposed α-helices. Psf1 has more arginine residues overall. While no single feature can be accredited to the cold adaptivity of Psf1, a number of the mutations and their impact on the stability/flexibility of Psf1 in comparison to P5A_FcnA may be responsible.

The potential immuno-regulatory effect observed in vitro of the degradation products resulting from Psf1 action on the *S. latissima* fucoidan was noteworthy. Our results thus indicated that treatment of DCs with either the high or medium molecular weight fucoidan samples led to a tendency of increased secretion of IL-12p40 and decreased secretion of IL-10, compared with the negative control, resulting in PI>1, suggesting that Sl Native and Sl Psf1 MMW induce an inflammatory response. This is consistent with previous studies demonstrating that native fucoidan from various species of brown seaweed can induce DC maturation in vitro, increase their IL-12p40 secretion, and promote Th1 cell responses in both human and mouse models [55,56]. In contrast, Sl Psf1 LMW fucoidan treatment significantly decreased IL-12p40, in comparable levels to the well-documented ability of VitD3, to inhibit IL-12 secretion from DCs and macrophages [57] in a dose-dependent manner. IL-10 secretion was unaffected by Sl Psf1 LMW treatment; taken together, these results suggest an overall anti-inflammatory effect of the Sl Psf1 LMW on the DCs activation [58]. The observed differences in immunomodulatory activity between the LMW and MMW fractions suggest potential differences in receptor binding, uptake, or intracellular trafficking. However, it might rather reflect that the LMW fraction is more homogenous and likely less viscous, which may facilitate enhanced interaction with specific pattern recognition receptors. Previous studies have shown that molecular weight and post-degradation modifications can influence the bioactivity and physicochemical properties of fucoidans [59,60]. Based on this, we hypothesize that differences in molecular weight may lead to distinct receptor binding, internalization mechanisms, and subcellular localization patterns. One possibility could be that LMW fucoidan modulates signalling pathways e.g., via TLR4, potentially by partially blocking LPS binding or activating regulatory feedback mechanisms, leading to NF-κB or STAT1 inhibition. It may also engage scavenger receptors or C-type lectins like DC-SIGN, which can suppress TLR-driven inflammation through Raf-1–mediated modulation of transcription [61]. In contrast, MMW fucoidan may favour more conventional pro-inflammatory signalling. These contrasting effects may reflect size-related differences in receptor accessibility, signalling outcomes, or intracellular trafficking. DCs matured in the presence of Sl Psf1 LMW fucoidan significantly caused co-cultured allogeneic $CD4^+$ T-cells to secrete lower levels of IFN-γ without affecting the IL-17 secretion, which is consistent with reduced IL-12p40 secretion. It cannot be determined whether the decrease in IL-10 concentration in the co-culture supernatant is because of decreased secretion by DCs or regulatory T-cells as both cell types can produce IL-10. Thus, the decreased level of IL-10 may indicate a pro-inflammatory response. However, previous studies have shown that reduced IL-10 secretion in the co-culture does not affect the ability of reduction of IL-12p40 to affect IFN-γ secretion by co-cultured allogeneic $CD4^+$ T-cells [62]. Importantly, although significant cytokine modulation was observed, it remains necessary to consider whether these effects could be partially attributed to altered cell proliferation or viability. A recent study by Saliba and colleagues [63] demonstrated that certain LMW fucoidans exhibit antiproliferative and proapoptotic effects on murine splenocytes. In the present study, routine microscopic examination and viability assessment using Trypan Blue exclusion revealed no morphological abnormalities or notable differences in viability and cell number between control and treatment cell cultures. These findings suggest that cytotoxicity is unlikely. However, the possibility of more subtle antiproliferative effects influencing cytokine profiles cannot be fully excluded. Since the IL-12p40 secretion from DCs decreased when treated with Sl Psf1 LMW under LPS stimulation and subsequently the IFN-γ secretion by $CD4^+$ T-cells was reduced in co-culture, it may be speculated that the Psf1 LMW fucoidan sample might be inducing an inhibition of the nuclear factor-κB activation [52,64]. This has already been demonstrated in a study with human keratinocytes treated with commercial fucoidan [65]. Therefore, despite the decreased IL-10 concentration observed in the co-culture supernatant, we suggest that Sl Psf1 LMW fucoidan has the potential to function as an anti-inflammatory agent.

5. Conclusions

This work studied the psychrophilic Psf1 enzyme originating from *Pseudoalteromonas* sp. S3178 isolated from a surface swap of a shrimp caught in the Arctic Ocean. The stable and active fucoidanase was successfully heterologously expressed, purified, and characterized. Psf1 was suggested to be an *endo*-α(1 → 3)- fucoidanase that catalyzes the hydrolysis of α(1 → 3) linked fucose residues in the backbone of fucoidan from *S. latissima*. These results also indicate that Psf1 might be an interesting candidate for industrial applications in fucoidan oligosaccharide production where low temperatures could be beneficial.

While high and medium molecular weight fucoidans, including the native *S. latissima* fucoidan and the MMW fraction resulting from Psf1 treatment, induced an inflammatory response in DCs, the low molecular weight fucoidan fraction (Sl Psf1 LMW) demonstrated a dose-dependent anti-inflammatory effect by significantly reducing IL-12p40 secretion by DCs and IFN-γ secretion without affecting IL-17 levels in co-cultures of DCs and allogeneic $CD4^+$ T-cells. This suggests that Sl Psf1 LMW may have potential as an anti-inflammatory against e.g., chronic inflammatory or autoimmune diseases. This study was designed to specifically investigate potential anti-inflammatory effects on DC function by measuring their cytokine secretion, and subsequently their interaction with T cells (DC-T cell crosstalk). This is due to their pivotal role in initiating and modulating immune responses. We acknowledge the potential relevance of other APCs and consider this an important avenue for future research. In addition, the Psf1 released fucoidan oligosaccharides from *S. latissima* fucoidan may be relevant for other applications, such as cosmetics and pharmaceuticals.

CRediT authorship contribution statement

Vo Thi Dieu Trang: Writing – review & editing, Writing – original draft, Visualization, Methodology, Formal analysis, Data curation, Conceptualization. **Maria Dalgaard Mikkelsen:** Writing – review & editing, Writing – original draft, Validation, Project administration, Methodology, Investigation, Data curation, Conceptualization. **Monica Daugbjerg Christensen:** Writing – review & editing, Writing – original draft, Visualization, Methodology, Formal analysis. **Sebastian Meier:** Writing – review & editing, Visualization, Validation, Methodology, Formal analysis. **Cameron James Hunt:** Writing – review & editing, Software, Methodology, Formal analysis. **Jesper Holck:** Writing – review & editing, Methodology, Formal analysis. **Guðmundur Óli Hreggviðsson:** Writing – review & editing, Supervision, Methodology. **Jona Freysdottir:** Supervision, Methodology. **Hang Thi Thuy Cao:** Supervision, Methodology. **Huynh Hoang Nhu Khanh:** Supervision. **Anne S. Meyer:** Writing – review & editing, Validation, Supervision, Resources, Project administration, Investigation, Funding acquisition, Conceptualization.

Declaration of competing interest

All authors confirm that there are no known conflicts of interest associated with this publication and that there has been no significant financial support for this work that could have influenced its outcome.

Acknowledgments

This project was funded by MARIKAT JPI Cofund Blue BioEconomy Project Grant No. 9082-00021B and by the Technical University of Denmark. M.C. and T.R. acknowledge support from ANR under grant ANR-10-BTBR-04 (investment expenditure program IDEALG). This work was supported by grant from the Vietnam Academy of Science and Technology (Grant No. VAST02.01/23-24). The 800 MHz NMR spectra were recorded at the NMR Center DTU, supported by the Villum

Foundation. We acknowledge Ocean Rainforest for providing the *Saccharina latissima* seaweed. We would like to thank Professor Lone Gram for providing the Psf1 encoding DNA sequence for our work.

Appendix A. Supplementary data

Supplementary data to this article can be found online at https://doi.org/10.1016/j.ijbiomac.2025.145930.

Data availability

Data will be made available on request.

References

[1] M. Santiago, C.A. Ramírez-Sarmiento, R.A. Zamora, L.P. Parra, Discovery, molecular mechanisms, and industrial applications of cold-active enzymes, Front. Microbiol. 7 (2016) 1–32, https://doi.org/10.3389/fmicb.2016.01408.
[2] F. Sarmiento, R. Peralta, J.M. Blamey, Cold and hot extremozymes: industrial relevance and current trends, Front. Bioeng. Biotechnol. 3 (2015) 1–15, https://doi.org/10.3389/fbioe.2015.00148.
[3] M. Kuddus, Cold-active enzymes in food biotechnology: an updated mini review, Appl. Biol. Biotechnol. 6 (2018) 58–63, https://doi.org/10.7324/JABB.2018.60310.
[4] M.T. Ale, J.D. Mikkelsen, A.S. Meyer, Important determinants for fucoidan bioactivity: a critical review of structure-function relations and extraction methods for fucose-containing sulfated polysaccharides from brown seaweeds, Mar. Drugs 9 (2011) 2106–2130, https://doi.org/10.3390/md9102106.
[5] M.T. Ale, A.S. Meyer, Fucoidans from brown seaweeds: an update on structures, extraction techniques and use of enzymes as tools for structural elucidation, RSC Adv. 3 (2013) 8131–8141, https://doi.org/10.1039/c3ra23373a.
[6] M.I. Bilan, A.A. Grachev, A.S. Shashkov, M. Kelly, C.J. Sanderson, N.E. Nifantiev, A.I. Usov, Further studies on the composition and structure of a fucoidan preparation from the brown alga *Saccharina latissima*, Carbohydr. Res. 345 (2010) 2038–2047, https://doi.org/10.1016/j.carres.2010.07.009.
[7] B. Li, F. Lu, X. Wei, R. Zhao, Fucoidan: structure and bioactivity, Molecules 13 (2008) 1671–1695, https://doi.org/10.3390/molecules13081671.
[8] Y. Wang, M. Xing, Q. Cao, A. Ji, H. Liang, S. Song, Biological activities of fucoidan and the factors mediating its therapeutic effects: a review of recent studies, Mar. Drugs 17 (2019) 15–17, https://doi.org/10.3390/md17030183.
[9] M.T. Ale, H. Maruyama, H. Tamauchi, J.D. Mikkelsen, A.S. Meyer, Fucoidan from *Sargassum sp.* and *Fucus vesiculosus* reduces cell viability of lung carcinoma and melanoma cells *in vitro* and activates natural killer cells in mice *in vivo*, Int. J. Biol. Macromol. 49 (2011) 331–336, https://doi.org/10.1016/j.ijbiomac.2011.05.009.
[10] N. Kirsten, J. Ohmes, M.D. Mikkelsen, T.T. Nguyen, M. Blümel, F. Wang, D. Tasdemir, A. Seekamp, A.S. Meyer, S. Fuchs, Impact of enzymatically extracted high molecular weight fucoidan on lipopolysaccharide-induced endothelial activation and leukocyte adhesion, Mar. Drugs 21 (2023) 1–16, https://doi.org/10.3390/md21060339.
[11] M.S. Nielsen, M.D. Mikkelsen, S.H. Ptak, E.K. Hejbøl, J. Ohmes, T.N. Thi, V.H. N. Tran, X. Fretté, S. Fuchs, A.S. Meyer, H.D. Schrøder, M.J. Ding, Efficacy of marine bioactive compound fucoidan for bone regeneration and implant fixation in sheep, Biomed. Mater. Res. A. 110 (2022) 861–872, https://doi.org/10.1002/jbm.a.37334 (Epub 2021 Nov 18).
[12] J. Ohmes, M.D. Mikkelsen, T.T. Nguyen, V.H.N. Tran, S. Meier, M.S. Nielsen, M. J. Ding, A. Seekamp, A.S. Meyer, S. Fuchs, Depolymerization of fucoidan with endo-fucoidanase changes bioactivity in processes relevant for bone regeneration, Carbohydr. Polym. 286 (2022) 1–12, https://doi.org/10.1016/j.carbpol.2022.119286.
[13] J. Ohmes, Y. Xiao, F. Wang, M.D. Mikkelsen, T.T. Nguyen, H. Schmidt, A. Seekamp, A.S. Meyer, S. Fuchs, Effect of enzymatically extracted fucoidans on angiogenesis and osteogenesis in primary cell culture systems mimicking bone tissue environment, Mar. Drugs 18 (2020) 1–18, https://doi.org/10.3390/md18090481.
[14] P. Dörschmann, M.D. Mikkelsen, T.N. Thi, J. Roider, A.S. Meyer, A. Klettner, Effects of a newly developed enzyme-assisted extraction method on the biological activities of Fucoidans in ocular cells, Mar. Drugs 18 (2020) 1–16, https://doi.org/10.3390/md18060282.
[15] T.T. Nguyen, M.D. Mikkelsen, V.H.N. Tran, V.T.D. Trang, N. Rhein-Knudsen, J. Holck, A.B. Rasin, H.T.T. Cao, T.T.T. Van, A.S. Meyer, Enzyme-assisted fucoidan extraction from brown macroalgae *Fucus distichus* subsp. *evanescens* and *Saccharina latissima*, Mar. Drugs 18 (2020) 1–18, https://doi.org/10.3390/md18060296.
[16] V.H.N. Tran, T.T. Nguyen, S. Meier, J. Holck, H.T.T. Cao, T.T.T. Van, A.S. Meyer, M.D. Mikkelsen, The Endo-alpha(1,3)-Fucoidanase Mef2 releases uniquely branched oligosaccharides from *Saccharina latissima* Fucoidans, Mar. Drugs 29 (2022) 1–22, https://doi.org/10.3390/md20050305.
[17] E. Drula, M.L. Garron, S. Dogan, V. Lombard, B. Henrissat, N. Terrapon, The carbohydrate-active enzyme database: functions and literature, Nucleic Acids Res. 50 (2022), https://doi.org/10.1093/nar/gkab1045. D571–D577.
[18] M.D. Mikkelsen, V.H.N. Tran, S. Meier, T.T. Nguyen, J. Holck, H.T.T. Cao, T.T. T. Van, P.D. Thinh, A.S. Meyer, J.P. Morth, Structural and functional characterization of the novel endo-alpha(1,4)-fucoidanase Mef1 from the marine bacterium *Muricauda eckloniae*, Acta Crystallogr. D Struct. Biol. 79 (2023) 1026–1043, https://doi.org/10.1107/S2059798323008732.
[19] V.T.D. Trang, M.D. Mikkelsen, M. Vuillemin, S. Meier, H.T.T. Cao, A.S.M. J. Muschiol, V. Perna, T.T. Nguyen, V.H.N. Tran, J. Holck, T.T.T. Van, The endo-α(1→4)-L fucoidanase Fhf2 from *Formosa haliotis* releases highly sulfated fucoidan oligosaccharides, Front. Plant Sci. 3 (2022) 1–16, https://doi.org/10.3389/fpls.2022.823668.
[20] M. Vuillemin, A.S. Silchenko, H.T.T. Cao, M.S. Kokoulin, V.T.D. Trang, J. Holck, S. P. Ermakova, A.S. Meyer, M.D. Mikkelsen, Functional characterization of a new GH107 Endo-α-(1,4)-Fucoidanase from the marine bacterium *Formosa haliotis*, Mar. Drugs 18 (2020) 1–17, https://doi.org/10.3390/md18110562.
[21] A.S. Silchenko, N.E. Ustyuzhanina, M.I. Kusaykin, V.B. Krylov, A.S. Shashkov, A. S. Dmitrenok, R.V. Usoltseva, A.O. Zueva, N.E. Nifantiev, T.N. Zvyagintseva, Expression and biochemical characterization and substrate specificity of the fucoidanase from *Formosa algae*, Glycobiology 27 (2017) 1, https://doi.org/10.1093/glycob/cww138.
[22] T. Sakai, T. Kawai, I. Kato, Isolation and characterization of a fucoidan-degrading marine bacterial strain and its fucoidanase, Mar. Biotechnol. 6 (2004) 335–346, https://doi.org/10.1007/s10126-003-0033-5.
[23] S. Colin, E. Deniaud, M. Jam, V. Descamps, Y. Chevolot, N. Kervarec, J.C. Yvin, T. Barbeyron, G. Michel, B. Kloareg, Cloning and biochemical characterization of the fucanase FcnA: definition of a novel glycoside hydrolase family specific for sulfated fucans, Glycobiology 16 (2006) 1021–1032, https://doi.org/10.1093/glycob/cwl029.
[24] C. Vickers, F. Liu, K. Abe, O. Salama-Alber, M. Jenkins, C.M.K. Springate, J. E. Burke, S.G. Withers, A.B. Boraston, Endo-fucoidan hydrolases from glycoside hydrolase family 107 (GH107) display structural and mechanistic similarities to -L-fucosidases from GH29, J. Biol. Chem. 293 (2018) 18296–18308, https://doi.org/10.1074/jbc.RA118.005134.
[25] A.O. Zueva, A.S. Silchenko, A.B. Rasin, M.I. Kusaykin, R.V. Usoltseva, A. I. Kalinovsky, V.V. Kurilenko, T.N. Zvyagintseva, P.D. Thinh, S.P. Ermakova, Expression and biochemical characterization of two recombinant fucoidanases from the marine bacterium *Wenyingzhuangia fucanilytica* CZ1127T, Int. J. Biol. Macromol. 164 (2020) 3025–3037, https://doi.org/10.1016/j.ijbiomac.2020.08.131.
[26] O. Joffre, M.A. Nolte, R. Spörri, C.R.E. Sousa, Inflammatory signals in dendritic cell activation and the induction of adaptive immunity, Immunol. Rev. 227 (2009) 234–247, https://doi.org/10.1111/j.1600-065X.2008.00718.x.
[27] M. Cabeza-Cabrerizo, A. Cardoso, C.M. Minutti, M.P. Costa, C.R. Sousa, Dendritic cells revisited, Annu. Rev. Immunol. 39 (2021) 131–166, https://doi.org/10.1146/annurev-immunol-061020-053707.
[28] L. Sun, Y. Su, A. Jiao, X. Wang, B. Zhang, T cells in health and disease, Sig. Transduct. Target Ther. 8 (2023) 1–50, https://doi.org/10.1038/s41392-023-01471-y.
[29] S. Hirohata, T. Yanagida, Human Thl responses driven by IL-12 are associated with enhanced expression of CD40 ligand, Jpn. J. Clin. Immunol. 21 (1998) 67–76, https://doi.org/10.2177/jsci.21.supplement_67. Suppl.
[30] L. Zhou, I.I. Ivanov, R. Spolski, R. Min, K. Shenderov, T. Egawa, D.E. Levy, W. J. Leonard, D.R. Littman, IL-6 programs TH-17 cell differentiation by promoting sequential engagement of the IL-21 and IL-23 pathways, Nat. Immunol. 8 (2007) 967–974, https://doi.org/10.1038/ni1488.
[31] L. Gram, J. Melchiorsen, J.B. Bruhn, Antibacterial activity of marine culturable bacteria collected from a global sampling of ocean surface waters and surface swabs of marine organisms, Mar. Biotechnol. 12 (2010) 439–451, https://doi.org/10.1007/s10126-009-9233-y.
[32] S.S. Paulsen, M.L. Strube, P.K. Bech, L. Gram, E.C. Sonnenschein, Marine chitinolytic *Pseudoalteromonas* represents an untapped reservoir of bioactive potential, M. Syst. 4 (2019) 1–12, https://doi.org/10.1128/msystems.00060-19.
[33] T.T.T. Thanh, V.T.T. Tran, Y. Yuguchi, L.M. Bui, T.T. Nguyen, Structure of fucoidan from brown seaweed *Turbinaria ornata* as studied by electrospray ionization mass spectrometry (ESIMS) and small angle x-ray scattering (SAXS) techniques, Mar. Drugs 11 (2013) 2431–2443, https://doi.org/10.3390/md11072431.
[34] P.D. Thinh, R.V. Menshova, S.P. Ermakova, S.D. Anastyuk, B.M. Ly, T. N. Zvyagintseva, Structural characteristics and anticancer activity of fucoidan from the brown alga *Sargassum mcclurei*, Mar. Drugs 11 (2013) 1453–1476, https://doi.org/10.3390/md11051456.
[35] R.V. Usoltseva, O.S. Malyarenko, S.D. Anastyuk, N.M. Shevchenko, A.S. Silchenko, T.N. Zvyagintseva, V.V. Isakov, P.D. Thinh, H.H.N. Khanh, C.T.T. Hang, D. T. Trung, S.P. Ermakova, The structure of fucoidan from *Sargassum oligocystum* and radiosensitizing activity of galactofucans from some algae of genus *Sargassum*, Int. J. Biol. Macromol. 183 (2021) 1427–1435, https://doi.org/10.1016/j.ijbiomac.2021.05.128.
[36] M.I. Bilan, A.A. Grachev, A.S. Shashkov, T.T.T. Thuy, T.T.T. Van, B.M. Ly, N. E. Nifantiev, A.I. Usov, Preliminary investigation of a highly sulfated galactofucan fraction isolated from the brown alga *Sargassum polycystum*, Carbohydr. Res. 377 (2013) 48–57, https://doi.org/10.1016/j.carres.2013.05.016.
[37] O.S. Vishchuk, S.P. Ermakova, T.N. Zvyagintseva, Sulfated polysaccharides from brown seaweeds *Saccharina japonica* and *Undaria pinnatifida*: isolation, structural characteristics, and antitumor activity, Carbohydr. Res. 346 (2011) 2769–2776, https://doi.org/10.1016/j.carres.2011.09.034.
[38] X. Robert, P. Gouet, Deciphering key features in protein structures with the new ENDscript server, Nucleic Acids Res. 42 (2014) W320–W324, https://doi.org/10.1093/nar/gku316.
[39] M.M. Bradford, A rapid and sensitive method for the quantitation of microgram quantities of protein utilizing the principle of protein-dye binding, Anal. Biochem. (1976) 248–254, https://doi.org/10.1016/0003-2697(76)90527-3.

[40] T.L. Biel-Nielsen, K. Li, S.O. Sørensen, J.J.P. Sejberg, A.S. Meyer, J. Holck, Utilization of industrial citrus pectin side streams for enzymatic production of human milk oligosaccharides, Carbohydr. Res. 519 (2022) 1–8, https://doi.org/10.1016/j.carres.2022.108627.

[41] J. Jumper, R. Evans, A. Pritzel, T. Green, M. Figurnov, O. Ronneberger, K. Tunyasuvunakool, R. Bates, A. Žídek, A. Potapenko, A. Bridgland, C. Meyer, S.A. A. Kohl, A.J. Ballard, A. Cowie, B. Romera-Paredes, S. Nikolov, R. Jain, J. Adler, T. Back, S. Petersen, D. Reiman, E. Clancy, M. Zielinski, M. Steinegger, M. Pacholska, T. Berghammer, S. Bodenstein, D. Silver, O. Vinyals, A.W. Senior, K. Kavukcuoglu, P. Kohli, D. Hassabis, Highly accurate protein structure prediction with AlphaFold, Nature 596 (2021) 583–589, https://doi.org/10.1038/s41586-021-03819-2.

[42] H.T.T. Cao, M.D. Mikkelsen, M.J. Lezyk, L.M. Bui, V.T.T. Tran, A.S. Silchenko, M. I. Kusaykin, T.D. Pham, B.H. Truong, J. Holck, A.S. Meyer, Novel enzyme actions for Sulphated Galactofucan Depolymerisation and a new engineering strategy for molecular stabilisation of Fucoidan degrading enzymes, Mar. Drugs 16 (2018) 1–18, https://doi.org/10.3390/md16110422.

[43] T. Sakai, T. Kawai, I. Kato, Isolation and characterization of a Fucoidan-degrading marine bacterial strain and its Fucoidanase, Mar. Biotechnol. 6 (2004) 335–346, https://doi.org/10.1007/s10126-003-0033-5.

[44] C. Zhu, Z. Liu, L. Ren, S. Jiao, X. Zhang, Q. Wang, Z. Li, Y. Du, J.J. Li, Overexpression and biochemical characterization of a truncated endo-α(1 → 3)-fucoidanase from *Alteromonas* sp. SN-1009, Food Chem. 353 (2021) 129460, https://doi.org/10.1016/j.foodchem.2021.129460.

[45] K.S. Siddiqui, R. Cavicchioli, Cold-adapted enzymes, Annu. Rev. Biochem. 75 (2006) 403–433, https://doi.org/10.1146/annurev.biochem.75.103004.142723.

[46] N. Tatsumi, Y. Kumamoto, Role of mouse dendritic cell subsets in priming naive CD4 T-cells, Curr. Opin. Immunol. 83 (2023) 102352, https://doi.org/10.1016/j.coi.2023.102352.

[47] K.L. Hilligan, F. Ronchese, Antigen presentation by dendritic cells and their instruction of CD4+ T helper cell responses, Cell. Mol. Immunol. 17 (2020) 587–599, https://doi.org/10.1038/s41423-020-0465-0.

[48] A. Zayed, D.A. Al-Saedi, E.O. Mensah, O.N. Kanwugu, P. Adadi, R. Ulber, Fucoidan's molecular targets: a comprehensive review of its unique and multiple targets accounting for promising bioactivities supported by in silico studies, Mar. Drugs 22 (2024) 29, https://doi.org/10.3390/md22010029.

[49] M. Collin, V. Bigley, Human dendritic cell subsets: an update, Immunology 154 (2018) 3–20, https://doi.org/10.1111/imm.12888.

[50] Q. Peng, X. Qiu, Z. Zhang, S. Zhang, Y. Zhang, Y. Liang, J. Guo, H. Peng, M. Chen, Y.X. Fu, H. Tang, PD-L1 on dendritic cells attenuates T-cell activation and regulates response to immune checkpoint blockade, Nat. Commun. 11 (2020) 1–8, https://doi.org/10.1038/s41467-020-18570-x.

[51] A.V. Skriptsova, N.M. Shevchenko, T.N. Zvyagintseva, T.I. Imbs, Monthly changes in the content and monosaccharide composition of fucoidan from *Undaria pinnatifida* (Laminariales, Phaeophyta), J. Appl. Phycol. 22 (2010) 79–86, https://doi.org/10.1007/s10811-009-9438-5.

[52] S.P. Ermakova, R.V. Menshova, S.D. Anastyuk, O.S.M. Vishchuk, A.M. Zakharenko, P.D. Thinh, B.M. Ly, T.N. Zvyagintseva, Structure, chemical and enzymatic modification, and anticancer activity of polysaccharides from the brown alga *Turbinaria ornata*, J. Appl. Phycol. 28 (2016) 2495–2505, https://doi.org/10.1007/s10811-015-0742-y.

[53] L. Chevolot, B. Mulloy, J. Ratiskol, A. Foucault, S. Colliec-Jouault, A disaccharide repeat unit is the major structure in fucoidans from two species of brown algae, Carbohydr. Res. 330 (2001) 529–535, https://doi.org/10.1016/S0008-6215(00)00314-1.

[54] R.V. Menshova, N.M. Shevchenko, T.I. Imbs, T.N. Zvyagintseva, O.S. Malyarenko, T.S. Zaporoshets, N.N. Besednova, S.P. Ermakova, Fucoidans from brown alga *Fucus evanescens*: structure and biological activity, Front. Mar. Sci. 3 (2016) 1–9, https://doi.org/10.3389/fmars.2016.00129.

[55] L. Liu, X. Yang, P. Yuan, S. Cai, J. Bao, Y. Zhao, A. Aimaier, A. Aipire, J. Lu, J. Li, *In vitro* and *in vivo* dendritic cell immune stimulation effect of low molecular weight Fucoidan from New Zealand *Undaria pinnatifida*, Mar. Drugs 8 (2022) 1–16, https://doi.org/10.3390/md20030197.

[56] M. Yang, C. Ma, J. Sun, Q. Shao, W. Gao, Y. Zhang, Z. Li, Q. Xie, Z. Dong, X. Qu, Fucoidan stimulation induces a functional maturation of human monocyte-derived dendritic cells, Int. Immunopharmacol. 8 (2008) 1754–1760, https://doi.org/10.1016/j.intimp.2008.08.007.

[57] D. D'Ambrosio, M. Cippitelli, M.G. Cocciolo, D. Mazzeo, P. Di Lucia, R. Lang, F. Sinigaglia, P. Panina-Bordignon, Inhibition of IL-12 production by 1,25-dihydroxyvitamin D3. Involvement of NF-kappaB downregulation in transcriptional repression of the p40 gene, J. Clin. Invest. 101 (1998) 252–262, https://doi.org/10.1172/JCI1050.

[58] S. Rutella, S. Danese, G. Leone, Tolerogenic dendritic cells: cytokine modulation comes of age, Blood 108 (2006) 1435–1440, https://doi.org/10.1182/blood-2006-03-006403.

[59] G.J. Wu, S.M. Shiu, M.C. Hsieh, G.J. Tsai, Anti-inflammatory activity of a sulfated polysaccharide from the brown alga *Sargassum cristaefolium*, Food Hydrocoll. 53 (2016) 16–23, https://doi.org/10.1016/j.foodhyd.2015.01.019.

[60] L. Liu, X. Yang, P. Yuan, S. Cai, J. Bao, Y. Zhao, A. Aimaier, A. Aipire, J. Lu, J. Li, In vitro and in vivo dendritic cell immune stimulation effect of low molecular weight fucoidan from New Zealand *Undaria pinnatifida*, Mar. Drugs 20 (2022) 197, https://doi.org/10.3390/md20030197.

[61] S.I. Gringhuis, J. Dunnen, M. Litjens, B.v.H. Hof, Y.v. Kooyk, T.B.H. Geijtenbeek, C-type lectin DC-SIGN modulates toll-like receptor signaling via Raf-1 kinase-dependent acetylation of transcription factor NF-κB, Immunity 26 (2007) 605–616, https://doi.org/10.1016/j.immuni.2007.03.012.

[62] J. Freysdottir, M.B. Sigurpalsson, S. Omarsdottir, E.S. Olafsdottir, A. Vikingsson, I. Hardardottir, Ethanol extract from birch bark (*Betula pubescens*) suppresses human dendritic cell mediated Th1 responses and directs it towards a Th17 regulatory response *in vitro*, Immunol. Lett. 136 (2011) 90–96, https://doi.org/10.1016/j.imlet.2010.12.009.

[63] J. Saliba, C. Manseur, H. Groult, H. Akil, M. Tannoury, D. Troutaud, T. Maugard, J. Feuillard, I. Arnaudin, C. Jayat-Vignoles, Anti-proliferative and pro-apoptotic vLMW Fucoidan formulas decrease PD-L1 surface expression in EBV latency III and DLBCL Tumoral B-cells by decreasing actin network, Mar. Drugs 21 (2023) 132, https://doi.org/10.3390/md21020132.

[64] M. Tabarsa, E.H. Dabaghian, S.G. You, K. Yelithao, R.A. Cao, M. Rezaei, M. Alboofetileh, S. Bita, The activation of NF-κB and MAPKs signaling pathways of RAW264.7 murine macrophages and natural killer cells by fucoidan from *Nizamuddinia zanardinii*, Int. J. Biol. Macromol. 148 (2020) 56–67, https://doi.org/10.1016/j.ijbiomac.2020.01.125.

[65] M.J. Ryu, H.S. Chung, Anti-inflammatory activity of fucoidan with blocking NF-κB and STAT1 in human keratinocytes cells, Nat. Prod. Sci. 21 (2015) 205–209.

Appendix A: Cytokine secretion induced by investigated compounds

Table 10. Cytokine secretion by dendritic cells, treated with different poly–and oligosaccharides from brown, green and red seaweed, respectively.

Fucoidan and Fucoidan Oligosaccharides					
Species and samples	**Cytokines**				**Pro- or anti-inflammatory***
S. latissima			**IL–12p40**	**IL–10**	
SLORF3 deacetylated			(↓)	↓	
SLORF3 HMP (Mef2)			↓	–	
SLORF3 LMP (Mef2)			↓	(↓)	
SLORF2 (thuti) deacetylated			–	(↓)	
SLORF2 HMP (mef2)			–	–	
SLORF2 LMP (mef2)			(↓)	–	
SLORF3 (TVTD) Native			↑	↓	
SLORF3 HMP (Mef4)			↑	–	
SLORF3 LMP (Mef4)			↓	–	Anti-inflammatory
SLORF3 HMP (Mef3)			↑	↓	
SLORF3 LMP (Mef3)			↓	↓	Anti-inflammatory

SLORF3de. Mef2 HF3			(↑)	↑	
SLORF3de. Mef2 HF4			(↑)	–	
SLORF3de. Mef2 HF5			↑	–	Pro-inflammatory
SLORF3de. Mef2 HF6			↑	–	
SLORF3de. Mef2 HF7			–	(↓)	
F. evanescens					
FeF2 (TVTD) Native			(↑)	–	
FeF2 HMP (Fhf1)			(↑)	(↑)	
FeF2 HMP (Fhf2)			(↑)	(↑)	
FeF2 LMP (Fhf2)			–	–	
FeF3 (Vyha) Native			–	–	
FeF3 LMP (Fhf1)			–	–	
FeF4 (2M) HMP (Mef2)			(↑)	↑	
FeF4 (2M) LMP (Mef2)			–	–	
Ulvan and Ulvan Oligosaccharides					
Species and samples	**Cytokines**				**Pro- or anti-inflammatory**
***U. lactuca* (DTU)**	**TNF-α**	**IL-6**	**IL–12p40**	**IL–10**	
U. lac Crude			↑	↑	
U. lac F1			↑	↑	
U. lac F2			↑	↑	

U. lac F3			↑	↑	
U. palmata (DTU)					
U. pa Crude			↑	–	
U. pa F1			–	(↑)	
U. pa F2			–	(↑)	
U. pa F3			(↑)	(↑)	
Elicityl Ulva fine grade (Lund)					
Ulvan fine grade					
Ulvan mix B			–	–	
Ulvan mix C			–	–	
U. lactuca (Lund)					
LL-Control	(↑)	↑	(↑)		Only one data point for IL-12p40
LL-Sample	-	(↑)	(↑)		Only one data point for IL-12p40
Ulca sp. (Lund)					
IH-Control	(↑)	↑	(↑)		Only one data point for IL-12p40
IH-Sample	-	(↑)	-		Only one data point for IL-12p40
Ulva papenfussii					
LP-Control	(↑)	↑	(↑)		Only one data point for IL-12p40
LP-Sample	-	(↑)	-		Only one data point for IL-12p40
Palmaria cell wall sugars and Oligosaccharides					
Species and samples	**Cytokines**				**Pro- or anti-inflammatory**

P. palmata			**IL–12p40**	**IL–10**	
Palmaria 308			–	–	
Palmaria 308 D10–E8			–	↑	
Palmaria 308 E10–F4			–	–	
Palmaria 308 F8–F12			–	(↓)	Pro-inflammatory due to decreased secretion of IL–10
Palmaria 209			(↓)	↑	Anti-inflammatory, due to increased IL–10 secretion, but, this sample have not been purified on the Superdex30 column, thus the strong effect observed can be due to impurities in the sample.
Palmaria 209 E11–F1			↓	↓	
Palmaria 209 F4–F7			(↓)	↓	
Palmaria209 F9–F11			↓	↓	
Palmaria 209 F12–G3			↓	↓	
Palmaria 209 G4–H8			↓	↓	
Palmaria 209 H9–H10			(↓)	–	

*Significant pro-or anti-inflammatory effect of a given sample, $p \leq 0.05$; –, indicate no difference of cytokine secretion compared to a negative control; ↑, indicates significantly increased cytokine secretion; (↑), indicates a trend towards an increased cytokine secretion, but not significant; ↓, indicates significantly decreases cytokines secretion; and (↓), indicates a trend towards decreased cytokine secretion, but not significantly.

Table 11. Cytokine secretion from dendritic cells, treated with different compounds.

***β*–glucans with different origin**					
Species and samples	**Cytokines**				**Pro- or anti-inflammatory***
A. faecaeli			**IL–12p40**	**IL–10**	
Curdlan			–	–	Anti-inflammatory
Curdlan DP5 (linear)			–	–	
Curdlan DP8 (branched)			(↓)	(↓)	
Curdlan DP11 (branch on branch)			(↓)	(↑)	Anti-inflammatory
Species and samples	**Cytokines**				**Pro- or anti-inflammatory**
S. cerevisiae			**IL–12p40**	**IL–10**	
Nutramunity™ (Algalíf)			↓	↑	Anti-inflammatory
Nutraminity oligo F1					
Nutraminity oligo F2					
Nutraminity oligo F3					
Nutraminity oligo F4					
Other compounds					
Species and samples	**Cytokines**				**Pro- or anti-inflammatory**
C. crispus (carrageenan samples)			**IL–12p40**	**IL–10**	
C. crispus 61			–	(↑)	
C. crispus 61 D–E–F (fraction)			–	↑	
Species and	**Cytokines**				**Pro- or anti-inflammatory**

samples					
Chondroitin Sulfate			**IL–12p40**	**IL–10**	
Chondroitin Sulfate AC DP4			↓	–	Anti-inflammatory
GalNac4S			↓	–	
Species and samples	**Cytokines**				**Pro- or anti-inflammatory**
Exopolysaccharides from R. marinus			**IL–12p40**	**IL–10**	
EPS 493			–	↑	
EPS 6611			–	(↑)	
EPS 493 defined media			↑	–	